CHARACTRISTICS OF HYDROCYCLONE FLOWS

Mustafa Al kayed

A Thesis

in

The Department

of

Building, Civil and Environmental Engineering

Presented in Partial Fulfilment of Requirements

For the Degree of Master of Applied Science at

Concordia University

Montréal, Québec, Canada

December 2008

Your file Votre référence
ISBN: 978-0-494-63330-4
Our file Notre référence
ISBN: 978-0-494-63330-4

ABSTRACT

CHARACTERISTICS OF HYDROCYCLONE FLOWS

Mustafa Al kayed

The hydrocyclone is a very useful tool which utilizes high centrifugal forces to separate solids from liquids. Its success is primarily due to the simplicity of construction and operation, versatility in application, and relative insensitivity to changes in design.

In the present study, the Laser Doppler Anemometry (LDA) has been deployed to measure the mean velocities in the 6" hydrocyclone. Traditionally, a flat surface box or jacket is used to encase the hydrocyclone in an auxiliary box to minimize the refraction effects of laser beams which is caused by the curved solid wall of the hydrocyclone and the refractive index of the test medium. A new procedure is developed to reorient the laser beams that permit one to measure two velocity components at a single point. In this new procedure, the probe is tilted by 45° (called the transform position) to force the four laser beams of the LDA to intersect at the same point. Therefore, the tangential and axial velocities yet fully characterized and measured. The measured axial velocity profiles in the transform position were all corrected for index of refraction effects. This gives approximately the same results for this velocity in the traditional optical probe position (called the regular position). The

conclusion developed from these experiments enables one to use the LDA directly in the hydrocyclone wall without recourse to auxiliary attachments such as an enclosing box. Further, the new procedure permits the determination of the turbulent intensity as the fluctuations of two velocity components can be measured at the same point.

Flow visualization by droplet dye injection shows five different kinds of flow field patterns inside the hydrocyclone. The features of the flow field in the hydrocyclone, as seen in the dye tests, were confirmed by the flow patterns derived from LDA experimental data. The number of turns associated with the flow in the hydrocyclone was also determined.

Prediction of flow field characteristic was also achieved by a very short study related to Computational Fluid Dynamic (CFD) modeling. A 3-D turbulence model that uses the Reynolds Stress Model (RSM) was adopted to simulate the flow field patterns. RSM predicted the velocity field in the hydrocyclone very well. The predicted velocities agree well with the experimental results by LDA and flow visualization study.

ACKNOWLEDGMENTS

I wish to thank my supervisor Professor A.S. Ramamurthy for suggesting the research subject.

I also would like to thank Dr. José Angel Delgadillo Gómez, Dr. Diep Vo, Mr SangSoo Han and Mr Lang Vo for their assistance.

Finally, the support and encouragement given by my family is greatly appreciated. I take the opportunity to thank my family, my wife Majeda and my children Noor, Nazek and Gheed, without their love and patience this thesis would never have been completed.

This thesis is dedicated to my wife Majeda for her encouragement and support.

TABLE OF CONTENTS

List of Figures

List of Tables

Nomenclature

B_c: Inlet width, m

CFD: Computational Fluid Dynamics

D: hydrocyclone wall thickness, 6.35mm

D_c: the hydrocyclone diameter, (6″) 152.4mm

dp: cut diameters, Eq. 2.3, m

ϵ: the probe movement

f_d: Doppler Frequency

H_c: Height of inlet, m

L_c: Height of cylinder section, m

LDA: Laser Doppler Anemometry

n: a constant Eq. 2.1

n_a: n_{air} : the refractive index of air, 1.0

n_g: n_{glass} : refractive index of glass,1.5

N_t: effective number of turns made by fluid in cyclone

n_w: n_{water} : the refractive index of water(1.33348)

ρ_g: gas density (kg/ m^3)

ρ_p: particle density, (kg/m^3)

PIV: Particle Imaging Velocimetry

Q: the feed volumetric flow rate, m^3/sec

R: the radius, Eq. 2.1

R_c: the radius of hydrocyclone, 76.2mm

t_r : the residence time of the fluid stream, sec.

V: the volume of cyclone, m^3

V_a: Axial (vertical) velocity

V_r: Radial velocity

v_i: inlet velocity (m/s)

V_θ: Tangential velocity

y': the focal point of laser beams, point "O" in Fig.4.24

Z_c: Height of cone section, m

λ : Light wave length of laser

Δx : the displacement of probe volume in water

θ : intersection angle between the two beams

$\theta_a, \theta_{g_1}, \theta_{g_2}$: the refractive angles in air and glass in Case B respectively

μ : viscosity, (kg / m^2)

δ : the fringe spacing, m

Chapter 1

INTRODUCTION

1.1 Physical Description

Hydrocyclone is a device which utilizes a high centrifugal force to separate, classify or clarify specific solid and liquid components in a feed stream. Cyclones are used for solid-liquid separation. They are widely used in chemical, mineral and powder processing industries. While the cyclone uses gas as medium, a liquid cyclone uses water as the fluid medium. Hydraulic cyclone has been abbreviated as "Hydrocyclone" and even as "Hydroclone". The term used in this study will be "Hydrocyclone". It consists of a cylindrical top section connected to a lower conical section, a central upper overflow tube (Vortex Finder) and a central lower discharge tube (apex) as shown on Fig. 1.1 .

The hydrocyclone has an entry section attached to the top section of the cylindrical part and two outlets. They are at the top (Vortex finder) called the overflow and at the bottom (apex) called the underflow. In general, the underflow outlet, or both the underflow and the overflow outlets discharge into atmospheric pressure.

The flow enters the hydrocyclone tangentially in the cylindrical upper zone, which generate the centrifugal acceleration inside the hydrocyclone. Therefore, the fluid pressure head of the feed flow is converted into rotational motion. The downward moving flow is formed close to the wall and the upward moving flow tends to stay close to the hydrocyclone axis, as in Fig. 1.2.

1.2 Historical Background

According to Bradley (1965), the cyclone chamber has been patented in U.S.A. by Bretney (1891). The early use of cyclone was limited to separate particles from the carrier air. In 1939, Driessen of the Dutch State Mines used the cyclone as a thickener in a coal cleaning process, which led to international interest for using liquid (water) as the carrying medium (Bradley, 1965). After that, the hydraulic cyclone has become more popular as a liquid – solid separation device.

1.3 Applications of Hydrocyclones

Hydrocyclones are widely used and have the following advantages:

(1) Simplicity

In both construction and operation, no moving parts are present. There is ease and low cost of installation. It has a low cost maintenance.

(2) Small space requirement are needed for this equipment.

(3) Low energy consumption and high capacity are its desirable features.

(4) Versatility in application is also attributed to it.

The hydrocyclone applications can be divided into different phase separations, Bradley (1965) and Svarovsky (2000) summarize it as follows:

- Separate solids from liquids
- Separate solids from solids
- Separate liquids from liquids
- Separate gas from liquid

The disadvantages of hydrocyclones are the following:

They are limited in terms of the degree of separation achieved. They can cause erosion of walls, especially in the conical part (Wang et al., 2007). Also, the

presence of shear causes its inability to manipulate flocculant material and act as gravitational thickener. However, the advantages have proved to outweigh the disadvantages by far, and due to the capability of performing many different duties and applications, the prevalence of hydrocyclone as a separation equipment is competitive.

1.4 Objectives of the present study

The overall objective of this study is to investigate the flow field characteristic within the hydrocyclone, which will lead to improve the understanding of flow patterns and permit one to know the relation between the hydrocyclone parameters. LDA was the major experimental tool used to achieve this task.

Toward this goal four major tasks were completed during the course of this study:

1- Develop a hydrocyclone system (design, draw and fabricate) for the hydrocyclone studies.

2- Measure the mean velocities in a hydrocyclone using Laser Doppler Anemometry (LDA) (chapter 4):

Deploy the LDA to measure the mean velocities directly without using any box or jacket to encase the hydrocyclone that was generally used to avoid the refraction of laser beams which is caused by the curved solid wall of hydrocyclone. The data collection was conducted at two different positions. Firstly, the planes in which laser beams are present form a 90° angle; one of these planes contains the axis of the hydrocyclone (Figs. 3.15 and 3.18). This is the regular position traditionally used by LDA to

measure the mean tangential and axial velocity components. However, the two pairs of the beams do not meet at the same point. To force the two beam pairs to meet at the same point, the probe was tilted by 45° (Figs. 3.16 and 3.19) to measure the two mean velocities (tangential and axial). This is a new method, which uses the probe positioning differently to measure the mean velocity components in a hydrocyclone in the absence of a flat surface box or jacket to surround the hydrocyclone, as done by earlier hydrocyclones researchers who used the LDA. The data of both positions were collected, analyzed and verified for precision of measurement.

3- To observe the motion of droplets dye using flow visualization technique for the following purposes (chapter 5):

   a- Study some flow field characteristics inside the hydrocyclone: Record the flow pattern on video to know the flow characteristics.

   b- Compute the key parameters denoting the number of turns (N_t) made by the water within hydrocyclone. Verify this result related to N_t by approximate mathematical computations

4- A short study related to the simulation of flow field patterns within the hydrocyclone using the Computational Fluid Dynamics (CFD) package FLUENT software. To this end the Reynolds Stress Model (RSM) was adopted as the turbulence model. The model

predictions are compared with the experimental data and the flow visualization study (chapter 6).

1.5 Outline of the thesis

Chapter 2 details general background about hydrocyclones and there flow field patterns. Also, it reviews related literature with an emphasis on the researchers' studies that used LDA to measure the mean velocity components in hydrocyclone. Sections 2.4 and 2.5 introduce the factors affecting the performance of hydrocyclone and cyclone respectively. Chapter 3 reviews the experimental apparatus, the lab setup and procedures of the experiments by using LDA and flow visualization techniques. Chapter 4 reviews the effects of LDA optical probe positions on the measured mean velocities within a 6″ hydrocyclone. Chapter 5 attempts to describe the flow field patterns through injection of droplets dye and by tracing the motions of the dye and clarifies the features of the flow field in a hydrocyclone will be clarified.

The number of turns made by the injected droplets dye was measured to compute the separation efficiency of a hydrocyclone. This is described briefly. The comparison between the visual observations and the experimental data are also provided in section 5.1. Chapter 6 is another attempt to predict the flow field patterns using FLUENT. The turbulence model used is the Reynolds Stress Model (RSM). Comparison between CFD simulation and the experimental results in chapters 4 and 5 are discussed. Chapter 7 details the conclusions of this research and suggests topics for further studies.

Figures Chapter 1

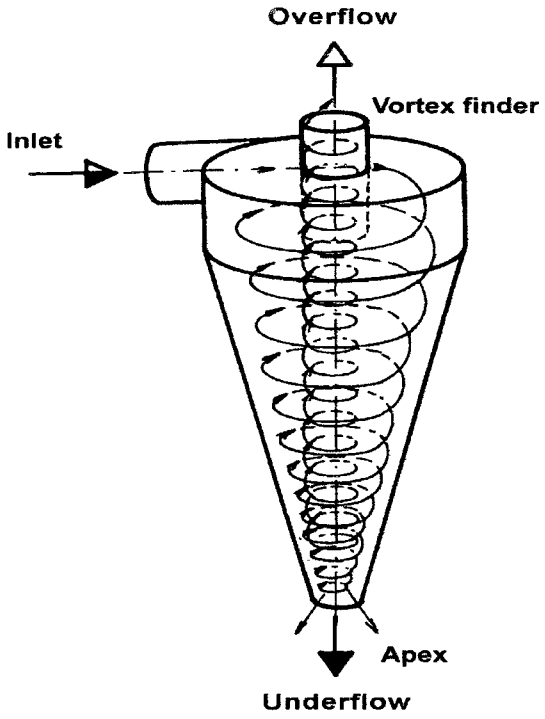

Figure 1.1 Hydrocyclone Geometry

(Bradley 1965)

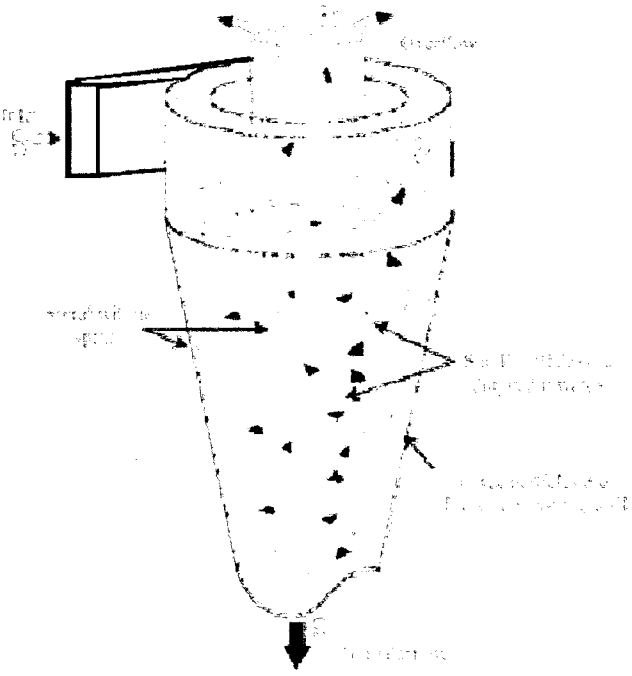

Figure1.2 Hydrocyclone Flow

Pattern (Cullivan et al. 2004)

Chapter 2

Literature Review

This review section is basically concerned with the scanning of literature related to solid - liquid separation in a hydrocyclone.

2.1 Design of a Hydrocyclone

Although the gas cyclone has a typical conventional design (Lapple 1951) as in Fig. 2.1, the hydrocyclone has two well-known geometries [Bradley 1965 and Rietema 1961]. Fig. 2.2 illustrates the dimensions of the two geometries along with the comparison. The hydrocyclone might be conical or cylindrical (flat bottom) in shape. The conical shape has the most widespread appeal and is popular.

2.2 The Flow Pattern

Although the hydrocyclone is simple in structure, the fluid motion inside it is extremely complicated. The complex flow field of hydrocyclone has been the subject of numerous investigations. The basic ideas of design hydrocyclones were traced to the pioneering studies of Kelsall (1952), Bradley and Pulling (1959), Rietema (1961), Svarovsky (2000) and others, to this day hydrocyclones still follow many of their design recommendations.

The velocity field in hydrocyclone can be categorized into three components:

a) Tangential velocity (V_θ)

b) Axial (vertical) velocity (Va)

c) Radial velocity (Vr)

Fig. 2.3 depicts the various velocities. The tangential velocity is the most important one of the three velocity components for the performance of the hydrocyclone. The higher the tangential velocity (V_θ) the larger the centrifugal force imposed on the particles and smaller is the diameter of a particle that can be separated .The next part of this chapter focuses on these velocity components.

As the feed slurry enters the hydrocyclone tangentially, the swirling motion generates a centrifugal force. This can be several hundred times greater than the gravity field. This centrifugal force creates the separation process. When the density of solid particles is higher than the fluid density, these particles are driven towards the wall and move downwards to leave the hydrocyclone through the underflow (apex). The particles with lighter density leave the hydrocyclone with the flow directed upward towards the overflow exit (vortex finder), Fig. 1.2 illustrates the process.

The wall friction at the roof of the hydrocyclone causes the swirling flow (tangential velocity) to attain low speed at this region. Therefore, a small amount of feed flow (15% by Kelsall 1952) will move from the upper part of the hydrocyclone to the bottom of the vortex finder entering in the overflow forming the so-called short-circuit Flow (Bradley 1965), as shown in Fig. 2.4.

It is well known that the short circuit flow is obviously deteriorating the separation efficiency of a hydrocyclone, because part of the feed flow is taking a shortcut to the vortex finder (Bergström et al. 2007, Bradley and Pulling

1959).Therefore, the vortex finder is projected into the cylindrical section of the hydrocyclone to lessen the effect of short circuit flow (Bergström et al. 2006). Kelsall (1952) described the short circuit as "a source of inefficiency". Although Bradley and Pulling (1959) proposed to use a "skirt" to decrease the effect of short circuit flow, Kelsall (1952) observed that tests had shown that a "skirt in a hydraulic cyclone was virtually useless". Rietema et al. (1983) used a "disk" at the bottom of vortex finder of a large cone angle to block what is stated to be a secondary liquid flow in referring to short circuit flow. Wang et al. (2008) proposed a mantle shaped vortex finder to improve the hydrocyclone performance.

Bradley and Pulling (1959) ascribed the reason for the presence of the short circuit flow to the difference in pressure with displacement along the radius from large radius (near wall, feed inlet) with high pressure to the small radius (toward the vortex finder) where the pressure is low. Wang et al. (2007) used a numerical study to confirm the presence of short circuit.

The second flow pattern in a hydrocyclone is the eddy flow as shown in Fig. 2.4. By using a dye injection, Bradley and Pulling (1959) visualized circulatory eddy flow that had the tendency of becoming trapped in eddies (Bergström et al. 2007 and Bradley 1965).

The third interesting flow pattern in the hydrocyclone is the "Locus of zero vertical velocity" which is termed by Bradley and Pulling (1959) as "the Mantle". More discussion about this flow pattern will further illustrated in this chapter under "vertical (axial) velocity", Svarovsky (2000) agreed with Bradley (1965) to

define the locus of zero vertical velocities (LZVV) and its presence in the hydrocyclone.

The last flow pattern of the qualitative flow field in the hydrocyclone is the presence of an air core. When the overflow and/or underflow outlets are opened to the atmosphere, the low pressure at the center axis of the hydrocyclone (which is due to the rotation of the fluid) creates a rotating air-column called the air core, which is developed from the underflow. Fig. 2.5 depicts the shape of air core inside a hydrocyclone.

The stability and shape of the air core has been the subject of several empirical investigations. The majority of researchers focused on the strong influence of the air core on the operational efficiency of the hydrocyclone. It is clear that the presence of air core is impairing the stability and separation efficiency of the hydrocyclone. Therefore, several authors proposed methods to eliminate or reduce the effect of the air core to improve the separation efficiency of hydrocyclone. Some researchers like Dabir et al. (1985) operated the hydrocyclone without air core. Fanglu et al. (1987) conclude from their experiments that the reducing of air core diameter made the flow pattern in the hydrocyclone more stable and that the velocity of the central flow became higher. Thus, they reported that by eliminating the air core, the complex three phases matter in the cyclone would become two phases, which will improve the separation effectiveness.

Qian et al. (1992) studied the effected of unstable air core on the flow field in hydrocyclone. According to their investigation, the air core has an unstable size, a varying shape and space position. Hence it strengthens the turbulence and asymmetry of the flow field and disturbs the regular distribution of solid particles

within hydrocyclone. It is related to the fact that the axis of the air core does not coincide with that of the hydrocyclone. Therefore, the physical centre of the hydrocyclone always deviates from the geometrical center. They briefly state that "when the air core lies in the centre of the vortex finder, the flow area within the vortex finder is symmetrical and particles with same size distribution report to overflow in every directions, but when the air core waves to one side, the symmetry is destroyed and particles entering into the vortex finder in different directions have different size distribution, leading to a low classification efficiency". At the end, they proposed to introduce a solid core to occupy the air core position. Fig.2.6 represented the relation between feed pressure and air core diameter as given by Qian el al. (1992).

Martinez et al. (2007) studied the effect of the vortex finder length on air-core precession; according to their measurements, the introduction of the vortex finder in the conical section causes a stabilization of flow lines. Chu et al. (2004) inserted a 6 mm, solid core through the hydrocyclone from the vortex finder (at the top) to the underflow pipe (at the bottom) and fixed outside the overflow and underflow regions. This eliminated the air core and improved the separation efficiency compared to that with air. Also, Sripringe et al. (2007) inserted a solid rod to eliminate the air core and to create a suitable flow for separation. They suggested that the height of solid rod could be reduced if its diameter increased or the inlet flow rate increased. Chu et al. (2002) introduced a winged core fixed below the vortex finder to control the turbulence structure, which led improved the hydrocyclone performance.

2.2.1 Tangential velocity

On the hydrocyclone there are two regions of flow:

1- Forced vortex region (core region), or inner region.

2- Free vortex region, outer region.

The tangential velocity increases with decrease in radius, therefore, the relationship can be written as:-

$$V_\theta . R^n = \text{constant} \qquad (2.1)$$

Here "V_θ" is the tangential velocity, "R" is the radius and "n" is a constant.

The maximum tangential velocity is on the inner region, n = -1

Therefore, in the inner region (also termed a solid body rotation):

$$V_\theta R^{-1} = \text{constant}$$

In the outer region "n" varies. Kelsall (1952) measured the value of "n" to range from 0.84 to 0.75 if the split Ratio (overflow rate / underflow rate) was varied between ∞ and 0 operated with the air core. The tangential velocity reached the maximum value and then it rapidly decreases (Fig. 2.7).

Fig. 2.8 illustrates the tangential velocity without air core that was adopted by Knowles et al. (1973).They used cine photography to measure the tangential velocity. The value of "n" as in Eq.1was varied between 0.2 and 0.4 for operations without an air-core.

Dabir and Petty (1986) used the Laser Doppler Anemometry (LDA) to measure the tangential velocity in a hydrocyclone operated without air-core (Fig. 2.9) and the value of "n" was 0.62 , when the split Ratio was 4, i.e. (Qo = 4 Qu).

In the hydrocyclone the tangential velocity is the dominating velocity component, which has been studied frequently. Most studies present similar results and confirmed the presence of two regions as previously mentioned. In a recent study of Wong et al. (2007), the tangential velocity was measured using Laser Doppler Anemometry (LDA) and Particle Imaging Velocity (PIV) and the results qualitatively agreed with previous studies (Fig. 2.10). As the pressure increases, the tangential velocities increase, this is due to the fact that a higher pressure is always accompanied by a large flow rate (Fanglu 1987).

2.2.2 Axial velocity

The second type of velocities in the hydrocyclone is the axial (vertical) velocity; refer to Fig. 2.3. It has a negative value from the inner wall of the hydrocyclone to the zero point, and positive value from the zero point to the central axis (air core). Vertical velocity distributions obtained by Kelsall (1952) is shown in Fig. 2.11.

Bradley (1965) located the zero vertical velocity in Kelsall's (1952) study and initiated the term "Mantel" Fig. 2.12. Kelsall (1952) referred to the zero vertical velocity as an envelope by connecting each zero point at each cross section.

The flow outside zero point (below zero value) flow downwards and discharged through underflow outlet, while the flow inside zero point (positive values) flow upwards and discharge through overflow outlet. This indicates the presence of two recirculation flows. Bradley (1965) discovered that there are three curved surfaces

in the hydrocyclone: The solid wall surface, the mantle surface and the air core surface (Chine and Concha, 2000).

The difference between the "mantle" (Bradley 1965) and the "envelope" (Kelsall 1952) is that the envelope shows a conical surface, while Bradley (1965) found, by using dye injection, that the mantle is a cylindrical surface and continues in the conical section (with diameter equal 0.43 Dc) increases as the cone angle increases and ends at level 0.7 Dc in conical part (Fig. 2.12). The reason for such discrepancy is traced to the abnormally long vortex finder used by Kelsall (1952) and Bradley (1965).

Dabir and Petty (1986) used a 2:1 contraction at the top of the vortex finder and discovered several individual counter current axial flows including a downward flow just below the vortex finder due to the presence of a 2:1 contraction. Fig. 2.13 illustrates the flow patterns observed by Dabir and Petty (1986).

Wong et al. (2007) got similar results for the vertical velocity profiles (Fig. 2.10). They confirmed that the distribution of vertical velocity is reasonable, and that the fluid entering the cyclone tangentially moves toward the wall forming an outer downward vortex flow under the strong action of the centrifugal force, and after reacting at the bottom it turns upward.

2.2.3 Radial Velocity

The radial velocity is much smaller than the tangential velocity and the axial (vertical) velocity; therefore, it becomes difficult to measure. Unlike the other velocities (tangential and vertical), the radial velocity was not studied in detail

(Bergström 2007, Sevilla and Branion 1997, Hsieh and Rajamani 1991 and Devulapalli and Rajamani 1994).

Kelsall (1952) calculated the radial velocity as shown in Fig. 2.14, which illustrates the result of Kelsall's calculation, in which the inward velocity was greatest close to the hydrocyclone wall and decreased as the radius decreased, Kelsall (1952) assumed axi-symmetric flow. It may be noted that the radial velocity is generally not measured due to the difficulty in setting the LDA beams to intersect in the flow region, which could be only from the top or even the bottom of the hydrocyclone.

Dabir and Petty (1986) also assumed axi-symmetric flow, and used Laser Doppler Anemometry (LDA) to measure the tangential and axial velocity, and from these two velocities they indirectly obtained the radial velocity, Fig. 2.15 shows their result for radial velocity.

Fisher et al. (2002) found experimentally that the absolute values of the radial velocity was only 2% of the tangential velocity , zero all over the radius for cylindrical section and in the conical section it raised upward through radius from hydrocyclone wall to center axis, which is similar to the results of Luo et al (1989). They used LDA to measure the tangential, vertical and radial velocity for two different designs of hydrocyclones. One of them was operated without air core Fig. 2.16(b).

From the above, it's clear that most investigators computed the radial velocity indirectly without measuring it. Typical flow profile indicates that the radial velocity is inward in the outer part, and outward in the inner part, although more

recent studies find inward radial velocity that increases towards the hydrocyclone axis as in Fig. 2.16 (Fisher et al. 2002, Lou et al. 1989 and Chu et al. 1993).

The radial velocity shows highly varying results between researchers, depending on the hydrocyclone geometry, the type of feed particles and the methods of measurement.

2.3 Measurement Techniques

Several studies experimentally measure the velocity inside the hydrocyclone. Intrusive probes (pilot tube) were used earlier for measuring the flow velocity at a local spot (Lilge 1962). Kelsall (1952) used optical methods for velocity data collection. Bradley and Pulling (1959) have illustrated the flow patterns in the hydrocyclone using dye injection. Boadway (1984) used visual observations of the air core, and Laser Doppler Anemometer (LDA) for measuring the mean velocity components. Smyth et al. (1984) too used LDA for the internal flow field measurements. Bhattacharyya (1984) used visual and photographic observations with dye injection to describe the flow field inside a hydrocyclone. Dabir (1983), and Dabir and Petty (1984 and 1986) used LDA to measure the mean velocity profiles in hydrocyclones. Fanglu et al. (1987) used LDA in their study. Chu et al. (2004) also used LDA with and without an air core.

Laser Doppler Velocimetry (LDV) has been used by several researchers, such as Monredon et al. (1992), Chine et al. (2000), Hwang et al (1993), Fisher et al. (2002) and Coghe et al. (2002). Peng et al. (2001) used LDA and compared the results with that of three-dimensional Computation Fluid Dynamics (CFD) simulation done by other authors for cyclones. Recently, Wong et al. (2007) used

both LDA and Particle Imaging Velocimetry (PIV) to measure the flow field inside a cylinder-on-cone cyclone.

Laser Doppler Anemometry (LDA) has been widely deployed to measure the mean velocity inside the cyclone and hydrocyclone as an ideal non-contact (non-intrusive) velocity measurement method in cyclones and hydrocyclones. The LDA technique has proven its accuracy and capability to measure velocity in hydrocyclone. It is noteworthy to mention that, it is experimentally not possible to measure fluid velocity by LDA in slurries even at low concentrations (1% by volume) as stated by Slack et al. (2004) and Dabir (1983).

When two laser beams of the same wavelength meet at a small angle, a series of interference planes are produced where they intersect and particles in the fluid passing through these interference planes emit pulses of light which can be picked up by a photomultiplier (Boadway 1984).

Eq. (2) determines the value of velocity (Fig. 2.17):

$$V = \frac{\lambda}{2 \sin\frac{\theta}{2}} f_d \qquad (2.2)$$

Here, λ = Light wave length of laser, θ = Angle between the two beams, and f_d = Doppler Frequency.

LDA system consists of a laser (typically a continuous wave Ar-Ne-laser), fibre optics, signal processor, traversing system, and a computer to control the measurement and save data. In LDA the laser beam is first divided into two beams with equal intensities. The beams are then directed to optical fibres which deliver

them to the probe optics. The focal length of the front lens determines both the size and position of the crossing point of the

LDA system consists of a laser (typically a continuous wave Ar-Ne-laser), fibre optics, signal processor, traversing system, and a computer to control the measurement and save data. In LDA the laser beam is first divided into two beams with equal intensities. The beams are then directed to optical fibres which deliver them to the probe optics. The focal length of the front lens determines both the size and position of the crossing point of the two beams (also called the probe volume). In LDA optics guide the two laser beams into the measurement point (probe volume) where they form interference fringes of high intensity planes of light perpendicular to the laser beam plane. The flow is often seeded with small particles, which can follow the turbulent motion of the fluid. When these particles pass by the measurement volume they scatter light.

The intensity fluctuation of the scattered light depends on the velocity of the particle. The data analysis calculates the velocity of the particle by dividing the traveled distance "d_f" by the spend time (Fig. 2.18), "d_f" is the Doppler Frequency, $d_f = (2V/\lambda) \sin(\theta/2)$, where V is the velocity component perpendicular to the fringes.

2.4 Factors Affecting Hydrocyclone performance

The following factors affect hydrocyclone performance:

1- Hydrocyclone Geometry

2- Pressure drop

3- Cut Diameter (cut size, d_{50}) which defined as the size of particles collected, with 50% efficiency.

4- Centrifugal force, thus fluid flow rate.

5- Collection Efficiency.

6- Particle concentration

In literature, the majority of authors experimentally investigated the influence of operating parameters or geometry changes of the hydrocyclone on the separation process. The effects of operating parameters and / or geometry features on separation (collection) efficiency are discussed in the next section.

Martinez et al. (2007) focused their study on the effect of geometrical characteristic modifications on the separation efficiency, and they summarized this study as follows:

a- The effect of vortex finder: (Martinez et al. 2008)

- In the absence of vortex finder the short circuit flow increases and hence decreases the separation efficiency.
- The optimum vortex finder length value corresponds to a ratio of 0.1 of total length of hydrocyclone. If the vortex finder depth increases more, it causes a decrease in the separation, and if the vortex finder reaches the cone section it causes high turbulence and less efficient condition.

b- Increase in the length of cylindrical zone causes stabilization of flow lines, because the influence of vortex finder over the flow pattern decreases and the pressure drop also decreases. Near the tip of vortex finder high turbulence exists.

c- The study of Martinez et al (2007) showed a high turbulence zone in the region of transition between the conical and cylindrical part that leads to the minimum efficient point.

Fanglu et al. (1987) used LDA for measurement of velocity field in two types of cyclones (dense medium cyclone and water-only cyclone) and reported the following conclusions:

a- The increases in feed pressure (thus increase the flow rate) causes to increase the tangential velocity, and hence increases the separation efficiency.

b- The tangential velocity decreases with increase of the diameter of vortex finder, when the diameter of vortex finder increased, the air core will become larger than the apex diameter, thus decreasing the underflow which leads to decrease the separation efficiency.

c- The increase of vortex finder wall thickness increases the tangential velocity, because the increase of vortex finder wall thickness makes the space between the cyclone wall and vortex finder smaller and the flow layers become more stable.

d- The increase in the cone angle will reduce the tangential velocity at the conical section, and the axial velocity will decrease, as the mantle (axial-zero velocity) increase with increase of conic angle. High density material is discharged only by gravity force and the low density material leaves the cyclone with the flow going upward into vortex finder through overflow outlet.

e- The split ratio (ratio of the underflow rate to the overflow rate) strongly influences the separation efficiency, because if the split radio (Qu/Qo) is less than 0.50, the air core diameter is larger than that of underflow apex.

According to Pian et al. (1992) the presence of a core in a conventional hydrocyclone (Forced vortex) causes instability in the flow. They confirmed that "there is no separation process taking place within the forced vortex i.e. the air core, because the treated particles cannot enter the forced vortex. It is clear from Fig. 2.6 that the air core appears in a certain value of feed pressure and starts to increase rapidly until it becomes relatively stable (no change in air core diameter) and is not influenced by additional feed pressure.

Despite of the above, pressure turbulence is inevitable in practice because of the pump performance and the feed concentration rate. So, the presence of air core in practice is unavoidable and its diameter can be reduced to 6 mm (Fanglu et al. 1987) or less to have a stable flow with reasonable separation efficiency. The effect of air core in the performance of hydrocyclone was presented earlier in this chapter.

Chu et al. (2004) replaced the air core with a solid core, which resulted in higher separation efficiency. Kim et al. (2004) conducted an experiment with fluid flow at a low velocity and pressure drop in large hydrocyclone. They elaborated their results based on experimental and numerical studies, in which they confirmed that the increase in the inlet velocity will cause a linear increase of the internal flow, as well as the pressure distribution of the hydrocyclone. They further reported that the high velocities are present near the air core at the centre of hydrocyclone and

at the entrance of vortex finder. Besides that, they concluded that the increase in the underflow diameters will increase the collection efficiency until 50 mm. After 50 mm diameter, the efficiency is at a constant value. The studies of Narasimha et al. (2005) revealed that an increase in feed flow rate and decrease in underflow (apex) diameter the cyclone efficiency improves. Hwang et al. (2008) studies concluded that the increases of the inlet feed rate in a small hydrocyclone will increases the pressure drop under a fixed split ratio, which result to improve the separation efficiency.

Matvienko (2004) used a theoretical analysis to investigate the structure of flow in a hydrocyclone in the presence of turbulence. He reported that the hydrocyclone "can be considered as a hydraulic resistance in an inlet pipe". To overcome this hydraulic resistance, there must be a sufficient pressure immediately ahead of the inlet pipe. Then the centrifugal pressure increases as a result of the flow rotation and causes head losses. Only 20% of head losses occurred by the hydraulic resistance at the inlet. It is important to note that this analysis is valid with suspension particles in the fluid. Hence, the hydrocyclone capacity increases with increase in the total head and flow rate. It is noteworthy to mention that the pressure drop (or pressure loss) is defined as the difference in pressure between points immediately before feed entry and immediately after the overflow exit.

To end the effects of geometry and operation of hydrocyclone on the performance, it is important to refer to the classification of these variables as conducted by Bradley (1965), in the publication titled "The Hydrocyclone", Bradley divided the variables that affect the hydrocyclone performance into two groups:

1) Operating variables: are independent of the cyclone size. They are feed flow rate and feed composition (solids concentration, solids size and shape, solids density, and liquid medium density and viscosity)
2) Design variables: are dependent on the cyclone size, such as, feed size, overflow size, underflow size, apex size and cyclone size.

Bradley (1965) briefly illustrated the influence of above variables on the performance of hydrocyclone (chapters 6 & 7), which is related to the field's application. In a numerical study Wang and Yu (2006) concluded that a smaller cyclone is helpful to higher efficiency and lower pressure drop due to reduced tangential velocity and particle moving orbit but the feed capacity will be smaller, therefore, to balance between the prospective high efficiency and the reasonable feeding rate, the solution is to have several of smaller hydrocyclones in series.

2.5 Factors Affecting cyclone Performance

For cyclones the factors that control its performance include the centrifugal force, the cut diameter, the pressure drop and the collection efficiency.

The most important factor of the above is the cut diameter, which defined as the size (diameter) of particles collected with 50% efficiency.

The well known cut diameter for cyclone is the Lapple cut (Lapple 1951), $d_{p(cut)}$.

$$d_{p(cut)} = \sqrt{\frac{9\,\mu\,B_c}{2\,\pi\,N_t v_i \left(\rho_p - \rho_g\right)}} \qquad (2.3)$$

Where: μ = viscosity, (kg / m^2)

B_c = Inlet width, m

N_t = effective number of turn (5 to 10 for common cyclones)

v_i = inlet velocity (m/s)

ρ_p = particle density, (kg/m^3)

ρ_g = gas density (kg/ m^3)

Spellman (2005) states that the cut size depends on the particle properties, fluid properties, cyclone size and operating condition (number of turns made by the fluid). Therefore, the effective number of turns (N_t) is an important factor in determine the cut size, thus the cyclone efficiency. In spite of this, N_t is assumed to be 5 in the range of 5 and 10 and no study has provided a good procedure to get N_t.

Lapple (1951) considered the number of turns as an empirical quantity which must be determined experimentally, but it should be constant for any size of cyclone and for conventional / Lapple's cyclone (Fig. 2.1) it has been suggested to be 5. The relation between the particle size and separation (collection) efficiency is given by Lapple in Fig. 2.19.

In the next section, the effective number of fluid turns in cyclone will be briefly elaborated as reported in some sources that concerned about cyclones and centrifugal separators.

Zhang Y. (2005) summarized the concept of fluid turns in the cyclone, according to him; the fluid will turn one full revolution at one height of the inlet for the

upper cylinder, and half a revolution at one height of the inlet for the lower cone, which is represented mathematically as:

$$N_t = \frac{1}{H_C}\left(L_C + \frac{Z_C}{2}\right) \qquad \text{(Refer to Figure 2.1)} \qquad (2.4)$$

Where: N_t = Effective number of turns of fluid in cyclone

H_c= Height of inlet, m (in)

L_c= Height of cylinder section

Z_c = Height of cone section

Peavy et al. (1985) referred to Lapple's equation stated earlier, as the collection efficiency of particles that will be removed with 50 percent efficiency on a weight basis. They assumed that the number of effective turns within the cyclone (N_t) is approximately 5 turns.

Many authors such as Flagan and Seinfeld (1988) and Azbel et al. (1983) referred to Eq. 4 to compute the number of effective turns within the cyclone. Mackanzie et al. (1941) used Eq. 3 for cut diameter ($d_{0.50}$) the particle size for which the collection efficiency is 50 percent. They multiplied Eq. 4 by "π" to compute the effective number of turns (N_t) as follows:

$$N_t = \frac{\pi}{H_c}\left(L_c + \frac{Z_c}{2}\right) \qquad (2.5)$$

Here, L_c and Z_c are the length of the cylinder and cone respectively.

Mackenzie's Eq. (2. 5) yields a collection efficiency that will be high. Actual Eq. (2. 5) is rarely used, and Eq. (2. 4) is the popular one, as it gives more reasonable number of fluid turns within the cyclone.

Theodore et al. (1988) refer to Eq. (2.3) as the minimum particle diameter "$d_{p\ min.}$" that should be completely separated from the fluid in a cyclone. But they approached it by a different way to compute "N_t"; the number of turns made by fluid stream in cyclone. They confirmed that "N_t" in a conventional cyclone (Fig.(2. 1) has been found to be about 5, They emphasized that this values "N_t" typically ranges from 3 to 10, but may be as low as 0.50 in some designs, and they presented a theoretical approach as in Eq.(2. 6) below:

$$N_t = \frac{t_r v_i}{\pi D_c} = \frac{\frac{V}{Q} v_i}{\pi D_c} \qquad (2.6)$$

Here:

t_r is the residence time of the fluid stream, in sec.

v_i is the inlet velocity, ft/sec (m/sec)

V is the volume of cyclone, ft^3 (m^3).

Q is the feed volumetric flow rate, ft^3/sec (m^3/sec).

D_c is the cyclone diameter, ft (m)

2.6 Summary of literature on hydrocyclones and cyclones

The following can be concluded from the previous literature review:

1) There is a legion of literature available on hydrocyclones that investigated experimentally the influence of operating parameters or geometry changes on the separation result. Fewer experimental studies investigate the internal flow field characteristics.
2) LDA technique has been widely used to measure the mean velocity components inside hydrocyclones. The interesting point here, several researchers used a flat box or jacket to encase the hydrocyclone to avoid or even to eliminate the refraction of the laser beams on the hydrocyclone curved solid wall. Few researchers had used LDA directly without commenting the refraction effects on the measured velocity components. Therefore, this point deserves to be investigated briefly. The questions here, in case LDA used directly in the curved solid wall of hydrocyclone, how much the refraction of the laser beams influences the obtained results? What are the effects of the optical probe that positioned differently on the measured mean velocity components?
3) Flow visualization by dye injection has been used by several authors to investigate the flow patterns inside the hydrocyclone. It employed to identify specific regions within the flow domain, few researchers have tried to use flow visualization by droplet dye injection and traced the route of droplets dye within the entire flow field of hydrocyclone, to briefly illustrate the flow patterns within the hydrocyclone, which have complex patterns. This causes the authors to predict the flow patterns using numerical models or / and computational fluid Dynamics (CFD).

4) The collection efficiency of cyclone depends on the cut size (diameter) and the effective number of turns made by fluid stream within the cyclone is crucial parameters to compute the cut size. Many investigators used to assume the number of turns. Others used specific formulas to compute it. It is an empirical parameter, and should be determined experimentally. The cut size is applicable to compute the collection efficiency in a hydrocyclone. Therefore, the number of turns made by the liquid stream within a hydrocyclone was not subject to any investigation.

Figures Chapter 2

$B_c=D_c/4$, $D_e=D_c/2$

$H_c=D_c/2$, $L_c=2D_c$

$S_c=D_c/8$, $Z_c=2D_c$

J_c=Arbitrary, usually $D_c/4$

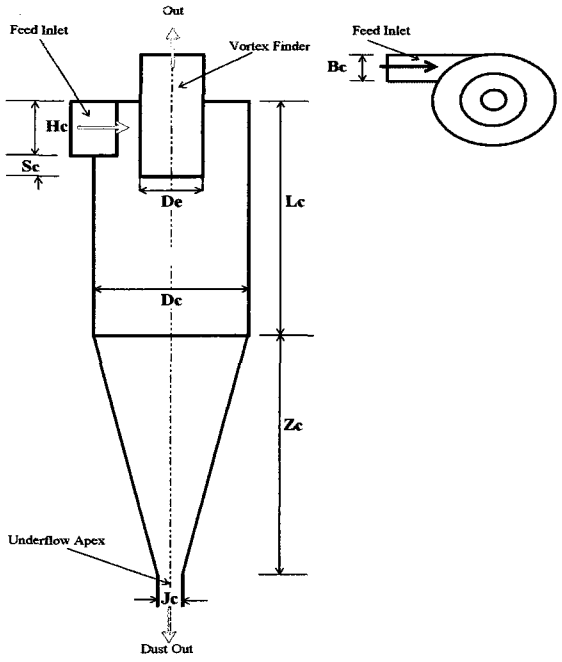

Figure 2.1 A conventional gas cyclone (Lapple, 1951)

H.Cyclone Type	Parameters						
	Di/Dc	Do/Dc	f/Dc	H2/Dc	L/Dc	Du/Dc	Cone Angle (θ)
Rietema	0.28	0.34	0.4	—	5	0.2	10°—20°
Bradley	0.133 (1/7)	0.2 (1/5)	0.33 (1/3)	0.5 (1/5)	6.85	0.07	9°

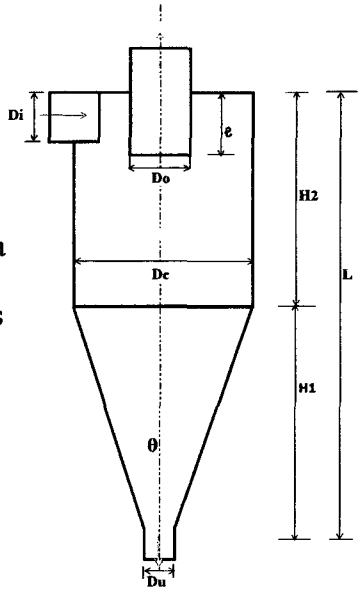

Figure 2.2 Hydrocyclone geometry by Rietema (1961) and Bradley (1965) with parameters comparison

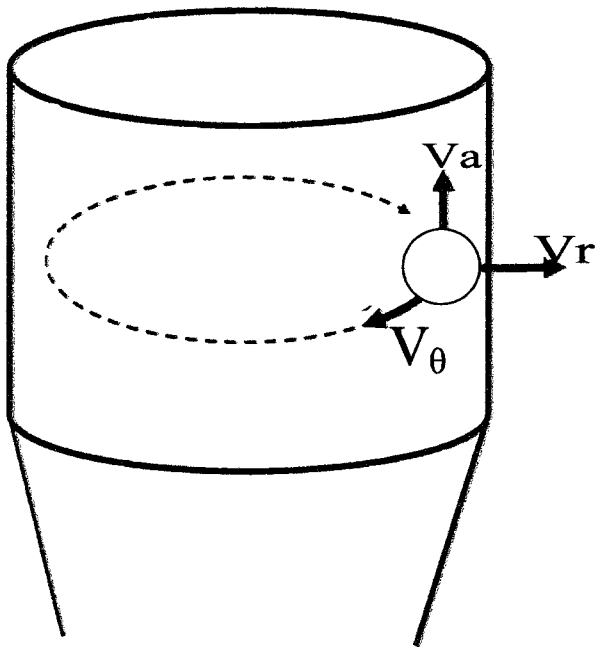

Figure 2.3 Illustration of hydrocyclone velocity components

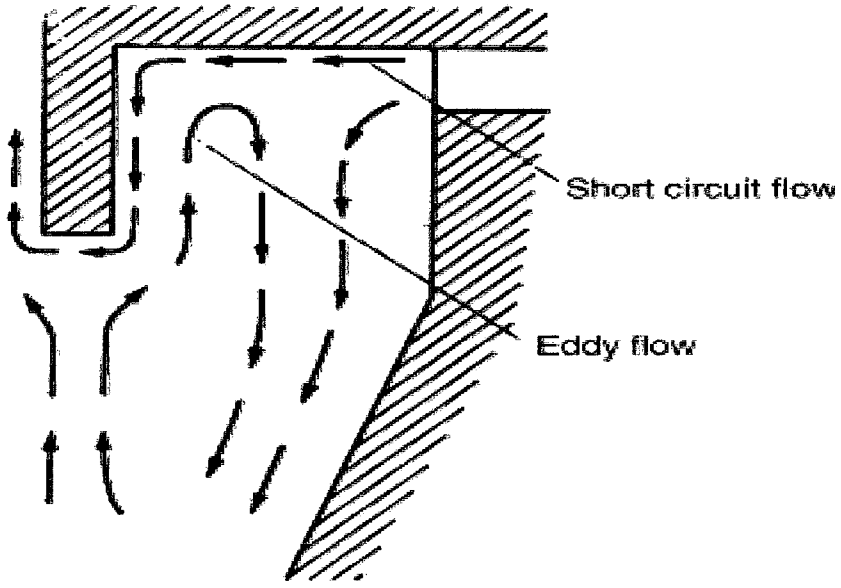

Figure 2.4 Schematic representations of the Short Circuit and Eddy Flows (Bradley, 1965)

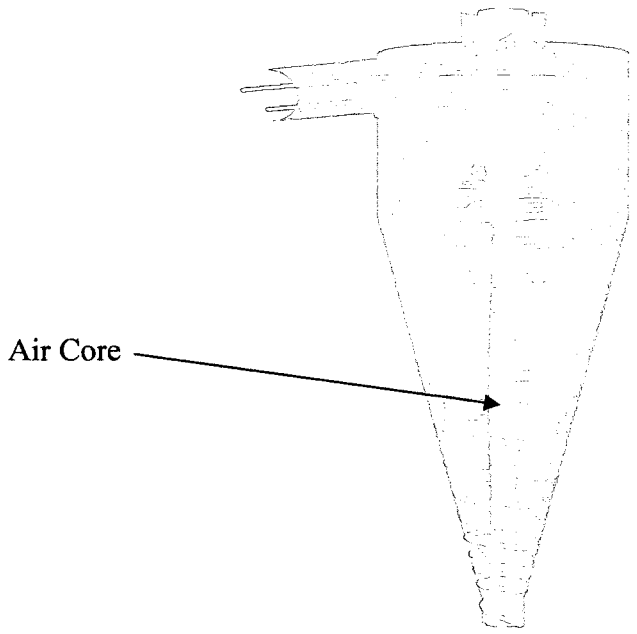

Figure 2.5The air core column that develop at the centre axis of hydrocyclone

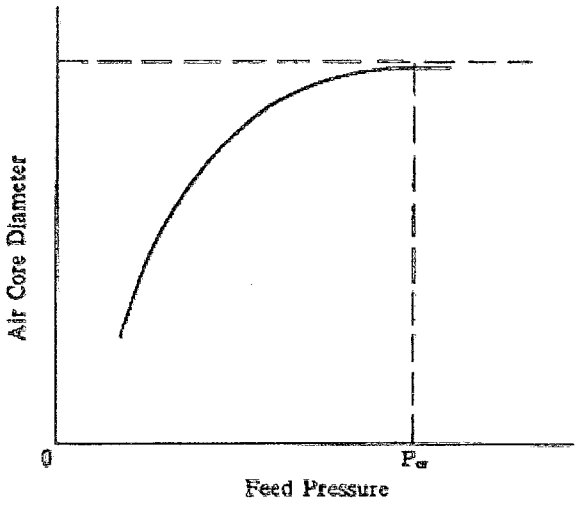

Figure 2.6 Air Core Diameter vs. Feed Pressure by Qian et al. (1992)

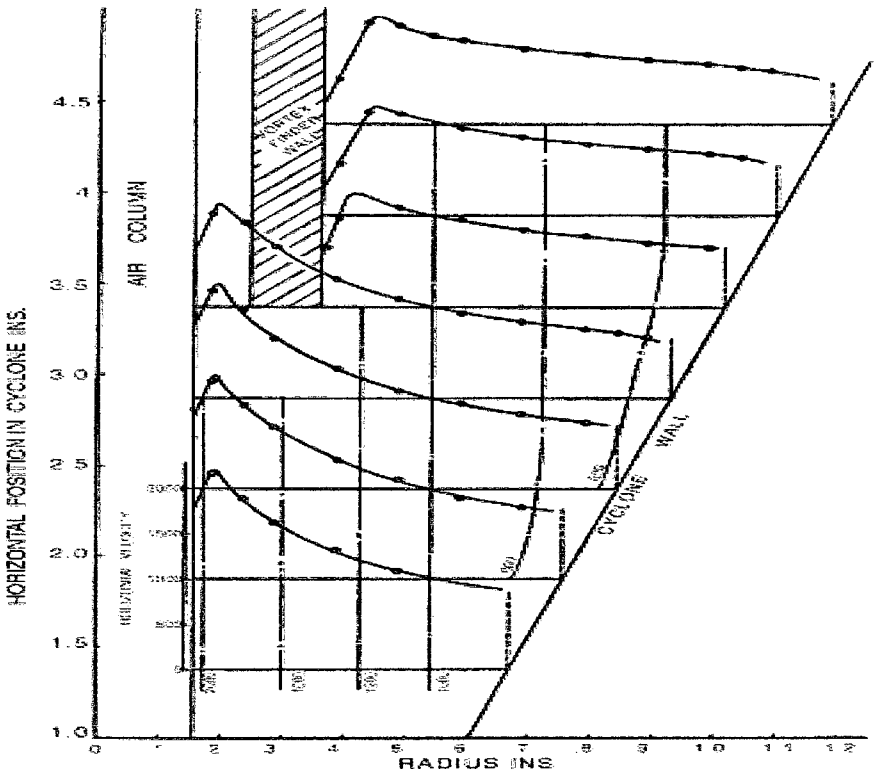

Figure 2.7 Tangential velocity profiles operated with air core by Kelsall (1952)

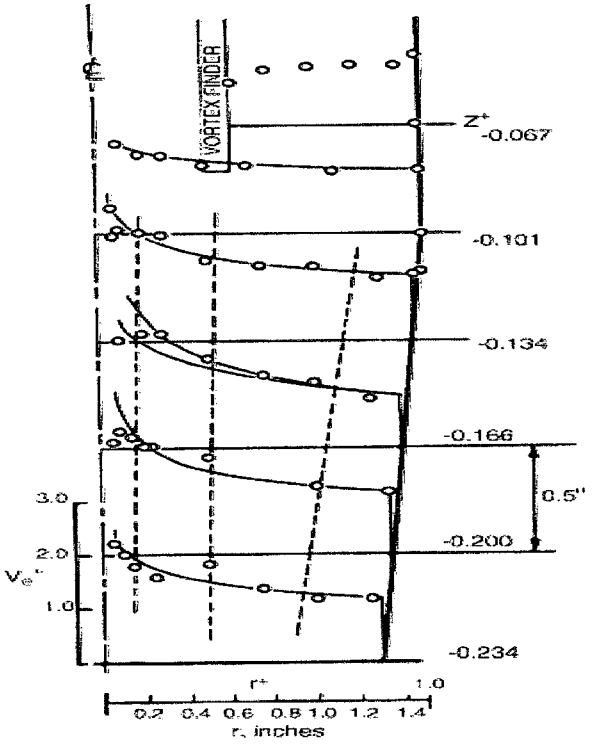

Figure 2.8 Tangential velocity profiles operated without air core by Knowles et al. (1973)

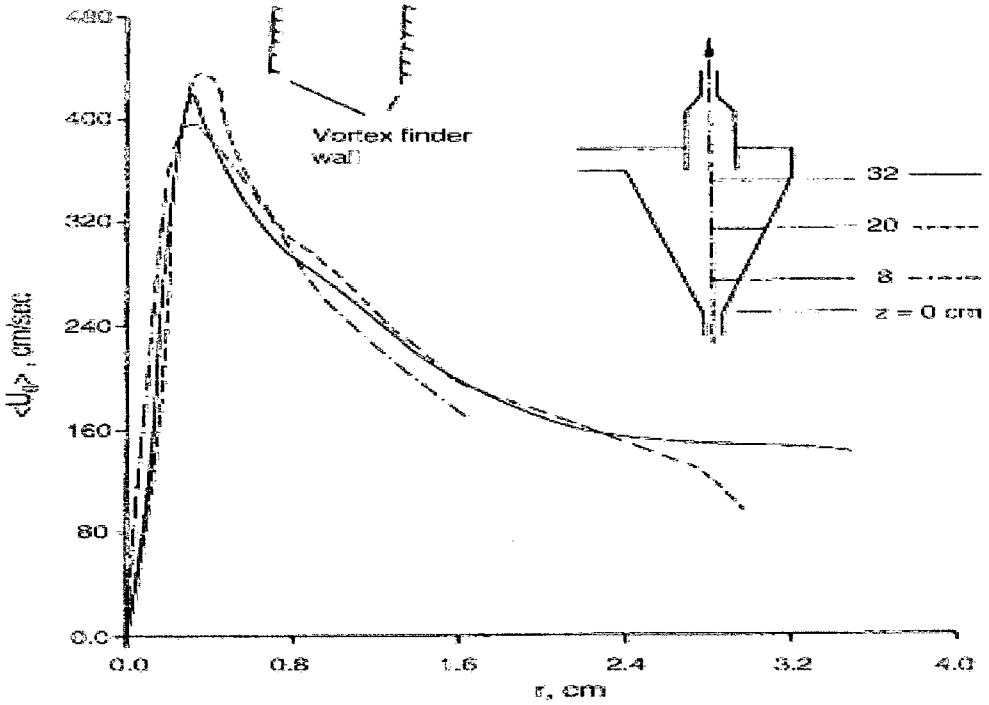

Figure 2.9 Tangential velocity profiles operated without air core by Dabir and Petty (1986)

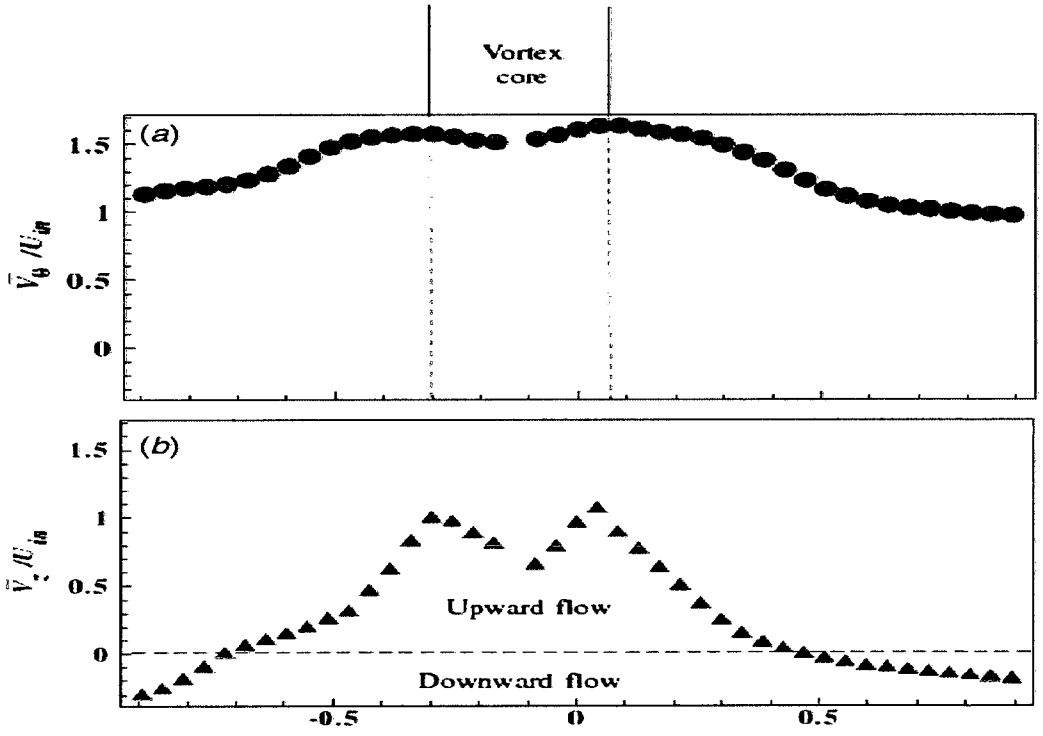

Figure 2.10 Tangential (a) and Axial (b) velocity profiles by Wong et al. (2007)

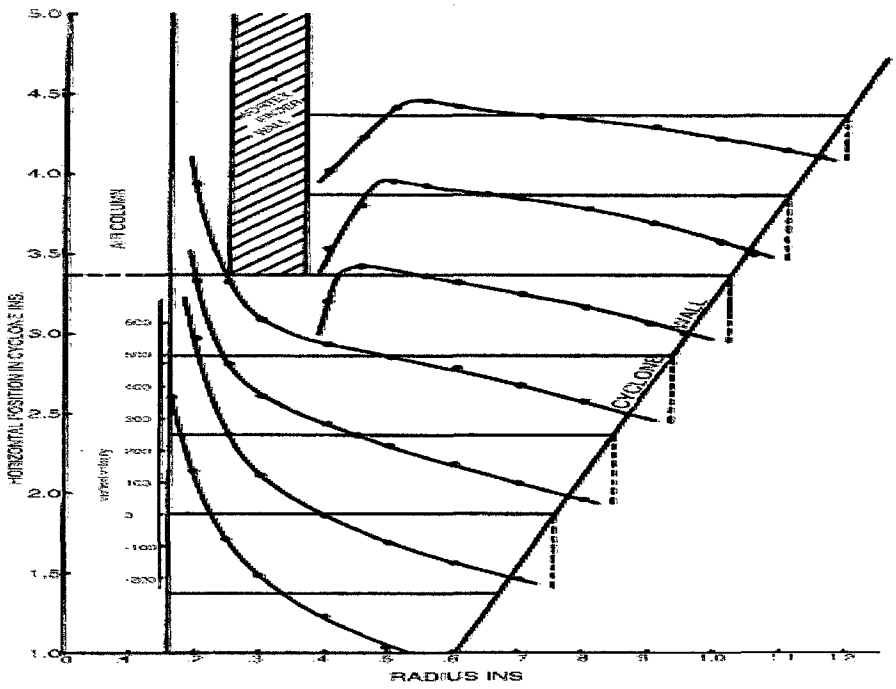

Figure 2.11 Axial velocity profiles by Kelsall (1952)

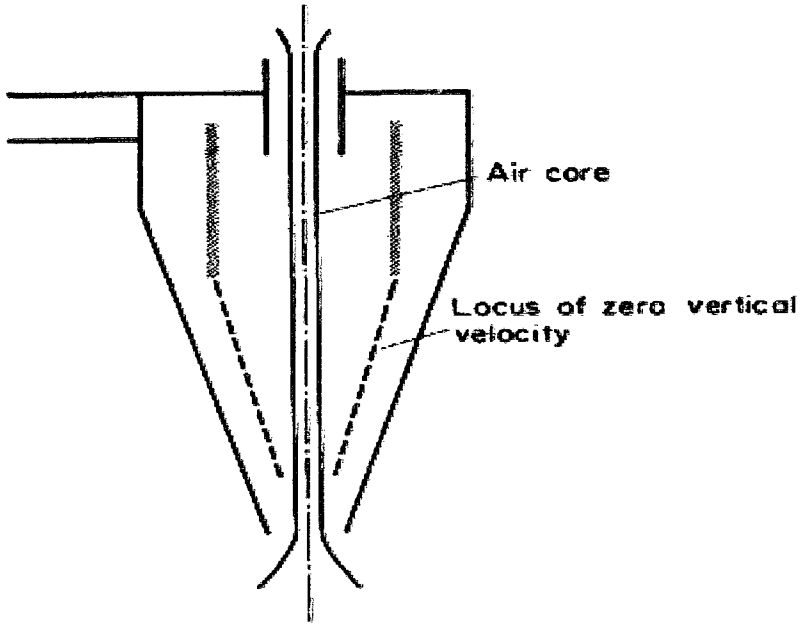

Figure 2.12The Mantle, Locus of Zero Vertical Velocity (LZVV) by Bradley (1965)

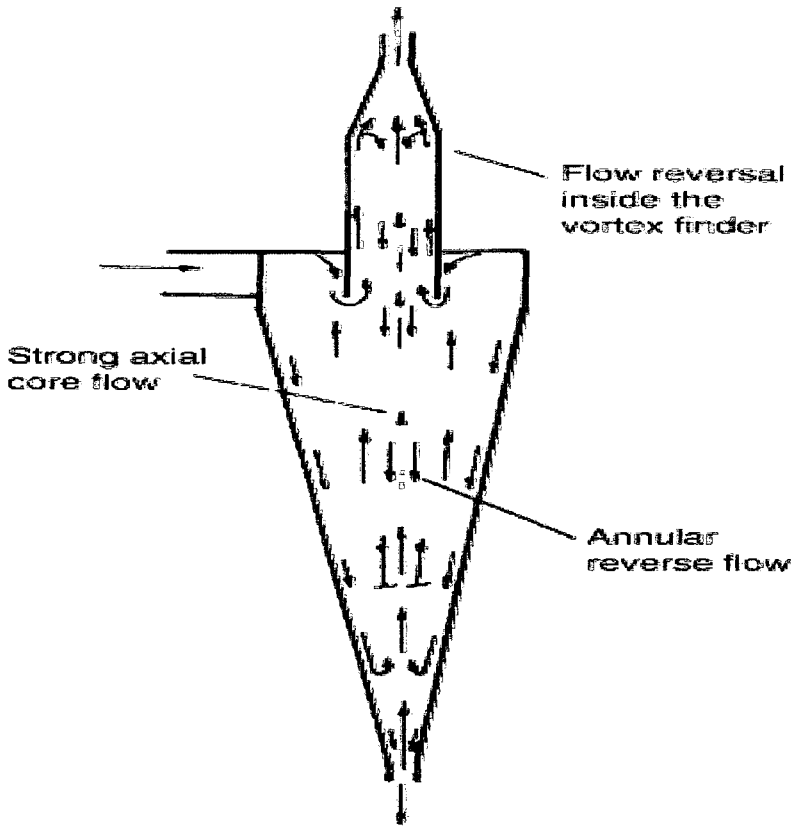

Figure 2.13 Flow patterns in the 3″ hydrocyclone using dye injection by Dabir and Petty (1986)

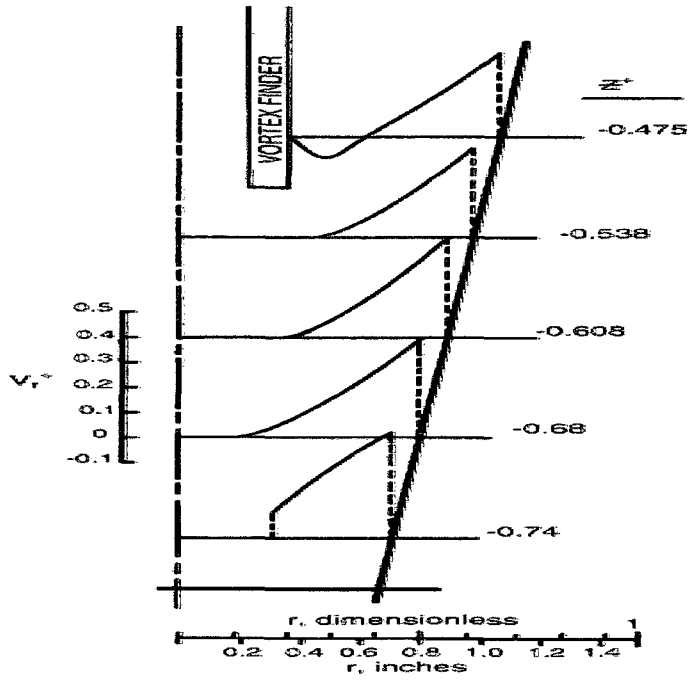

Figure 2.14 Radial velocity profiles by Kelsall (1952)

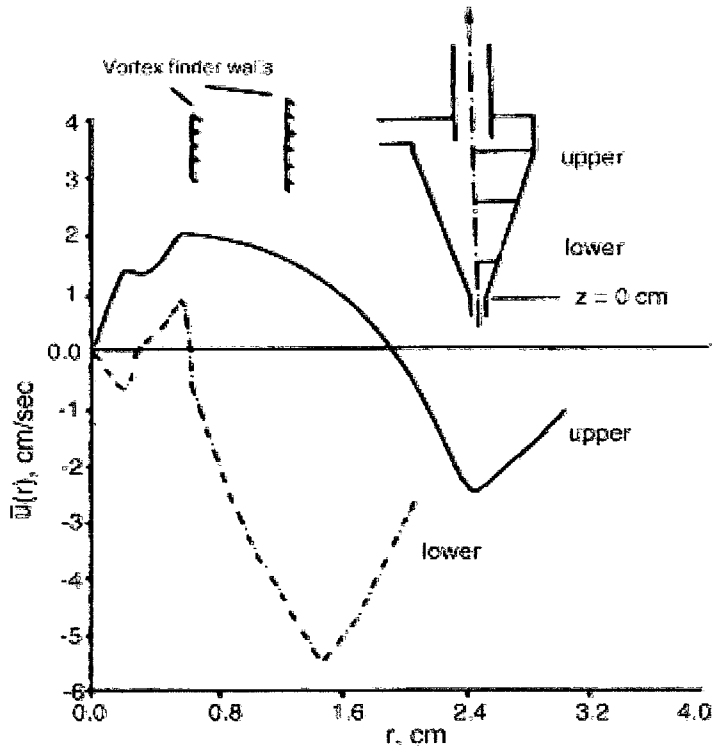

Figure 2.15 Radial velocity profiles as measured by Dabir and Petty (1986)

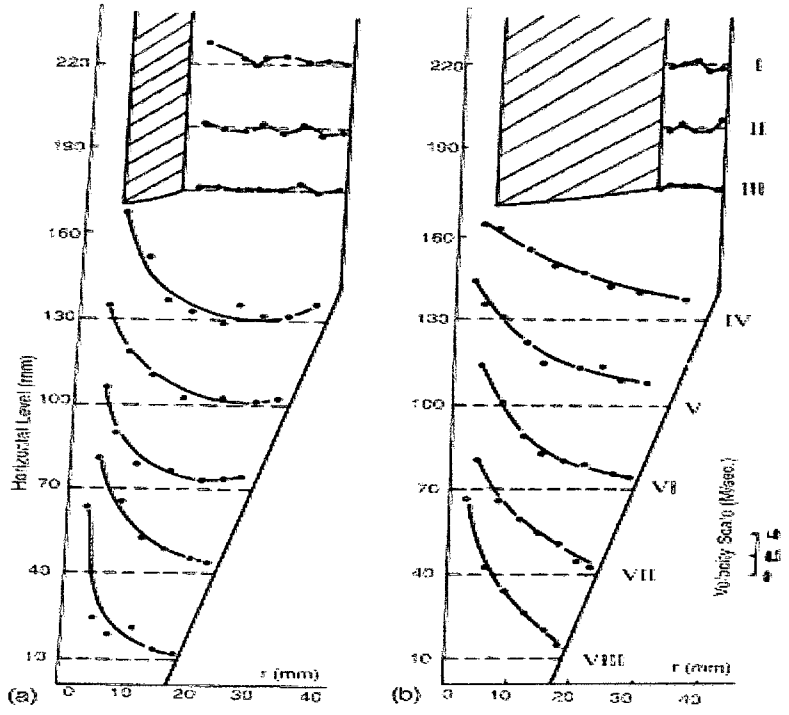

Figure 2.16 Radial velocity profiles by Luo et al. (1989). The hydrocyclone on the right side is operated without air core

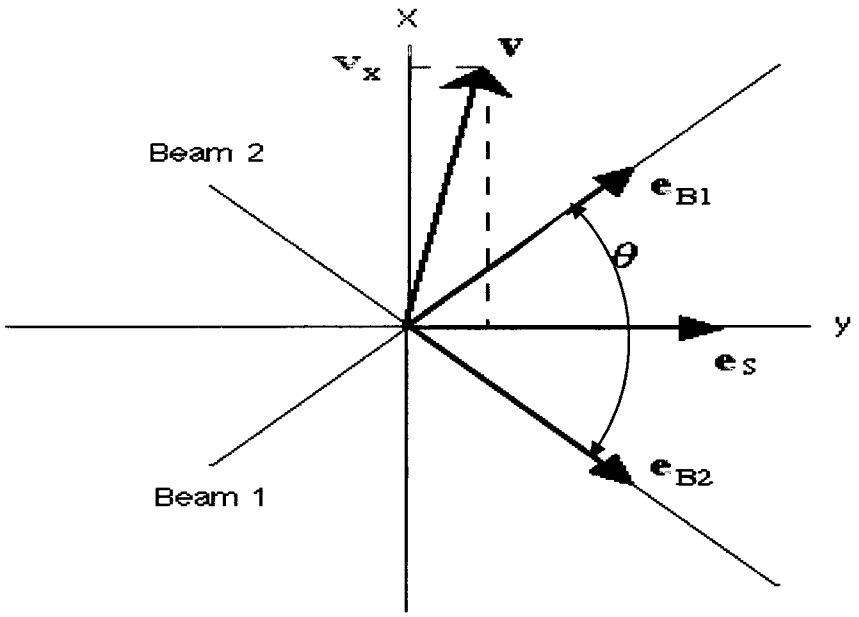

Figure 2.17 The geometry of the LDA measurement where "V" measured by Eq. 2.2

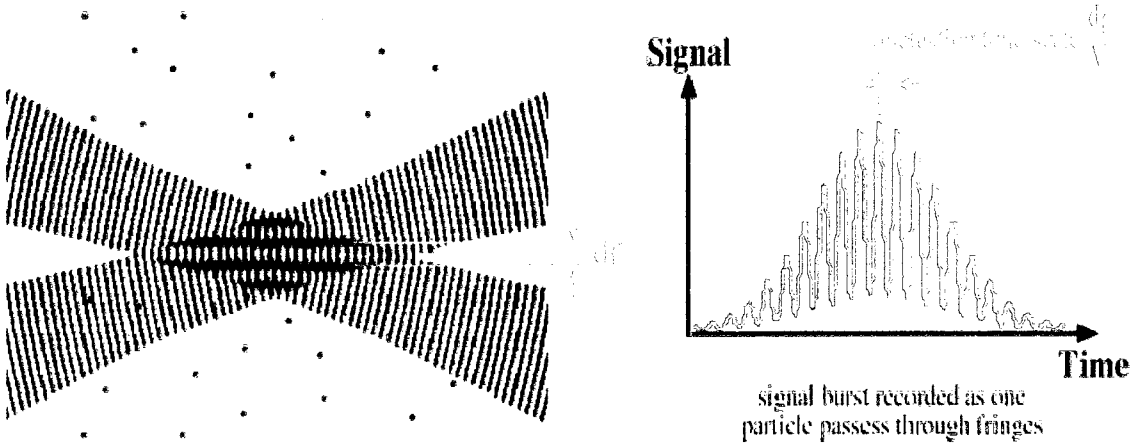

Figure 2.18 The principal theory of a Laser Doppler Anemometry (LDA) (www.dantecmt.com)

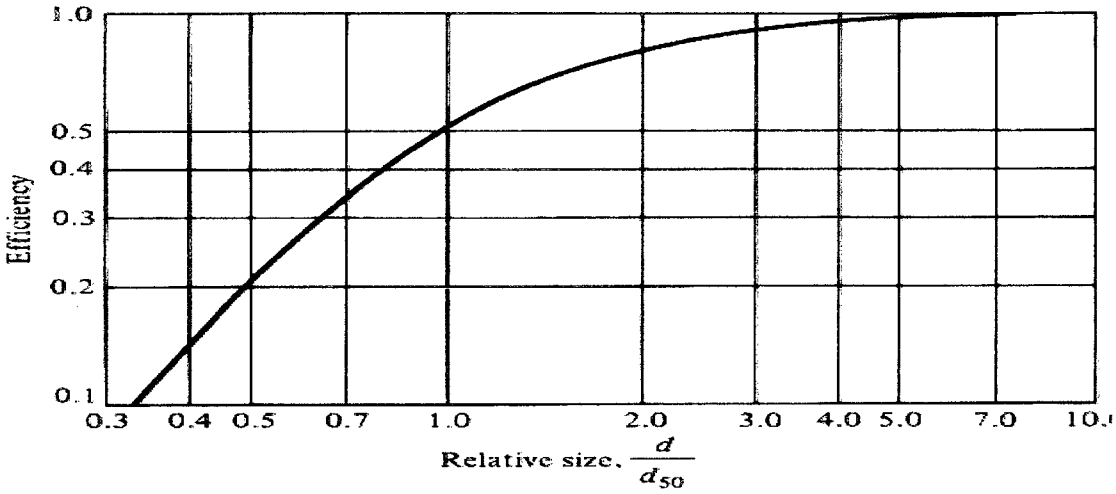

Figure 2.19 Relationship between Collection Efficiency and Particle size for Gas Cyclone by Lapple (1951)

Chapter 3

Experimental Apparatus and procedures

3.1 Flow loop

A schematic of flow loop used in this study is shown in Fig. 3.1. An over head tank (**4**) in the feed line helped to reduce pressure fluctuations and provide a low feed pressure to the system. The feed line to the hydrocyclone is 3″ in diameter and contained a single gate valve (**8**) and a pressure gauge (**7**).

The inlet valve (**8**), overflow (**9**) and underflow (**10**) outlet valves were used to adjust the flow rate, split ratio and pressure. The underflow and overflow pipes (Fig. 3.1) were connected to 60^{o} V-notch tanks (**6**) to measure the outlets flow rates.

Liquid used in the experiments was water and to generate tracer particles for the LDA measurements, latex paint particles were added to the fluid. In all the studies reported, the hydrocyclone operated without an air core, and the inlet and outlet valves were adjusted to have a steady flow inside hydrocyclone.

3.2 The Hydrocyclone

The hydrocyclone in this study was made of plexiglas it allowed complete optical access for the measurement through LDA.Figs.3.2 to 3.6 summarises the hydrocyclone dimensions and manufacturing details. The overall assembly of the hydrocyclone is given in Fig. 3.7. A transition piece of plexiglas was used to

connect the circular inlet 3" PVC pipe with the rectangular inlet section 3" x $2\frac{1}{2}$" at the hydrocyclone entry (item 12 in Fig. 3.1). A pressure gauge was installed on this transition piece, immediately before the inlet of hydrocyclone.

As seen in Fig. 3.2 and Fig. 3.7, the bottom of the inlet assembly layers was connected with the top flange of cylindrical part (H7). The inlet assembly body have an outer diameter of 11" and a 6" inner diameter, which made the width of the inlet assembly part 2.5" (63.5 mm). LDA was used to measure the mean velocity components at regions below the inlet assembly part. The first LDA data was obtained at an axial plane that was 140 mm below the roof of the hydrocyclone.

In chapter two under section 2.1 "Design of Hydrocyclone", the dimensions of cyclone and hydrocyclones were presented. Therefore, it is important to have comparisons between dimensions of the hydrocyclone used in this study and the two well-known hydrocyclone geometries designed by Rietema (1961) and Bradley (1965), besides Lapple's cyclone, (Table 3.1). The geometry of hydrocyclone used in this study looks similar to the geometry of Lapple's cyclone rather than the other well-known hydrocyclones of Rietema (1961) and Bradley (1965).

According to Svarovsky (1977), the principle is identical to gas cyclone and hydrocyclone, Svarovsky reported; "so as to have reasonably reliable designs, it is best to select a 'standard' or known design of cyclone or hydrocyclone, it could be a combination of relative geometrical proportions, even it could have a unique geometry, but the best design which gives high performance and separation efficiency".

The size of the hydrocyclone in this research, as well as the dimensions of the inlet, underflow and overflow was retained during the study. The flow was kept steady by adjusting the valves at the inlet, underflow and overflow (Fig. 3.1). Therefore, no air core exists during the data collection using LDA and flow visualization test. During the course of experiments, the flow conditions were monitored continuously, no significant changes occurred during any of the experiments, except the positions of the optical probe, as will be discussed later in Chapter 4.

3.3 Laser Doppler Anemometry (LDA)

The LDA technique permits a complete nonintrusive mapping of the flow field within hydrocyclones. The LDA used to measure the mean velocity of the liquid (water) by measuring the speed of small seed particles (latex in this study) that follow the liquid flow. The used LDA in this research was fabricated by Dantec (USA).

3.3.1 Set up of LDA

Further to the reviews stated earlier in section 2.4.3 (measurement techniques). The LDA system has a back scattered mode and comprises of the following:

1- A laser source: in this study it is an Ar-Ion laser.
2- A stand to hold the optical probe(mounted on a rail axis) and enable to control the position of the crossing point of the two laser beams (the probe volume). The stand moves the rail axis in Z (vertical) direction.
3- Fibre optics with a probe.

4- A signal processor.

5- A computer for processing and saving the data.

The probe was mounted on a traverse (rail axis) which allowed a horizontal movement (along the radius of the hydrocyclone) and it was attached to a vertical stand to allow vertical movements of probe, (Fig. 3.8 and Fig. 3.9).

The LDA probe was positioned on a specific axial station and aligned to be perpendicular to the wall of the hydrocyclone, because the curvature of the solid wall of hydrocyclone will cause an optical refraction of the laser beams. This was made many authors and researchers used a separation or protection flat box or jacket filled with water (or another liquid) surrounding the hydrocyclone to minimize the effect of beams refraction at the curved solid wall of the hydrocyclone (Dabir 1983, Dabir and Petty 1986, Chin et al. 2000, Chu et al. 2002, Fanglu et al. 1987, Peng et al. 2001).

3.3.2 Procedure of Measurements using LDA

a. It is essential at the beginning to know how much the laser beams move inside the hydrocyclone(i.e. in water) as the optical probe moves at the rail axis (in air). To clarify this point, a trial was conducted on a cylindrical pipe, identical to that erected on the hydrocyclone, and operating the LDA using the same optical probe mounted on the rail axis as stated above so as to locate the positions of crossing point (probe volume) as the probe moves in the radial direction. The result shown in Table 3.2. These position corrections are applied after completion the experiments, as will be shown later in "Characteristics of hydrocyclone flow field" (Chapter 4). It is noteworthy to mention that Dabir (1983) gave an expression that applied

to compute the position of the real probe volume as the test rig (i.e. laser optical probe) moves ,that is,

$$\Delta x = n_w \times \in / n_a$$

Where, $\in$ is the probe movement, Δx is the displacement of probe volume in water, n_w is the refractive index of water (1.33348) and n_a is the refractive index of air(1.0), therefore, when the probe moves 5 mm ($\in$) in air (Table 3.2), the probe volume moves in water by amount:

$$\Delta x = 1.33348 \times 5 \text{ mm} / 1.0 = 6.67 \text{ mm}$$

This is close to the experimental data in Table 3.2 (7 mm).

b. The mean velocity components were measured, and the axial plane measurement positions (stations) are shown in Fig. 3.10, all measurements are in millimetre. Measurements were performed at 21 different axial stations (i.e. 9 stations in the cylindrical part and 12 stations in the conical part). The first axial station (140 mm) measured from the roof of hydrocyclone. Therefore, the hydrocyclone roof is station 0.00 mm.

c. For the radial direction, the measurements covered the distance between the outside wall of the vortex finder and the inner wall of the hydrocyclone, for regions above the vortex finder, which complied with the laser beams movement as shown in Table 3.2, along the radius of the hydrocyclone. For regions below the vortex finder, the measurements covered the axial planes between the outside wall and the central axis of hydrocyclone.

d. To locate the central axis of the hydrocyclone, the following technique was followed: The probe was moved back and forth along the radius of the hydrocyclone, so as to locate the interference fringes or called a probe

volume (the crossing point of the two laser beams) close to the wall of the hydrocyclone, and observing the mean frequency or velocity on the readout display in the computer. If the crossing point is in the solid wall glass or outside the wall, the message window displays an error to acquire data, which gave an indication that the interference fringes were on the wall or outside it. So the probe moves forth to enter the crossing point immediately inside the wall. It is assumed that the velocity is zero or very small at the wall or near the wall and increases with distance (along the radius) from the wall (Wang et al., 2007). When the LDA acquired data close to the wall, it was assumed that the beam crossing point is 5 – 10 mm away from the wall. Hence, the center of the 6" hydrocyclone might be located accordingly. This location is marked as radius zero.

e. It is assumed that the inlet position is at angle zero, therefore the probe was located at 270° angle as indicated in Fig. 3.11 (Angular measuring station in the hydrocyclone).

The flow field in the hydrocyclone is an axi-symmetric flow except at the tangentially inlet side (Monredon et al. 1992, Dabir and Petty 1986, Knowles et al. 1973, Murphy et al. 2007 and Hsieh and Rajamani 1988 and 1991). In their study, Wong et al. (2007) measured the mean velocity using LDA and PIV techniques, and covered the entire diameter of the cylinder-on–cone cyclone and their research results revealed an axially symmetric flow within the cyclone used in the experiments.

The work of Martinez et al. (2008) confirmed that flow patterns in the hydrocyclone are a symmetric flow. Svarovsky (2000) defined the liquid

flow patterns in a hydrocyclone as "a circular symmetry flow, with the exception of the region and just around the tangential inlet duct".

The same assumption always made for the purpose of modelling, either by a numerical modelling or by predicts the flow field using Computational Fluid Dynamics (CFD) simulations (Cullivan et al. 2004, Sevilla and Branion 1997, Devulapalli and Rajamani 1994 and Delgadillo and Rajamani 2005).

Due to symmetry of the flow, the measurements in this investigation were conducted at an angle of 270°, where the LDA probe was placed during the experiments (Fig. 3.11).

f. In the experiments, the LDA measurements were taken with a four-beam LDA, the laser produced lights of two different colors (two green and two blue) which have wavelengths 514.5 nm and 488 nm respectively. For each measurement point, a sample of 5000 Doppler bursts was taken, and the measurement interval was 50 sec.

   The probe focal length was 399.3mm, and the used software was PDA flow and particle software 1.40 from Dantec, USA.

   The laser was an Ar-Ion A 35mW Model No. 5500 A-00.The experiments conducted on 168 points (87 points in cylindrical part and 81 points in conical part), on which the mean velocity profiles were measured.

3.3.3 Test procedure

By using LDA, two techniques were conducted to measure the mean velocity components in the hydrocyclone at the different axial stations, as stated in section 3.3.2(b) and (c) above. The techniques are summarized as follows:

Case (A): A typical probe positioned (Figs. 3.12 and 3.15) with a 90°angle between the two laser beams (green and blue) and the mean tangential velocity was measured on stations indicated in Fig. 3.10.

Case (B): The same probe was tilted by 45° (Figs. 3.13 and 3.16) and ran on the same stations and radial positions as illustrated in Fig. 3.10 and in case (A). This will be denoted as the "transform position". It is a new procedure to measure the mean velocity components (tangential and axial) in a hydrocyclone by LDA using a specific position for the optical probe (Figs. 3.13, 3.14 and Fig. 3.16) rather than using a flat box or jacket to surround the hydrocyclone as previously discussed. This will briefly discuss in Chapter 4.

3.4 Flow visualization experiment:

The purpose of this experiment is to explore the inner flow patterns in the hydrocyclone:

1- By means of droplets dye injection, as a technique to observe and clarify the features of the flow field in a hydrocyclone and motions of flow stream.
2- By examining the flow patterns, using visual and video record to observe the motion of dye droplets, the number of liquid turns could be measured.

3.4.1 Test set up and procedure:

Bradley and Pulling (1959) used radically protruding probes to inject the dye. Even though small in diameter they will still interfere with the flow by inducing secondary flow and braking the spin. To avoid this, on this investigation a small

tapping (¼") in the cylindrical section, 125 mm below the roof of hydrocyclone, was used to inject the dye from the wall, as shown in Fig. 3.17.

When the steady-state conditions were attained, by adjusting the valves at the inlet, overflow and underflow, the droplets dye were injected from the wall by a syringe. A video recording was obtained to enable on conduction of the flow visualization as stated above.

Figure Chapter 3

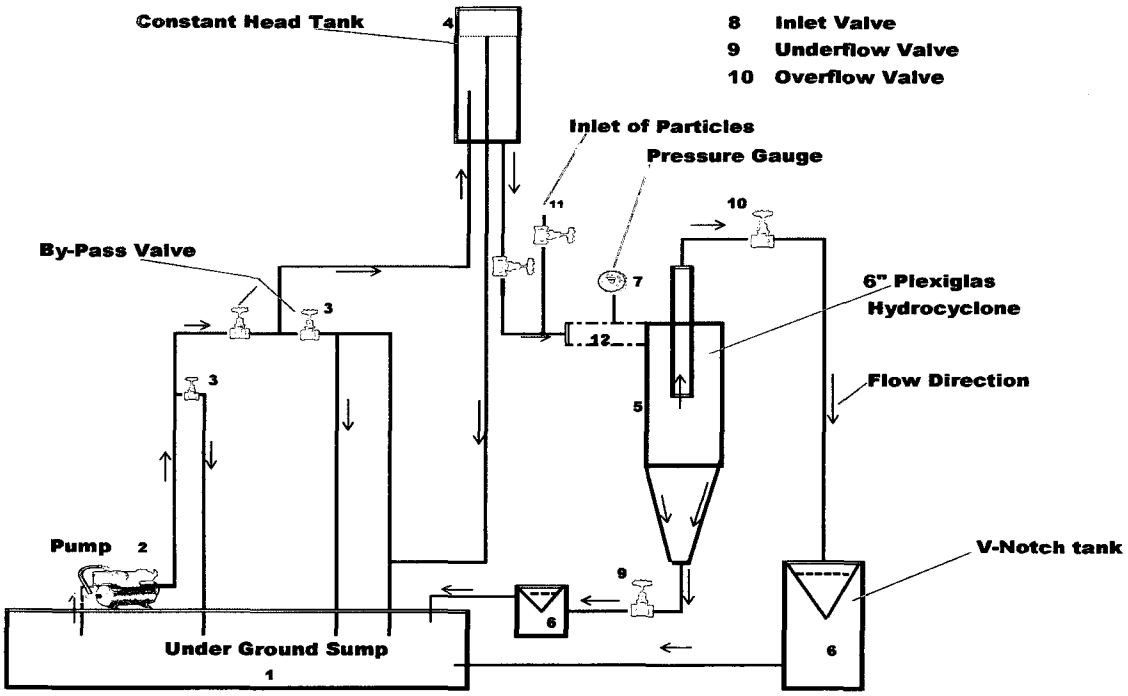

Figure 3.1

Schematic flow loops

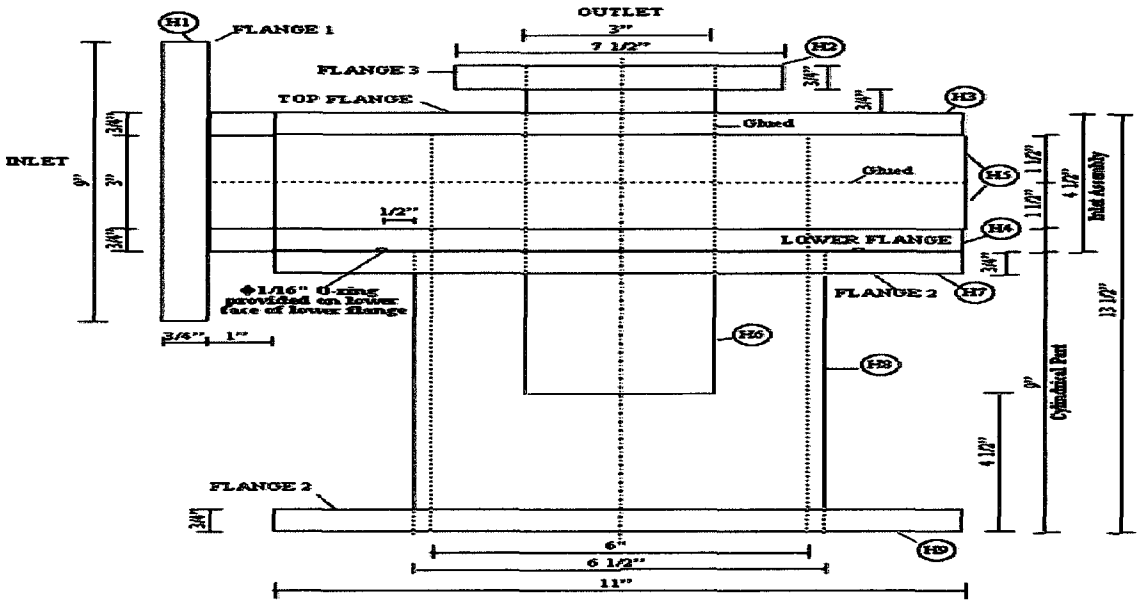

Figure 3.2 Hydrocyclone Inlet, Vortex Finder and Cylindrical section Assembly

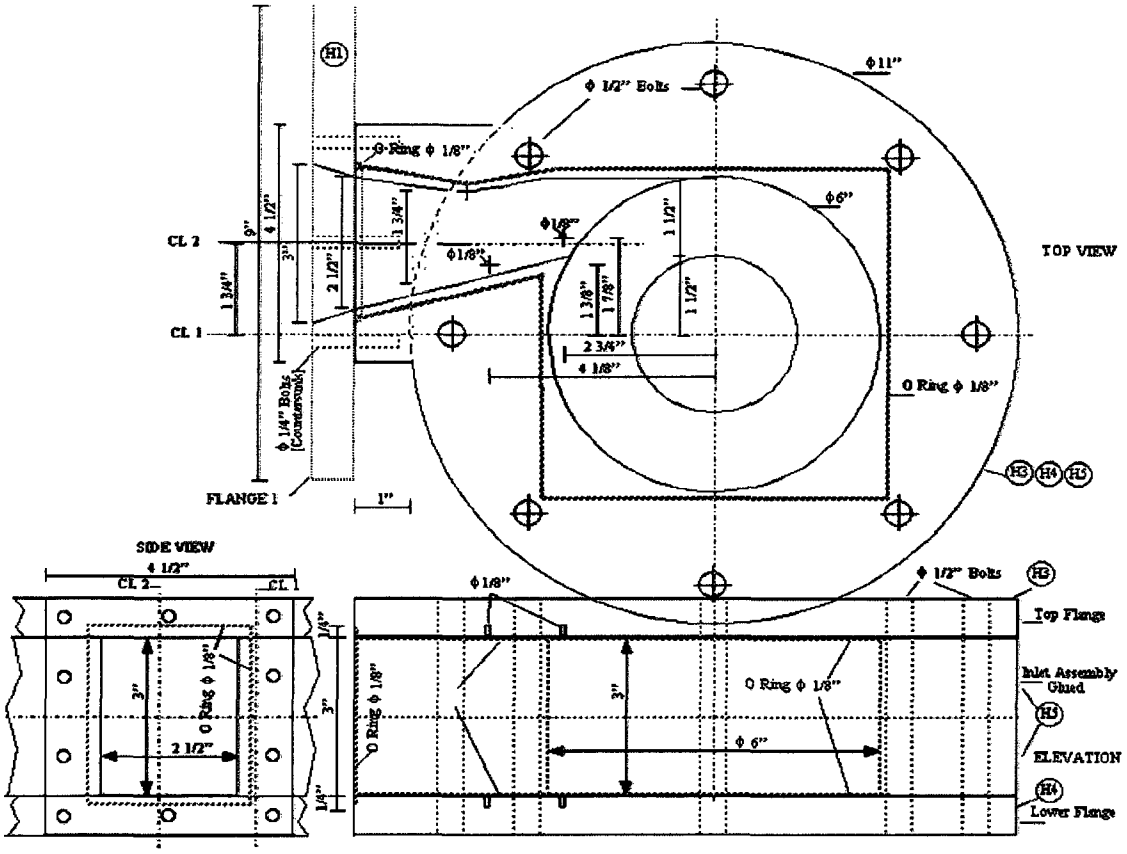

Figure 3.3 Inlet Assembly (1)

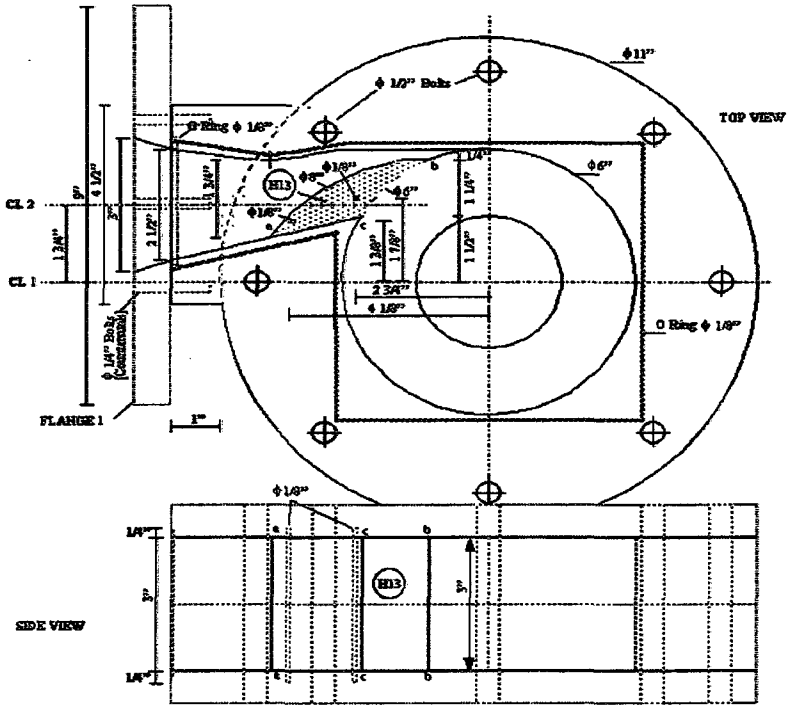

Figure 3.4 Inlet Assembly (2)

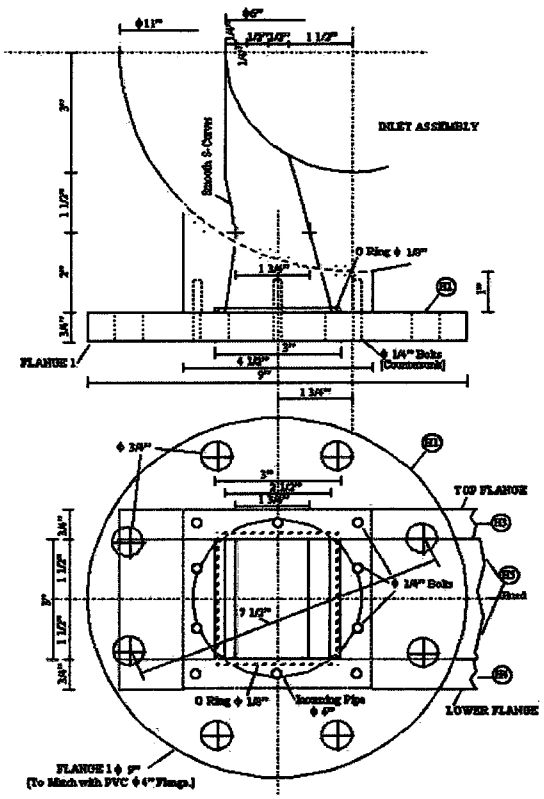

Figure 3.5 Hydrocyclone Inlet details

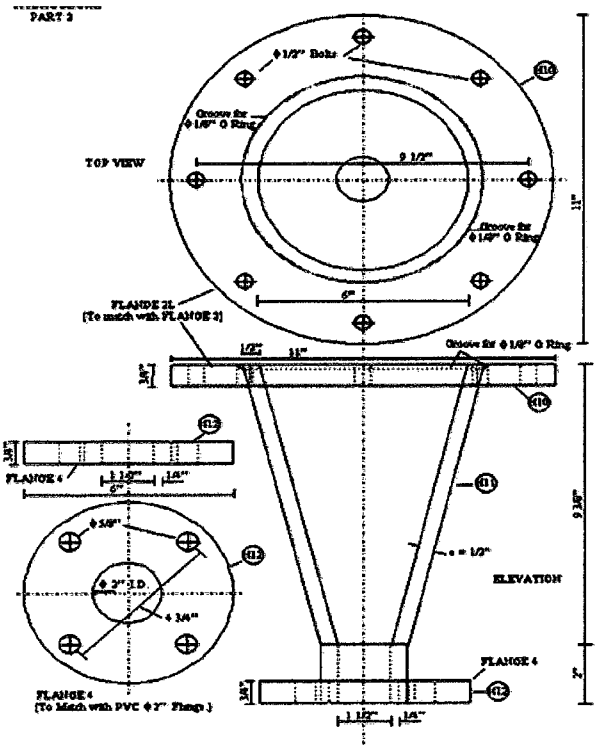

Figure 3.6 Cone Section Details

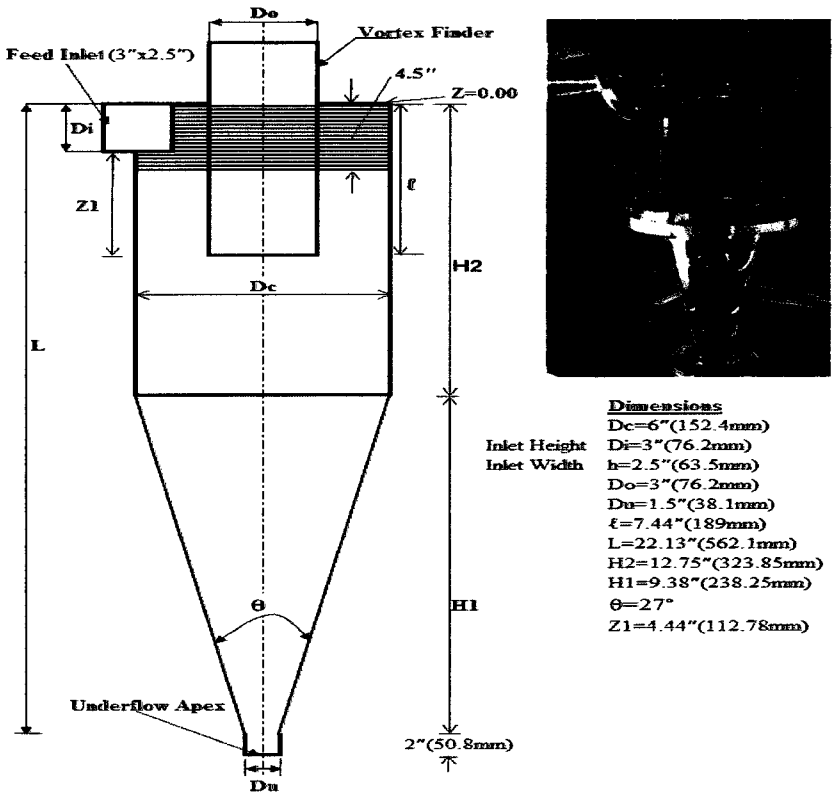

Figure 3.7 Hydrocyclone dimensions

Figure 3.8 The laser optical probe mounted on rail axis and stand (1)

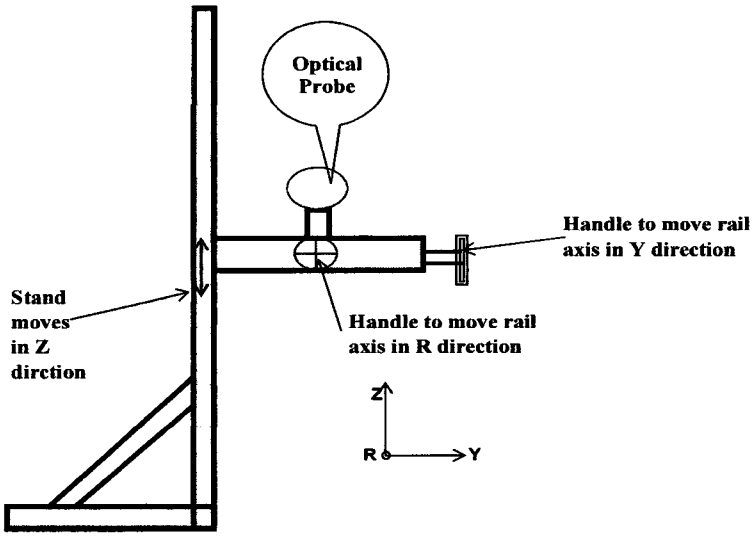

Figure 3.9 Optical probe mounted on rail axis and stand (2)

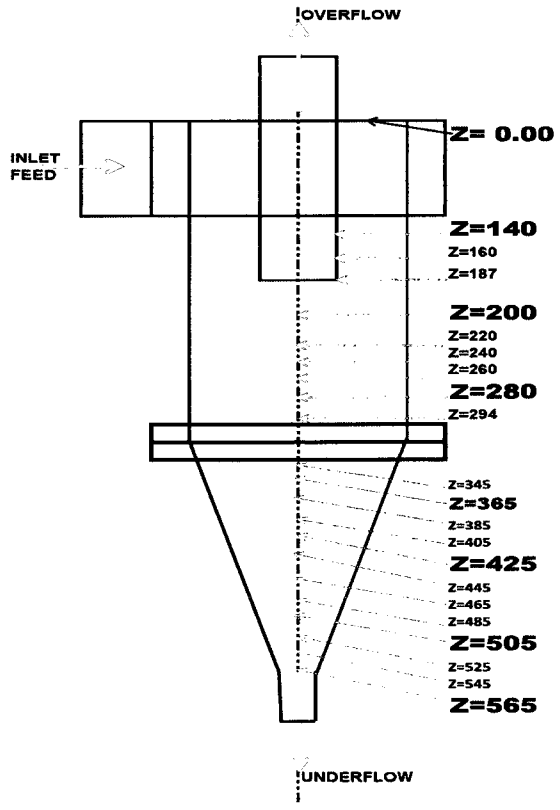

Figure 3.10 Laser Axial Stations (planes)

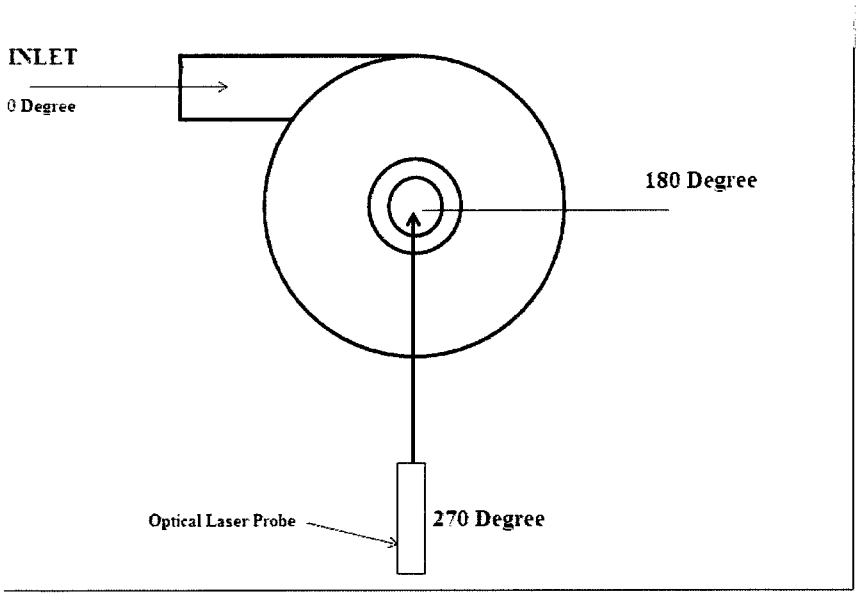

Figure 3.11: Angular measuring station in the hydrocyclone

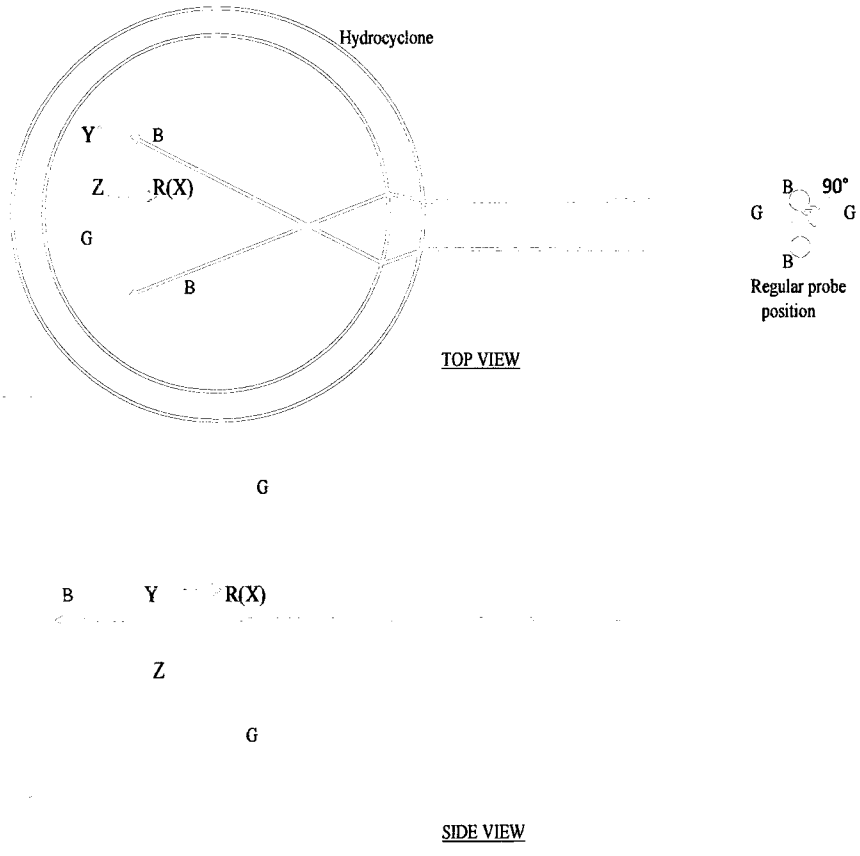

Figure 3.12 Regular LDA position, 90° angle between the laser beams (Case A)

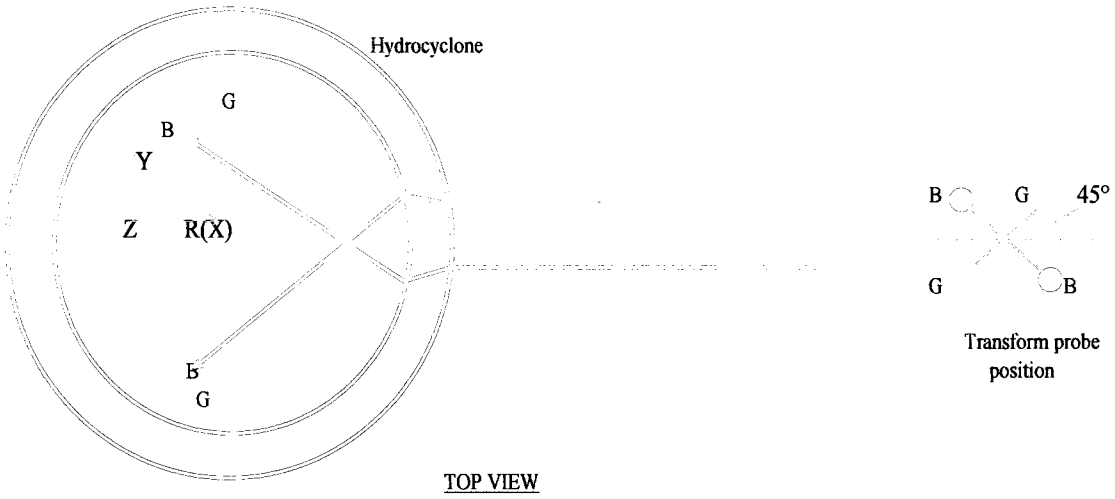

Figure 3.13 Transform position, 45° angle between the laser beams (Case B)

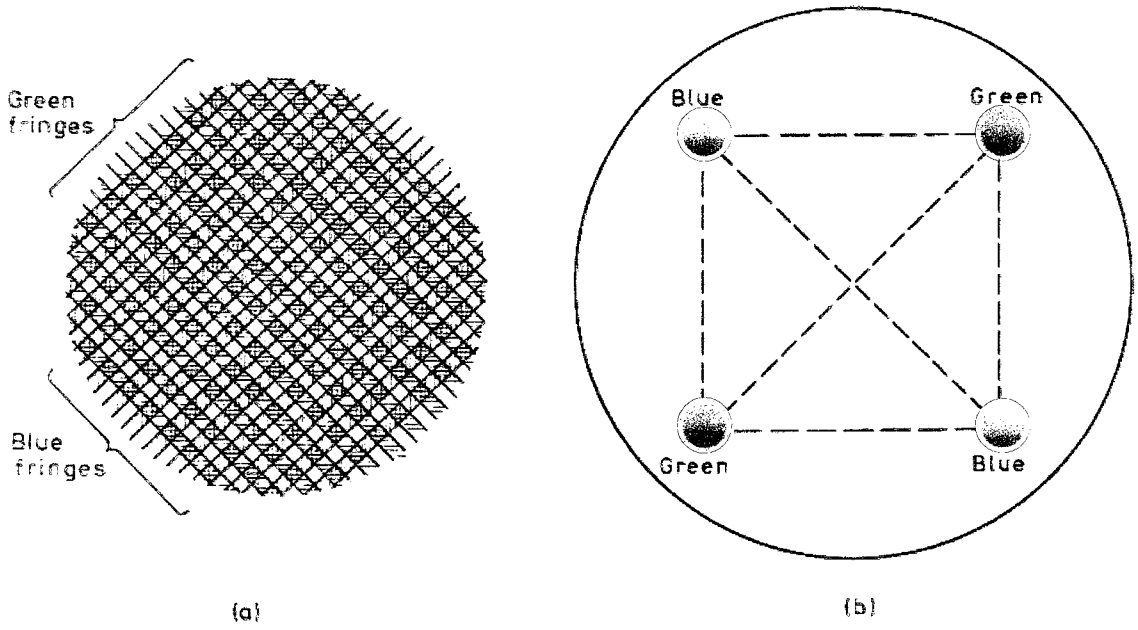

Figure 3.14 Optical probe rotates 45° in the transform position (Drain 1980)

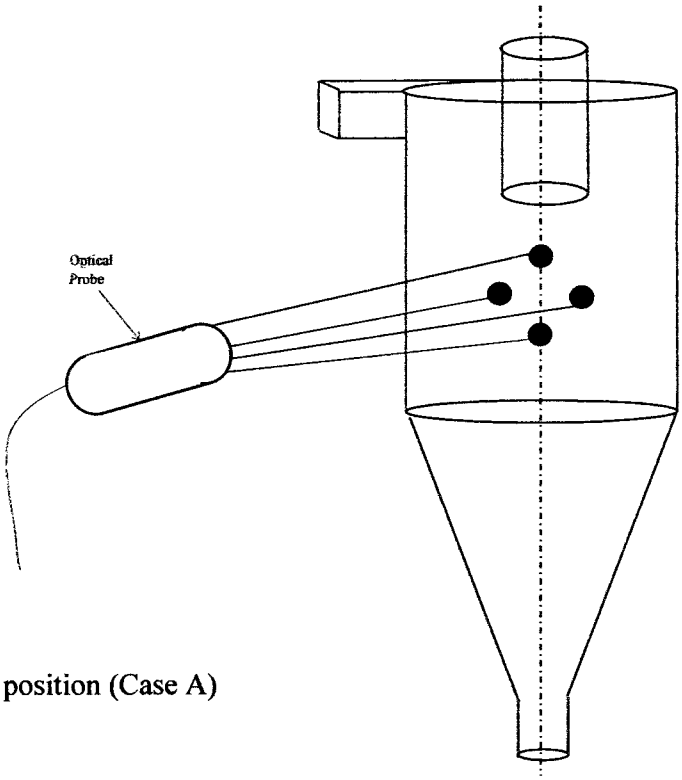

Figure 3.15 The regular probe position (Case A)

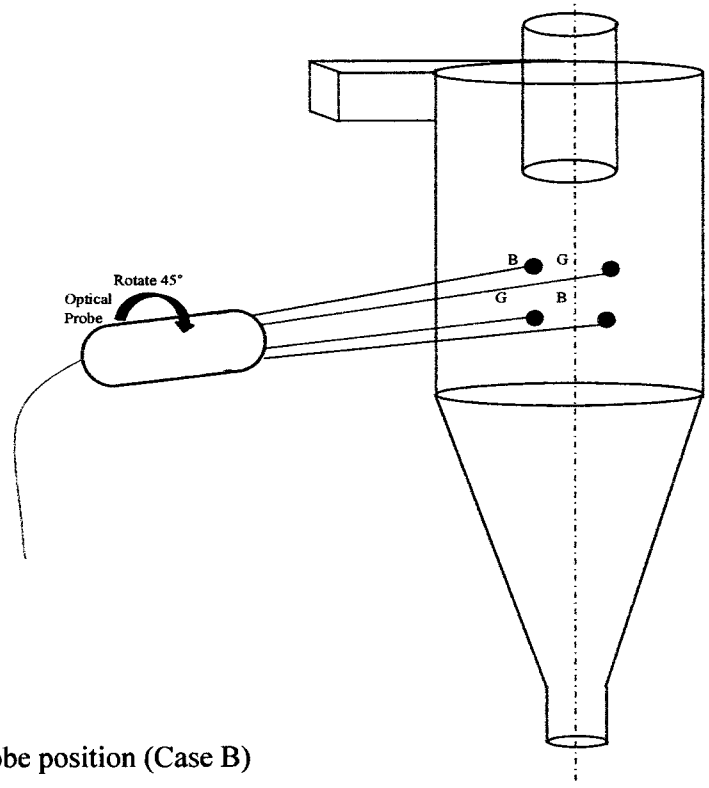

Figure 3.16 The transform probe position (Case B)

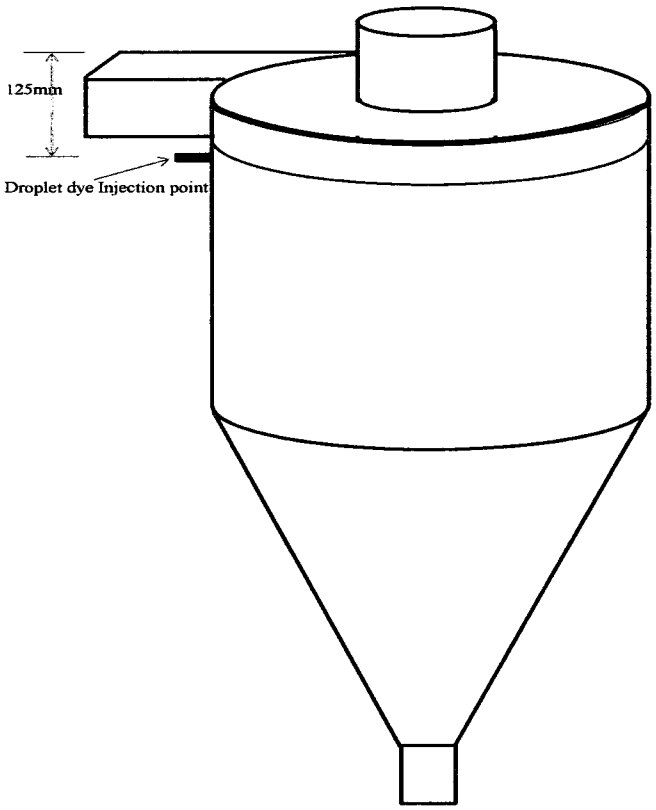

Figure 3.17 Droplet Dye injections for flow visualization experiment

Chapter 4

Characteristics of hydrocyclone flow field

4.1 Introduction

This chapter covers an analysis of the experimental results obtained to study the effects of LDA optical probe positions on the measured mean velocities in the hydrocyclone. The regular procedure to use the LDA in hydrocyclone is to encase it with a flat box or jacket filled with water or other material to reduce the effect of laser beams refraction, but in this study, the LDA used in absence of such box so as to investigate the effect of beams refraction on the measured mean velocities with two different optical probe positions.

Two sets of experiments were performed in this investigation:

1) First set where the probe was placed on a regular position, Fig. 3.12 and Fig. 3.15 (refer as regular position or Case A).
2) Second set when the same probe was tilted 45°, Fig. 3.13 and Fig. 3.16 (refer as transform position or Case B).

The mean velocities at different axial positions were measured. The main objective of these experiments is to answer the following question. What would be the result of the measured mean velocities, if the LDA was directly used in the curved solid wall of hydrocyclone? The answer to this question is provided in the subsequent sections.

4.2 Measurements of mean axial velocity V_a (Case A)

In the regular probe position (Case A) adopted traditionally (Fig. 3.12); there is in effect a position shift of the probe volume along the LDA axis due to the refraction of the laser beams. Therefore, the green and blue beams are not intersected in one crossing point along the LDA axis. This restricts one to measure only one component. Only the green beam of the argon laser (which perpendicular and parallel to the hydrocyclone axis) was used in the regular probe position (case A). It is not possible to measure both axial and tangential velocities at the same point. Therefore, only one velocity component, which is parallel to the laser beam plane (axial velocity), was measured by LDA in Case A. The results are illustrated below:

1) From Fig. 4.1 to Fig. 4.3 depict the mean axial velocity "Va" profiles were acquired at three different axial positions; 140 mm, 160 mm and 187 mm respectively, the latter axial level at the tip of vortex finder. These figures covered "Va" between the wall of vortex finder and the wall of the hydrocyclone.
2) From Fig. 4.4 to Fig. 4.9 are represented "Va" in the cylindrical part below the vortex finder and above the bottom flange of the cylindrical section.
3) From Fig. 4.10 to Fig. 4.21 covered "Va" on the conical part.
4) Tables 4.1 and 4.2 summarized the results of "Va" in Case A and tables 4.6 to 4.10 showed the LDA data.

All measurements were performed for the same flow conditions:

- Feed flow rate = 2.32x10^-3 m^3/sec (50 % reported to underflow and 50 % reported to overflow)
- Inlet pressure = 5 psi
- Water temperature 20° C - 21° C
- All measurements reported here are in lightly seeded water using Latex paint as a seeding particle

As stated earlier (Table 3.2), the crossing point of the laser beams occurred in the vicinity of hydrocyclone wall at radius 72 mm, which is 4.2 mm away from the solid wall. To confirm this result; the relationship given by Burst et al. (1981) was applied, according to Burst et al. (1981), the laser crossing position is "a function of the refractive indices of applied layers and the half-angle between the beams" page 19, which illustrated in this relationship:

$$y = [y' + d(1 - \frac{\cos\theta_a}{\sqrt{(\frac{n_g}{n_a})^2 - \sin^2\theta_a}})]\frac{1}{\cos\theta_a}\sqrt{(\frac{n_w}{n_a})^2 - \sin^2\theta_a} \qquad (4.1)$$

Here y' = 1 mm, θ_a = 2.724°, n_a = 1.0 refractive index of air, n_g = 1.5 refractive index of glass, n_w = 1.334 refractive index of water, d = 6.35 mm wall thickness, Fig. 4.24 depicts the details. The parameters y' and θ_a will be derived on next section 4.2.1a. Substituting in the relationship 4.1 gives y = 4.16 mm which indicates that the above experiment's result was correct. Also, Dabir (1983) computed the above distance to be 4.158 mm, for the case of parameters related to the present hydrocyclone using Dabir's equation (A.34).

The axial velocity profiles in Figs. 4.1 to 4.3 show direct evidence of the short circuit phenomenon. Here, the negative value indicates downward flow direction. In these three axial planes (140 mm, 160 mm and 187 mm below the hydrocyclone roof) above the bottom of vortex finder, the flow moves downward along the outer wall of the vortex finder. The positive values in the axial velocity refer to the upward flow, while the negative values refer to the downward flow, as shown in Va profiles below the vortex finder in the cylindrical part. Therefore, the locus of zero axial velocity (LZAV) shows the change in the flow directions.

Another noticeable feature in the axial velocity profiles is that the axial flow reverses along the conical part except at regions very close to the underflow (apex), as shown in the axial planes from 385 mm to 505 mm below the hydrocyclone roof (Figs. 4.12 to 4.18). It is obvious that more fluid reverses its direction in this region. It is noteworthy that there is a consistent lateral shift of the locus of zero axial velocity (LZAV) toward the centre axis below the vortex finder until the region of reversal flow.

Figs. 4.9 to 4.11 show the axial velocity profiles at the axial planes 294 mm, 345 mm and 365 mm, these profiles displayed a W-shaped distribution which reflects the fluctuating of axial velocity in this region, at top of the conical part, where the reversal flow presented. The axial velocity profiles below the vortex finder rising markedly near the central axis of hydrocyclone, which indicated an upwards flow exists in this area.

The measured axial velocity component obtained in this experiment, using LDA, were found similar in line with the experimental results of other authors who used the LDA to measure the mean velocities inside hydrocyclones, with some

discrepancies in magnitude depending on the experimental operating conditions and the hydrocyclone parameters (Chine and Concha 2000, Dabir 1983, Dabir and Petty 1986).

The flow patterns in a hydrocyclone are highly complex and any change in the geometry will consequently change the flow patterns, thus affecting the velocity profiles. According to Svarovsky (2000) "it may be incorrect to assume that precisely similar profiles occur in the cyclones with a considerably different geometry, so the velocity profiles in a hydrocyclone is only qualitative".

4.3 Measurements of mean velocities (Transform position/ Case B)

The experiments were conducted in order to investigate the effect of rotating the probe by 45° angle (Fig. 3.16) on measuring the mean velocities in a 6" hydrocyclone. The solid wall curvature of the hydrocyclone is taken into account to calculate precisely the optical trajectories of the laser beams and to locate the intersect point at the right place knowing the different refractive indices of air, glass and water. Before presenting the results of measured mean velocities using this method, it is important to compute the refracted angles in both cases and to know its effect on measuring the mean velocities.

According to Dabir (1983), the half angle of intersecting two laser beams (Θ_w) must be determined theoretically by using principles of geometric optics (Snell's Law) and trigonometry (Fig. 3.13). Dabir (1983) had used LDA to measure the mean velocities in a 3" hydrocyclone that satisfies the original design criteria of Rietema (1961). To reduce curvature effects he surrounded the hydrocyclone with a plexiglas box having flat surfaces and filled the space between the hydrocyclone

and the box by glycerol (index of refraction ≅ 1.46) and he chose the hydrocyclone made from pyrex (index of refraction ≅ 1.50 which is the same of water). Dabir (1983) had conducted brief computations to study the effects of refraction indices on the measured mean velocity by LDA. The difference between Dabir study and this research is that the LDA in the presented study was used without any flat box or jacket to encase the hydrocyclone, which was the case in Dabir's (1983) study. The effects of refraction indices were addressed in this study. Although the approaching to analyze the refraction effects is different in both studies but the ideas are the same, therefore, the present computations will be regularly compared with that conducted by Dabir (1983).

4.3.1 Refracted angles of laser beams in case A (Fig. 3.12)

According to the law of refraction the light beam is widened when it enters an optically dense medium (Durst et al. 1977, and Drain 1974). Fig. 4.22 depicts the path of the two laser beams which penetrates the glass layer and is refracted at the interface due to the different refractive indices of the layers, e.g. air and glass, glass and water. The angles in the figure have all been exaggerated for clarity.

The refractive indices n_{air}, n_{glass}, and n_{water} are:

$n_{air} = n_a \approx 1.0$, $n_{glass} = n_g = 1.5$, and $n_{water} = n_w = 1.33348$

According to Snell's Law, the relationship between the incident and refracted beam (Durrani et al. 1977, Durst et al. 1981 and Hecht et al. 1974) as below

$$n_a \times \sin \theta_a = n_g \times \sin \theta_g \qquad (4.2)$$

Also, $n_g \times \sin\theta_g = n_w \times \sin\theta_w$ (4.3)

Hence, $n_a \times \sin\theta_a = n_w \times \sin\theta_w$ (4.4)

Thus, the angle variation between any two layers is only a function of their relative refractive indices (n_a / n_w) and not dependent on the optical properties between them (Durst et al. 1981). This applied only on the regular probe position (case A), where the laser beams (green) is perpendicular to the solid wall and parallel to the hydrocyclone axis.

The focal length of the probe is 399.3 mm and the probe lens's width is 38 mm, which gives (Fig. 4.24):

$$\theta_a = \tan^{-1}\frac{19}{399.3} = 2.724°$$

Therefore, Eq. 4.4 may be rewritten to give:

$$1.0 \times \sin 2.724 = 1.334 \times \sin \Theta_w$$

Thus, $\theta_w = 2.04°$ (4.5)

Dabir (1983) gave an equation to compute this angle based on Snell's Law, that is,

$$\theta_w = n_a x / \theta_a \; n_w$$

Which gives the same result, $\theta_w = 2.04°$, for the case of parameters related to the present hydrocyclone using Dabir's equation

In Fig. 4.24:

$\cos \theta_a = \frac{y'}{OD} = 0.9989 = 1.0$ and ON $= \sqrt{399.3^2 + 19^2} = 399.75$mm

$$\frac{y'}{1} = \frac{399.75}{399.3} = 0.9989 = 1$$

Thus y' = 1.0 mm, is the focal point of laser beams (point "O" in Fig. 4.24) in case of ignoring the effects of the refractive indices for air, glass and water. As shown in Fig. 2.24 the differences in the index of refraction between the layers (air-glass and glass-water) cause the two refracted beams to intersect at point "A" rather than the focal point "O". To eliminate the effect of such beams refraction, the indices of refraction of the layers should be same, so the intersect point matching the focal point.

4.3.2: Refracted angles of laser beams in case B (Fig. 3.13)

Fig. 3.14 by Drain (1980) illustrates the position of rotated optical probe and the anticipated fringe shape (a). Fig. 4.23 and Fig. 4.24 depict the refracted laser beams inside the hydrocyclone in case B, the transform position. In LDA the laser beams spacing between the same colors is 40 mm and 20 mm between the green and blue colors (Fig. 4.25). The angles in the figures have all been exaggerated for clarity.

In Eq. 4.2 $n_a \times \sin \theta_a = n_g \times \sin \theta_{g_1}$

$$1.0 \times \sin 2.724° = 1.5 \times \sin \theta_{g_1} \text{ then } \theta_{g_1} = 1.816°$$

Fig. 4.25 illustrates, by scale, the laser beams trajectories, the laser route from "C" to "B" moves in two directions and the angle θ_{g_2} measure to be:

$$\theta_{g_2} = 2.003°$$

In Eq. 4.3 $n_g \text{ x } \sin \theta_{g_2} = n_w \text{ x } \sin \frac{y'}{1}$

$$1.5 \text{ x } \sin 2.003° = 1.334 \text{ x } \sin \theta_w$$

Hence, $\theta_w = 2.253°$ (4.6)

Dabir (1983) used a different approach to compute the above angle θ_w. This approach also depends on principles of geometric optics (Snell's Law) and trigonometry. For this, one gets $\theta_w = 2.256°$, for the case of parameters related to the present hydrocyclone using Dabir's equations (A.42 and A.47).

For LDA, Dantec devotes Eq. 2.2 to theoretically compute the magnitude of the velocity of particles, it is important to calculate the fringe spacing (the interference fringes are formed when the two laser beams intersect) from the formula:

Fringe spacing: $$\delta = \frac{\lambda}{2 \sin \frac{\theta}{2}}$$ (4.7)

Thus, the velocity of particles is:

$$V = \delta \text{ x } f_d$$ (4.8)

Here, λ = 514.5 nm = 514.5x10^-9 m (green) and 488 nm = 488x10^-9 m (blue), $\theta = 2\theta_w$ and f_d = 40 MHz = 40x10^6 s^{-1}

For regular probe position (case A):

λ = 514.5 nm = 514.5x10^-9 m (green), θ_w = 2.04°

Hence, fringe spacing δ is 7.23x10^-06 m, which gives V_a = 289.07 m/s.

For case B, the probe tilted 45°:

λ = 514.5 nm = 514.5x10^-9 m (green) and 488 nm = 488x10^-9 m (blue), θ_w = 2.253°

Therefore, fringe spacing δ is 6.54x10^-06 m and 6.21x10^-06 m for green and blue respectively. Therefore, V_a = 261.75 m/s and V_θ = 248.27 m/s respectively.

Therefore, as the angle between the two green laser beams increases 10.44 % the particle velocity inside the hydrocyclone decreases 10.42 % (green, V_a). The measured velocity of the particle is the velocity component normal to the fringe pattern, not the actual velocity, because the particle diameter may be very small, as the wavelength of the laser light, so the particles have approximately the same local velocity as the flow medium.

4.4 Experimental results in case B

The experiments conducted in case B proved that it is possible to measure both the axial and the tangential velocities at the same point since the intersecting point (the crossing point of the two green and blue colors) is the same. Therefore, two velocity components measured by the LDA in this case, the tangential and the axial velocities. The results are illustrated below:

a. Figs. 4.26 to 4.28 show the profiles of the mean tangential velocity Vθ at three different axial positions above the bottom of vortex finder. The locations were 140 mm, 160 mm and 187 mm respectively.
b. Figs. 4.29 to 4.34 show the variation of Vθ in the cylindrical part of the flow field that is below the vortex finder.
c. Figs. 4.35 to 4.46 cover the Vθ data in the conical part.
d. Figs. 4.47 to 4.49 show the axial velocity V_a data above the vortex finder at three axial levels, 140 mm, 160 mm and 187 mm respectively. These are the same radial positions in Case A that covered Va between the wall of vortex finder and the wall of the hydrocyclone.
e. Figs. 4.50 to 4.55 illustrate the axial velocity V_a data at the cylindrical part below the vortex finder.
f. Figs. 4.56 to 4.67 depict the axial velocity at the conical part.
g. Tables 4.3, 4.4 and 4.5 summarized the results of Vθ and V_a for case B (tables 4.11 to 4.15 show the LDA data).

The feed flow rate and inlet pressure were kept same, as in case A, to compare the effects of probe positions in the measured mean velocity components, while all parameters have been same, including the geometrical parameters of hydrocyclone.

It is clear from the figures that "Vθ" increased from the hydrocyclone wall towards the centre, reached a maximum value and then rapidly decreased. At horizontal levels above the bottom of the vortex finder, the tangential velocity increases from the hydrocyclone wall towards the outside wall of the vortex finder, reaches a maximum near the wall and then decreases quickly as the vortex finder wall is approached.

At horizontal levels below the bottom of the vortex finder, V_θ increases from the wall towards the centre of the hydrocyclone, reached a maximum value at a radius of 25 mm approximately equal to Rc / 3 (Rc is the radius of hydrocyclone; 76.2 mm) and decreases rapidly as the centre is approached. The same shape of V_θ continued at the conical section. V_θ increases downward reaching the maximum near the apex outlet.

These velocity profiles (V_θ) are similar to previous experimental studies of Wong et al 2007 (Fig. 2.10), Knowles et al. 1973 (Fig. 2.8), Dai et al. 1999 (Fig. 4.22) and Rajamani et al. 1992 (Fig. 4.23), which are closed to the typical shape of V_θ in literatures.

A net increase in the tangential velocities in the cylindrical part as well as in the conical part was observed and the magnitude of the tangential velocity decreases

with the radius.. The forced vortex can be seen in the central region and the free vortex prevails thereafter. Below the vortex finder, envelopes of constant tangential velocity profiles were observed, the gradient of the forced vortex in the conical part was nearly the same as in the cylindrical part.

A noticeable feature of both experimental cases (A and B) is that, the both axial velocity profiles are quite similar at different depths. However, the axial velocity components in case B must be corrected for index of refraction effects (Tables 4.3 to 4.5). Therefore, the magnitudes of V_a were increased by amount 10.42%. Figs. 4.68 to 4.88 illustrate the comparisons of axial velocity profiles between regular and transform (the probe tilted 45°) positions of the optical probe and the corrected profiles. The comparison shows reasonably good agreement as can be seen in these figures, it is noticed that Va values in regular case are always greater than that in the transform case (case B). Near the central axis of the hydrocyclone, the values of Va seem approximately same because they have small magnitudes. Both experiments show the same trends, for Va, and significant degrees of asymmetry, but Va values in case "B" have less values than in case A between 8 % to 11 % which abiding with the previous calculations of the optical and particle velocity(Eq. 4.13). The fact that the shape of Va velocity profiles are nearly identical throughout the cylindrical and conical parts, further confirms this point of view.

It is obviously clear that the corrections of the axial velocity profiles (Figs. 4.68 to 4.88) due to refraction phenomena produced symmetrical values closed to the measured Va in case A (regular position of the optical probe) which indicate that the applied corrections are correct. The tangential velocity in case B are not

corrected because there are no data obtained in case A for this velocity as discussed earlier, so to correct the tangential velocity in case B it should be compared with Va data that collected in a regular position of the optical probe, which only be done by immersed the hydrocyclone in a flat box or jacket filled with water or other suitable material, which is the traditional method when using the LDA in a hydrocyclone.

As elaborated earlier, and contrary to regular case A, the tangential velocity Vθ was measured by LDA in case B only. Here, the position of the tilted probe enables one to have the crossing point of the two laser beams at the same point. Therefore, the axial and the tangential velocities could be measured at the same location.

4.4.1 Turbulent intensity

In the transform position, the fluctuations of two mean velocity components can be measured at the same point. Using the LDA data in case B, the root mean square (RMS) values give the fluctuations of mean velocities (axial and tangential), the turbulence intensity can be calculated as shown in Fig. 4.89 and table 4.16. This profile represents the axial plane Z=280 mm below the roof of the hydrocyclone. It is choose, as an example, for an axial plane among the recirculation zone. The turbulent intensity profile illustrated in Fig. 4.89 shows that the intensity of fluctuations are greater near the hydrocyclone wall and near the central axis. It is obvious from the profile in Fig. 4.89 that the zero axial velocity is characterised by a higher turbulence, where the flow changes its direction.

The applied equations are:

$$\text{I: Turbulent Intensity (\%)} = u' / v \qquad (4.9)$$

Here, v is the mean axial velocity in the hydrocyclone = $4Q / (\pi Dc^2)$ = 0.127 m/s, and

u′ is the root-mean-square of the turbulent velocity fluctuations = $\sqrt{\frac{2}{3}K}$

k : is the turbulent energy (m^2 / s^2) which is given in the expression:

$$k = \frac{1}{2}(\overline{V_\theta'^2} + \overline{V_a'^2} + \overline{V_r'^2}) \qquad (4.10)$$

where, V_θ' and V_a' are given in table 4.16 and Vr′ is very small and not measured, therefore it is neglected.

This result for the turbulent intensity is in good agreement with the findings of Chine and Concha (2000) and Solero and Coghe (2002). In same procedure the turbulent intensity can be drawn for the other axial planes within the hydrocyclone using the LDA data obtained in the transform position of the optical probe.

4.5 Conclusion of the probe position experiments

In their experiments, while using LDA or LDV to measure the mean velocities inside hydrocyclones, other investigators used to immersed a hydrocyclone in a water-filled (or other materials as glycerine) flat surface jacket made of transparent glass to minimize the optical refraction of the laser beams (Hsieh and Rajamani 1988 and 1991, Devulapalli and Rajamani 1994, Dabir 1983, Dabir and Petty 1986, Chine and Concha 2000). Dabir (1983) suggested that the experimental test section might be designed to eliminate the refraction phenomenon, to achieve that, he recommended matching the refractive index of the test fluid and the glass walls of the hydrocyclone, which make easy for LDA to directly measure the mean velocities. According to Drain (1980) this in not

feasible if large quantities of fluid are involved and so the practical use of the index matching principle is limited.

By using LDA, the present study conducted to measure the mean velocities in 6″ hydrocyclone, in absence of any flat surface box or jacket that encase the hydrocyclone, to study the effects of optical refraction of the laser beams on the measured mean velocities. Two positions of the optical probe were used. One was a regular position with 90° angle between the two probe beams and the other position when the same optical probe was tilted 45°. From the discussion and results presented earlier, it is found that the half-angle (θ_w) of the intersecting of the two laser beams inside hydrocyclone, besides the refraction indices of phases (air, glass and water) have the major effects in the computed mean velocities inside a hydrocyclone, as the half-angle between these two intersecting beams increases, the measured particle velocity inside the hydrocyclone decreases nearly in the same amount. The regular probe position enables to measure only the axial velocity component (which is parallel to the beam plane) because the crossing points (the intersecting point of the two LDA laser beams) are not the same. Meanwhile, the second probe position in case B (where the probe tilted 45°) made the two beams intersecting at the same point, which enable to measure the tangential and axial velocity components. The axial velocity V_a profiles obtained in case B can be corrected by applying the foregoing results, in which, the curvature of the hydrocyclone wall together with the differences in the indices of refraction, are considered the major factors in computing the corrections amount.

The conclusion developed from these experiments has revealed that LDA is able to directly measure two mean velocities simultaneously at the same point in the

hydrocyclone depends on the position of the optical probe. When the probe is placed to have an angle of 90° between the two different colors of laser beams, the LDA will measure the mean axial velocity using the green laser beams (LDA set to have one component) which are perpendicular on the solid wall (parallel to the hydrocyclone axis) and ignoring the horizontal laser beams that penetrate on the side walls. As the optical probe is tilted 45°, the LDA acquired the capability to measure two mean velocity components (axial and tangential). The magnitude of measured mean velocities is less than that measured in the probe regular position depends on the half-angle between the intersecting laser beams inside hydrocyclone. As a general role, as the half-angle between the two intersecting laser beams increases, the measured mean velocity inside the hydrocyclone decreases nearly in the same amount, therefore, the corrections for the magnitude of mean velocity components may be done accordingly.

The experiment study supports the view that the measured velocity profiles offer some qualitative observations. Despite the refraction of the laser beams on the solid curved wall of a hydrocyclone; it is possible to measure accurately the mean velocities as the half-angle between the crossing beams is known and the optical probe positioned properly, thus, the velocity components can be corrected accordingly.

Figures Chapter 4

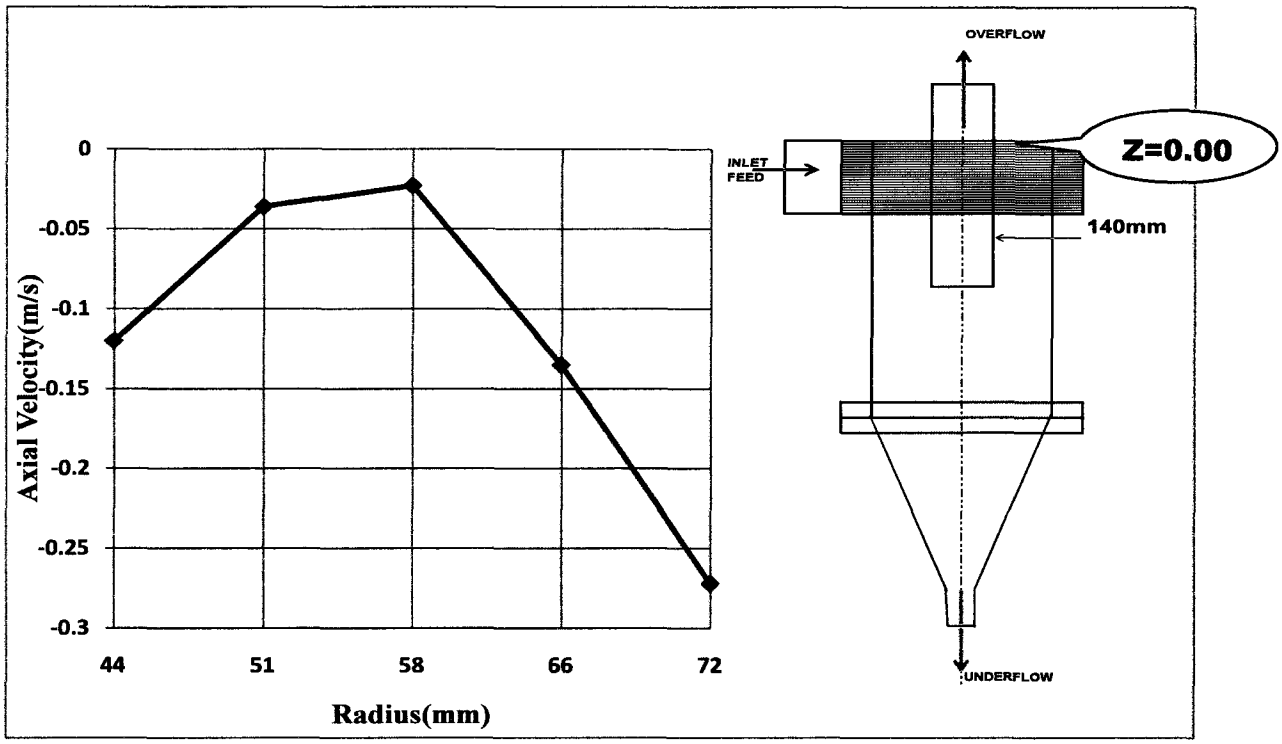

Figure 4.1 Axial velocity profile at Z=140mm (regular probe position)

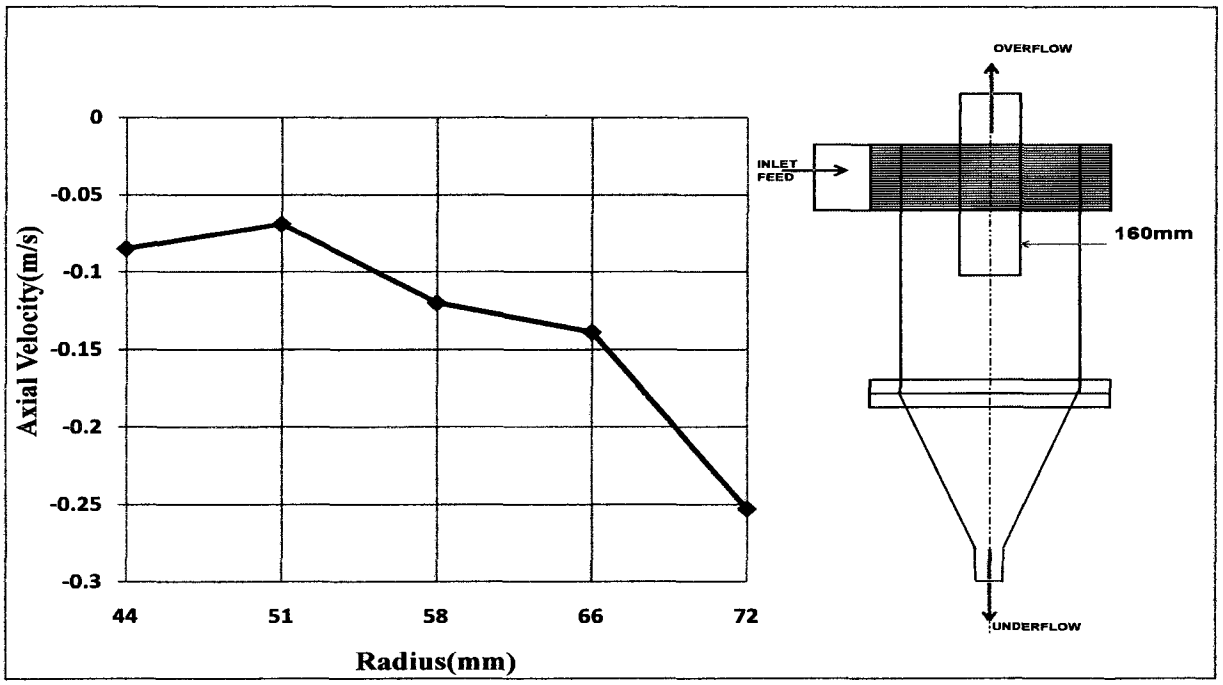

Figure 4.2 Axial velocity profile at Z= 160 mm (regular probe position)

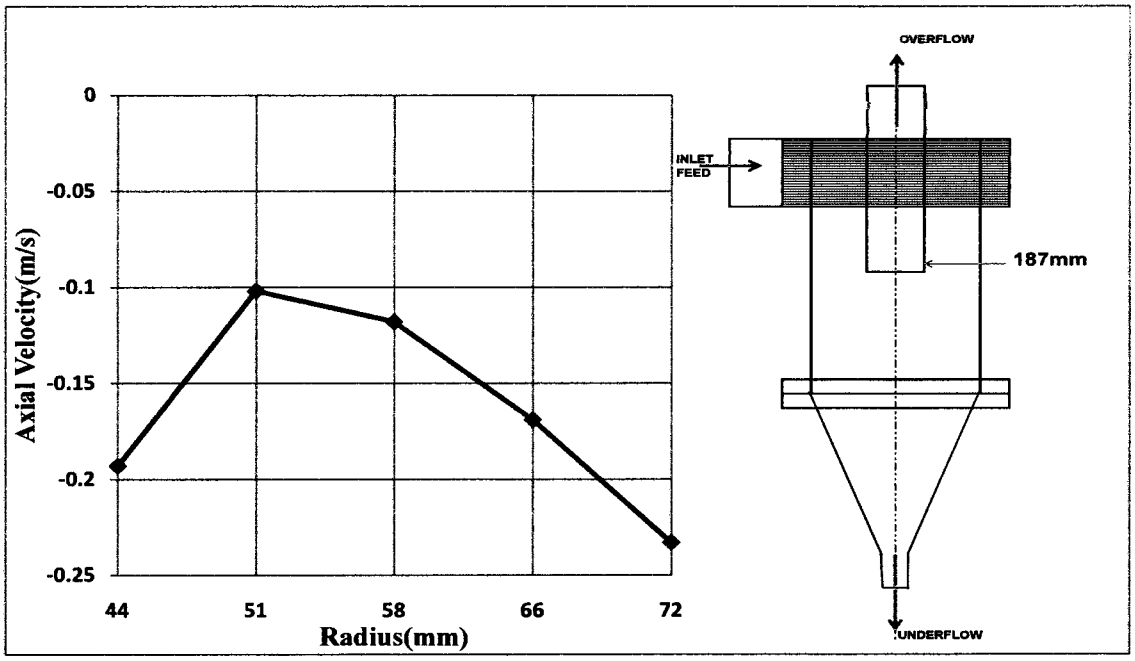

Figure 4.3 Axial velocity profiles at Z= 187mm (regular probe position)

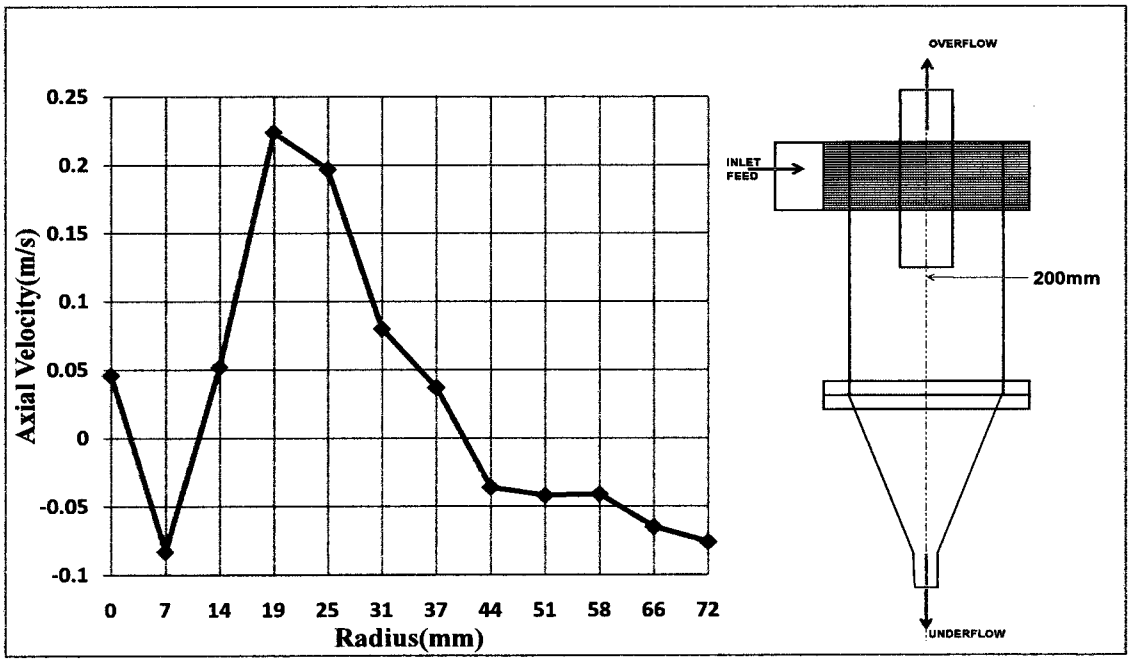

Figure 4.4 Axial velocity profiles at Z=200mm (regular probe position)

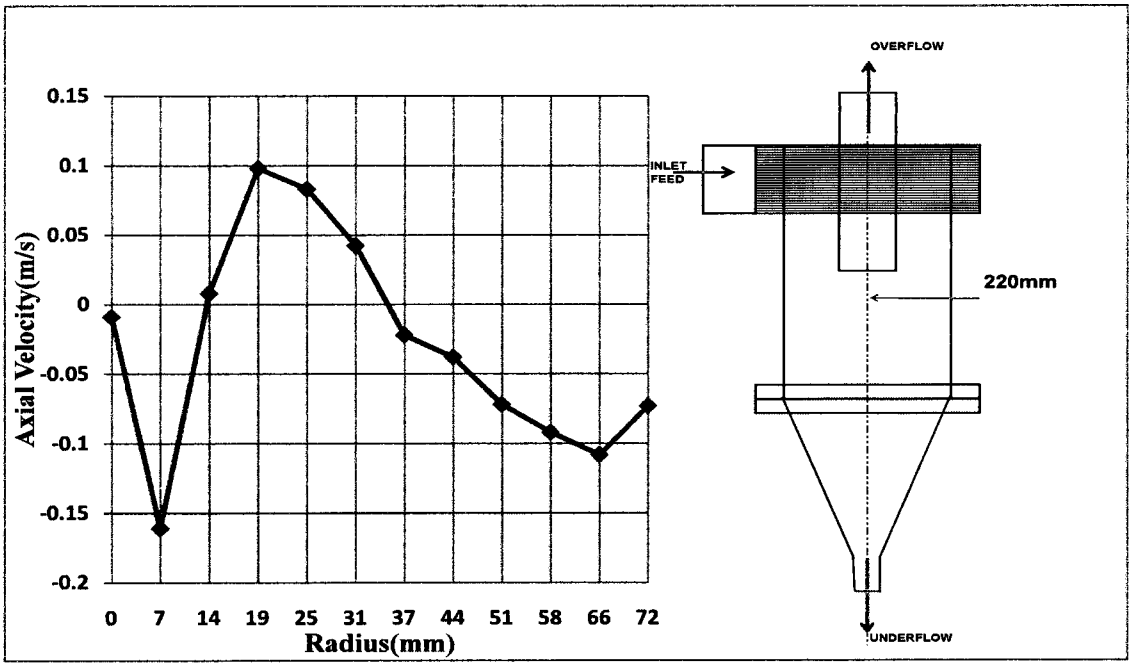

Figure 4.5 Axial velocity profile at Z= 220mm (regular probe position)

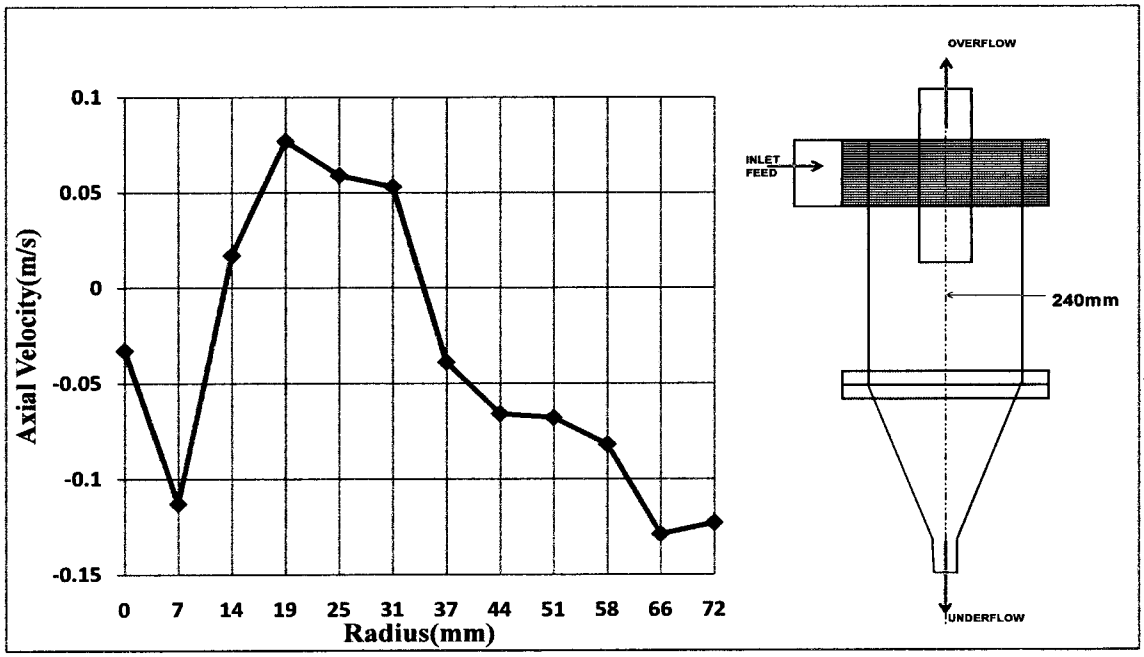

Figure 4.6 Axial velocity profile at Z=240mm (regular probe position)

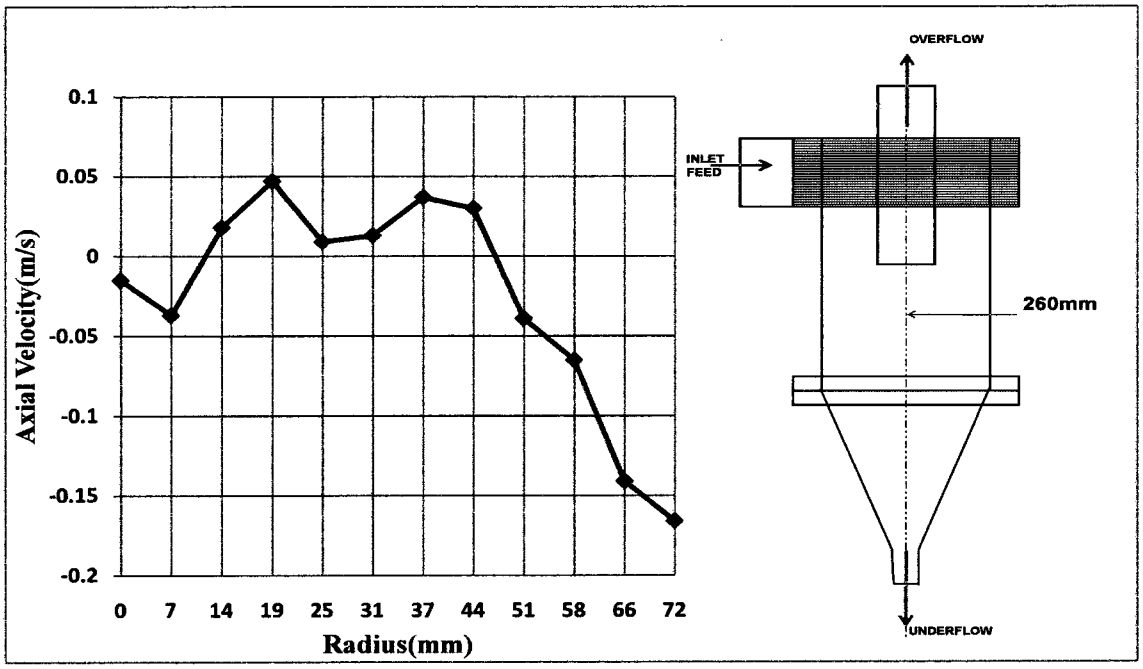

Figure 4.7 Axial velocity profile at Z= 260 mm (regular probe position)

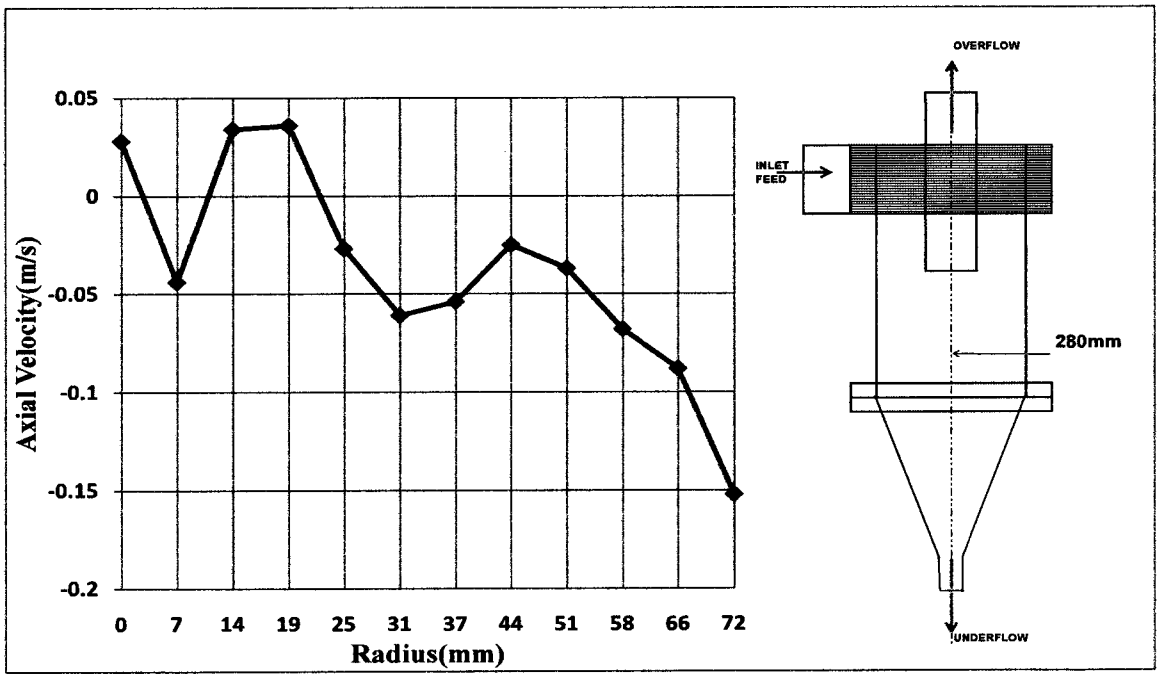

Figure 4.8 Axial velocity profile at Z=280mm (regular probe position)

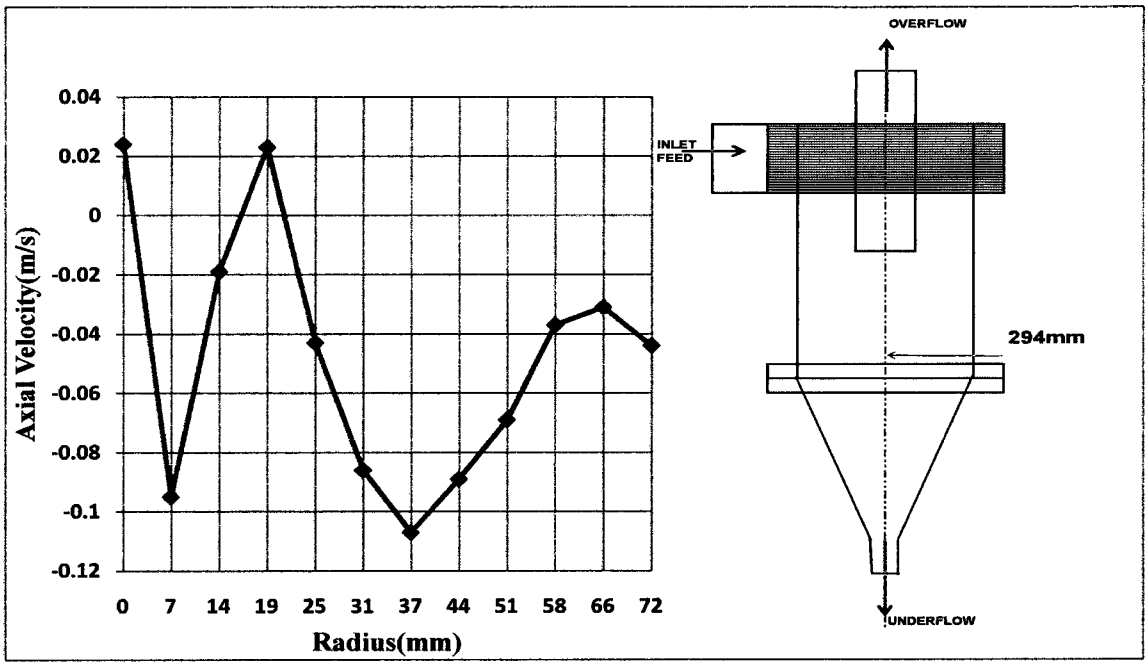

Figure 4.9 Axial velocity profile at Z=294 mm (regular probe position)

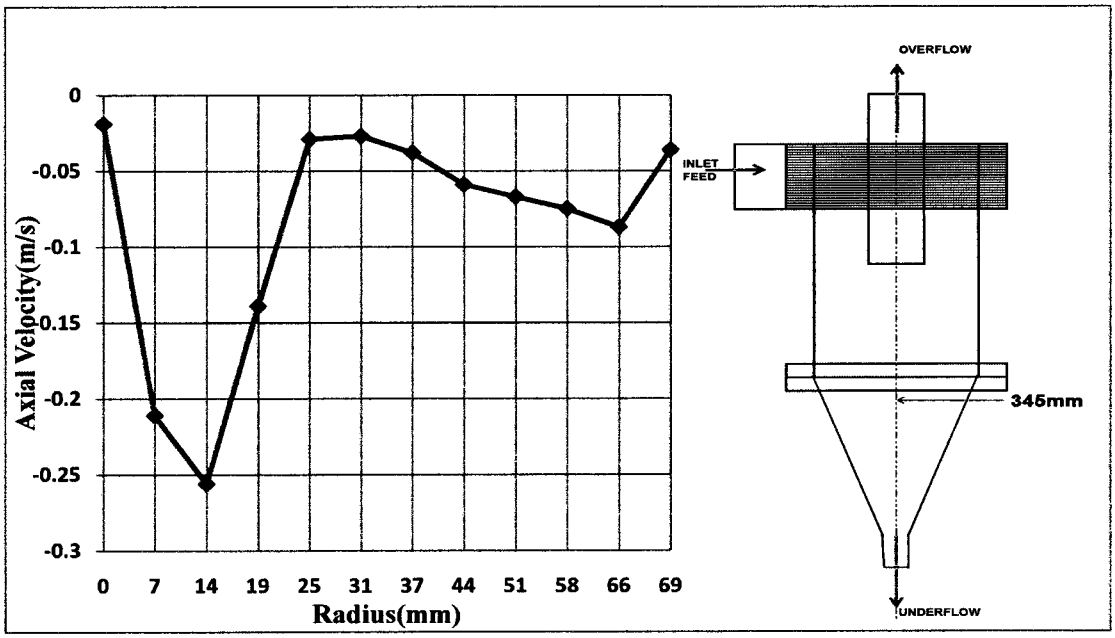

Figure 4.10 Axial velocity profile at Z=345 mm (regular probe position)

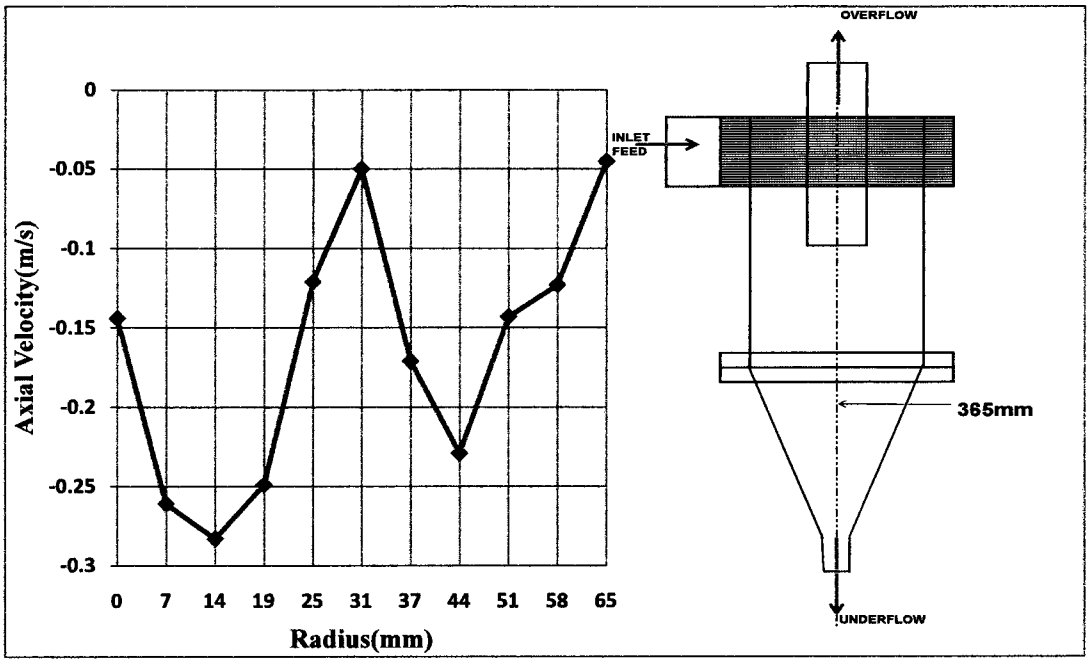

Figure 4.11 Axial velocity profile at Z= 365mm (regular probe position)

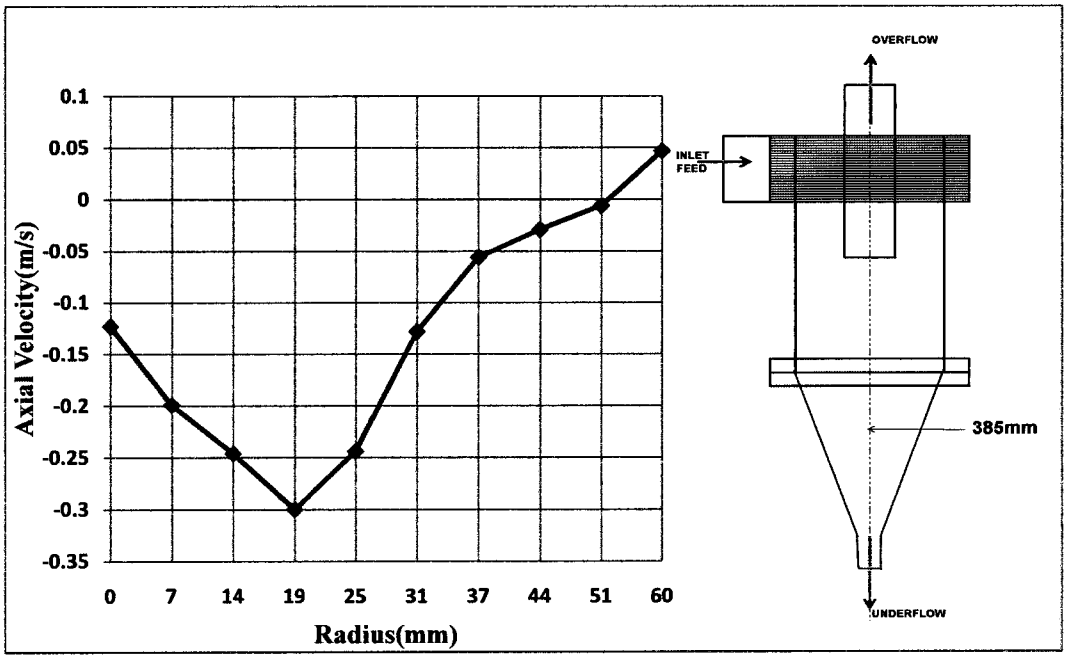

Figure 4.12 Axial velocity profile at Z= 385mm (regular probe position)

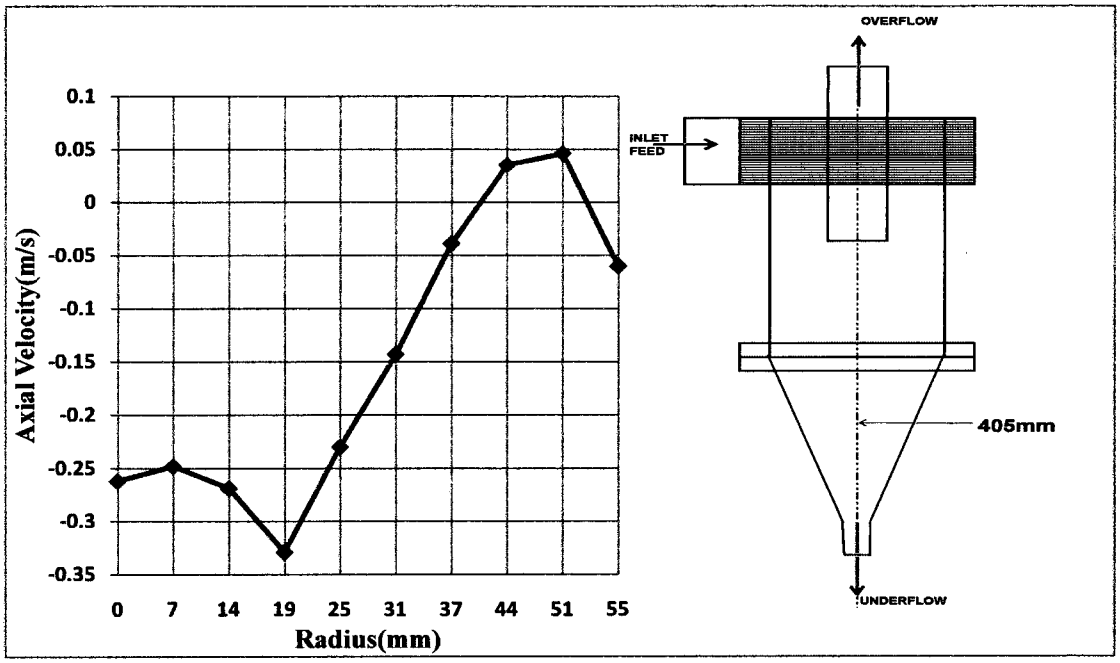

Figure 4.13 Axial velocity profile at Z=405mm (regular probe position)

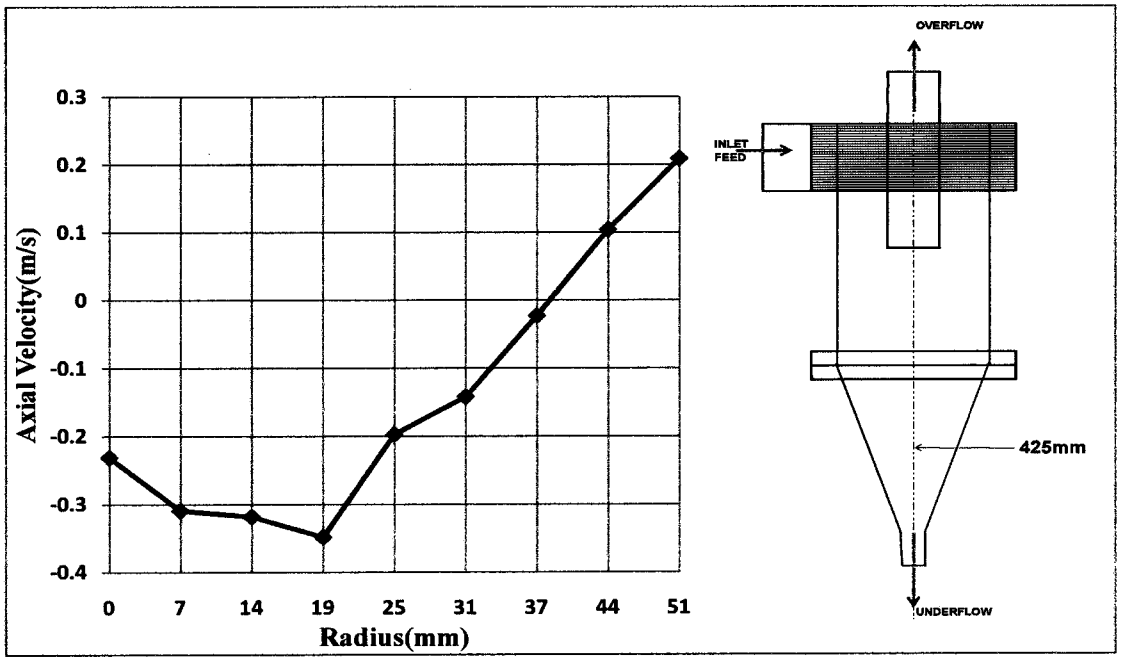

Figure 4.14 Axial velocity profile at Z= 425mm (regular probe position)

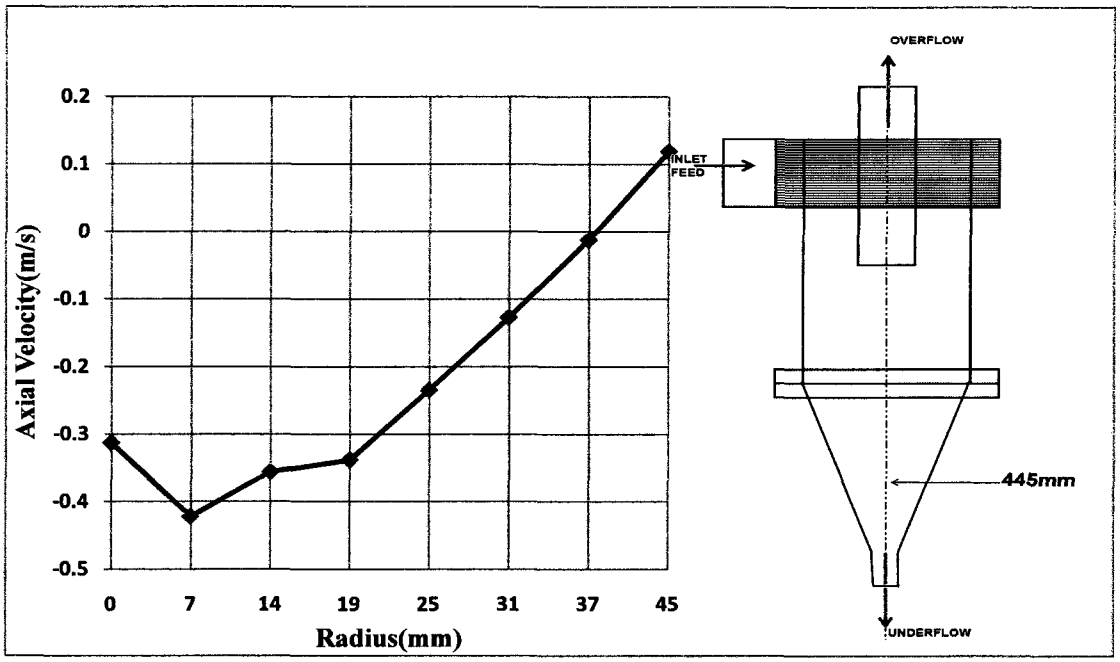

Figure 4.15 Axial velocity profile at Z=445mm (regular probe position)

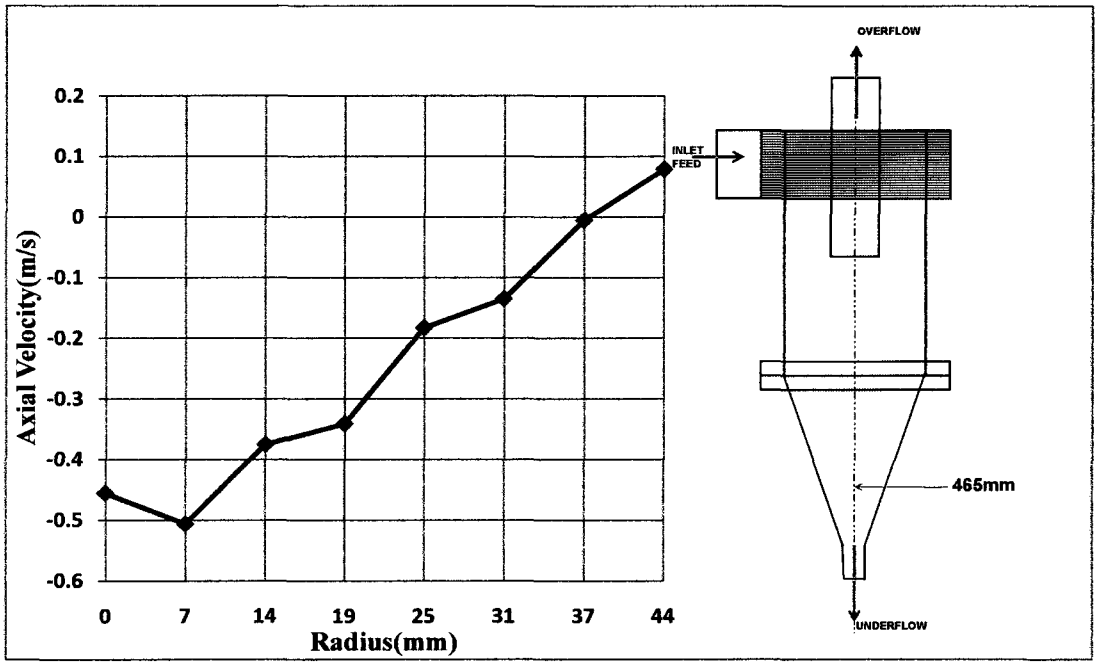

Figure 4.16 Axial velocity profile at Z= 465mm (regular probe position)

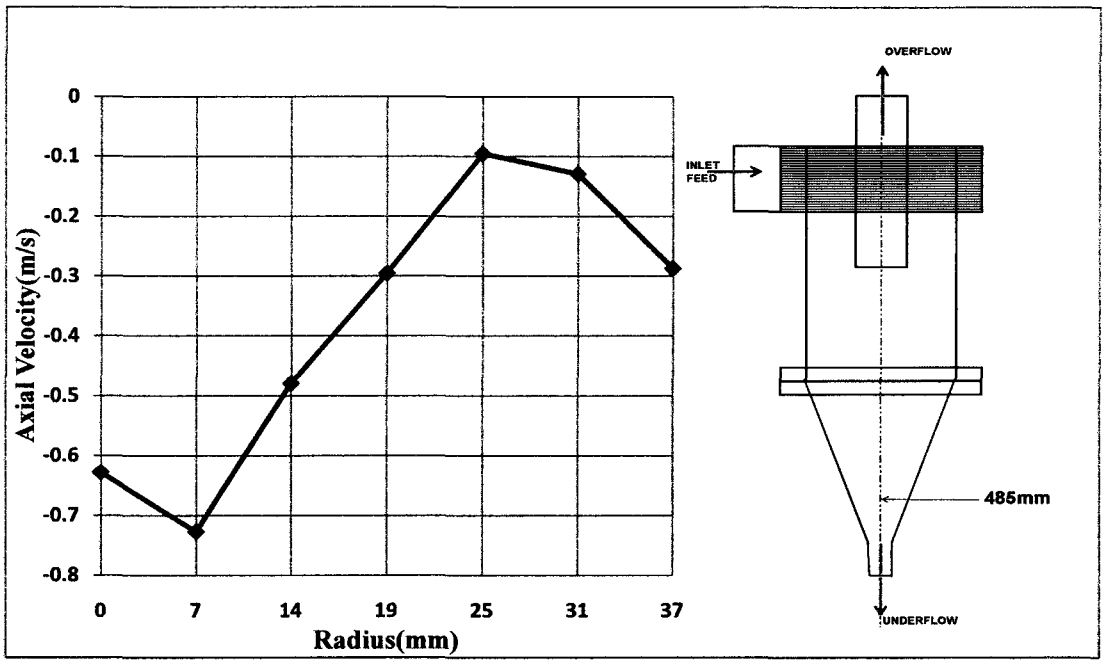

Figure 4.17 Axial velocity profile at Z= 485 mm (regular probe position)

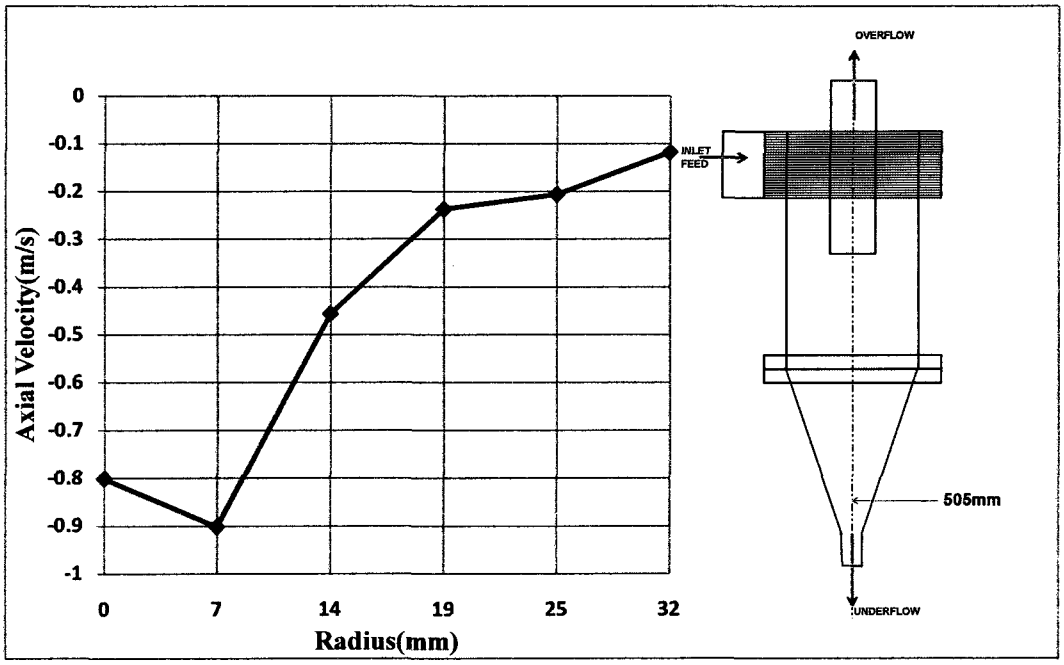

Figure 4.18 Axial velocity profile at Z= 505mm (regular probe position)

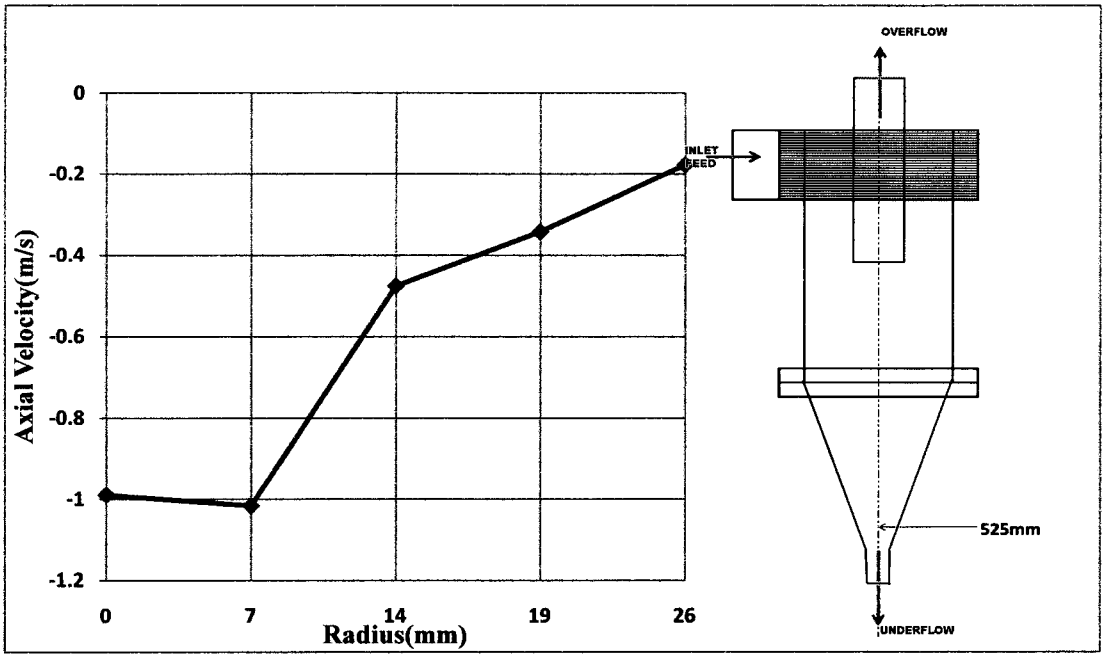

Figure 4.19 Axial velocity profile at Z= 525mm (regular probe position)

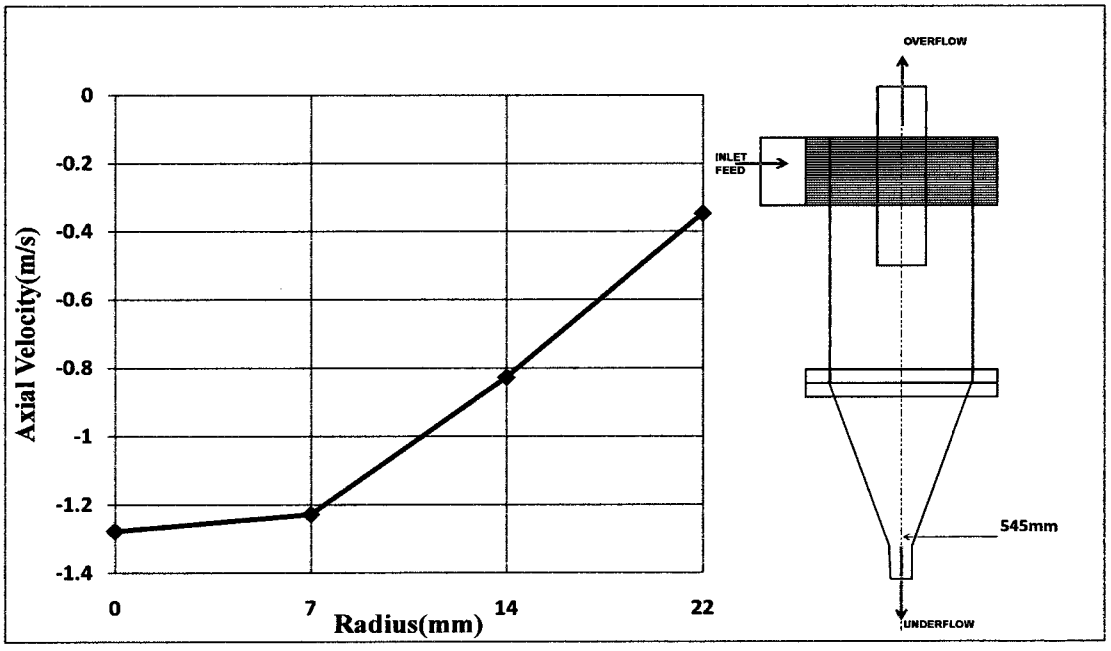

Figure 4.20 Axial velocity profile at Z= 545 mm (regular probe position)

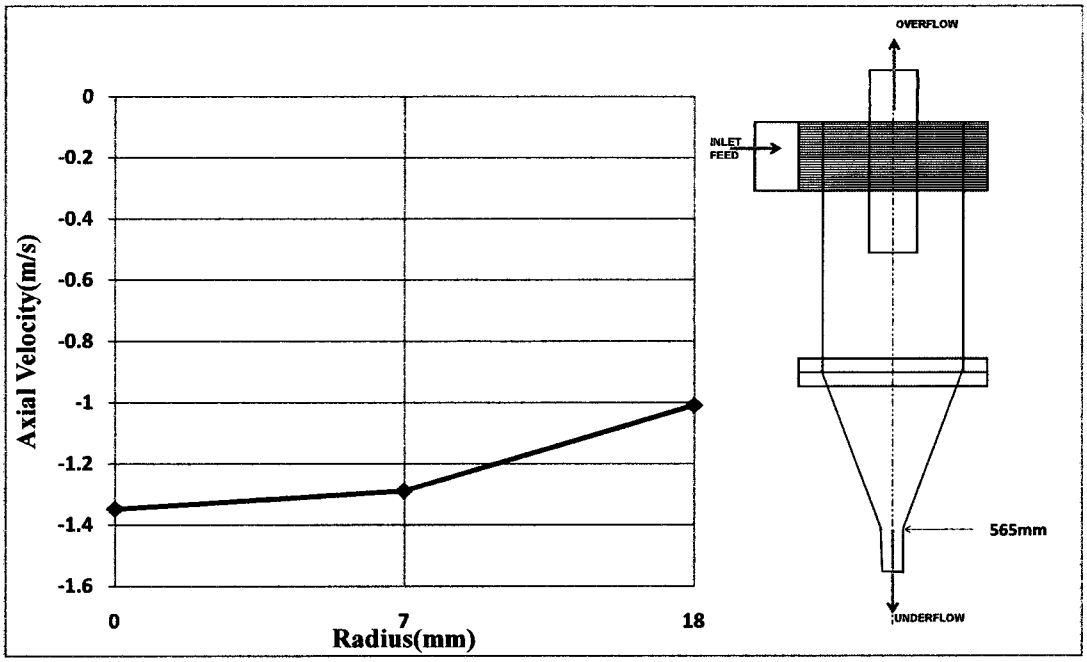

Figure 4.21 Axial velocity profiles at Z=565mm (regular probe position)

Fig. 4.22 Laser beams in regular position(Case A)

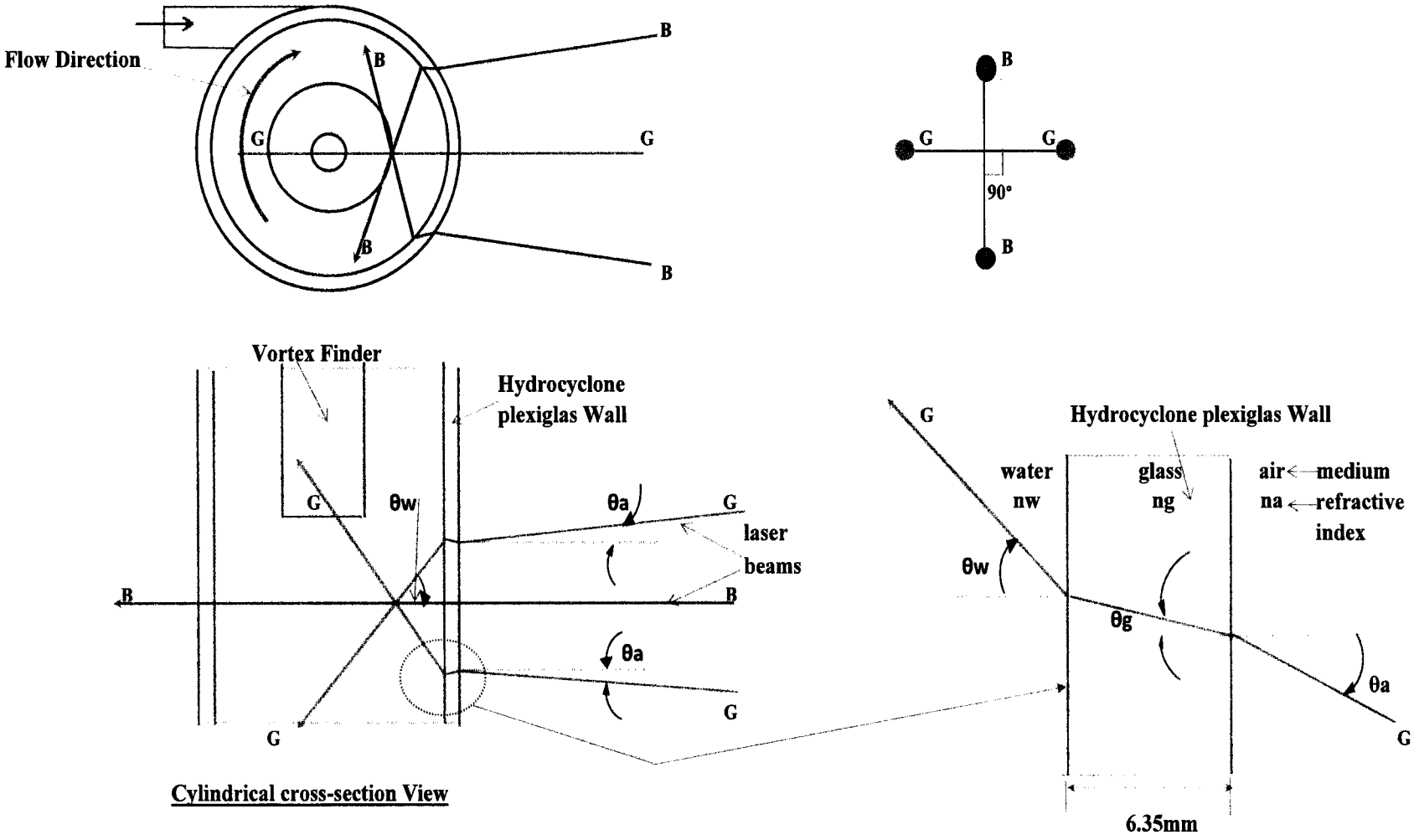

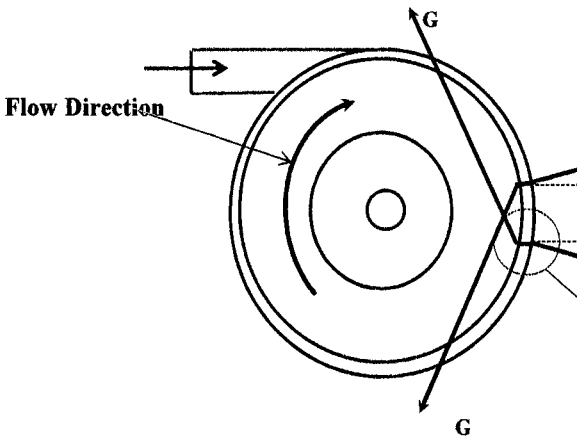
G
Flow Direction
G

Fig. 2.23 Laser beams where the probe tilted 45° (Case B)

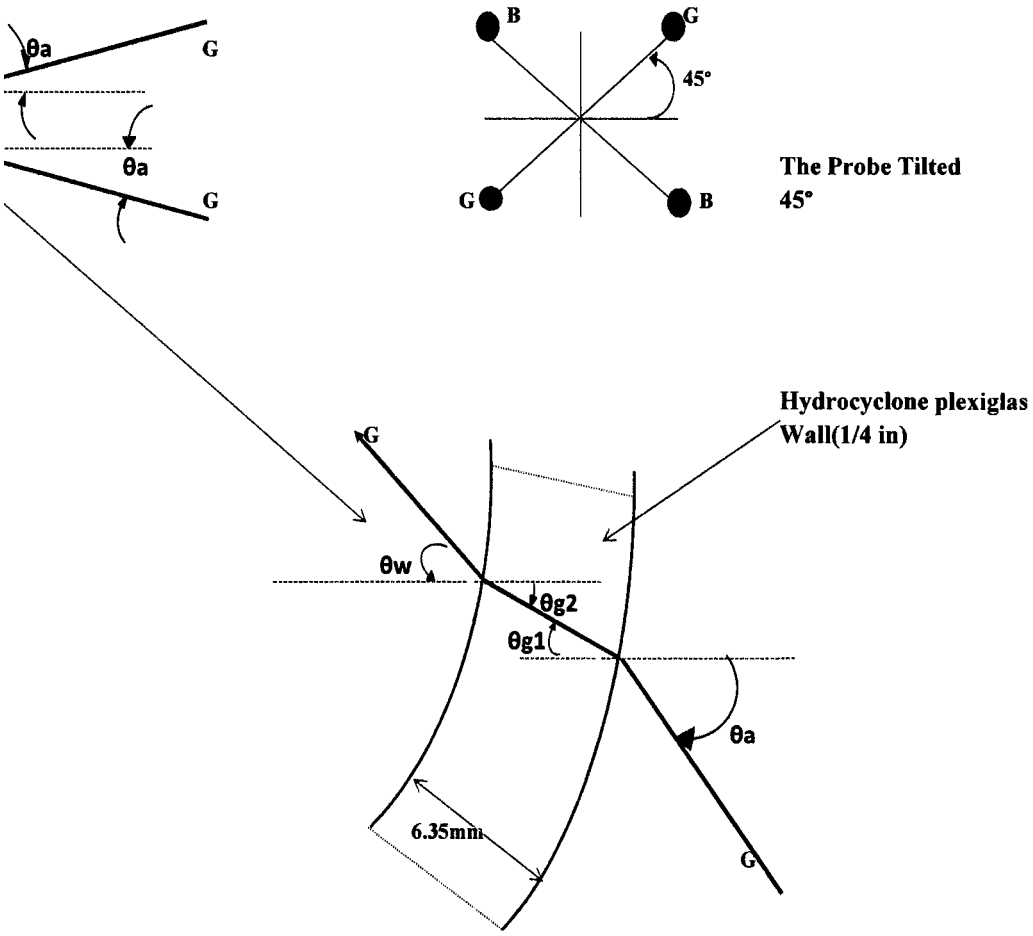

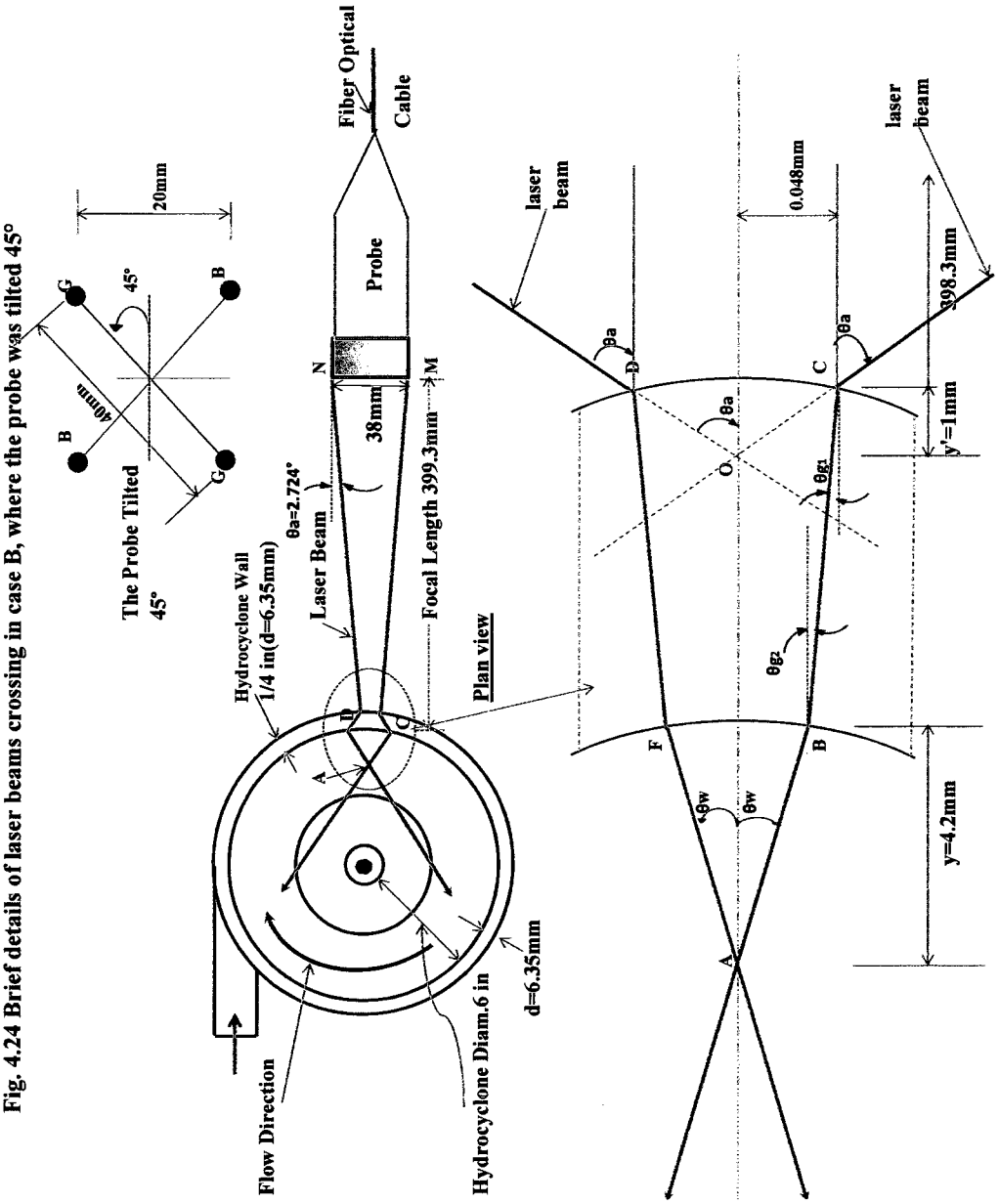

Fig. 4.24 Brief details of laser beams crossing in case B, where the probe was tilted 45°

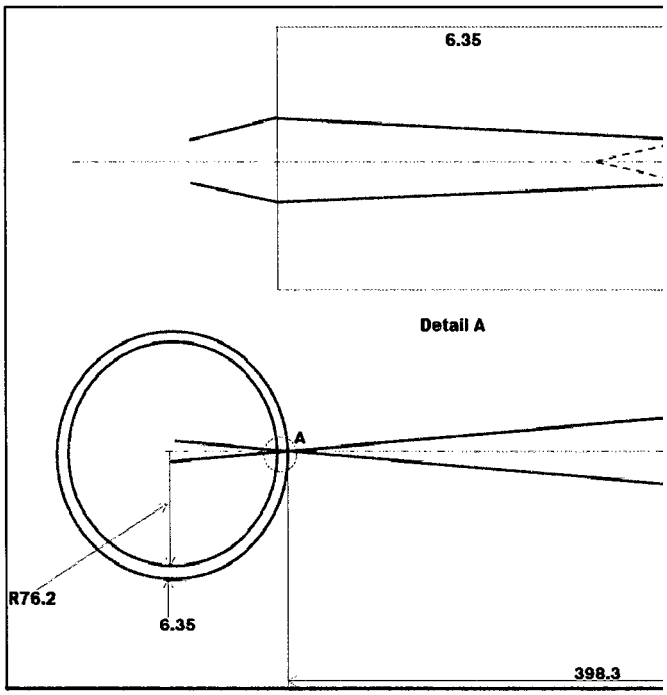
6.35
Detail A
A
R76.2
6.35
398.3

Figure 4.25 Schematic layout of two laser beams; draw to scale to measure the refractive angle θ_{g2}

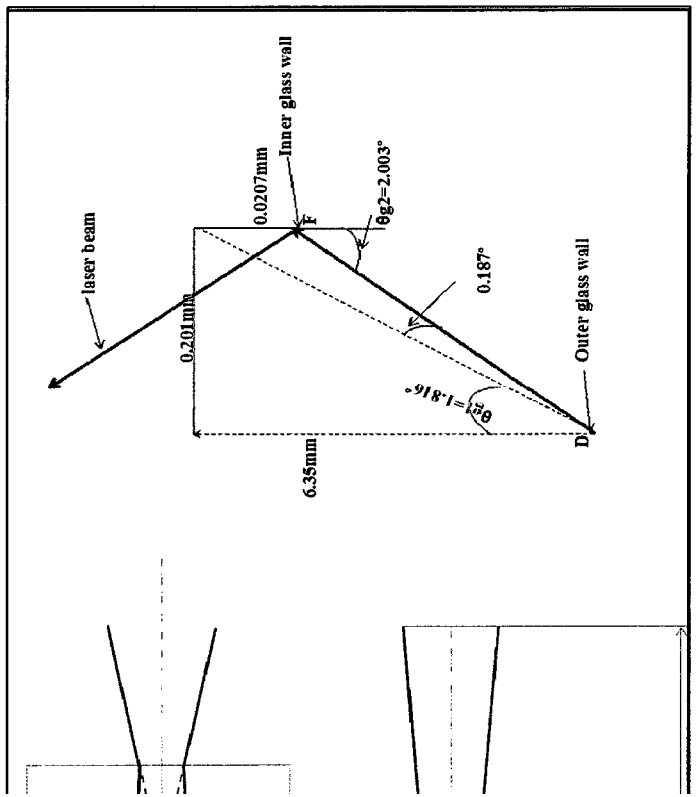

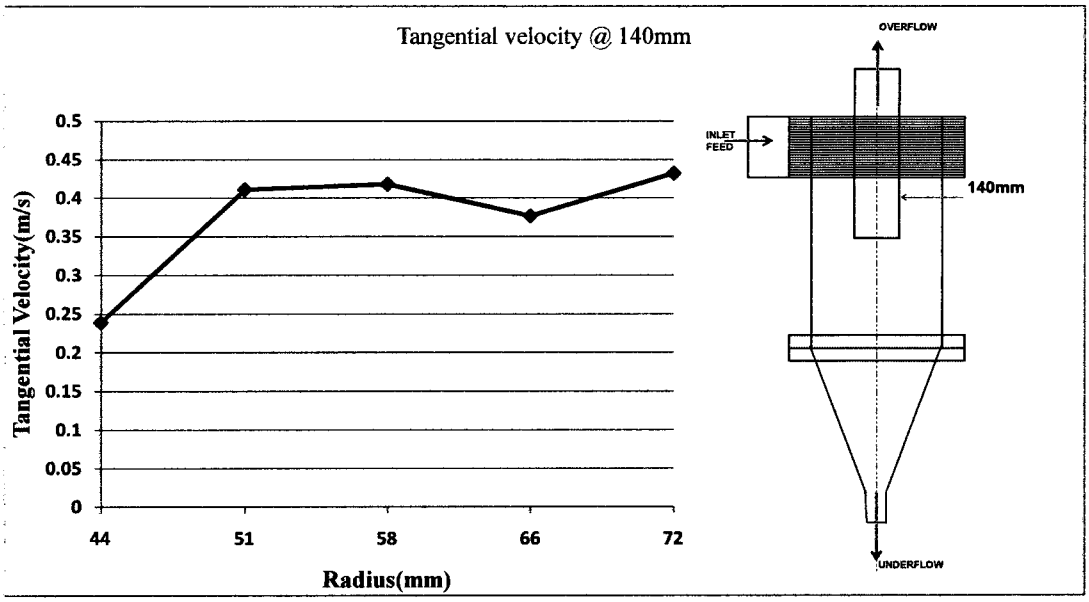

Figure 4.26 Tangential velocity profile at Z= 140mm (Case B, probe tilted 45°)

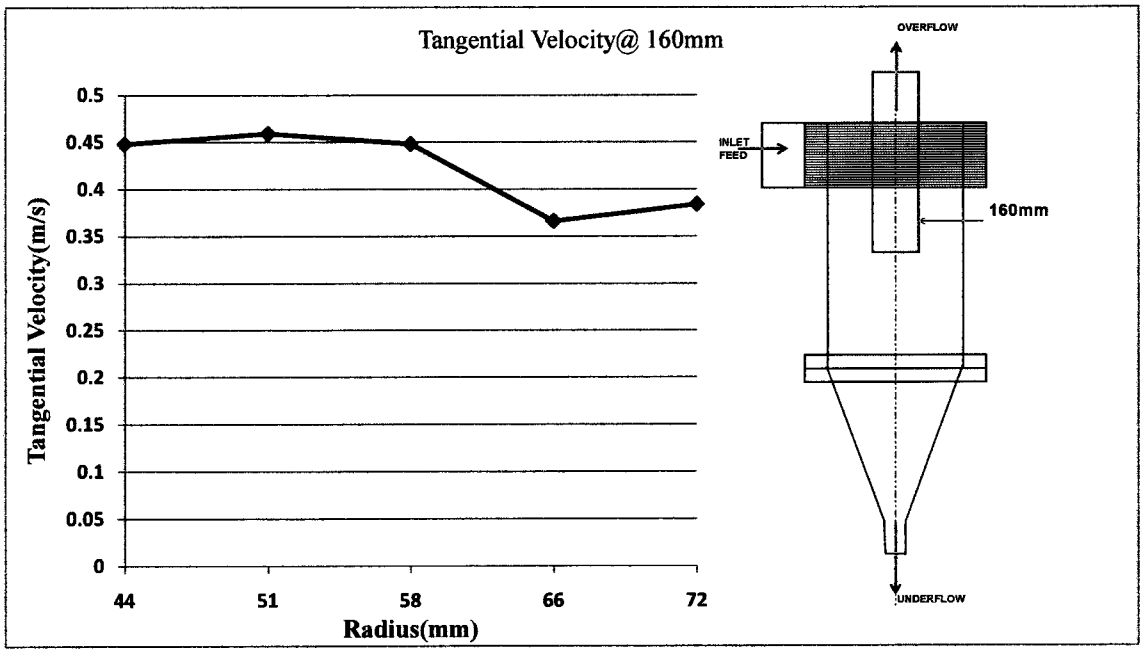

Figure 4.27 Tangential velocity profile at Z= 160mm (Case B, probe tilted 45°)

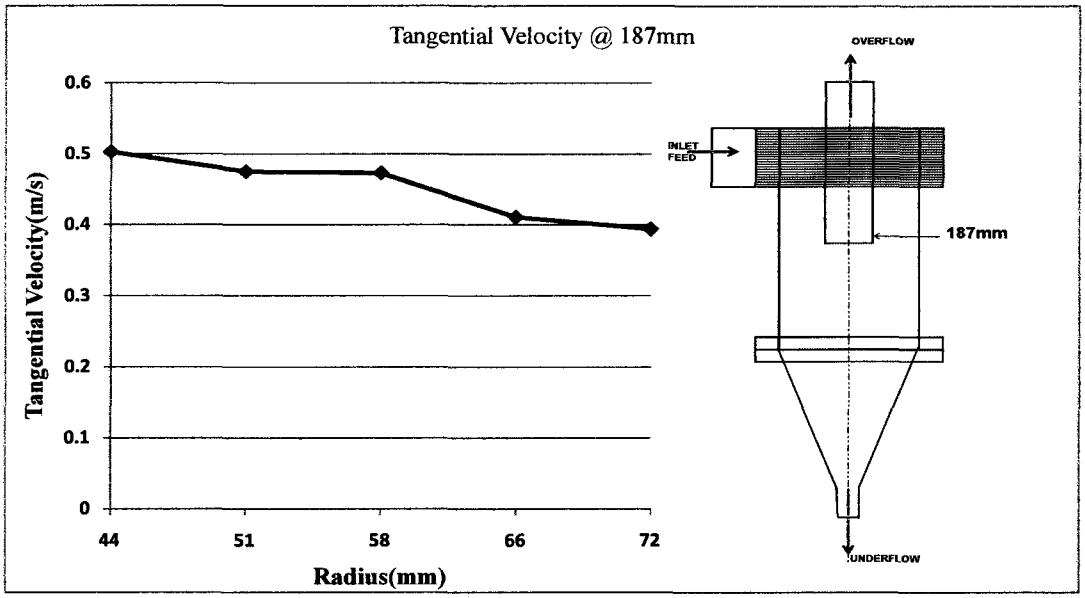

Figure 4.28 Tangential velocity profile at Z= 187mm (Case B, probe tilted 45°)

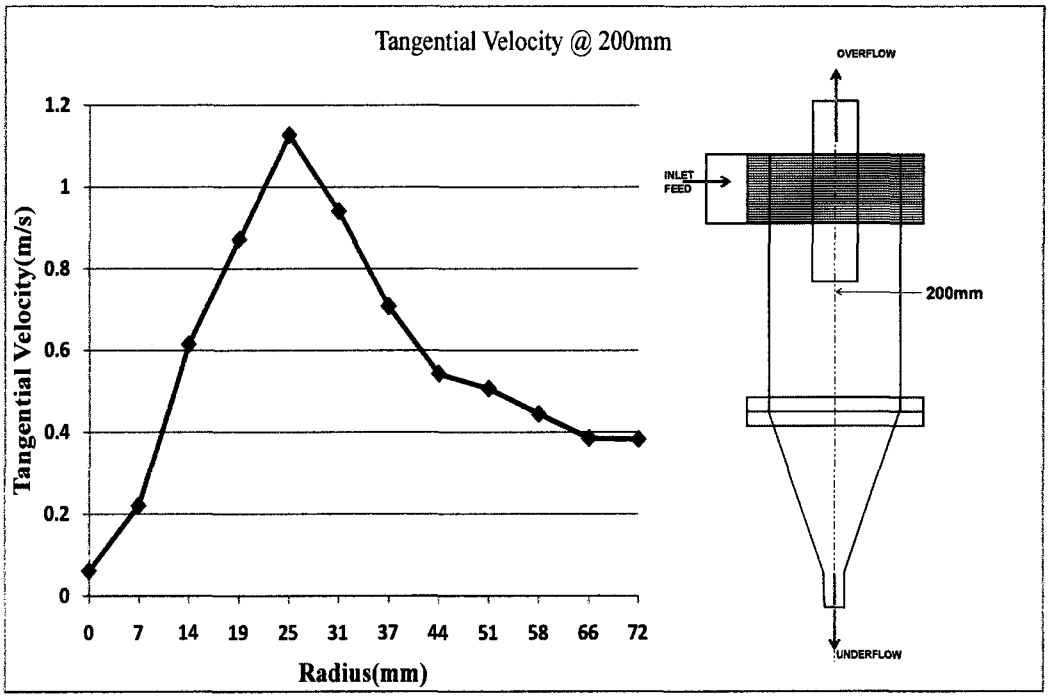

Figure 4.29 Tangential velocity profile at Z= 200mm (Case B, probe tilted 45°)

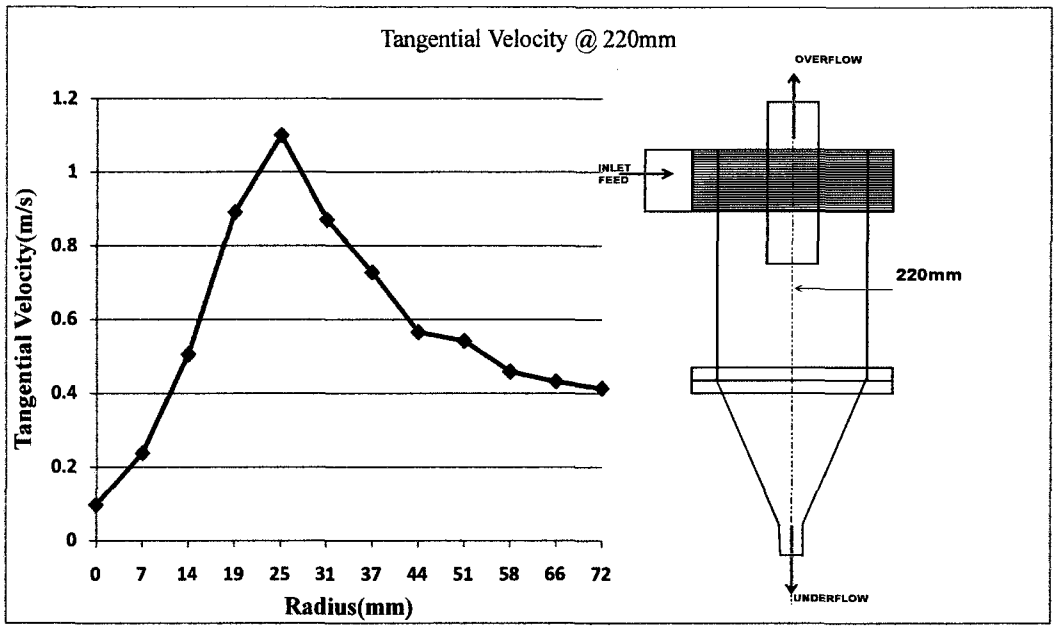

Figure 4.30 Tangential velocity profile at Z= 220mm (Case B, probe tilted 45°)

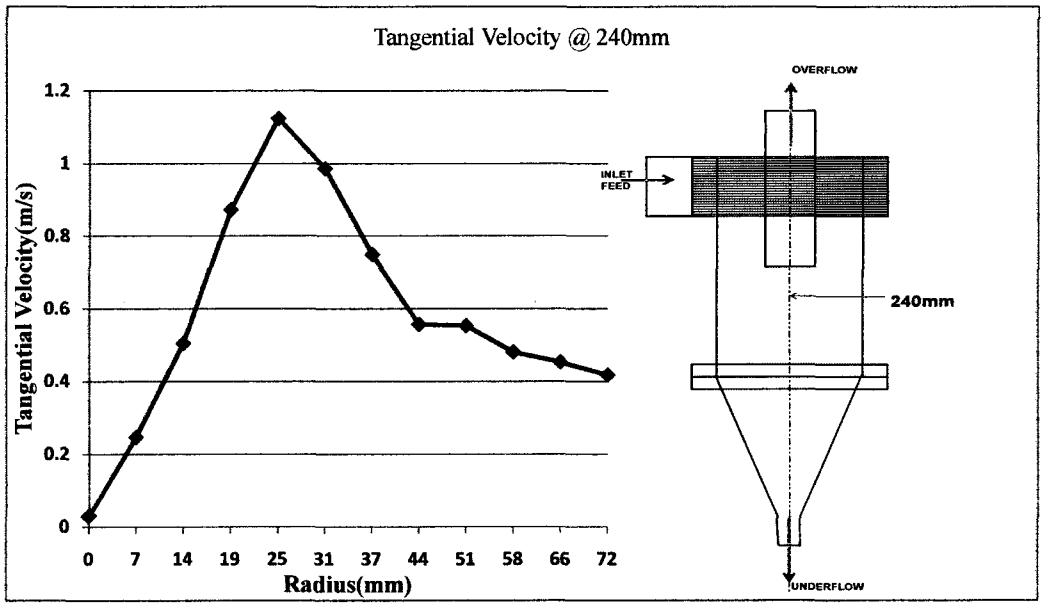

Figure 4.31 Tangential velocity profile at Z=240mm (Case B, probe tilted 45°)

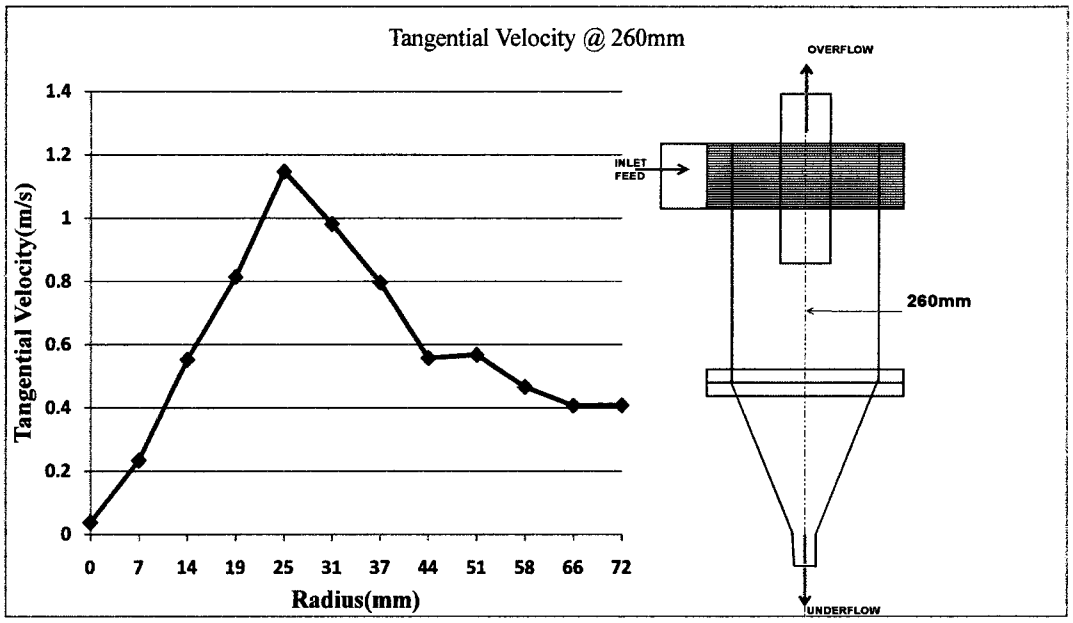

Figure 4.32 Tangential velocity profile at Z= 260 mm (Case B, probe tilted 45°)

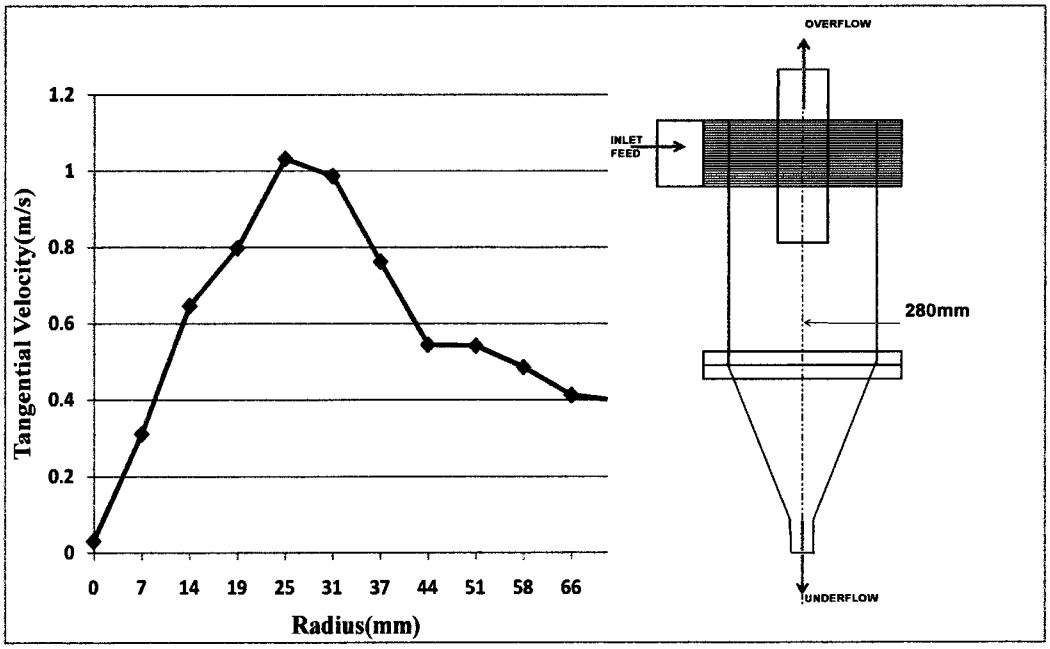

Figure 4.33 Tangential velocity profile at Z= 280mm (Case B, probe tilted 45°)

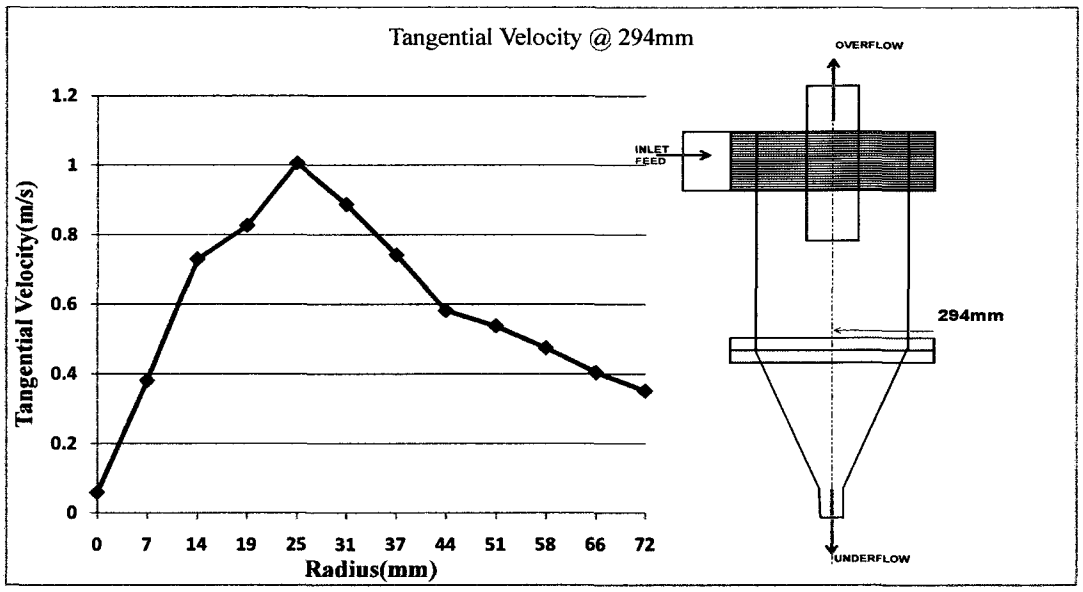

Figure 4.34 Tangential velocity profile at Z= 294mm (Case B, probe tilted 45°)

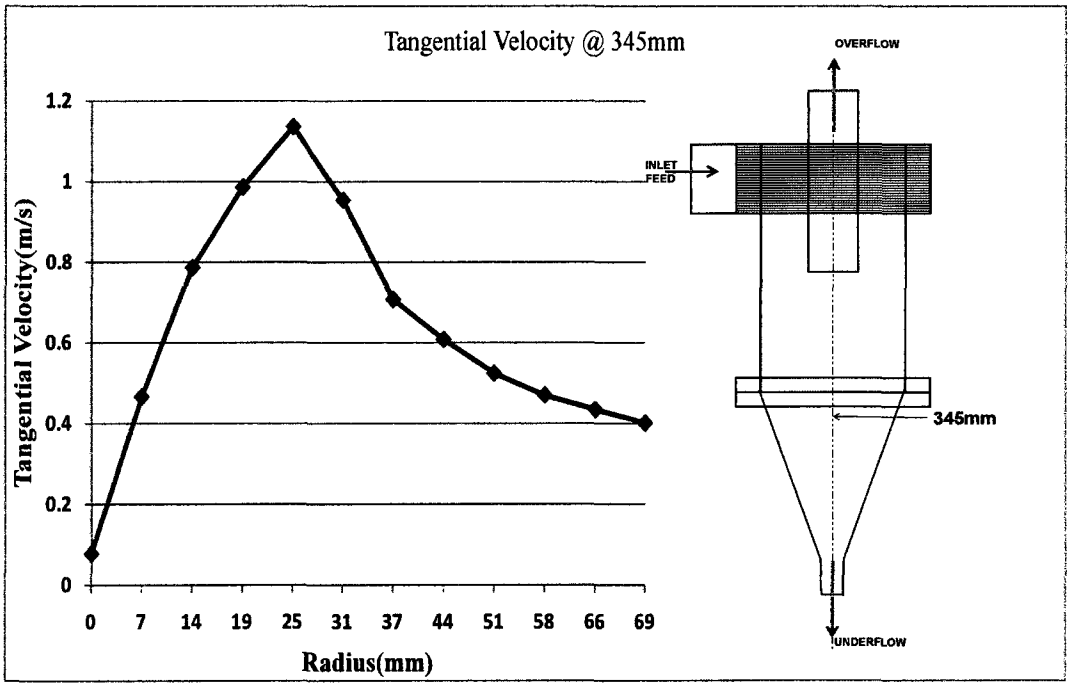

Figure 4.35 Tangential velocity profile at Z= 345mm (Case B, probe tilted 45°)

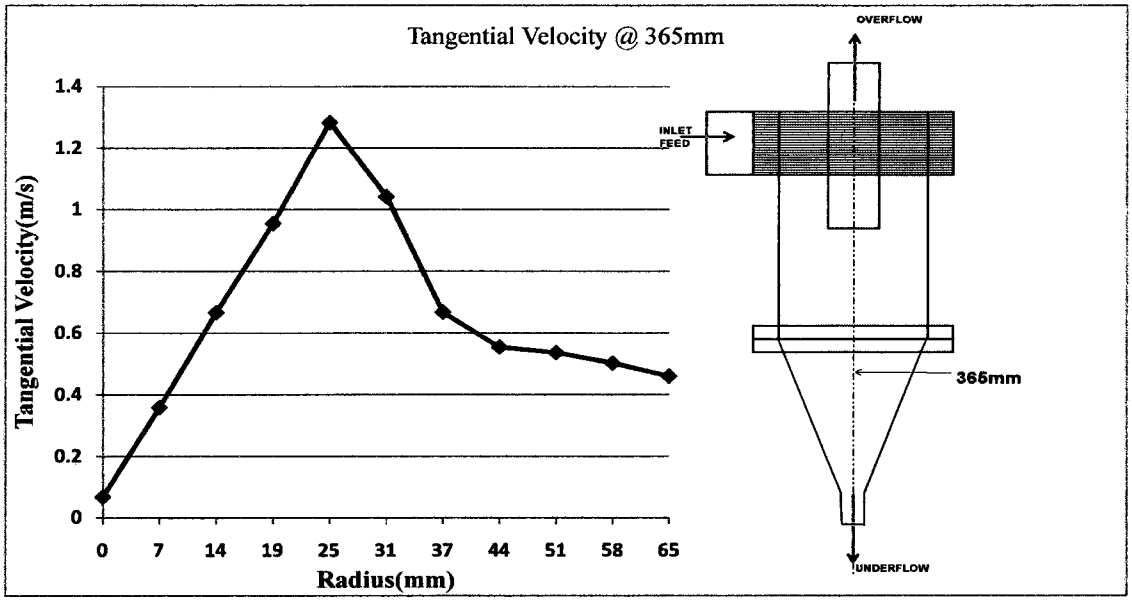

Figure 4.36 Tangential velocity profile at Z= 365mm (Case B, probe tilted 45°)

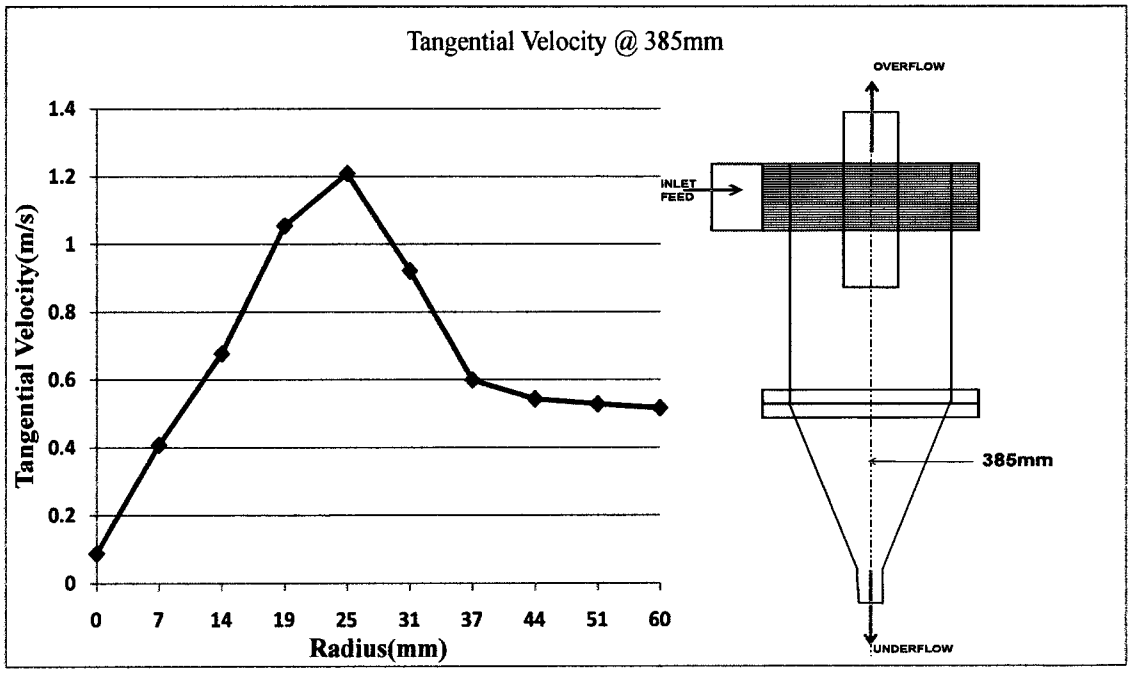

Figure 4.37 Tangential velocity profile at Z=385mm (Case B, probe tilted 45°)

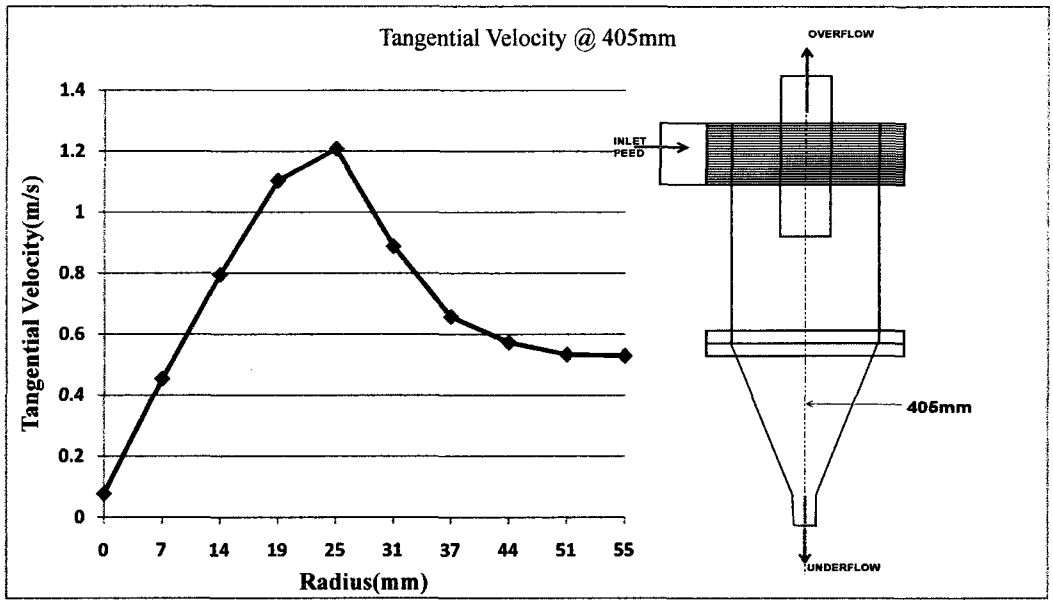

Figure 4.38 Tangential velocity profile at Z=405mm (Case B, probe tilted 45°)

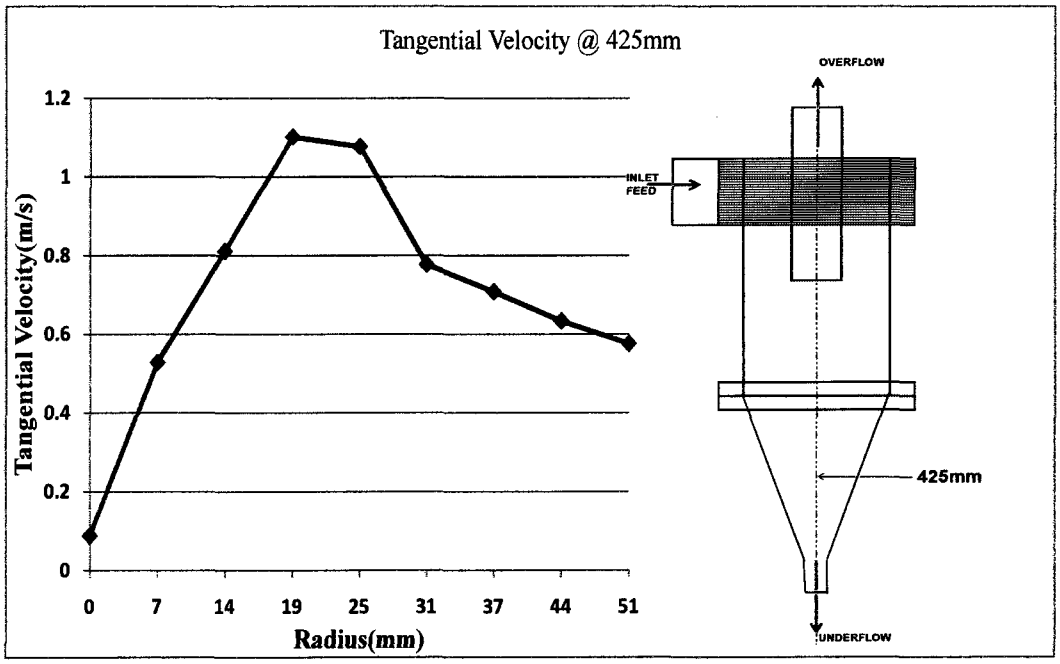

Figure 4.39 Tangential velocity profile at Z= 425mm (Case B, probe tilted 45°)

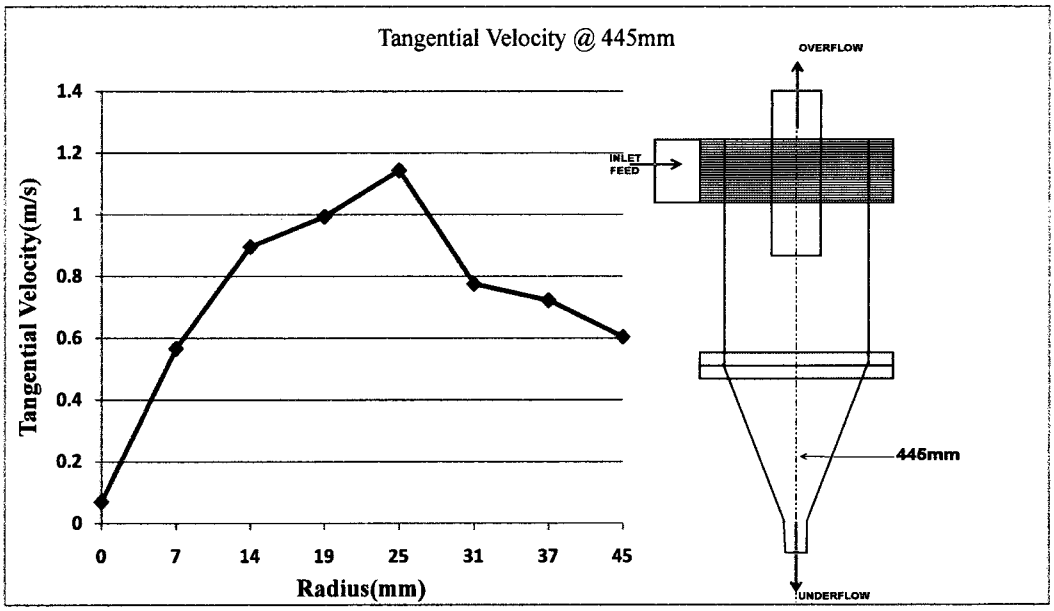

Figure 4.40 Tangential velocity profile at Z= 445mm (Case B, probe tilted 45°)

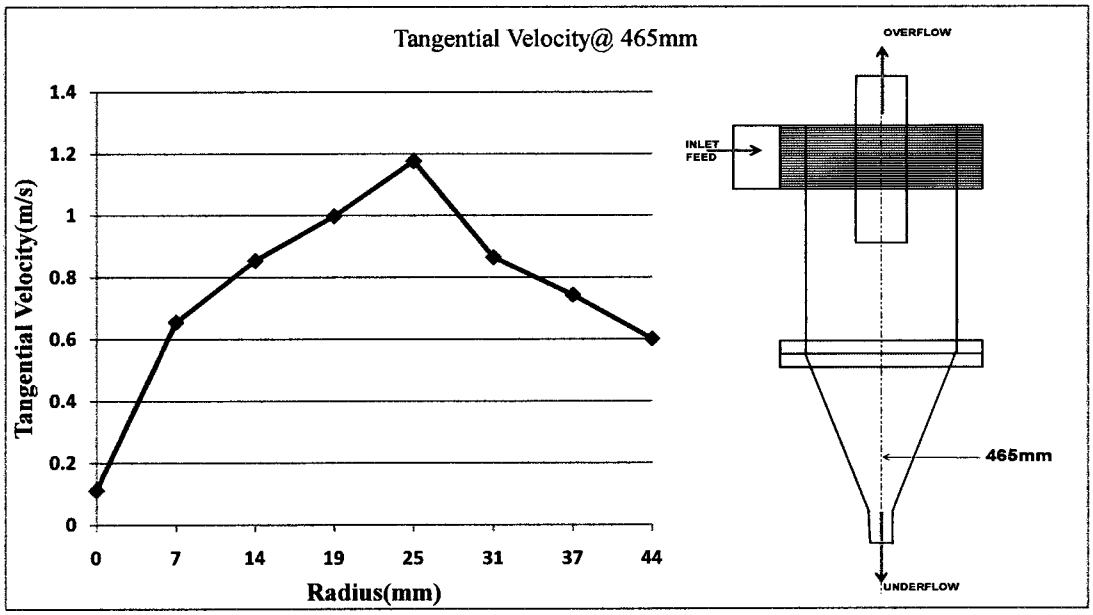

Figure 4.41 Tangential velocity profile at Z= 465mm (Case B, probe tilted 45°)

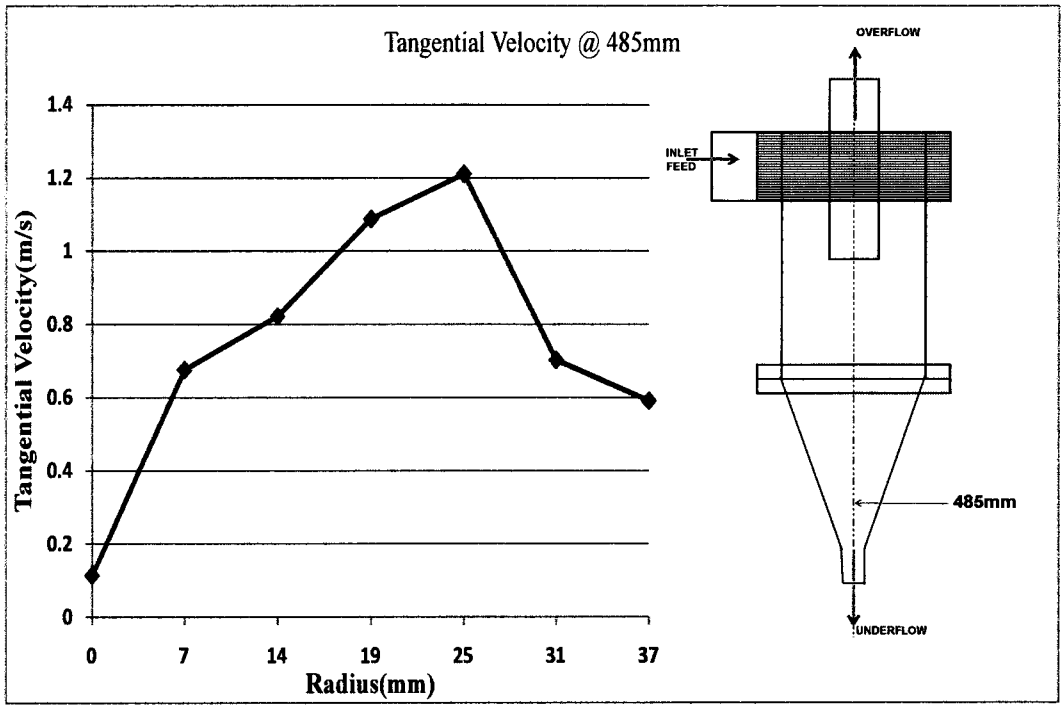

Figure 4.42 Tangential velocity profile at Z=485mm (Case B, probe tilted 45°)

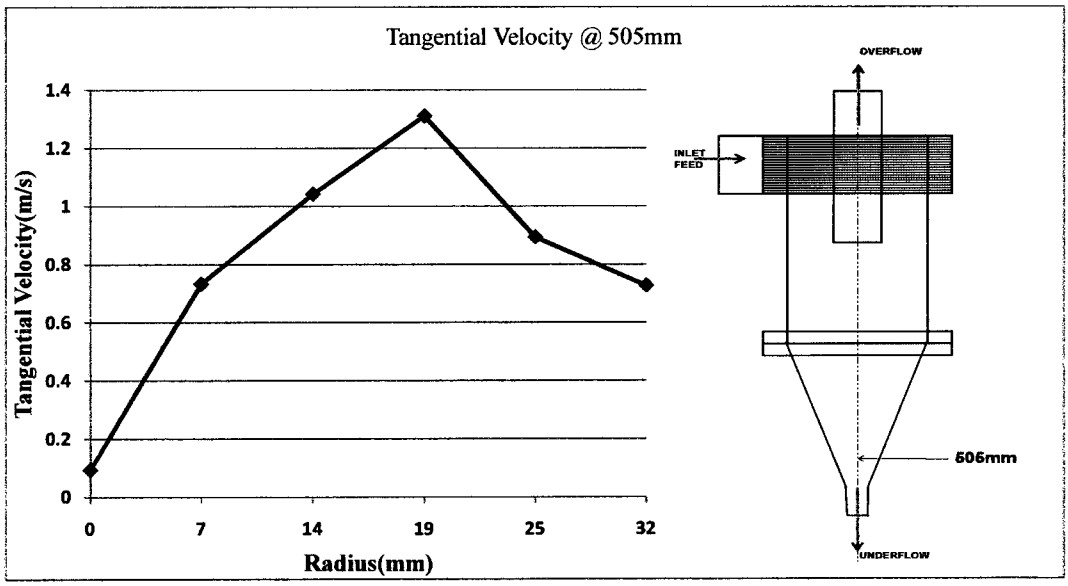

Figure 4.43 Tangential velocity profile at Z= 505mm (Case B, probe tilted 45°)

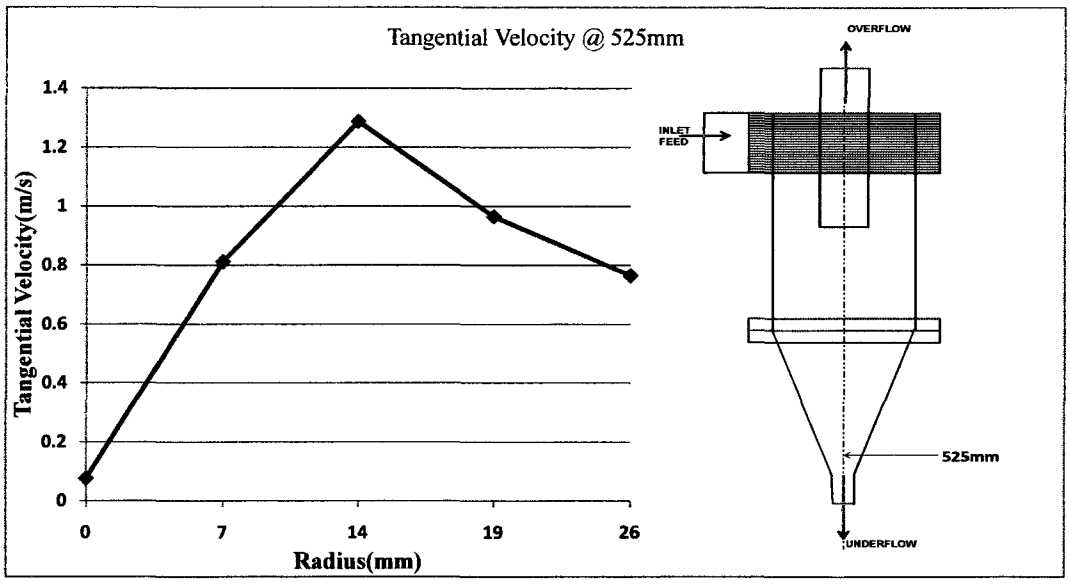

Figure 4.44 Tangential velocity profile at Z=525mm (Case B, probe tilted 45°)

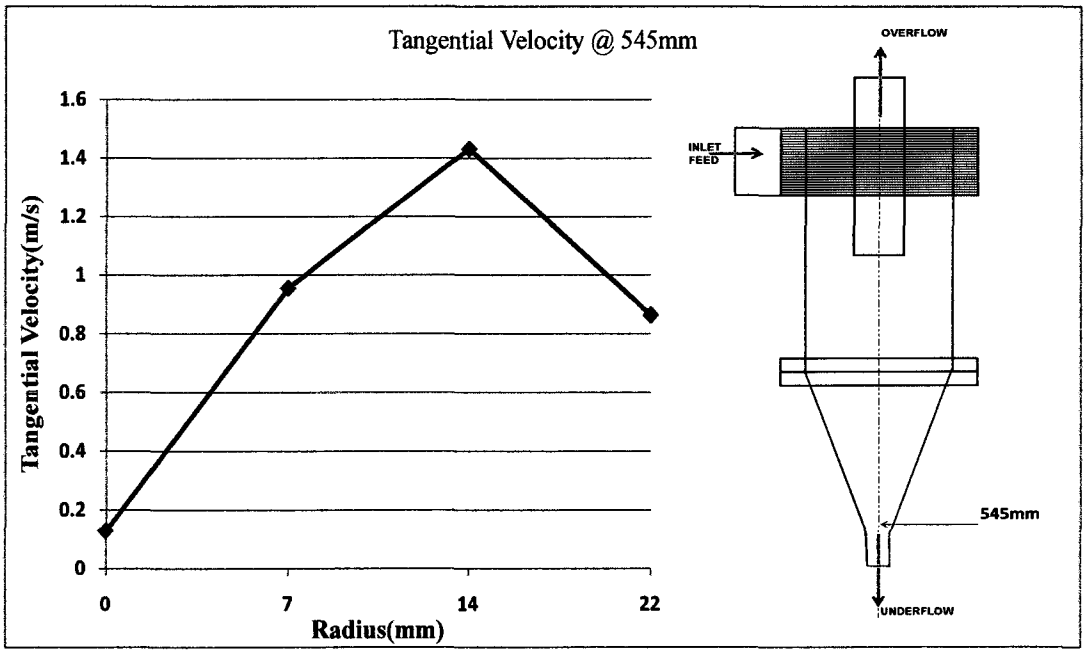

Figure 4.45 Tangential velocity profile at Z=545mm (Case B, probe tilted 45°)

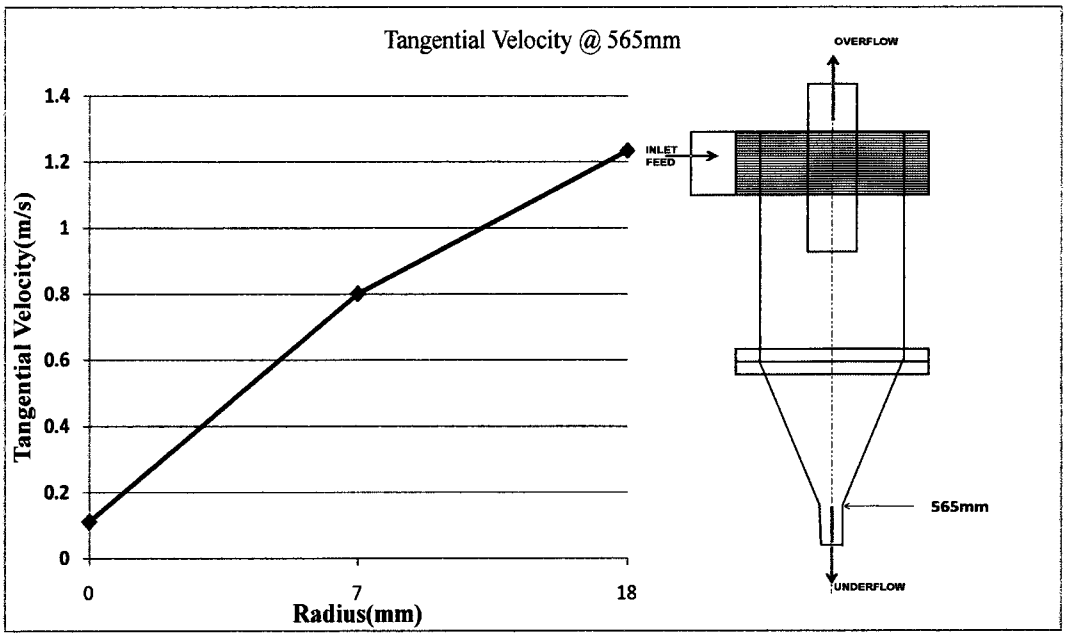

Figure 4.46 Tangential velocity profile at Z=565mm (Case B, probe tilted 45°)

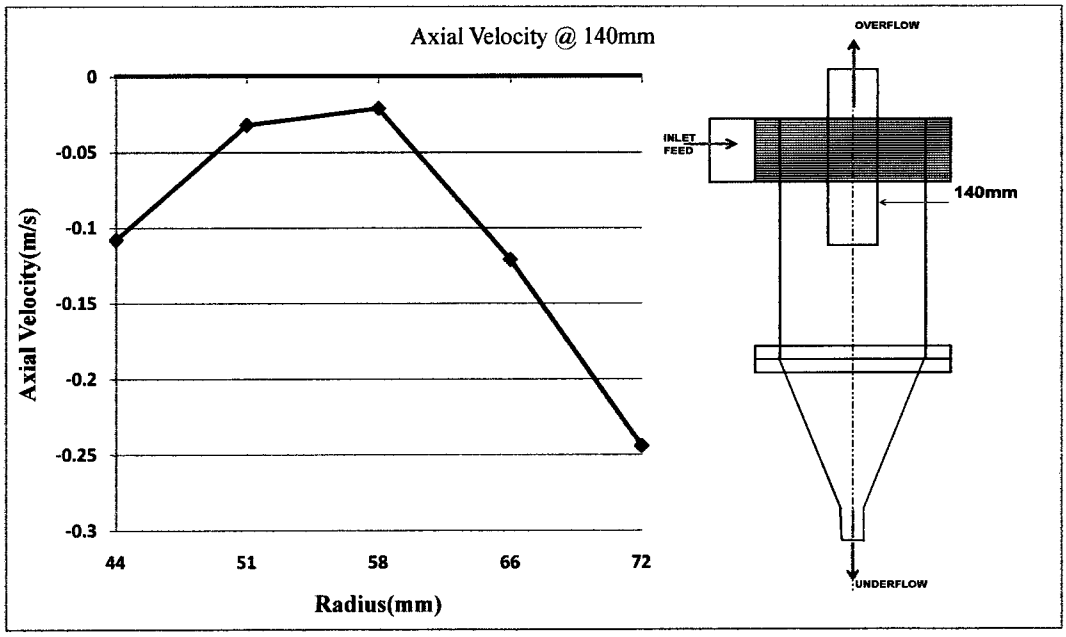

Figure 4.47 Axial velocity profile at Z=140mm (Case B, probe tilted 45°)

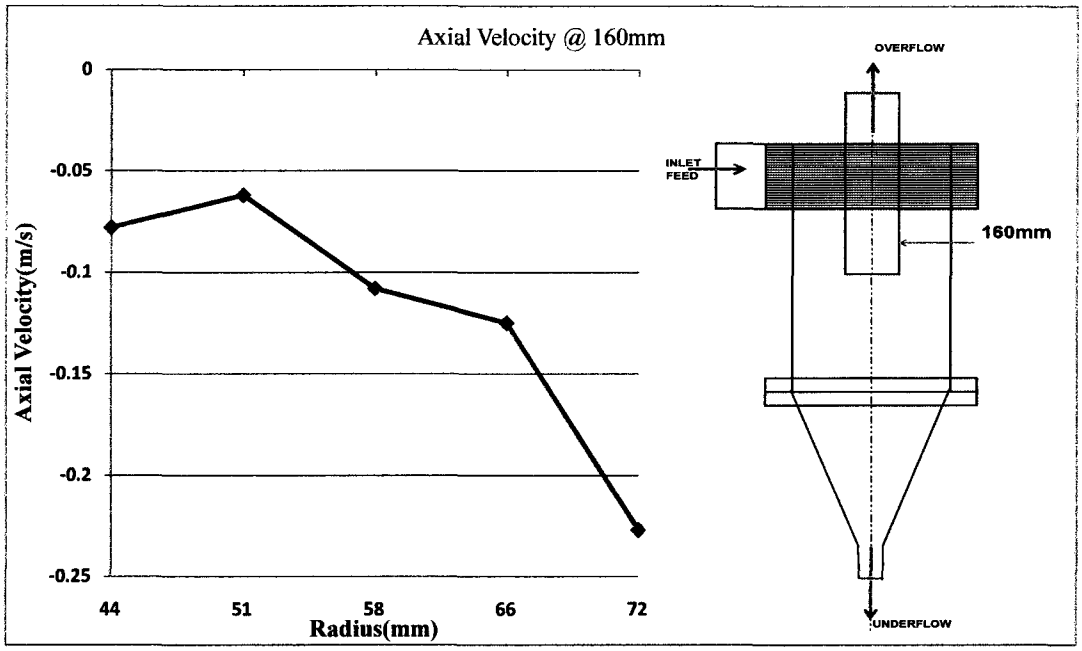

Figure 4.48 Axial velocity profile at Z=160mm (Case B, probe tilted 45°)

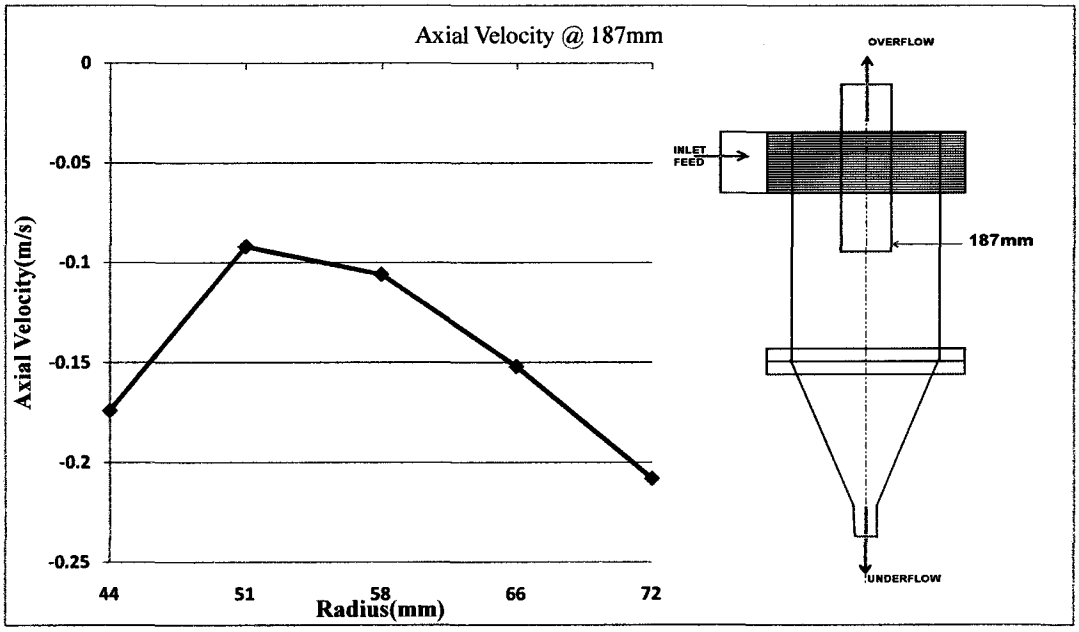

Figure 4.49 Axial velocity profile at Z=187mm (Case B, probe tilted 45°)

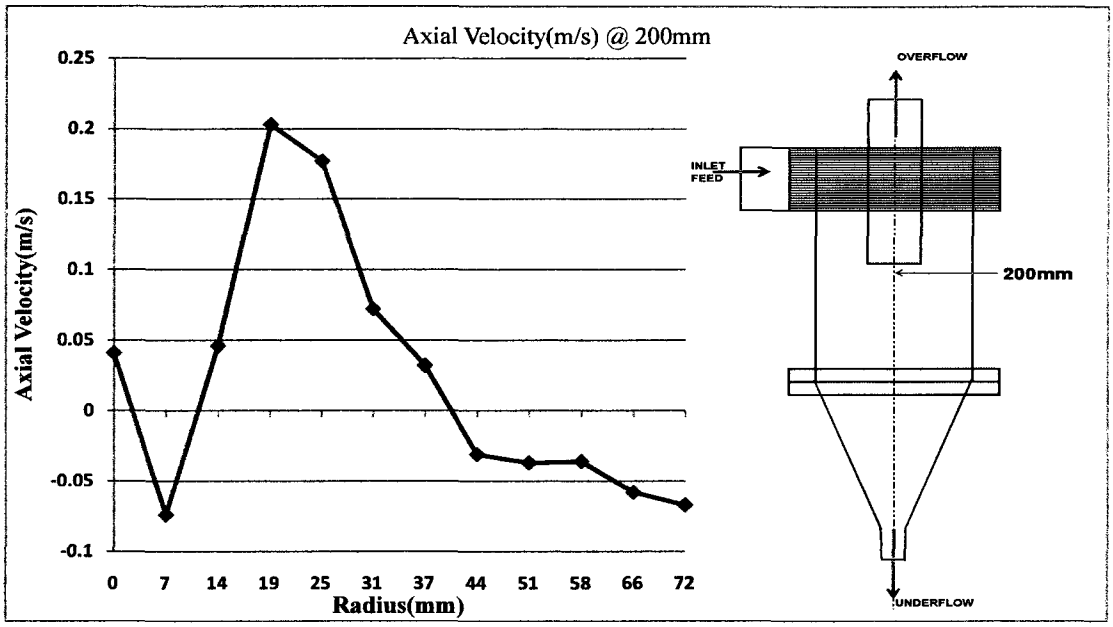

Figure 4.50 Axial Velocity profile at Z=200mm (Case B, probe tilted 45°)

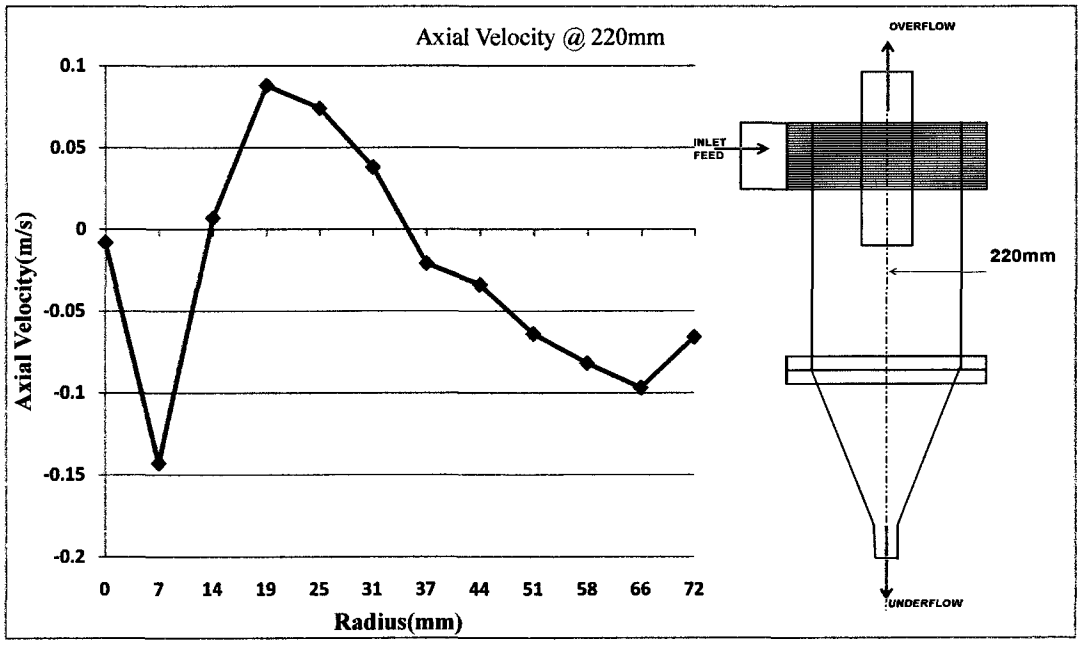

Figure 4.51 Axial velocity profile at Z=220mm (Case B, probe tilted 45°)

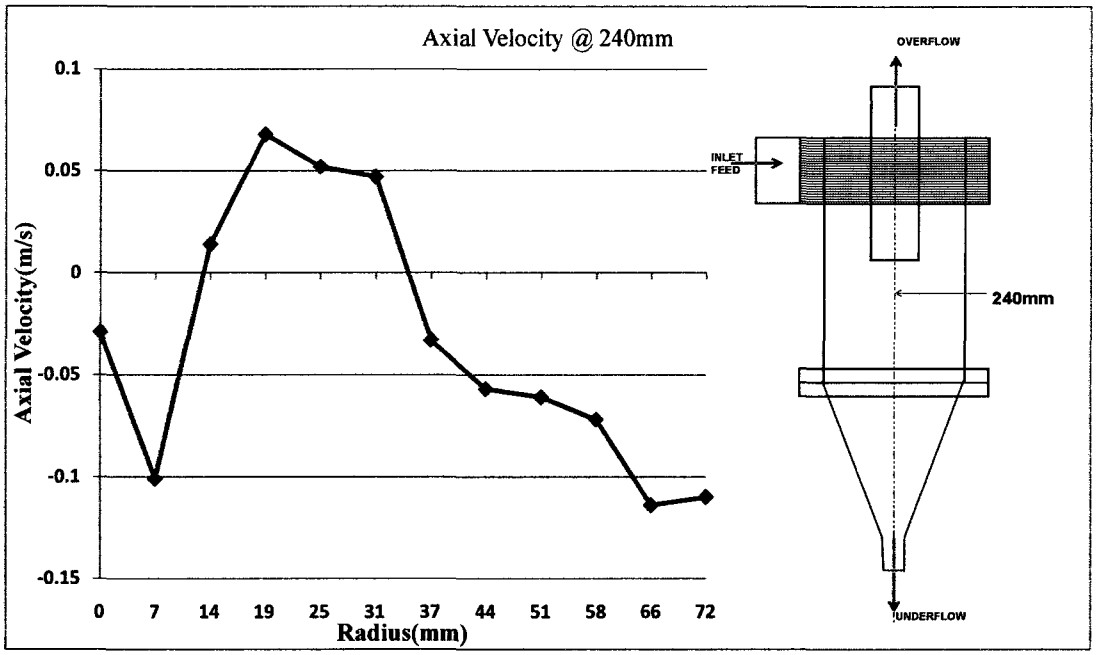

Figure 4.52 Axial velocity profile at Z=240mm (Case B, probe tilted 45°)

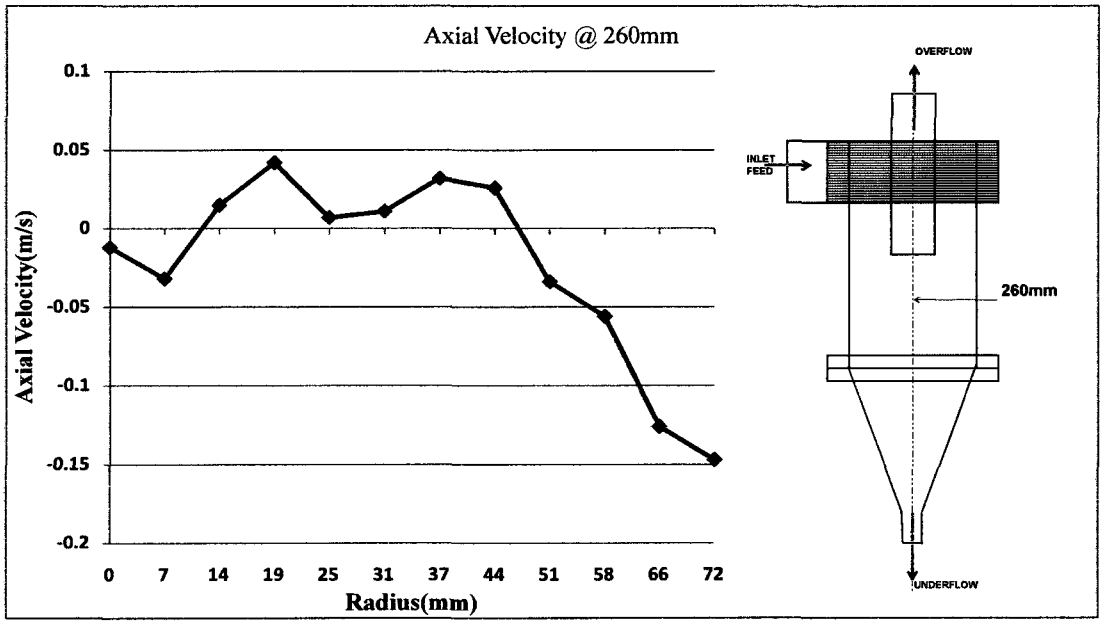

Figure 4.53 Axial velocity profile at Z=260mm (Case B, probe tilted 45°)

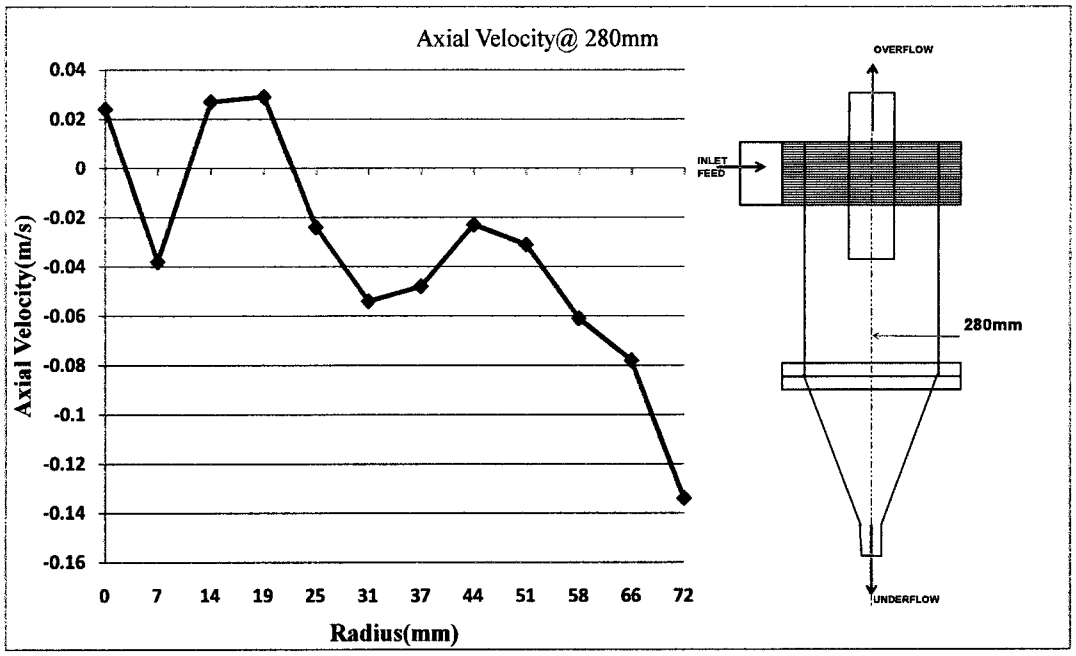

Figure 4.54 Axial velocity profile at Z=280mm (Case B, probe tilted 45°)

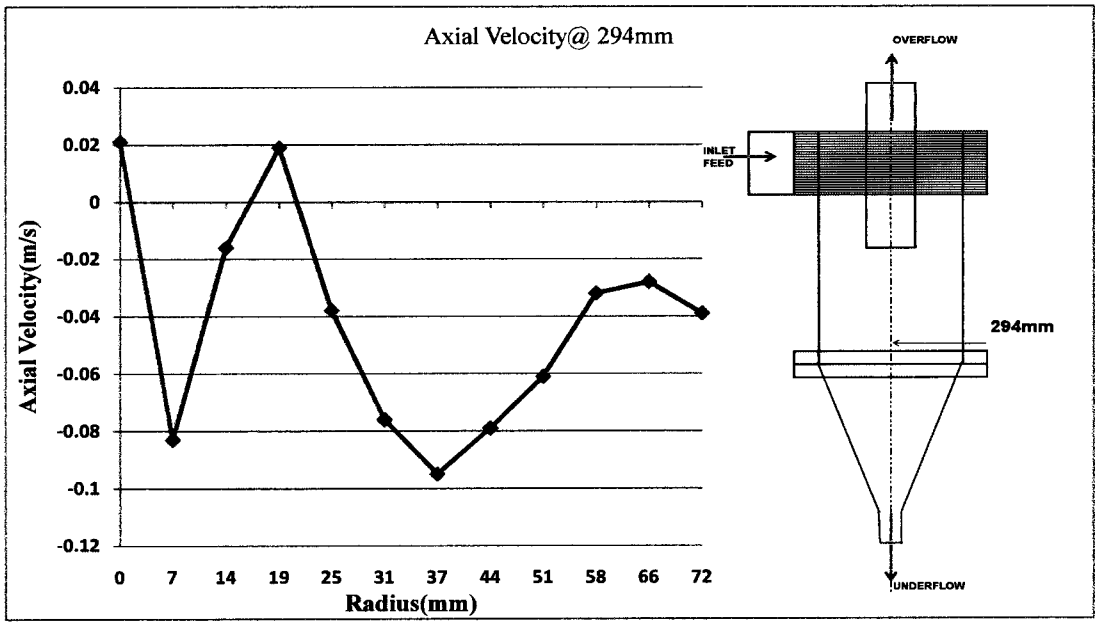

Figure 4.55 Axial velocity profile at Z=294mm (Case B, probe tilted 45°)

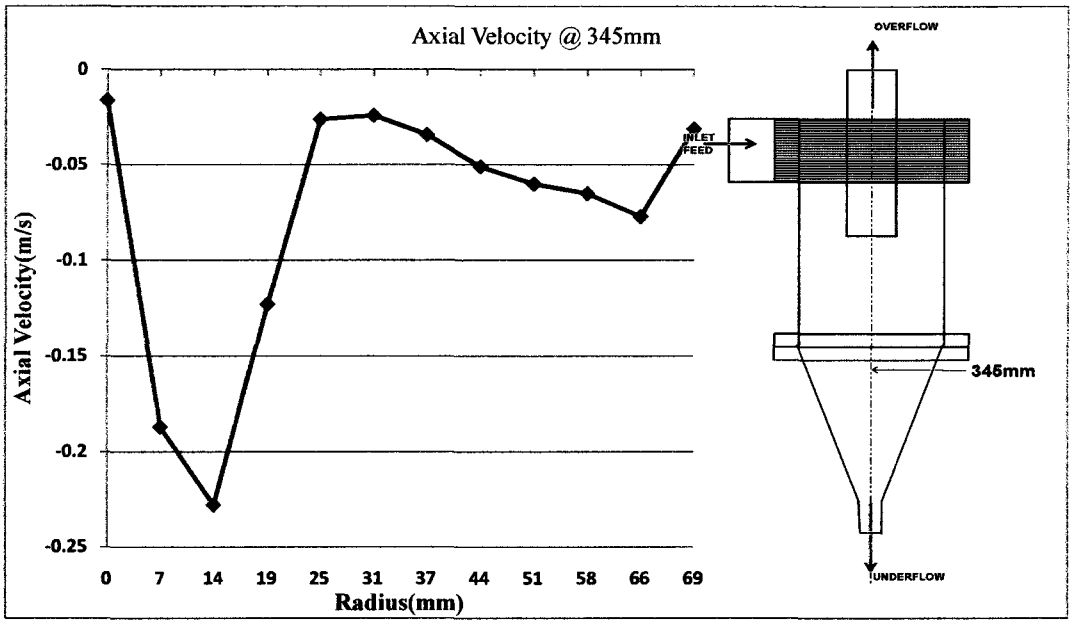

Figure 4.56 Axial velocity profile at Z=345mm (Case B, probe tilted 45°)

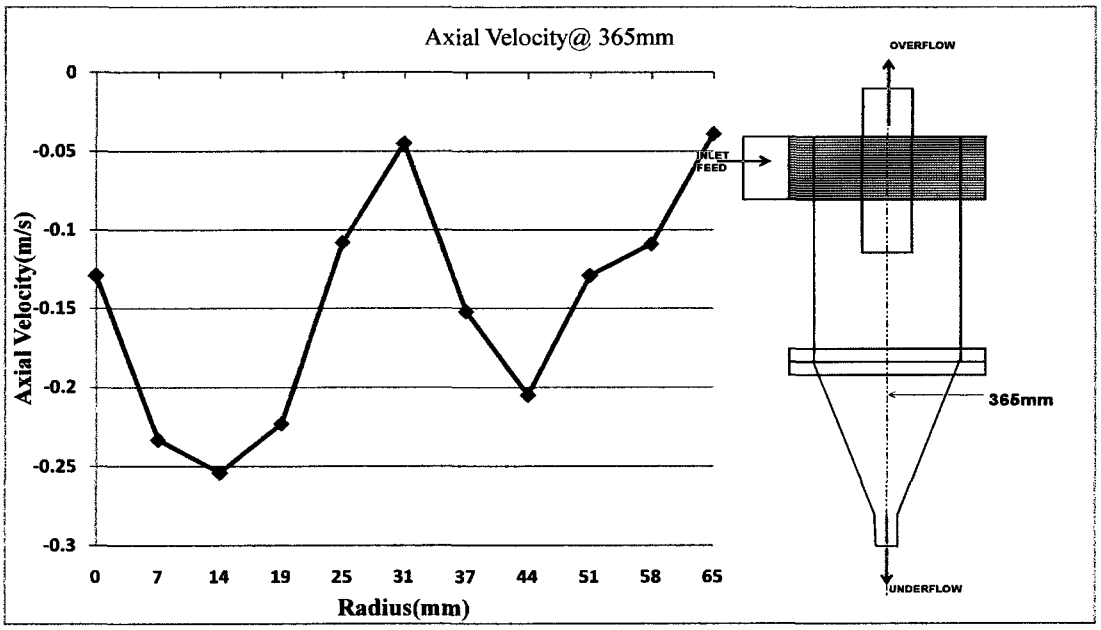

Figure 4.57 Axial velocity profile at Z=365mm (Case B, probe tilted 45°)

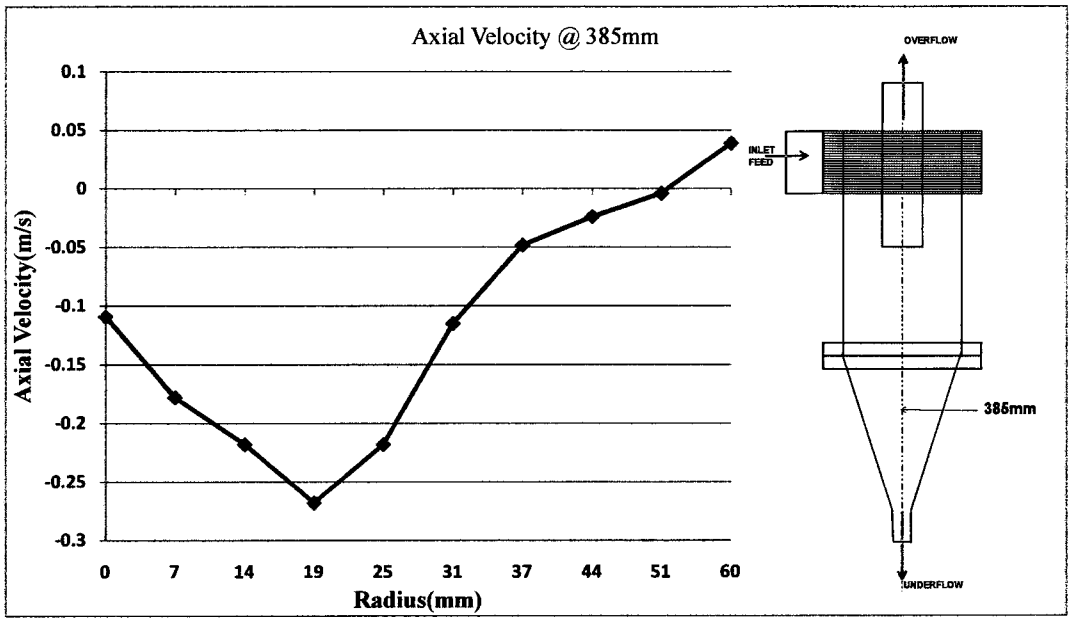

Figure 4.58Axial velocity profile at Z=385mm (Case B, probe tilted 45°)

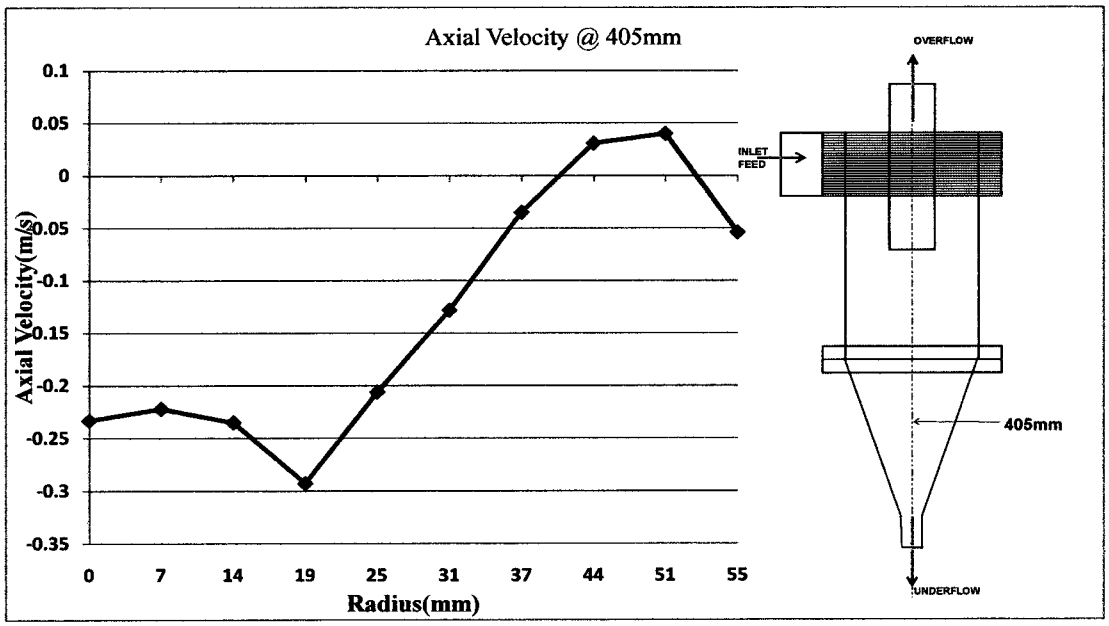

Figure 4.59 Axial velocity profile at Z=405mm (Case B, probe tilted 45°)

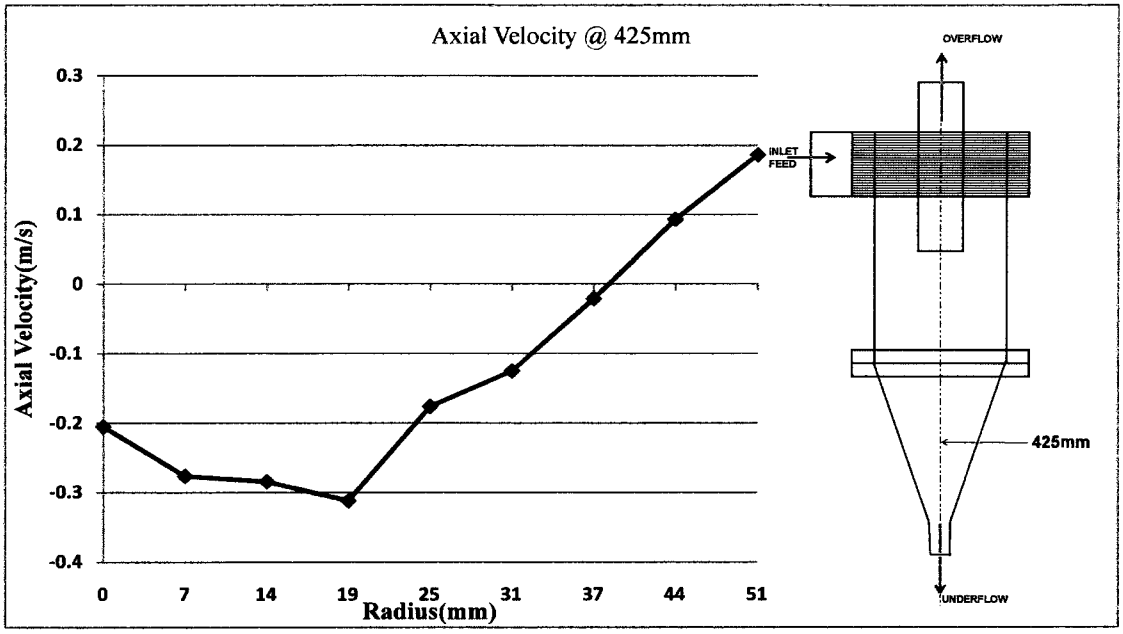

Figure 4.60 Axial velocity profile at Z=425mm (Case B, probe tilted 45°)

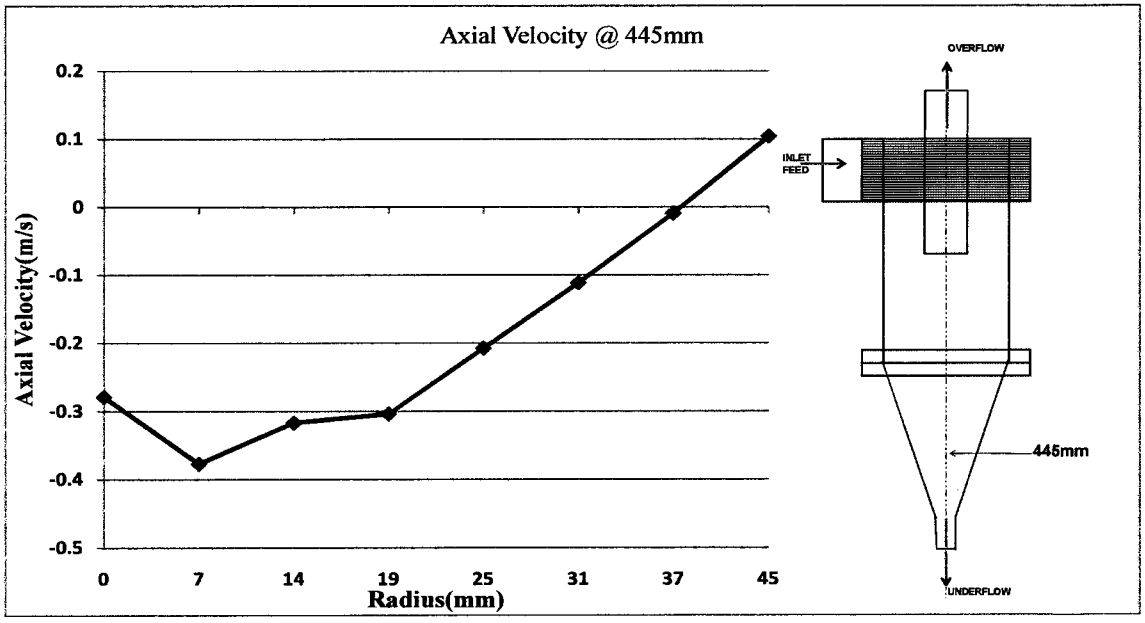

Figure 4.61 Axial velocity profile at Z=445mm (Case B, probe tilted 45°)

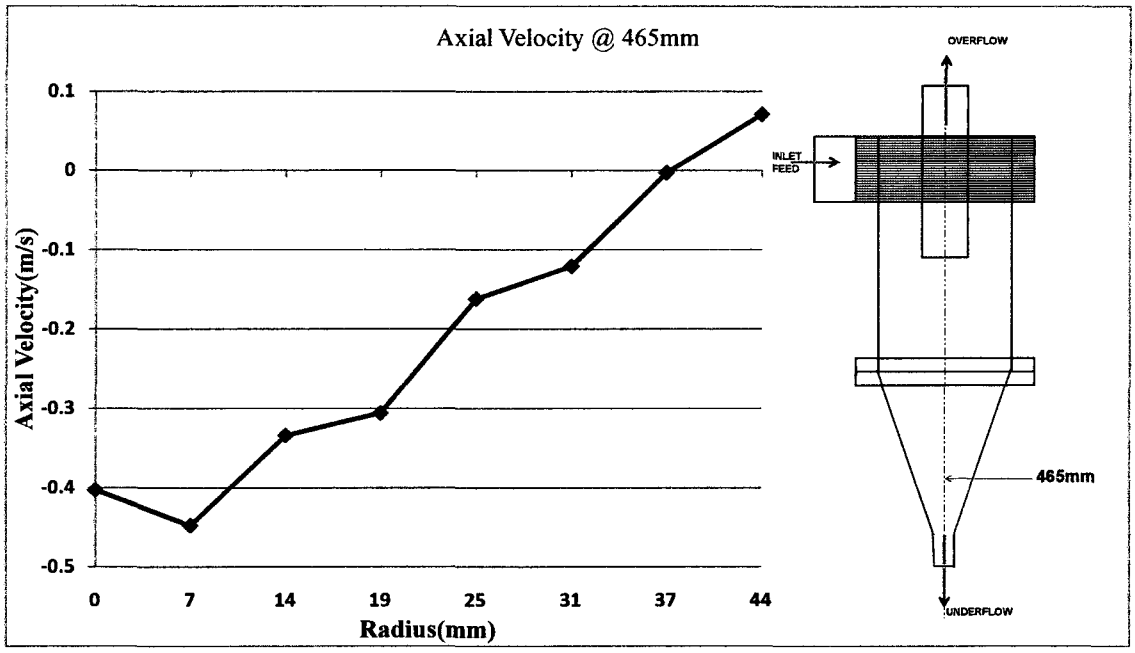

Figure 4.62 Axial velocity profile at Z=465mm (Case B, probe tilted 45°)

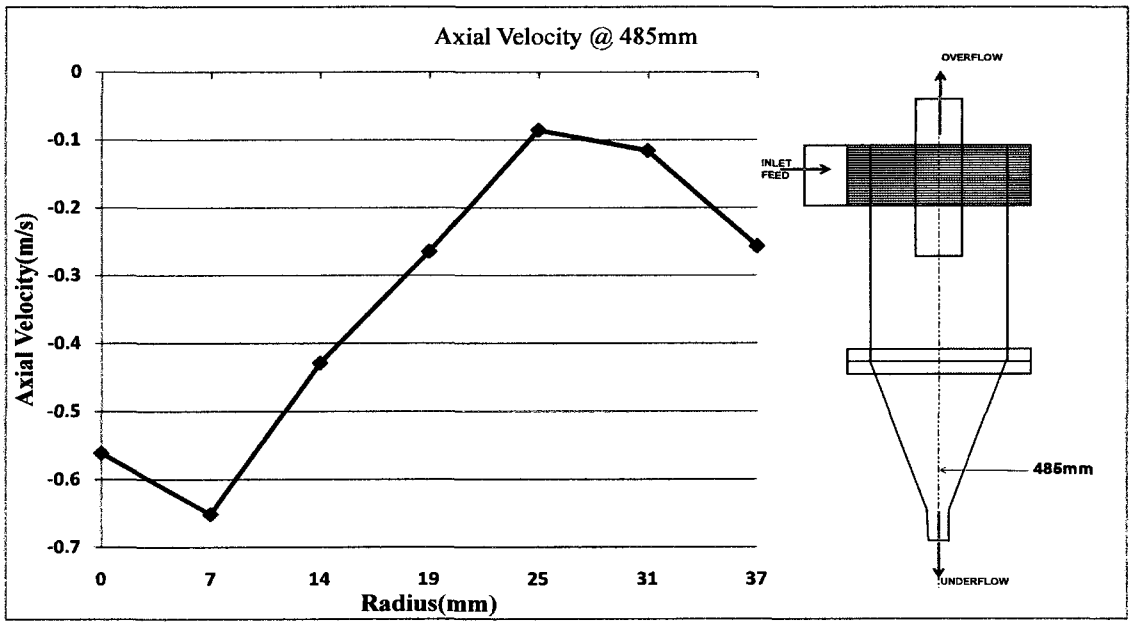

Figure 4.63 Axial velocity profile at Z=485mm (Case B, probe tilted 45°)

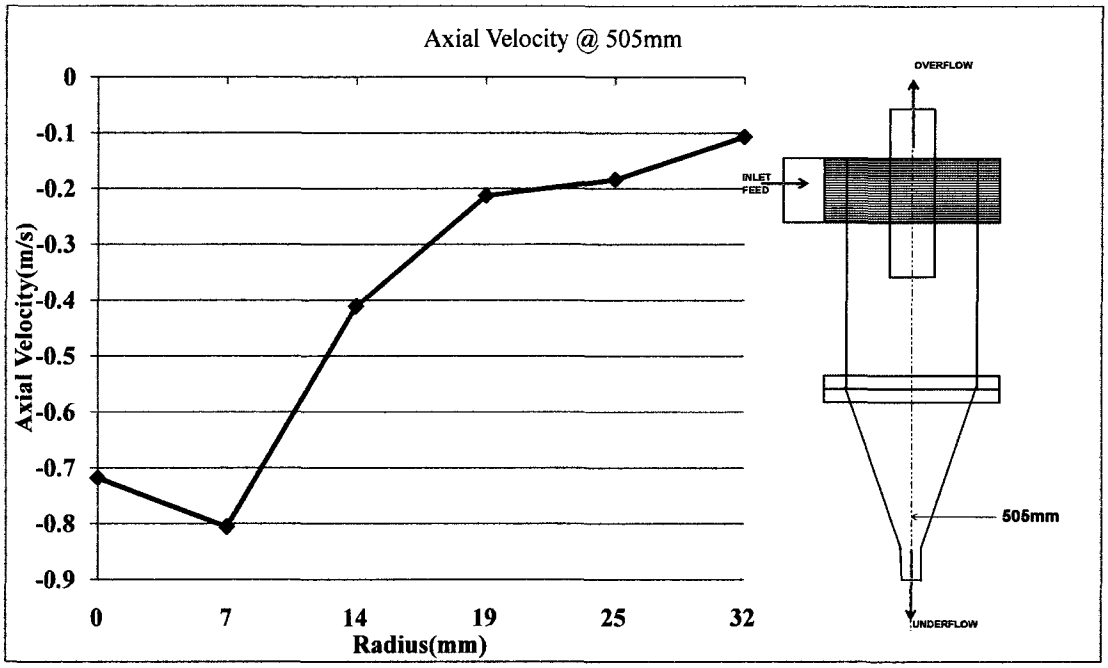

Figure 4.64 Axial velocity profile at Z=505mm (Case B, probe tilted 45°)

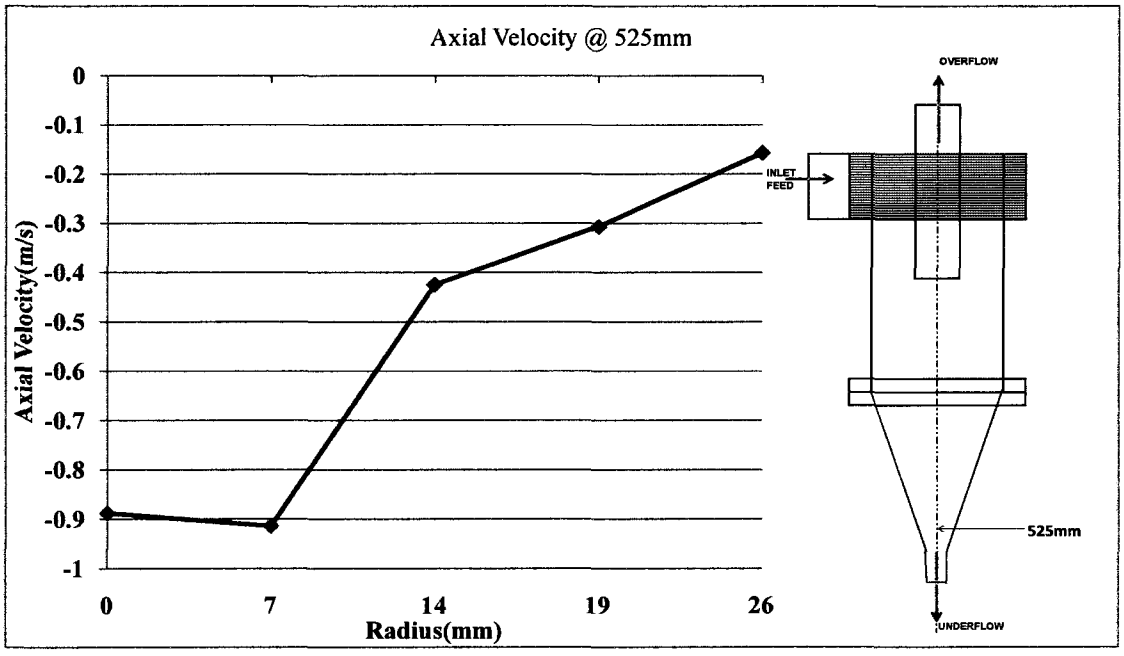

Figure 4.65 Axial velocity profile at Z=525mm (Case B, probe tilted 45°)

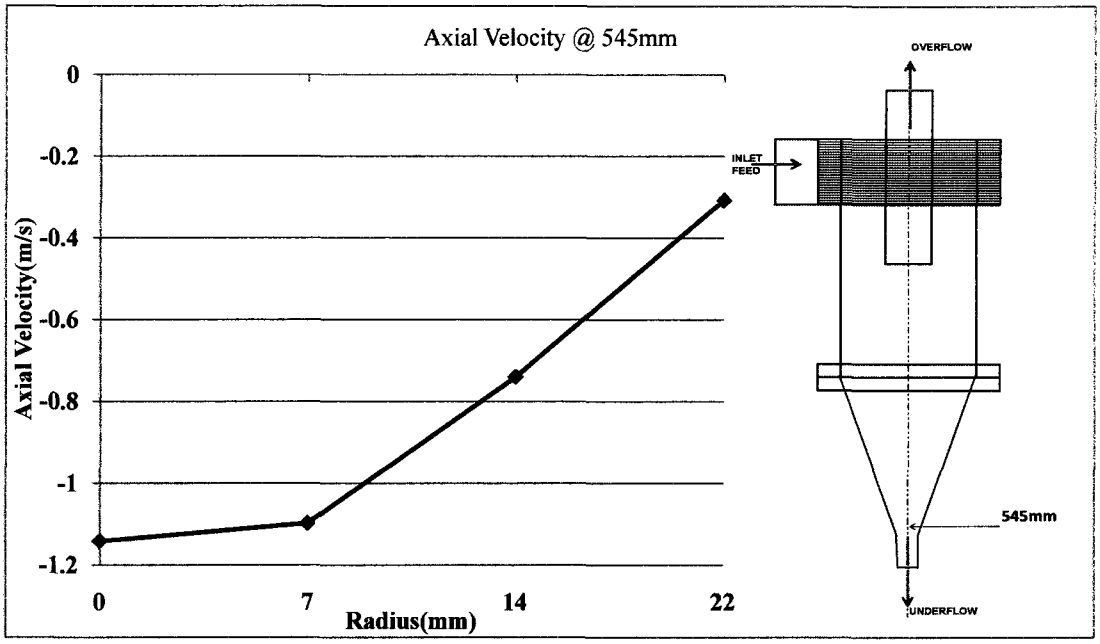

Figure 4.66 Axial velocity profile at Z=545mm (Case B, probe tilted 45°)

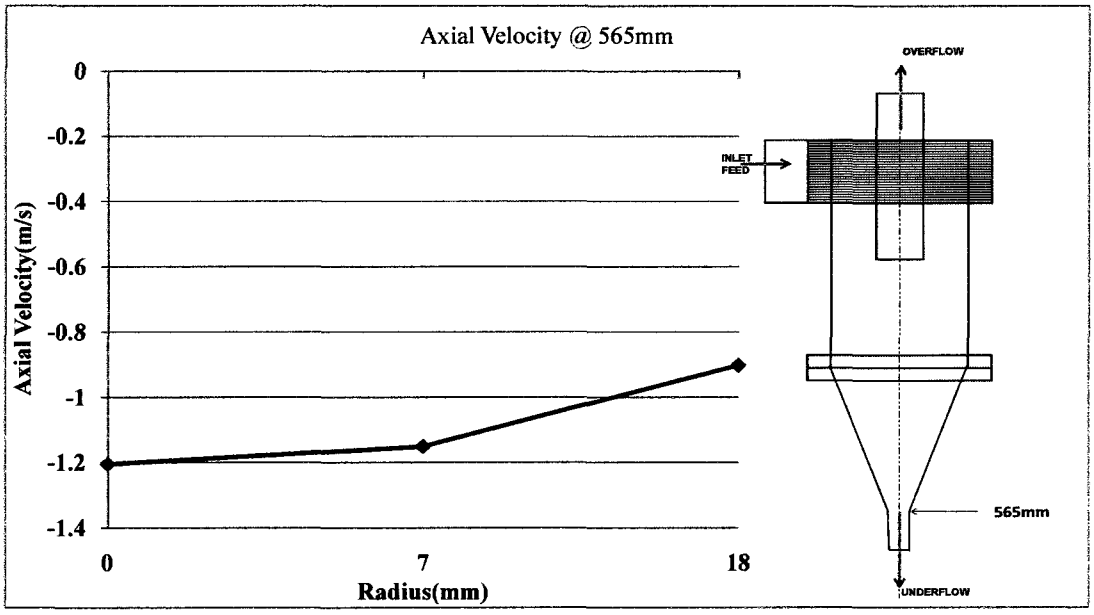

Figure 4.67 Axial velocity profile at Z=565mm (Case B, probe tilted 45°)

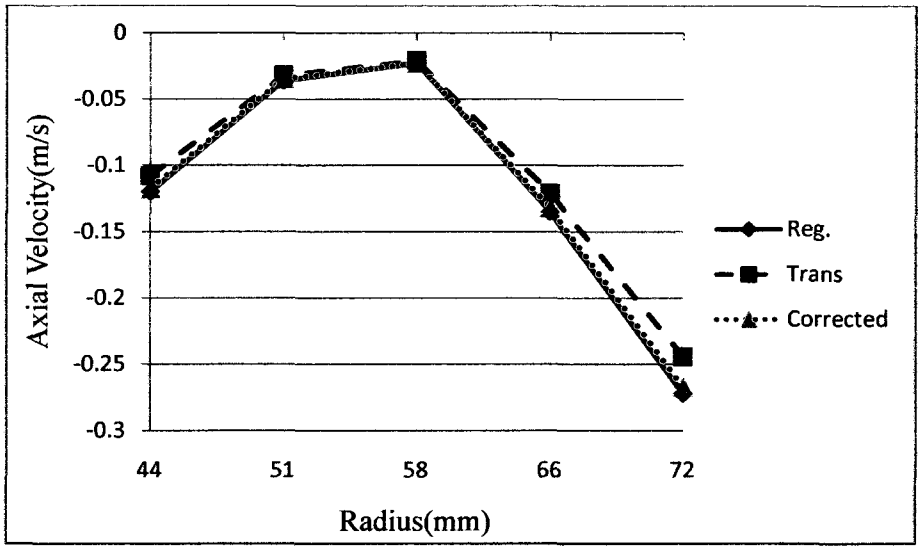

Figure 4.68 Axial velocity profiles comparisons at Z=140mm

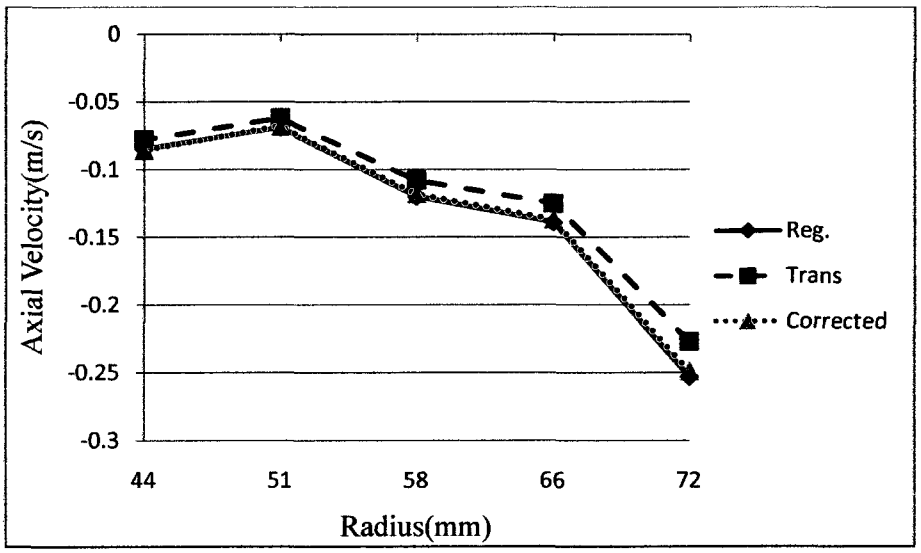

Figure 4.69 Axial velocity profiles comparisons at Z= 160 mm

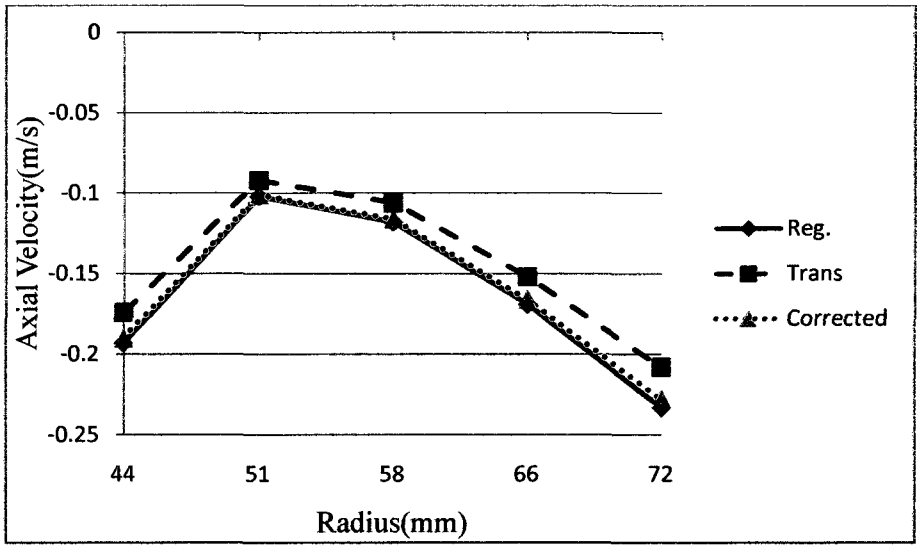

Figure 4.70 Axial velocity profiles comparisons at Z=187mm

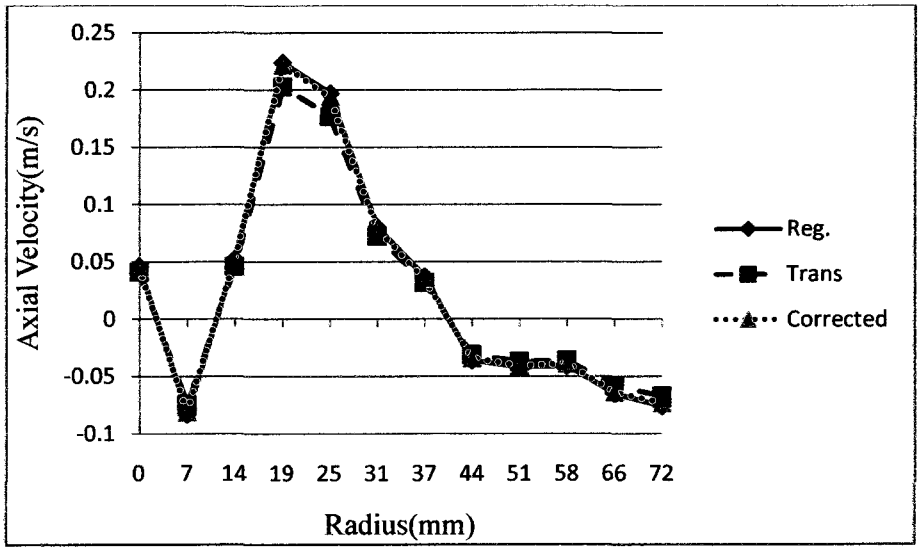

Figure 4.71 Axial velocity profiles comparisons at Z=200mm

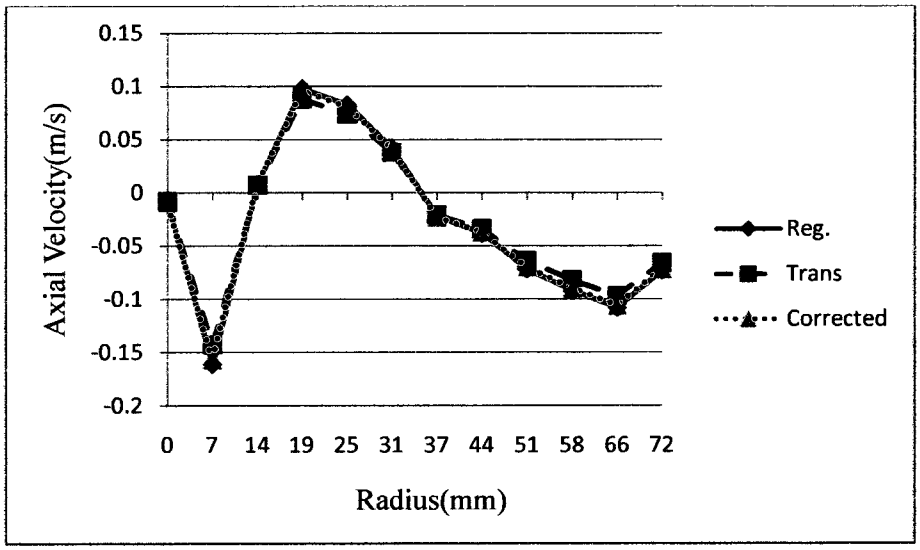

Figure 4.72 Axial velocity profiles comparisons at Z=220mm

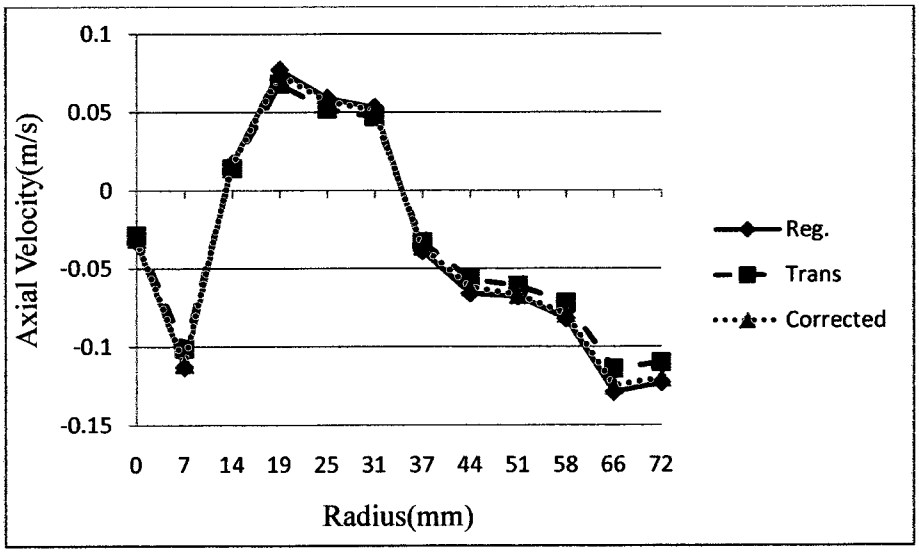

Figure 4.73 Axial velocity profiles comparisons at Z=240mm

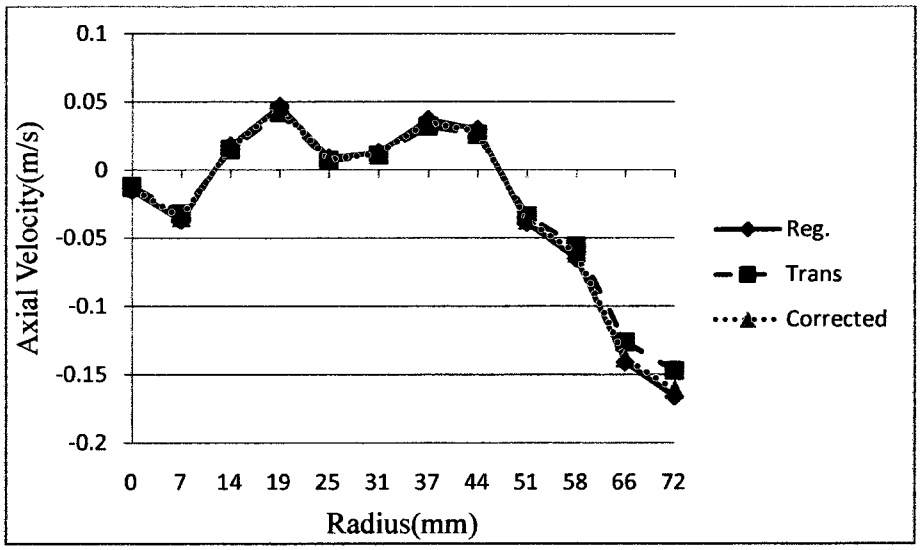

Figure 4.74 Axial velocity profiles comparisons at Z= 260mm

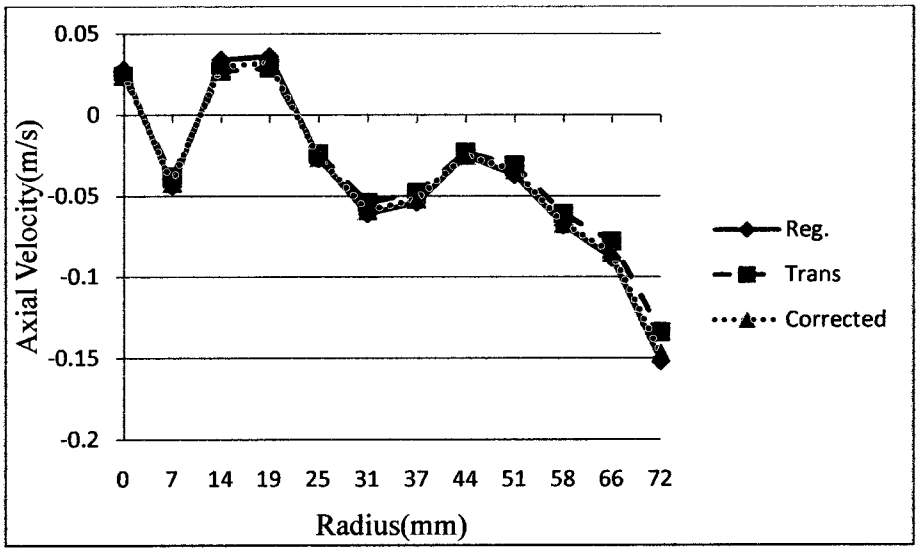

Figure 4.75 Axial velocity profiles comparisons at Z= 280mm

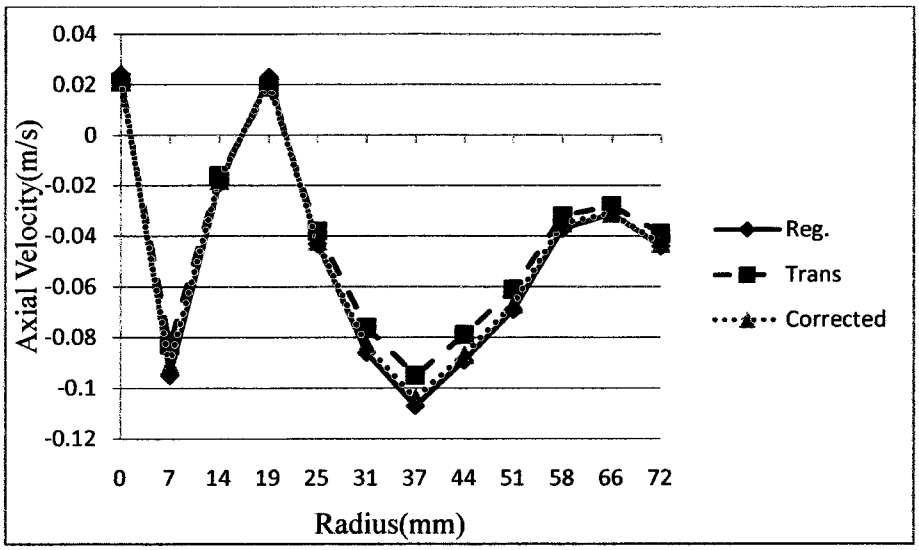

Figure 4.76 Axial velocity profiles comparisons at Z=294mm

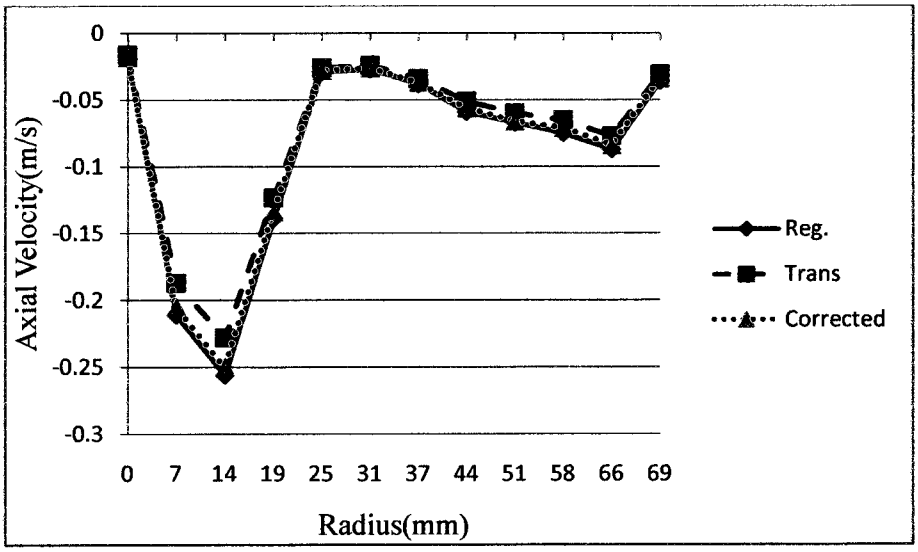

Figure 4.77 Axial velocity profiles comparisons at Z= 345mm

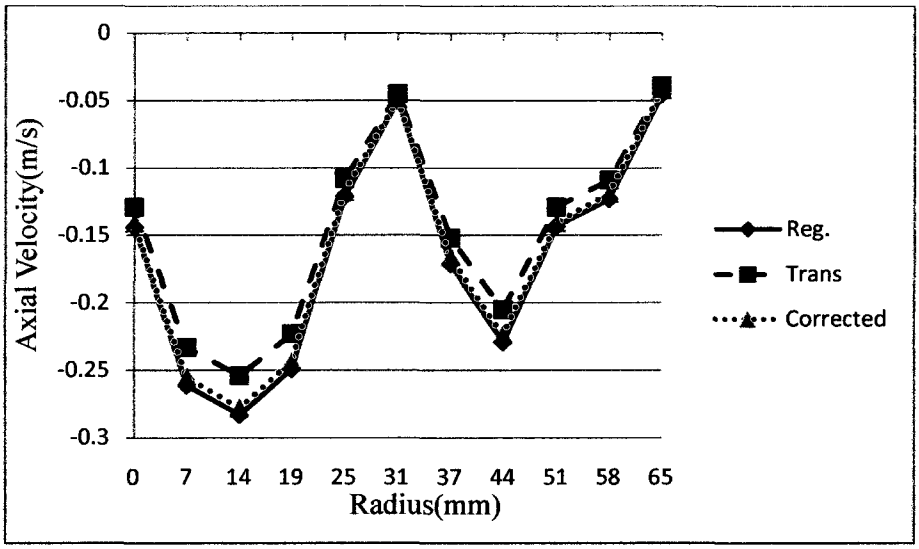

Figure 4.78 Axial velocity profiles comparisons at Z=365mm

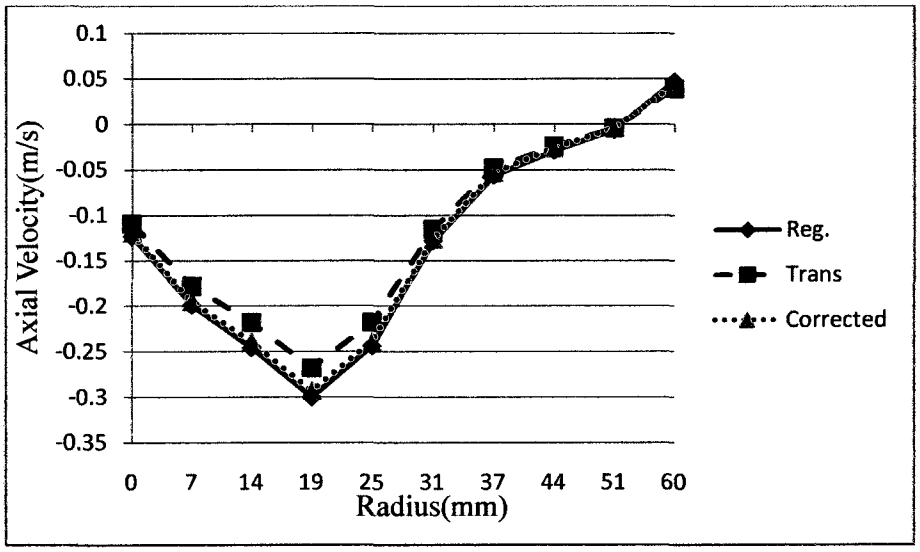

Figure 4.79 Axial velocity profiles comparisons at Z=385mm

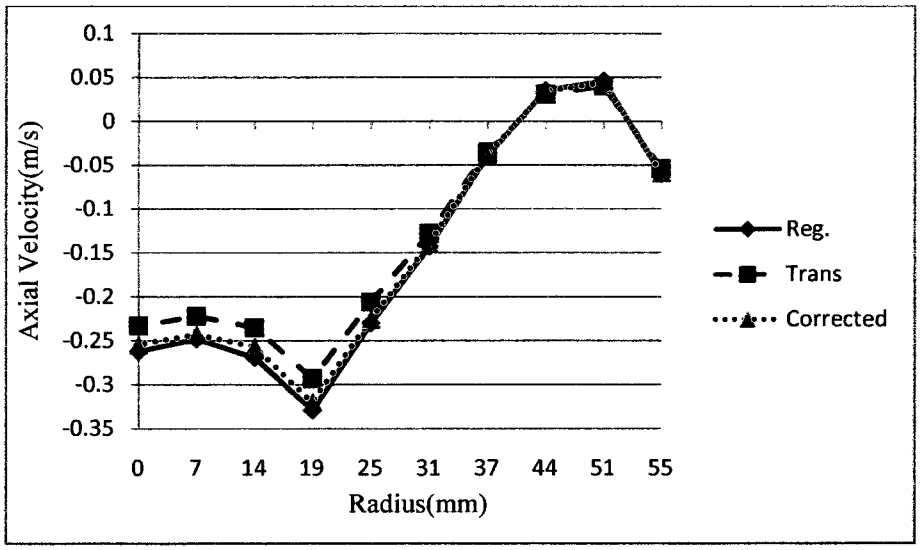

Figure 4.80 Axial velocity profiles comparisons at Z= 405mm

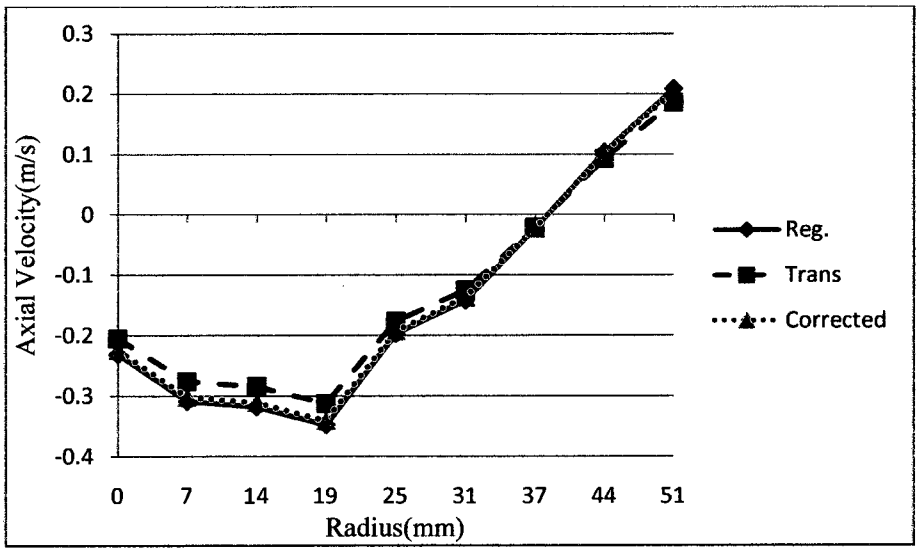

Figure 4.81 Axial velocity profiles comparisons at Z= 425mm

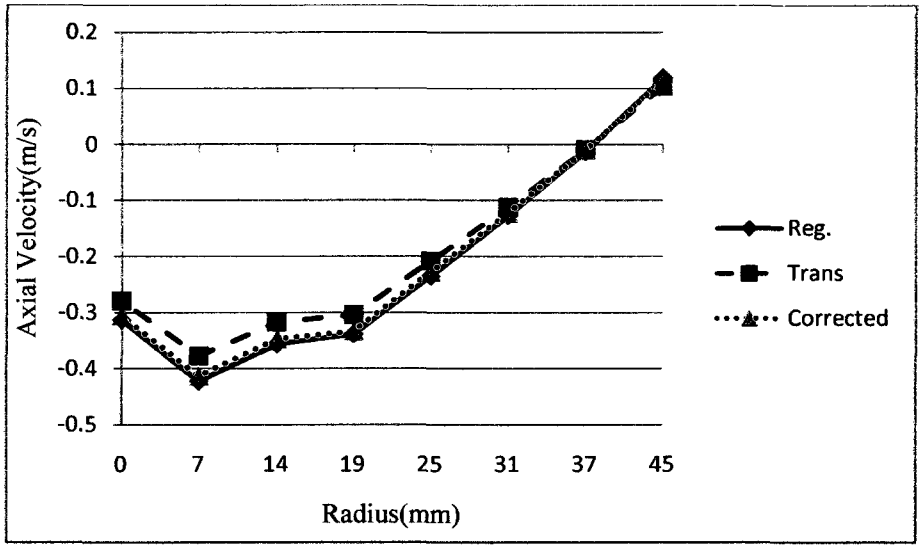

Figure 4.82 Axial velocity profiles comparisons at Z= 445mm

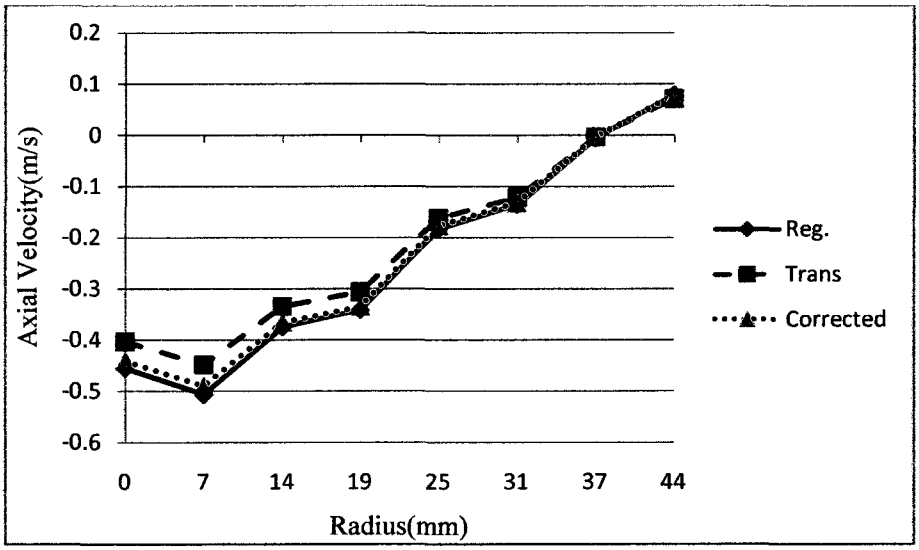

Figure 4.83 Axial velocity profiles comparisons at Z=465mm

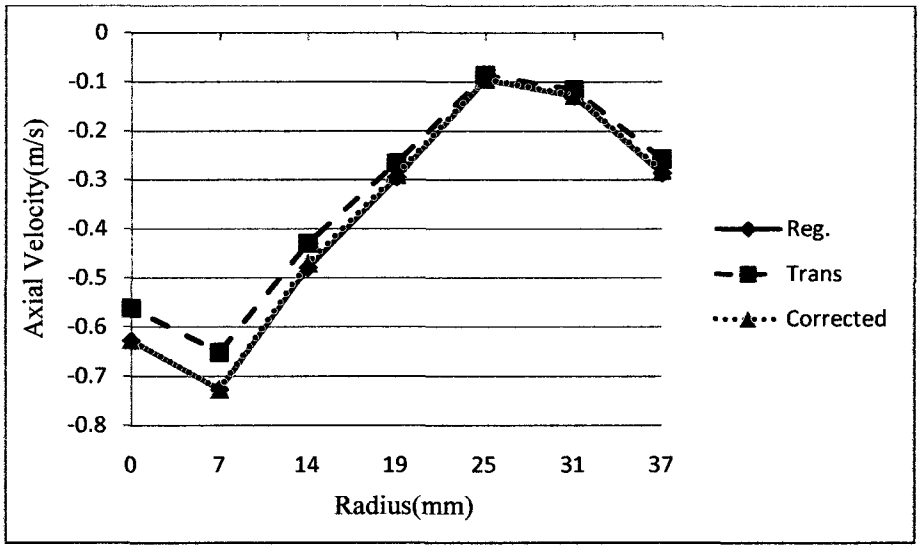

Figure 4.84 Axial velocity profiles comparisons at Z= 485mm

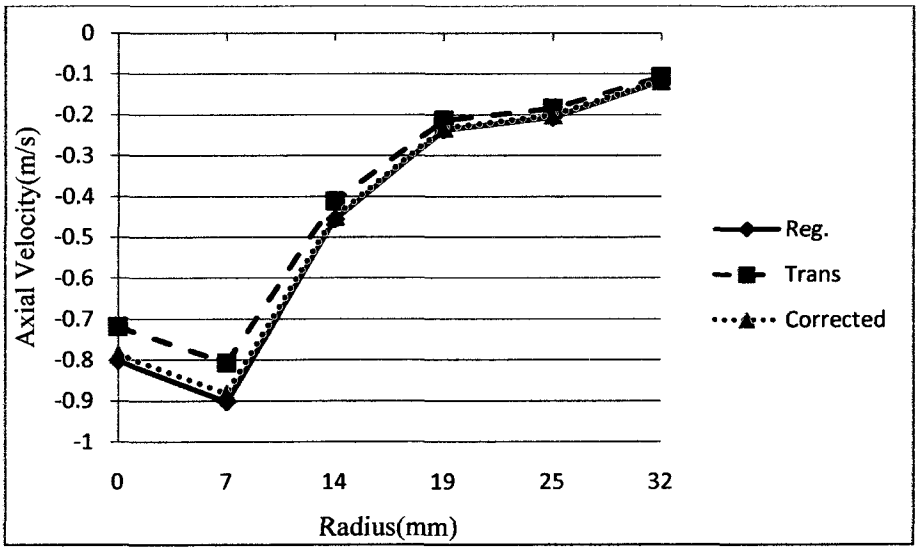

Figure 4.85 Axial velocity profiles comparisons at Z= 505mm

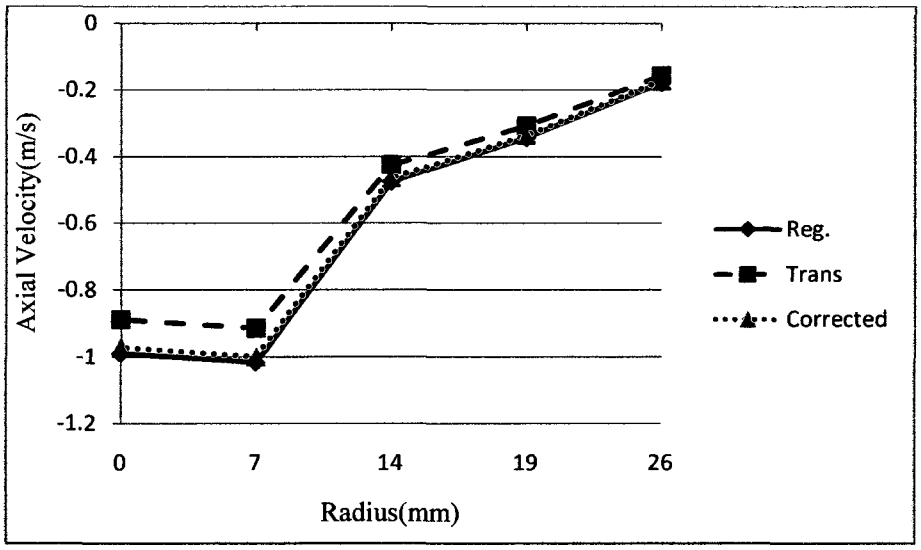

Figure 4.86 Axial velocity profiles comparisons at Z= 525mm

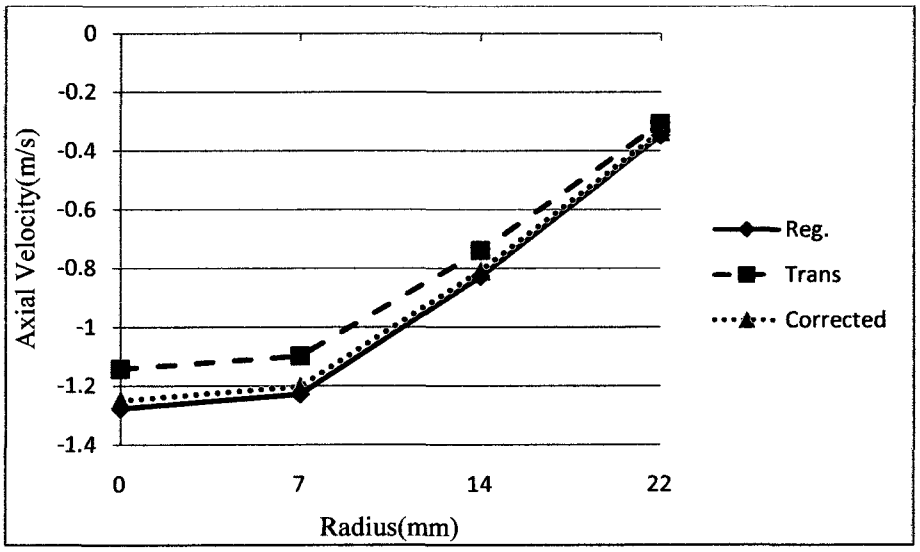

Figure 4.87 Axial velocity profiles comparisons at Z=545mm

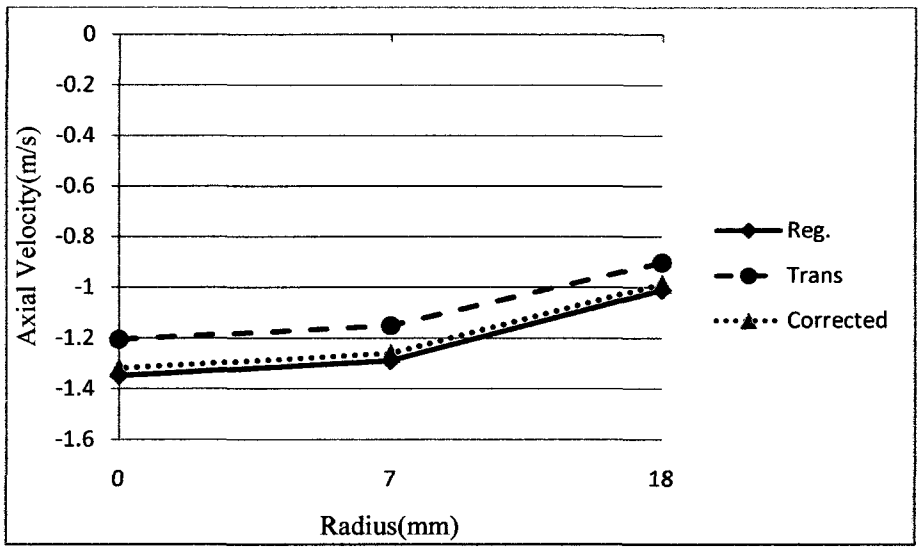

Figure 4.88 Axial velocity profiles comparisons at Z=565mm

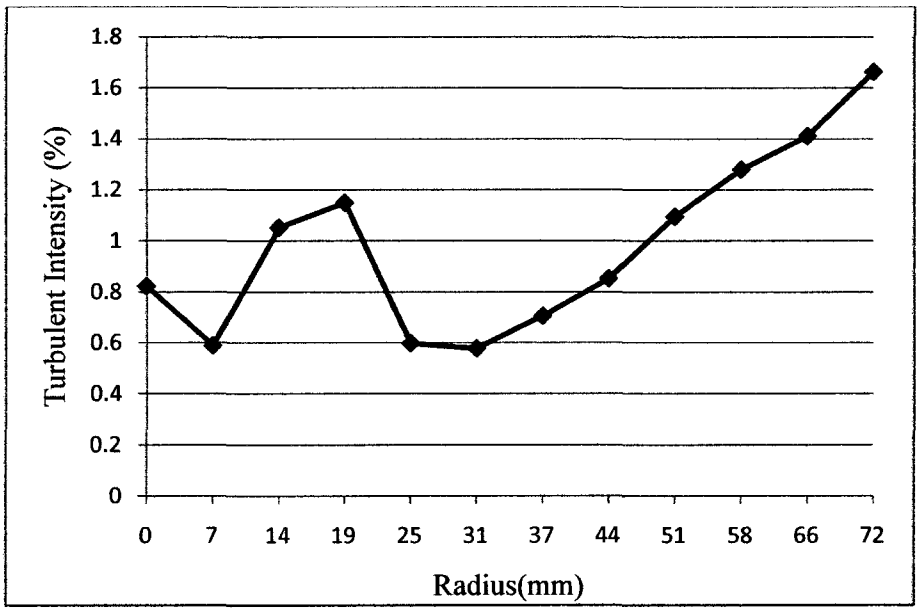

Figure 4.89 Turbulent Intensity at axial level Z = 280mm (case B)

Chapter 5

Result and discussion of Flow Visualization Studies

The qualitative flow patterns in a 6″ hydrocyclone were examined by droplet dye (a nail polish) injection. It permitted the visualization of the flow. The selected dye approved to be cohesive for sufficient time in water and it did not instantly dissipate. Therefore, it was easy to trace the trajectory of droplet dye within hydrocyclone. The results were filmed in a video. The objectives of these studies were:

1) Investigate the flow field patterns of 6″ hydrocyclone under the specified operating conditions.
2) Determined the number of turns made by flow in this hydrocyclone.

As stated earlier, a small tapping ($^1/_4$″) in the cylindrical wall, 125 mm below the roof of hydrocyclone was used to inject the droplet dye from the wall (Fig. 3.20) using a syringe and a video recording was obtained to investigate the two aforementioned objectives . Although the visual and video observations covered the regions below the tapping point that include part of cylindrical part and the entire conical part , the trajectories of dye droplet were visible and covered the entire hydrocyclone which enable to clearly observe the flow motions (Fig. 5.1) . The experiments were conducted at a low speed flow.

5.1 Flow Field Patterns:

It was observed from recorded video that the swirl flow initially develops against the outer wall and moves downward to the apex discharge. The droplet dyes are going down through the boundary layer and joining the underflow. But, a part of the droplet dyes comes out of the boundary layer and join the overflow and some of it trapped in a multi circulation zone. One of the main flow features in all hydrocyclones (Figs. 1.1 and 1.2) is the occurrence of a downward helical flow in the outer region and an upward helical flow in the centre (core) region. These are the major flow field patterns in a hydrocyclone. The followings were summarizing the flow field patterns that observed from the droplet dye movements (Fig. 5.2):

1- Part of the flow moves against the outer wall and leave from the underflow outlet.
2- Part of the flow reverses its direction at region in the conical part and joins the upward flow to the vortex finder (overflow).
3- Some flow goes through the short circuit flow and proceeds downward along the outside wall of vortex finders and join the upward flow (overflow).
4- Some droplets of the dye trapped in eddies formed multiple circulation zones (mantles) between the cylindrical part and the upper part of conical section.
5- A flow reversal within the vortex finder causes an annular flow countercurrent to the upward swirling flow which contains the axis (Fig. 5.2).

These quantitative visualizations are consistent with the results of other investigators (Bradley (1965), Dabir and Petty (1986), Bhattacharyya (1984),

Trawinski (1984)). With the experimental operating conditions presented in this study(Chapter 3), that is; low velocity flow and 50% of flow reported to overflow and 50% to the underflow, the results of flow visualization elaborate the flow field patterns and the droplets dye injection enable to capture these flow patterns easily.

Fig. 5.2 illustrates the flow patterns within the 6″ hydrocyclone. An interesting flow pattern occurred at centre of hydrocyclone between the apex and vortex finder. A downward annular flow countercurrent to the upward flow on the axis, which is contrary to the regular one shown in Figs. 1.1 and 1.2. Dabir (1983) was the first researcher who discovered such reversal flow within the vortex finder due to a 2:1 contraction he used (Fig. 2.13). For the present flow conditions (Chp.3), the valves at the overflow and underflow outlets were partially opened to control the flow and to eliminate the air core within hydrocyclone, therefore, the downward flow at the axis occurred due to changes in part of flow directions at the bend piece at top of vortex finder as shown in Fig. 5.1. Dabir (1983) had confirmed that the reversal flow within vortex finder still possible, without a 2:1 contraction in vortex finder, but it contain the axis, which happened in this study. It is noteworthy that the downward swirling flow in the centre runs countercurrent to an upward outer flow between the apex and vortex finder, which is contrary to that finding by Dabir (1983)(Fig. 2.13), which caused by a 2:1 contraction in vortex finder in his 3″ hydrocyclone.

Comparing the velocity profiles (Chapter 4) and the flow patterns found in the flow visualization experiment, there are good agreements. As mentioned earlier; the negative magnitudes of axial velocity refers to the downwards flow, while the positive values show the upwards flow, which indicates the presence of two

recirculation flows. For region above the vortex finder, the axial velocity has negative values (Figs. 4.47- 4.49), therefore , the entire flow moves downward, while the values below the vortex finder (Figs. 4.50 - 4.57) indicated that the flow goes downward near the wall and upward toward the centre. These kinds of flow represented the one visualized in this experiment (refer to the recirculation flow) and the locus of zero axial velocity (LZXV) moves toward the centre as the flow moves downward until it reaches an axial plane Z=385mm when the flow changed again its direction; upwards near the wall and downwards near the centre. Below axial level Z= 505mm the flow is downwards discharged through underflow outlet (apex), which in consistent with the observation of dye motions in this experiment.

The phenomenon of short circuit is obvious in the video observation and the tangential velocity profiles (Figs. 4.26 to 4.28) depict the trends of this kind of flow that is popular in all hydrocyclones and cyclones.

5.2 The parameter N_t denoting the number of turns in the Hydrocyclone

As illustrated in section 2.5, number of turns made by fluid is an important factor to determine the cut size, thus the separation efficiency in a gas cyclone (Eq. 2.3). In this experiment the number of turns made by fluid was determined by visual observation and compared with some approximate mathematical computations, the details in Appendix 2. This attempt is a contribution to provide an experimental data for this key parameter "N_t" that might be useful for researchers

who look to develop an expression for the separation efficiency of hydrocyclone using the one applied in the gas cyclone (section 2.5).

5.3 Conclusion of flow visualization experiment:

The objectives of flow visualization experiment was firstly to qualitatively investigate the flow field patterns of the 6″ hydrocyclone and to compare the results with that measured quantitatively in the experimental study (Chapter 4) using LDA, and secondly, to determine the number of turns made be fluid within a hydrocyclone, which could be used to compute the separation efficiency of a hydrocyclone.

5.3.1 Flow Patterns:

The use of dye for flow visualization enables to obtain information where velocities are generally low, which help clarifying the behavior of the flow field patterns. Results of this research show that the flow pattern inside hydrocyclone is very complicated. Changes in a hydrocyclone geometry or / and operating conditions cause different flow patterns.

Several reverse flows may occur in the upper portion of the conical part, multiple eddies or recirculation zones were occurred in the cylindrical part. The outer primary vortex is moving downwards from the feed level to the apex discharge and the inner or secondary vortex is moving upwards from underflow to overflow outlet. These two countercurrent vortex system generate eddies in the sense of turbulence.

Therefore, the presence of multiple recirculation zones or eddies is inevitable in practice. These eddies should be kept stable, otherwise the separation become unsatisfactory, smooth flow conditions therefore are important, especially in the region, where the feed and overflow outlet are situated. Generally speaking, the flow in the central core region should be kept stable to achieve sufficient performance (Dabir 1983, Bhattacharyya 1984, Bradley 1965).

The qualitatively results of flow visualization experiments validate the quantitatively measurements of mean velocities using LDA. Resulted flow patterns consistent with the findings of previous authors.

The important conclusion from Fig. 5.2 is that the annular downwards reverse flow in the hydrocyclone centre unambiguously comes from the outer flow above the vortex finder tube rather than inside the vortex finder which affects the flow patterns throughout the hydrocyclone. However, the effect of this interesting result on the hydrocyclone performance obviously deserves further study. The aim of this research was focused on studding the flow field patterns of water (without slurry) inside a hydrocyclone to provide some understanding of the flow types and measured experimentally the mean velocities within a specific operating conditions.

Figures Chapter 5

Figure 5.1 Flow visualization using droplet dye injection

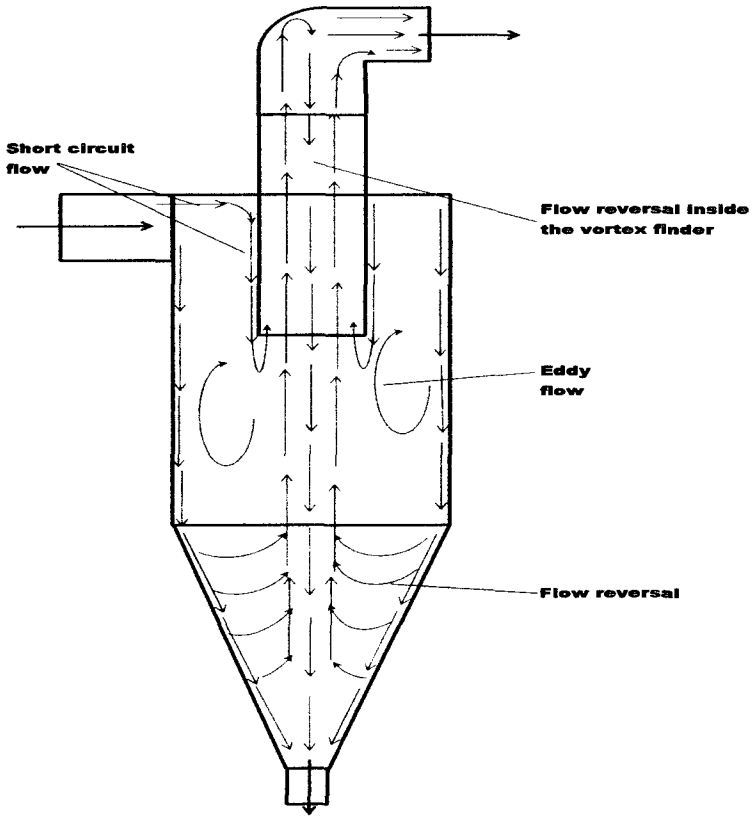

Figure 5.2 Flow field patterns as concluded from flow visualization experiment

Chapter 6

Simulation of Flow Patterns by CFD

6.1 Introduction

Computational Fluid Dynamics (CFD) is a versatile means to predict the characteristics of flow in fluid mechanics problems under a wide range of design and operating conditions. Applying the CFD in many engineering fields alleviates the problem of the usual engineering design. Recent advance in computational methods and computer technology make CFD an efficient means to study the dynamics of many physical systems.

Applications of CFD to simulate the specific flows in hydrocyclones have been examined by several researchers (Hsieh and Rajamani (1988 & 1991), Devulapalli and Rajamani (1994), Sevilla and Branion (1997), Cullivan et al. (2003), Schuetz et al. (2004), Narasimha et al. (2005), Nowakowski et al.(2004), Delgadillo and Rajamani (2005), Wang and Yu (2006 & 2008), Sripriya et al. (2007), Wang et al. (2007) and Hsu and Wu (2008)).

The objective of this short study simulation is to investigate the flow patterns in a 6″ hydrocyclone by CFD software package FLUENT (version 6.3.26) and to compare the numerical results with the experimental data related to LDA measurements of velocity.

6.2 Meshing and Boundary types

GAMBIT, which is the main preprocessor of FLUENT, was used to create geometry, specifying boundary types and meshing of hydrocyclone. Fig. 6.1 depicts the created geometry and Fig. 6.2 illustrates the meshing geometry. The simulation conducted in this chapter used some assistance provided by Dr. José Angel Delgadillo Gómez (Profesor Investigador, Universidad Autónoma de San Luis Potosí, Mexico) related mainly to the complex mesh generation and related computational procedures.

The numerical grids were developed three-dimensionally in an unstructured manner with meshing size equal 256,800 elements. For meshing, hexahedral mesh were used for cylindrical part, conical part, inlet, overflow and underflow sections of hydrocyclone as shown Figs. 6.3 and 6.4.

Boundary types are considered as mass flow for inlet, overflow and underflow as outflow. The flow rate of feeding inlet, overflow and underflow were known from the experimental data. The body of the hydrocyclone is considered as wall boundary type. FLUENT can read the created meshing geometry by GAMBIT and proceed with the simulation of the model.

6.3 Computational Modeling

According to Nowakowski et al. (2004) and Cullivan et al. (2003) the full three-dimensional modeling is essential in order to accurately model the hydrocyclone flow field; therefore, 3D modeling was used in this study. The flow pattern in hydrocyclone was modeled by Reynolds Stress Model (RSM). RSM can describe

the swirl flow field in a hydrocyclone accurately (Wang et al. (2007) and Schuetz et al. (2004)), especially in absence of an air core.

The applied solution parameters were PRESTO scheme, First Order Upwind and SIMPLEC discretization type for momentum and stress equations.

Hsu and Wu (2008), Wang et al. (2007) and Zhang (2005) illustrate the RSM governing equations which will be solved by FLUENT 6.3.26. The presence of air-core interface in hydrocyclone makes the flow unsteady and by removing the air-core, as in this study, makes the solution steady state. It took 30,000 iterations to converge for the single phase flow (water only) simulation.

6.4 Simulation results for velocities

In FLUENT, the contour and vector plots were used to analyze the simulation results. Some measured data in the experimental study as well as the operating conditions (Chp.3) were used in the FLUENT simulation as follows:

- Feed flow rate was 2.32×10^{-3} m^3/s.
- 50% of flow passed out as the overflow and 50% passed out as the underflow.
- The system operated without an air core using water only (single phase).

6.4.1 Flow Patterns

Figs. 6.5 and 6.6 illustrate the model predicted contours and vectors of velocity magnitudes of flow field patterns within hydrocyclone. The comparison with the test data are provided subsequently. The velocity vector displays some of the

minor flow patterns in the hydrocyclone flow field. As observed in Fig. 6.5, the velocity magnitude is more at the underflow section. Below the vortex finder of the hydrocyclone, the velocity magnitude is medium at some middle section and has minimum magnitude at the centre axis and at the upper portion of vortex finder. As described in the flow visualization study (Chp.5), the predicted flow by CFD matching with that observed earlier and for clarifying purposes, it will be discussed according to the types of flow pattern presented in Chp.5.

6.4.1.1 Short Circuit

Figs. 6.7 and 6.8 depict the short circuit phenomenon. The fluid is seen flowing downward along the outer wall of vortex finder and merges with the upward flow at the tip of vortex finder, which was observed in the flow visualization experiment (Chp.5) and this complied with the experimental data (Chp.4).

6.4.1.2 Eddy Flow

Figs. 6.9 and 6.10 show the recirculation (eddy) flows or eddies. A recirculation zone is seen clearly in the velocity vector plot (Fig. 6.9) at regions below the vortex finder which is in good agreement with the experimental results presented earlier.

6.4.1.3 Reversal Flow

Figs. 6.11 and 6.12 illustrate the reversal flow at the upper portion of conical part. As observed earlier, the flow reverses its direction along the wall of conical part (Fig. 6.12). This flow pattern is a common trend in all hydrocyclones.

6.4.1.4 Downward Reversal Flows within Vortex Finder

Figs. 6.13 to 6.16 show the small quantity of downward swirling flow in the centre runs countercurrent to an upward outer flow between the apex and vortex finder. The blue vectors represented the minimum downward flow at the axis of hydrocyclone which crosses the hydrocyclone from top of the vortex finder (Fig. 6.14) and the underflow region (Figs. 6.15 and 6.16), while the outer upward flows (Fig. 6.15) appear diminished as the flow moves down at the apex discharge region (Fig. 6.16) where the fluid accelerated toward the underflow. This supports the observations that the flow reversed its direction at the upper portion of the conical part rather than at the deep region in the apex zone, as reported in a few previous studies (Dabir, 1983).

6.4.2 Tangential Velocity

Figs. 6.17 and 6.18 depict the contours and vectors of tangential velocity within hydrocyclone. Fig. 6.17 shows the maximum tangential velocity as on the regions below the vortex finder while the minimum occurs in blue at the central axis, within the tube of vortex finder and at the outside walls of hydrocyclone. The tangential velocity computed by FLUENT will be briefly elaborated in next section (6.5).

6.4.3 Axial Velocity

Figs. 6.19 and 6.20 show the contours and vectors of axial velocity within hydrocyclone. It is obvious from Fig. 6.19 that the minimum axial velocity occurs at the underflow discharge and varies between medium and high at the rest of

hydrocyclone body. The maximum axial velocity occurs at entrance of the vortex finder as clearly shown in Fig. 6.19. In the next section (6.5) the computed axial velocity data characteristics using FLUENT will be briefly described.

6.4.4 Radial Velocity

Although the radial velocities are not measured during this study, CFD enables to predict this important velocity as shown in Figs. 6.21 and 6.22. This velocity is smaller than the tangential and axial velocities but has great effects on separation efficiency of a hydrocyclone.

6.4.5 Total Pressure Contours

Fig. 6.23 illustrates the plot of total pressure inside hydrocyclone. This figure obviously reveals that the maximum pressure occurs at the outer wall and decreases toward the central axis, where the pressure has minimum magnitudes. Wall pressures could be measured using wall taps. The delays in getting the fabricated micro manometer system prevented the collection of test data for wall pressures.

6.5 Comparison with the Experimental Data

The magnitudes of velocity components were given in Tables 6.1 to 6.21. Figs. 6.24 to 6.44 show the tangential and axial velocity profiles in different sections and covering the full axial plane from wall to wall so as to examine the sort of symmetry within hydrocyclone. It is obvious that there is a good symmetry in the flow within hydrocyclone especially in the tangential velocity profiles, so only one half of the hydrocyclone is needed to record velocity profiles. However, the

axial velocity profiles show some variations and asymmetry in the region below the vortex finder between the axial level 200 mm and 345 mm which denotes to the recirculation zone.

Figs. 6.45 to 6.65 represent the comparisons of the axial velocity profiles between the experimental data (V_a in both regular and transform positions along with the corrected data of LDA optical probe) and the CFD simulation. As can be seen in these figures, there is a reasonably good agreement between experimental and predicted results. There are some small differences in the magnitudes due to the assumptions made in the CFD simulation.

Figs. 6.66 to 6.86 depict the comparison of the tangential velocity profiles between the experimental data obtained in the transform position (dashed line) of LDA optical probe and CFD simulation. The model predictions for V_θ showed good quantitative agreement with the LDA measurements, the maximum levels of tangential velocity were predicted very well by the simulations. It is obvious that both LDA and CFD show the same trends and significant degrees of symmetry, this revealed that V_θ are predicted accurately.

6.6 Conclusion

The 3-D Reynolds Stress Model (RSM) predicts the velocity field in the hydrocyclone very well. There is good agreement between the measured and observed flow patterns. The simulation captures the flow characteristics inside the hydrocyclone. Results of this simulation clearly proved that the CFD

technique has great potential in understanding the fluid flow behavior in the hydrocyclone.

Figures Chapter 6

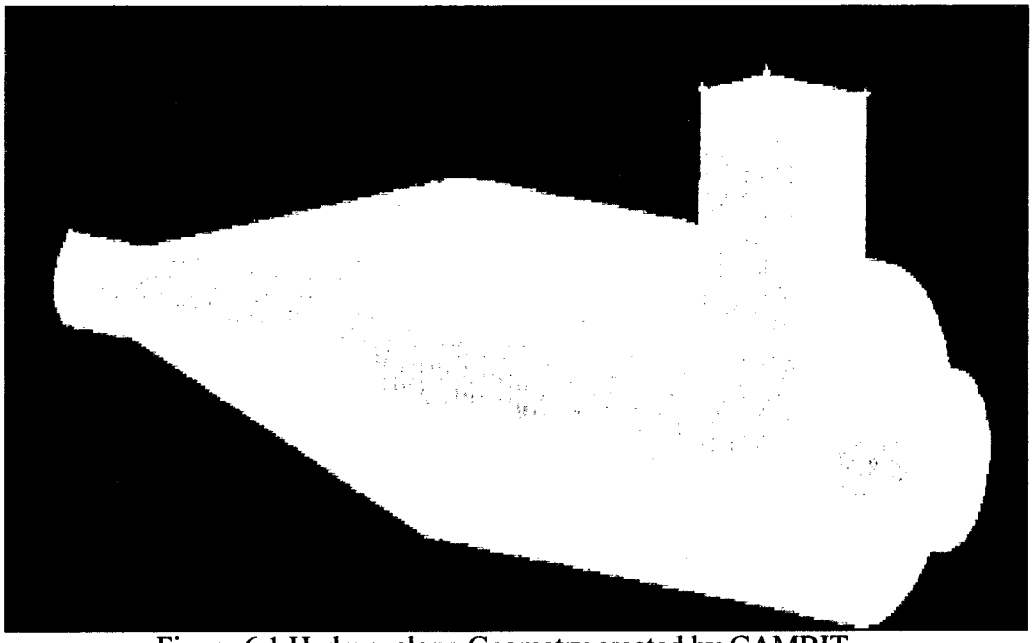

Figure 6.1 Hydrocyclone Geometry created by GAMBIT

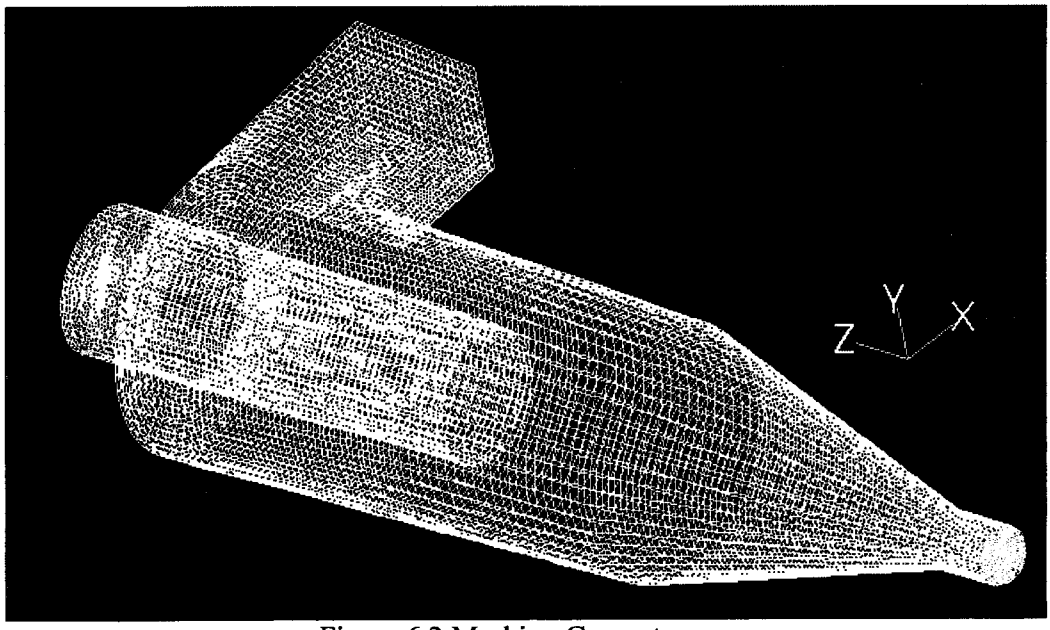

Figure 6.2 Meshing Geometry

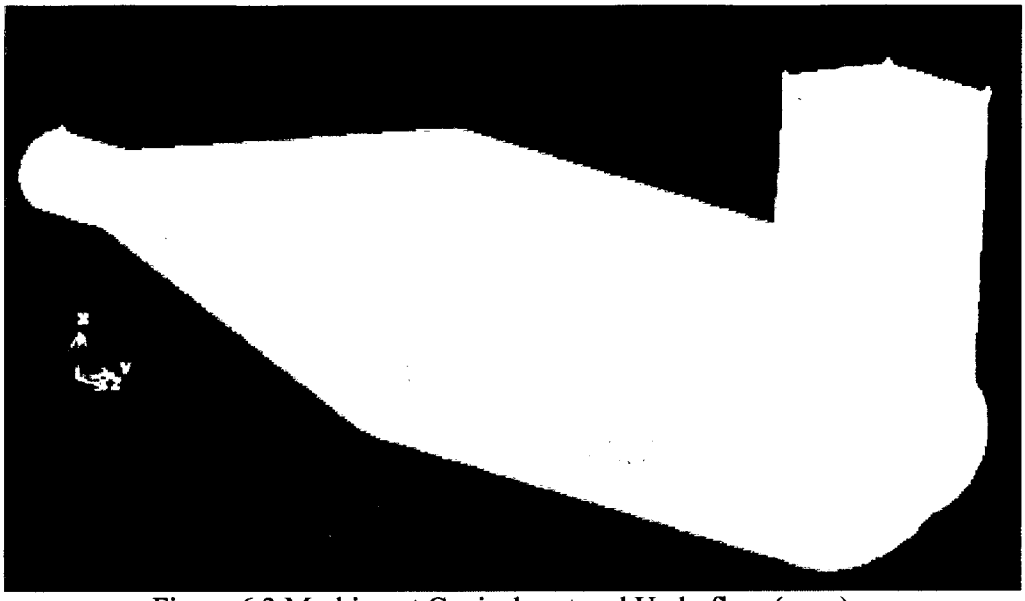

Figure 6.3 Meshing at Conical part and Underflow (apex)

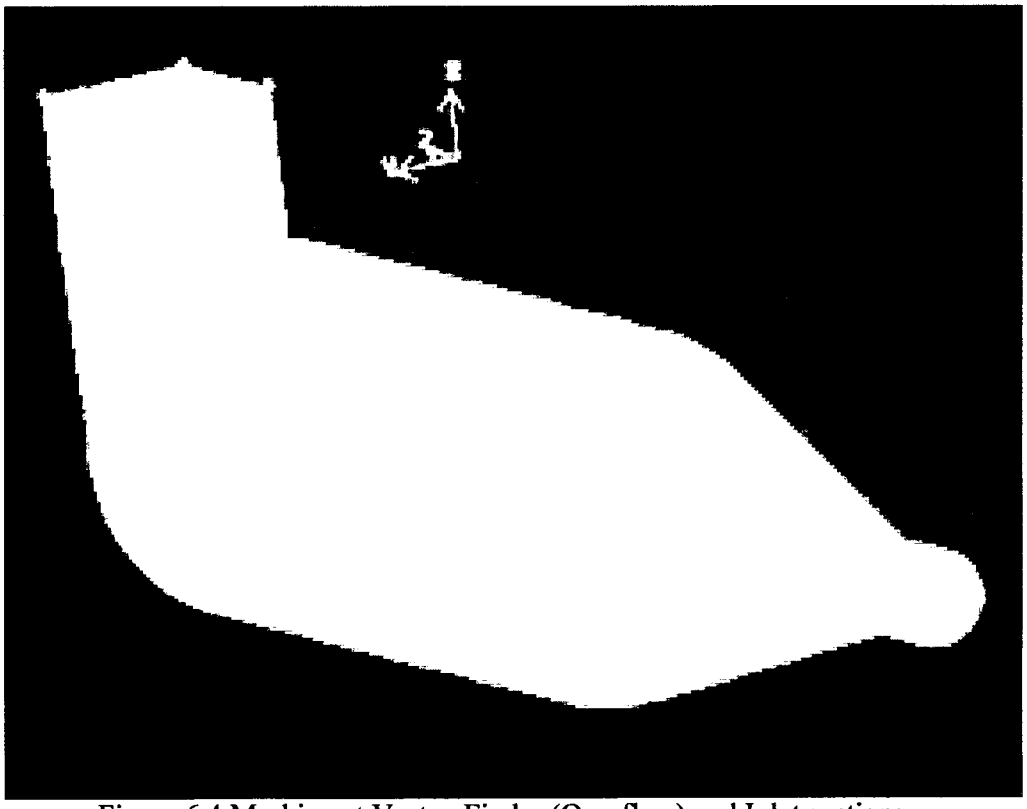

Figure 6.4 Meshing at Vortex Finder (Overflow) and Inlet sections

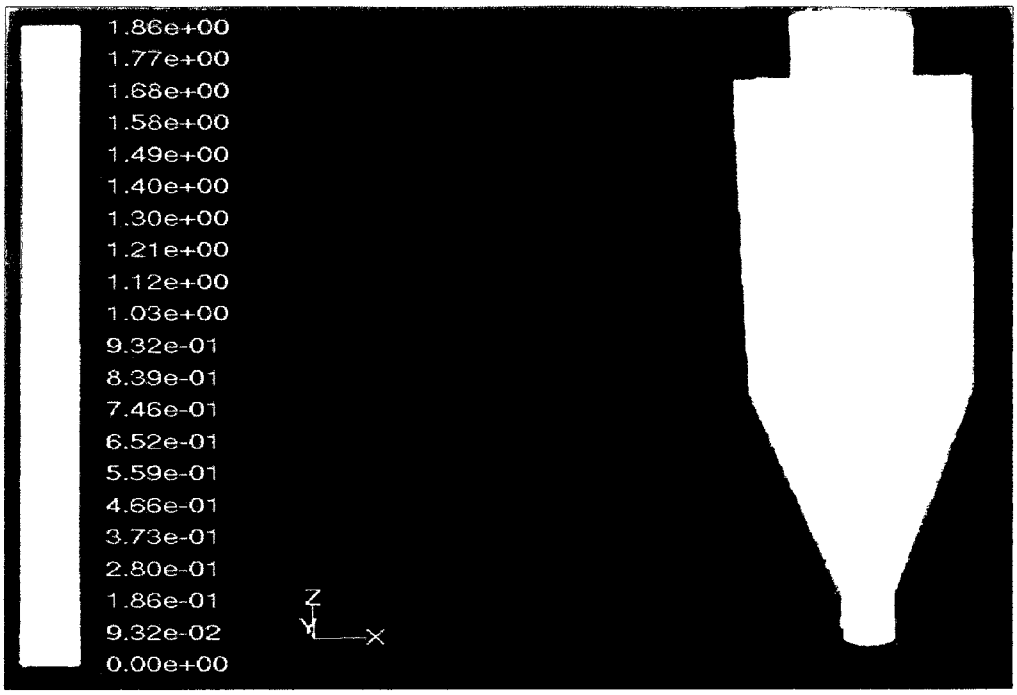

Figure 6.5 Contours Plot of Velocity magnitudes

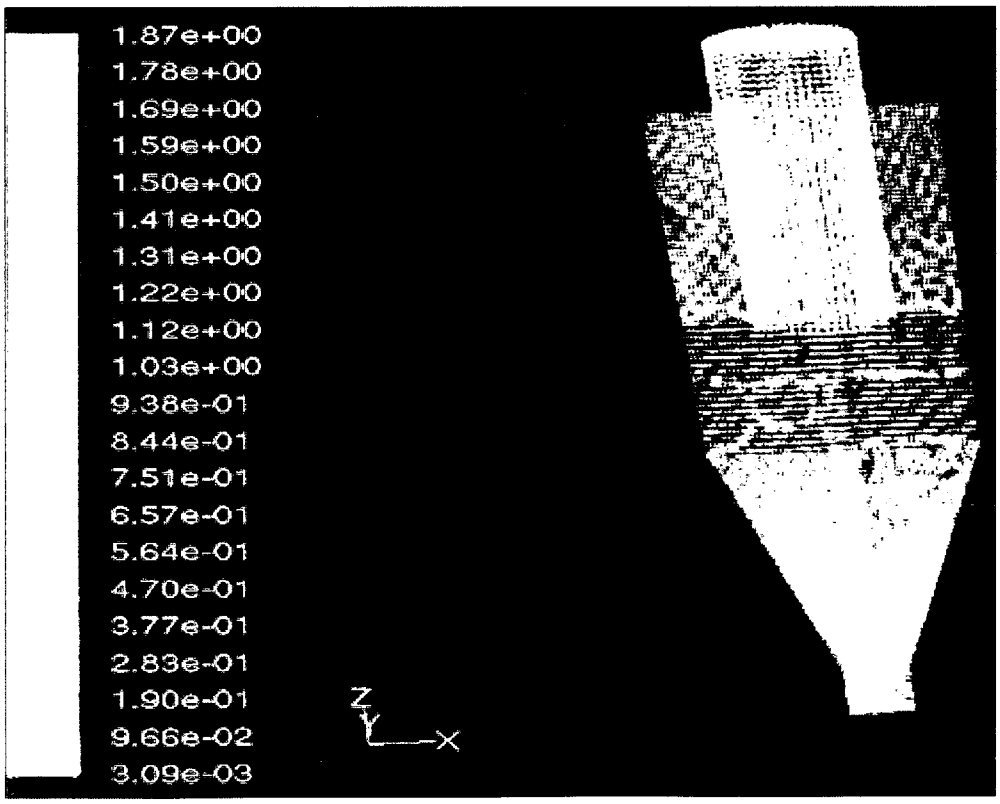

Figure 6.6 Velocity Magnitude Vectors

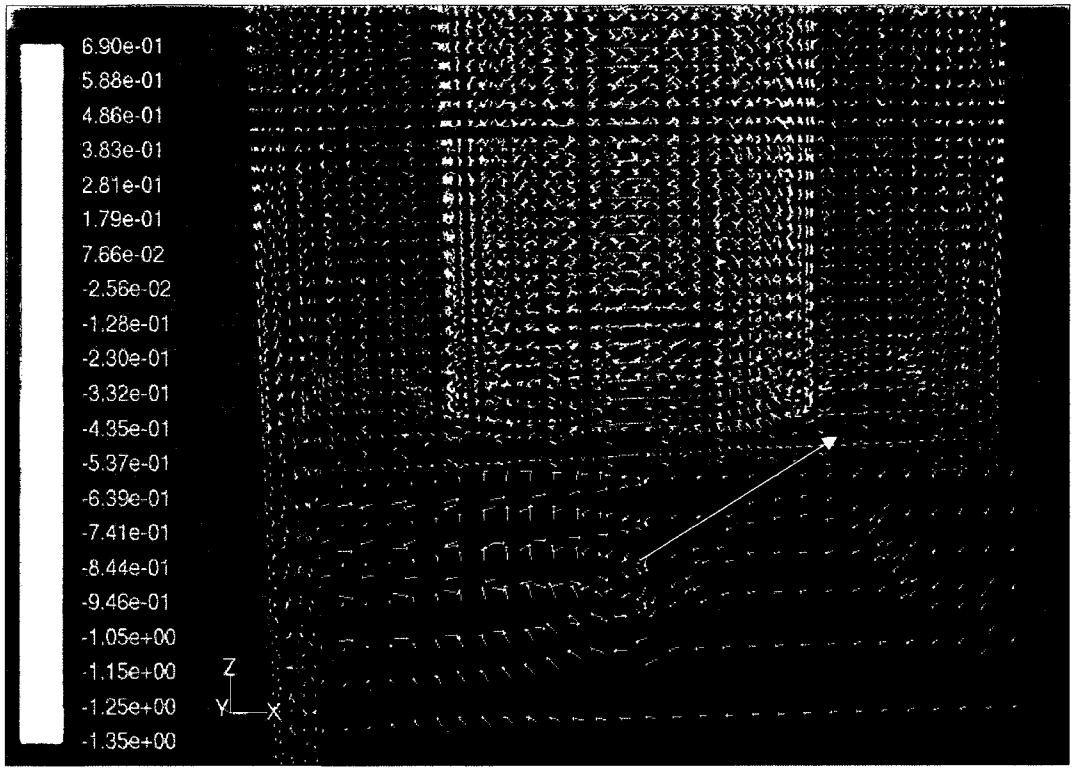

Figure 6.7 Short Circuit Flow

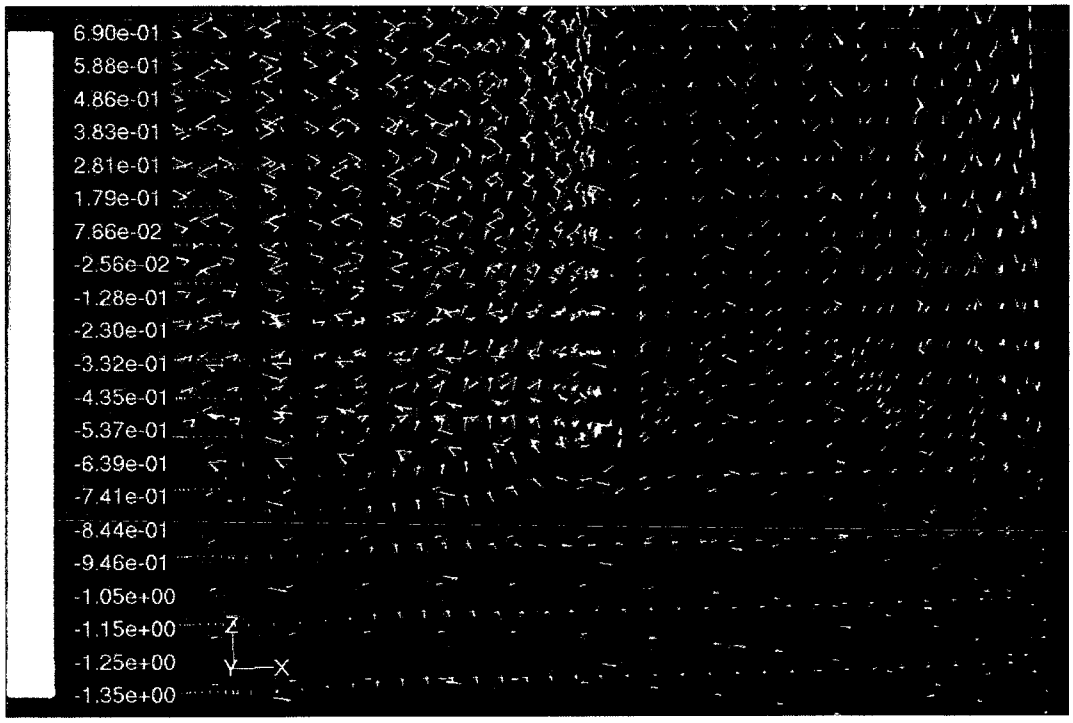

Figure 6.8 The Short Circuit Flow Phenomenon

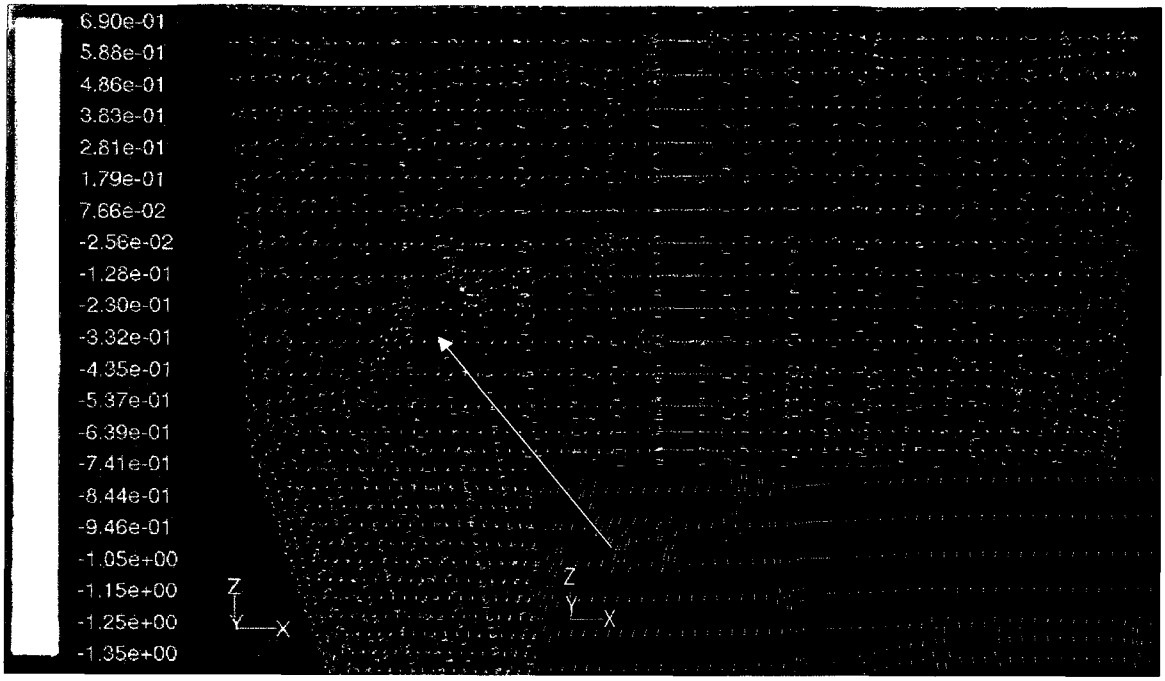

Figure 6.9 Recirculation (Eddy) Flow

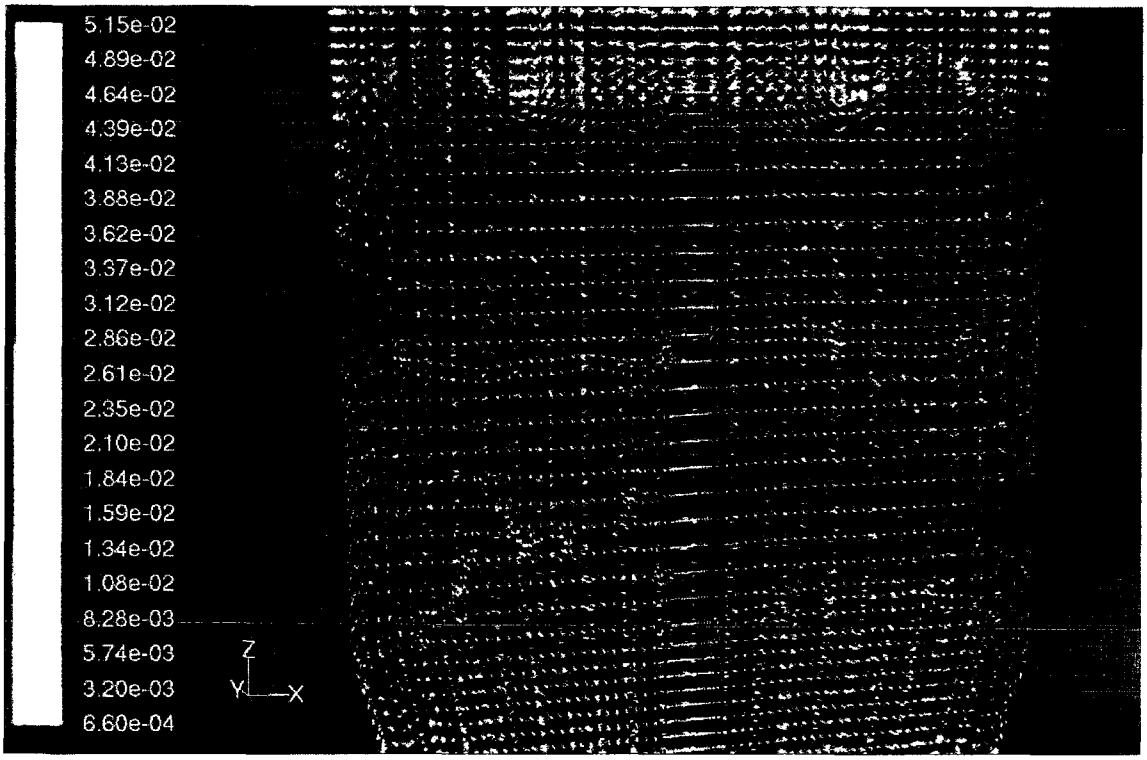

Figure 6.10 Recirculation (Eddy) Flow at cylindrical part

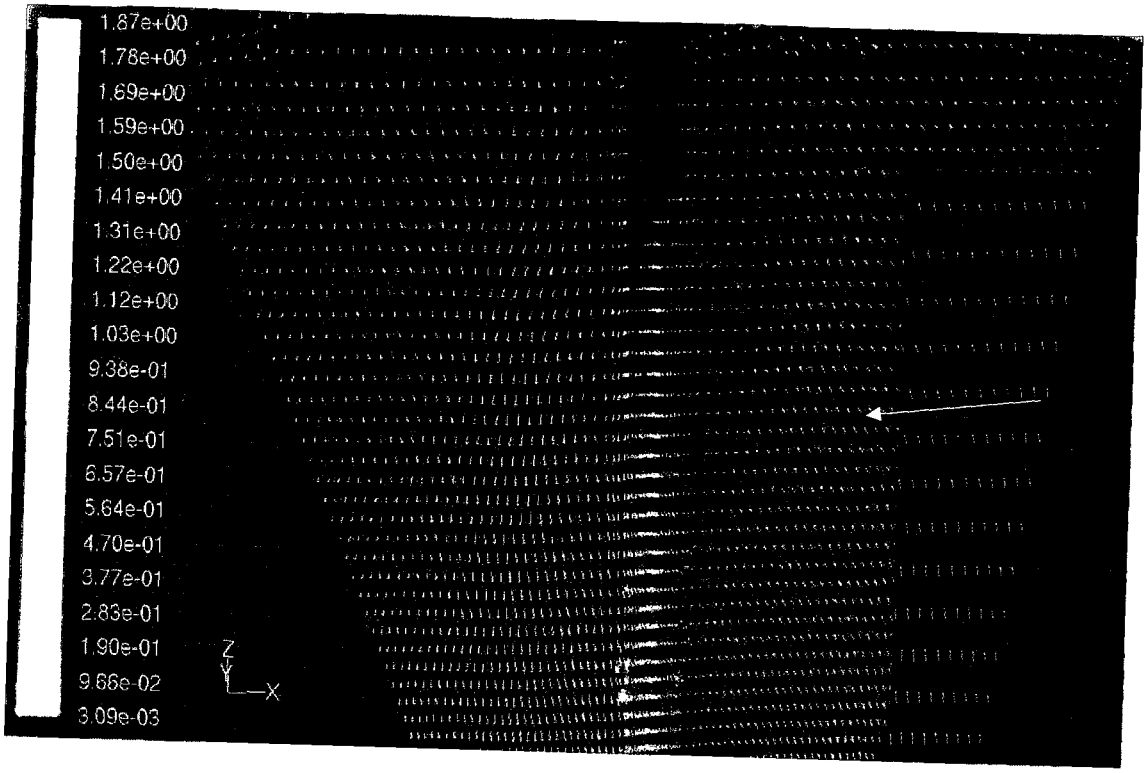

Figure 6.11 Reversal Flow at the upper portion of the conical part

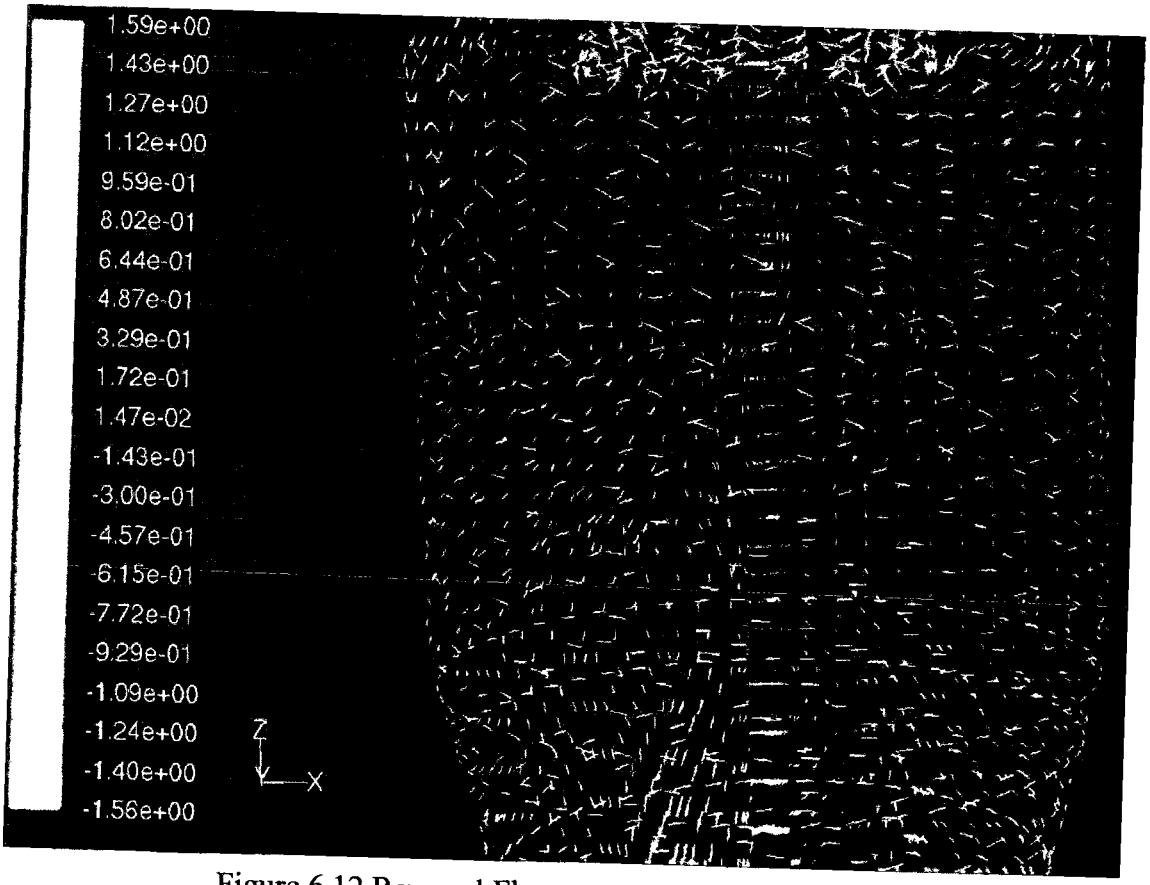

Figure 6.12 Reversal Flow moves upward

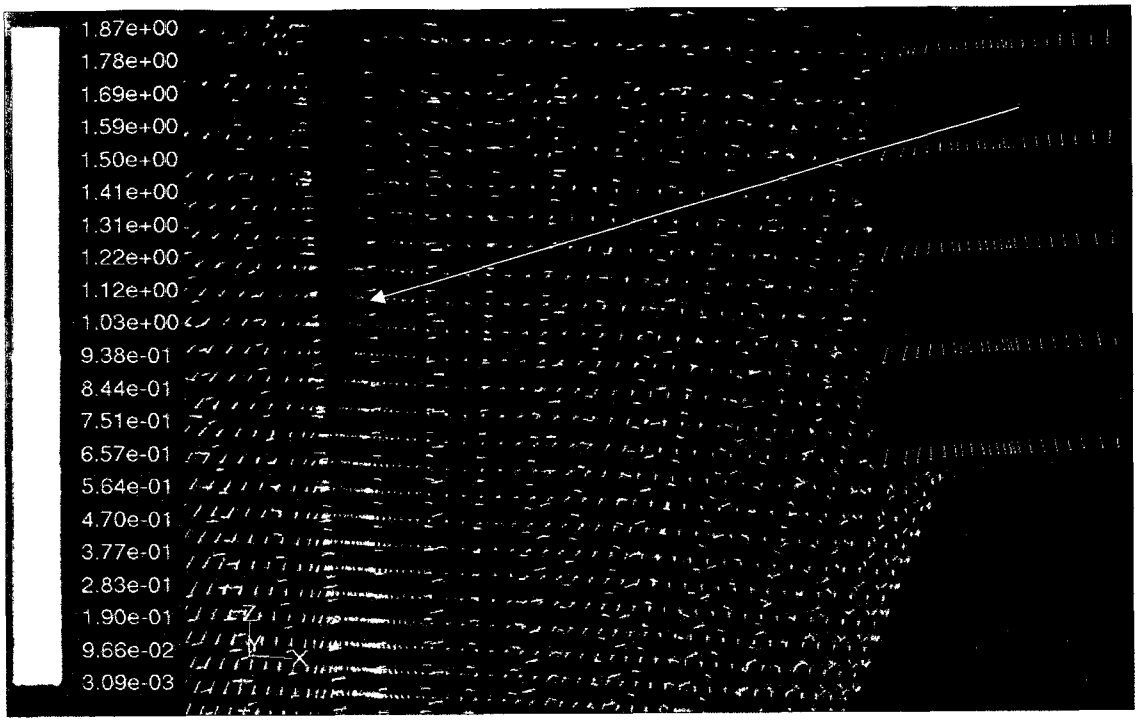

Figure 6.13 Downwards Flow at Axis Runs Countercurrent to an Outer Upwards Flow

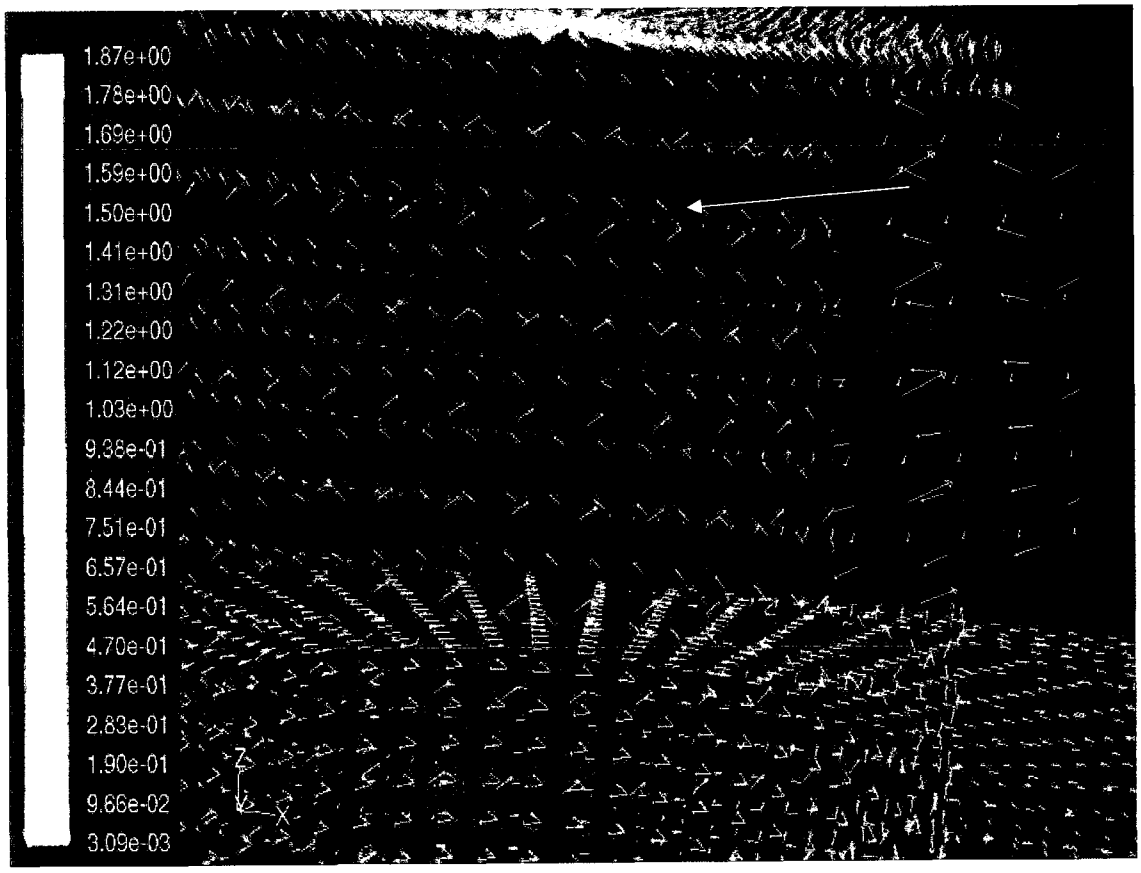

Figure 6.14 Downward Flow at centre of Vortex Finder

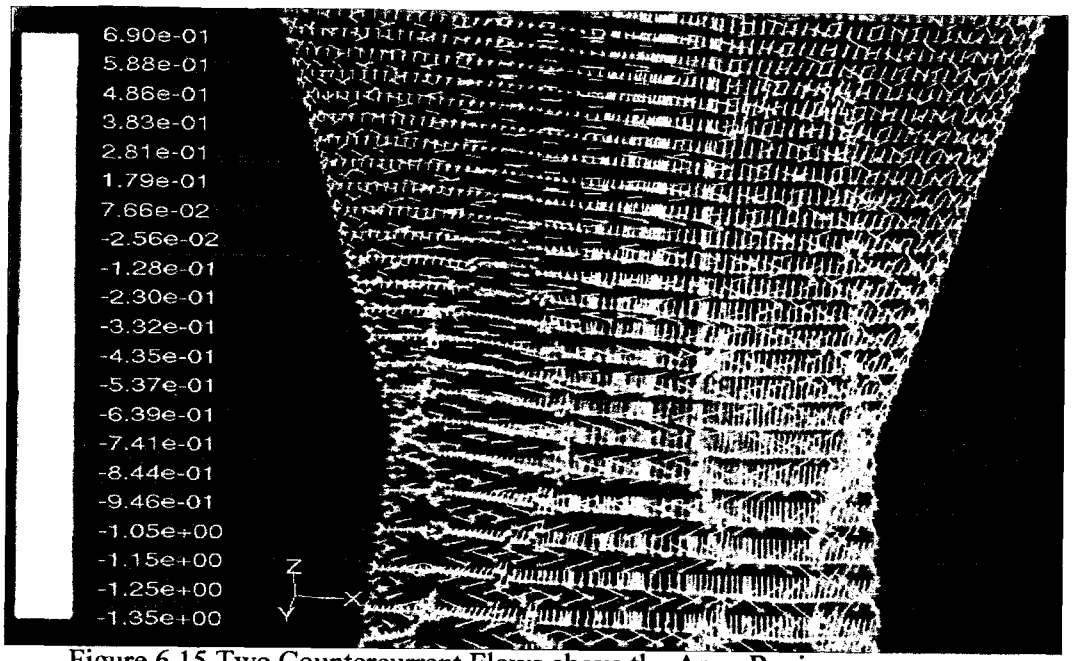

Figure 6.15 Two Countercurrent Flows above the Apex Region

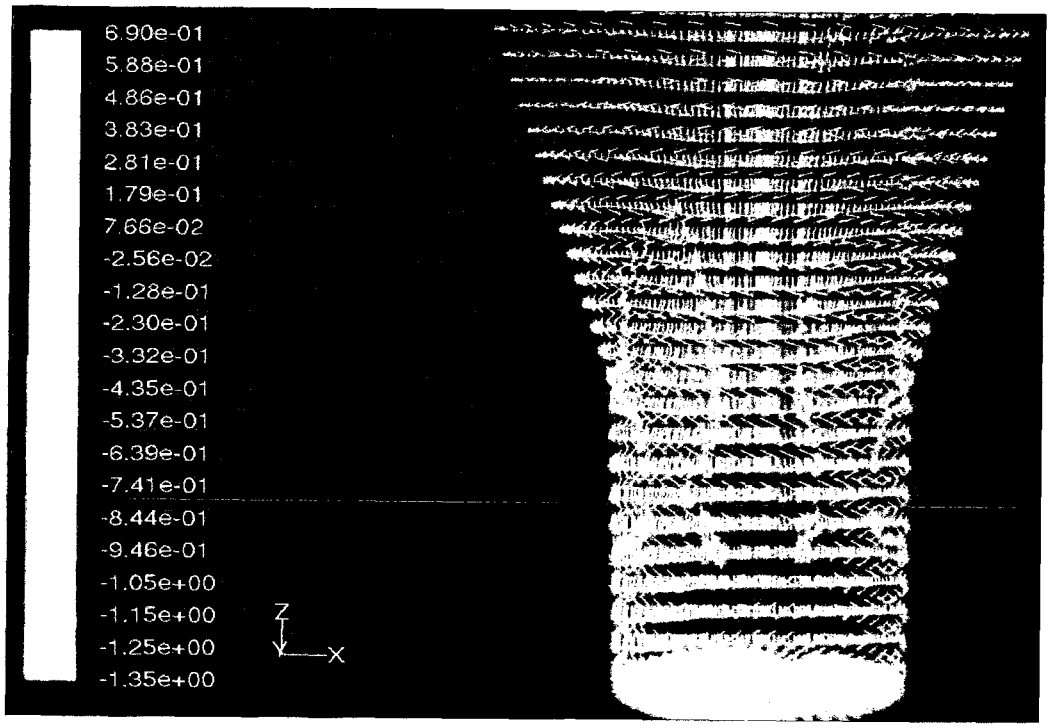

Figure 6.16 Two Countercurrent Flows at Underflow (apex) Region

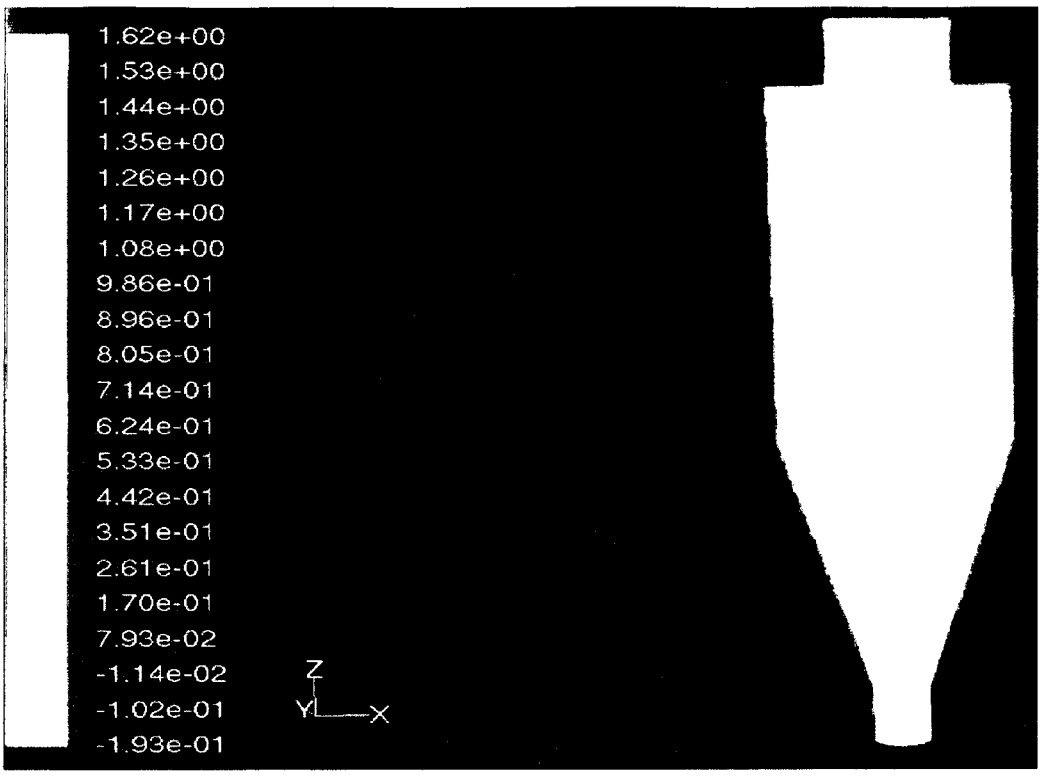

Figure 6.17 Contours of Tangential Velocity

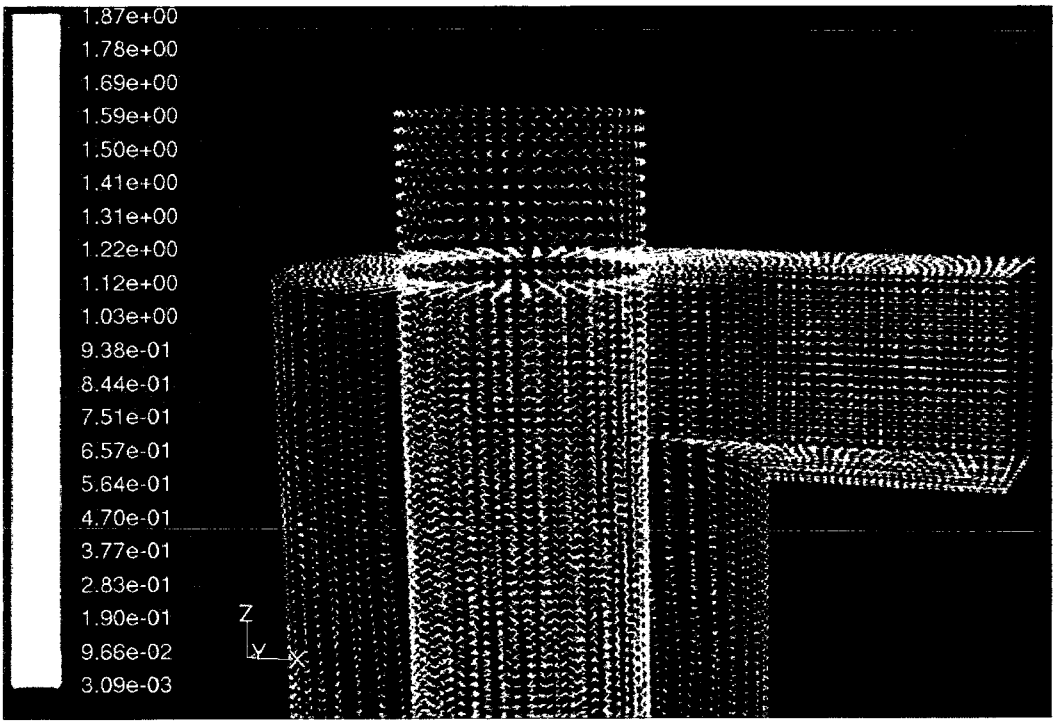

Figure 6.18 Tangential Velocity vectors plot

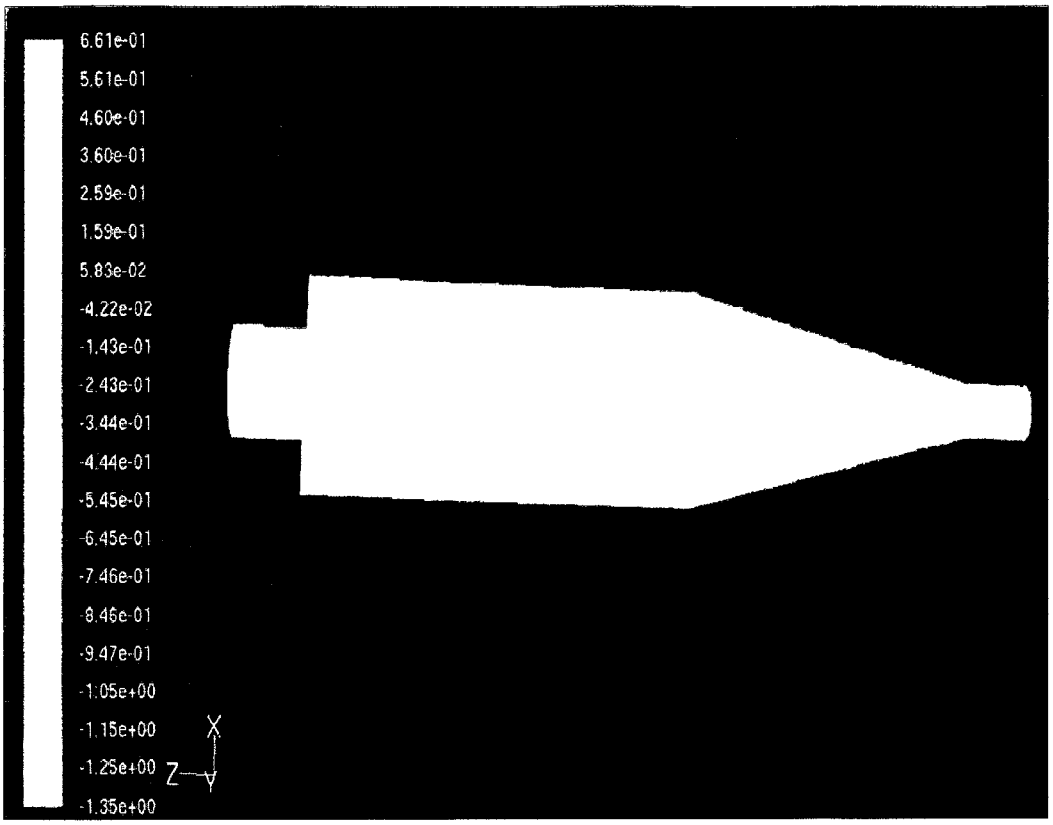

Figure 6.19 Contours of Axial Velocity

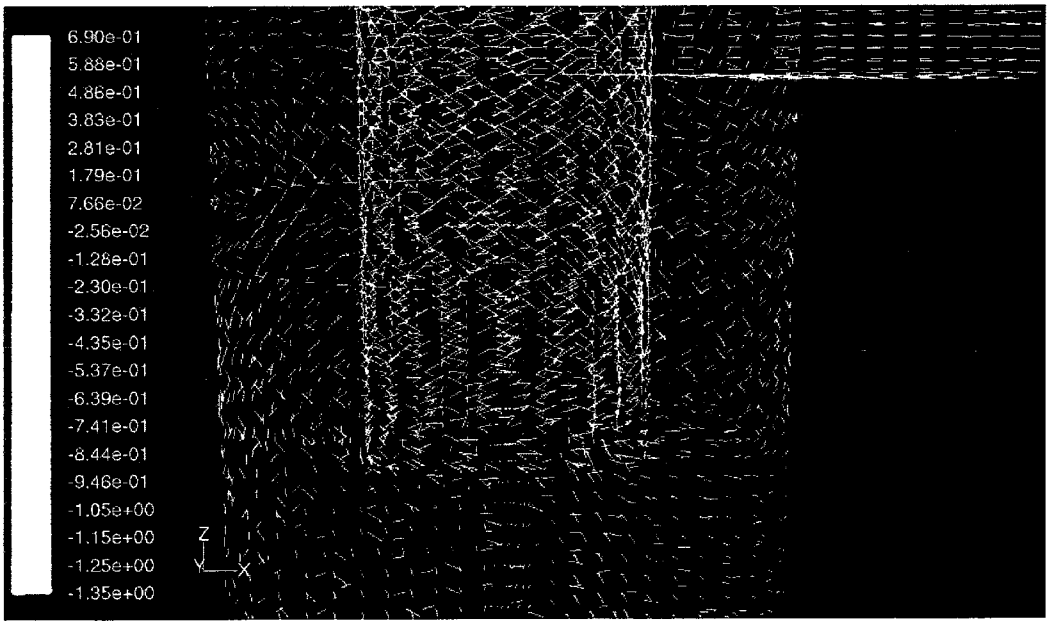

Figure 6.20 Axial Velocity Vectors at Vortex Finder and cylindrical part

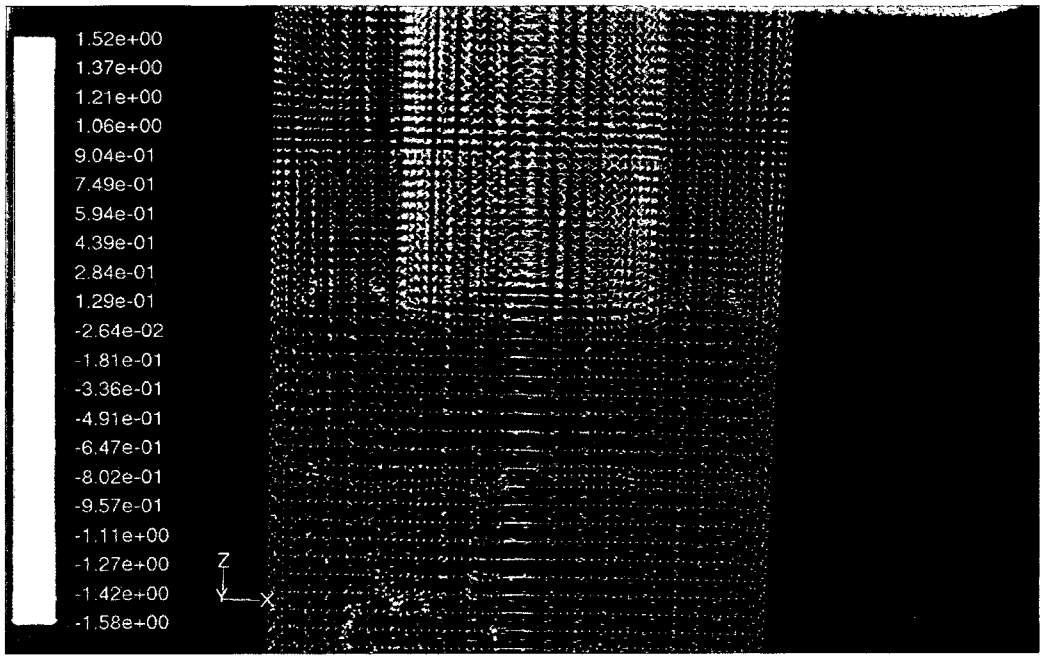

Figure 6.21 Radial Velocity Vectors

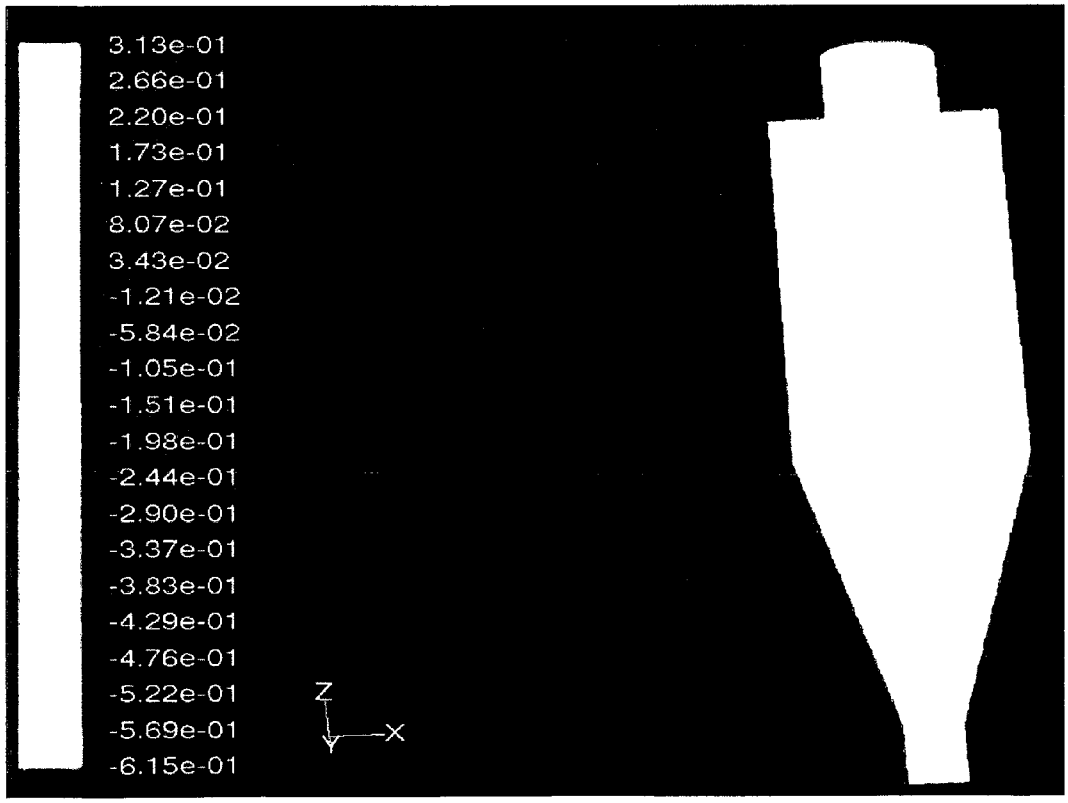

Figure 6.22 Contours of Radial Velocity

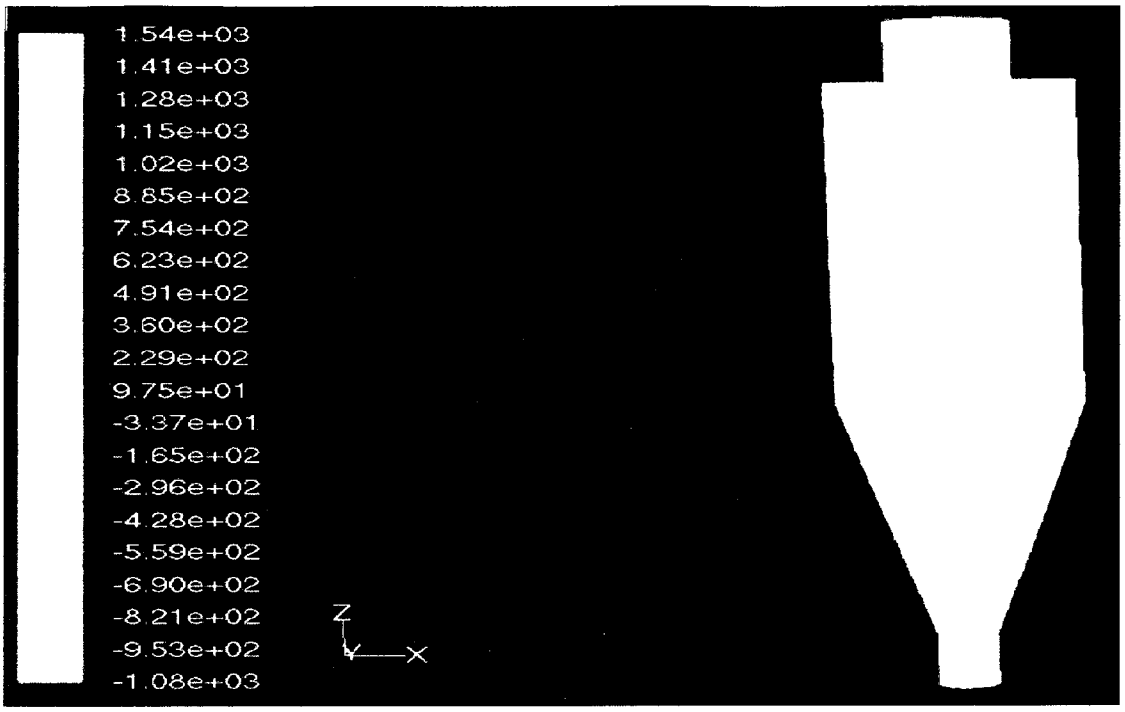

Figure 6.23 Contours of Total Pressure (Pascal)

Figure 6.24 Tangential and Axial Velocities at Axial Plane Z=140 mm

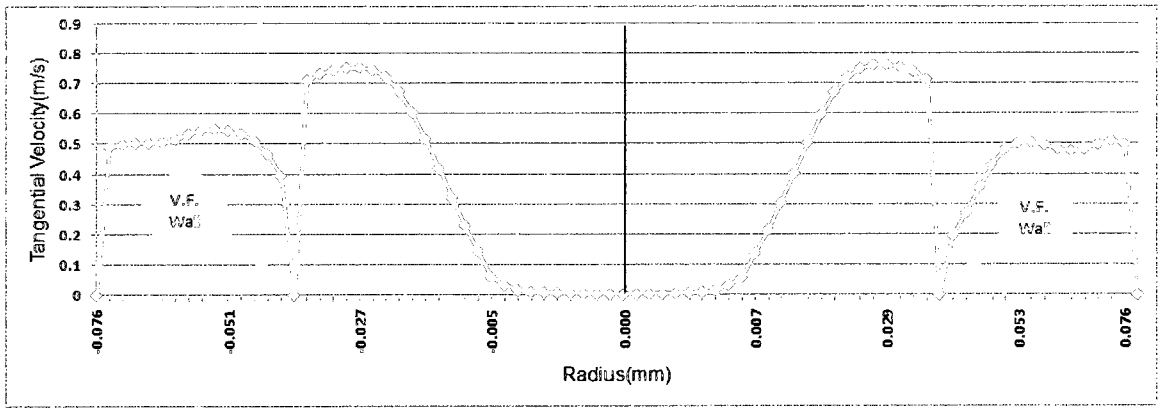

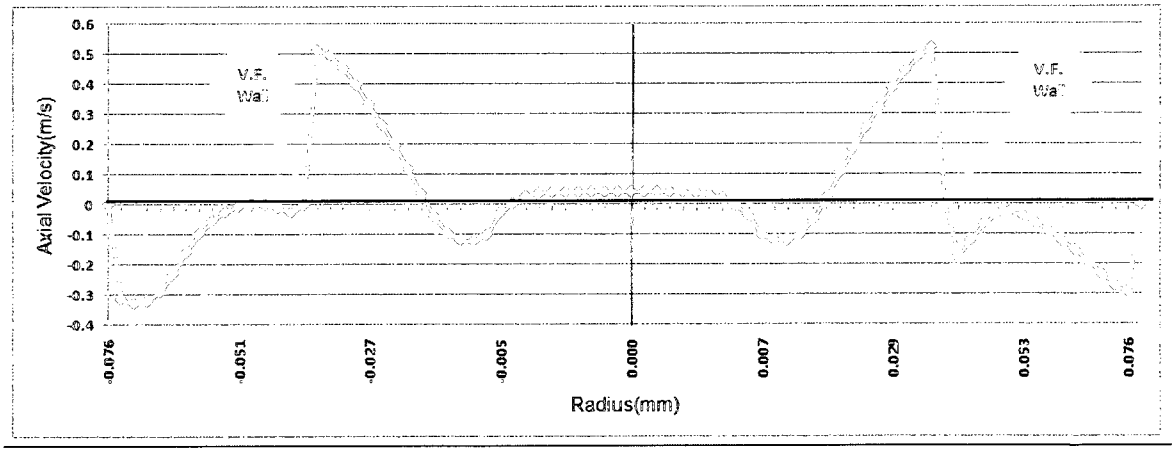

Figure 6.25 Tangential and Axial Velocities at Axial Plane Z=160 mm

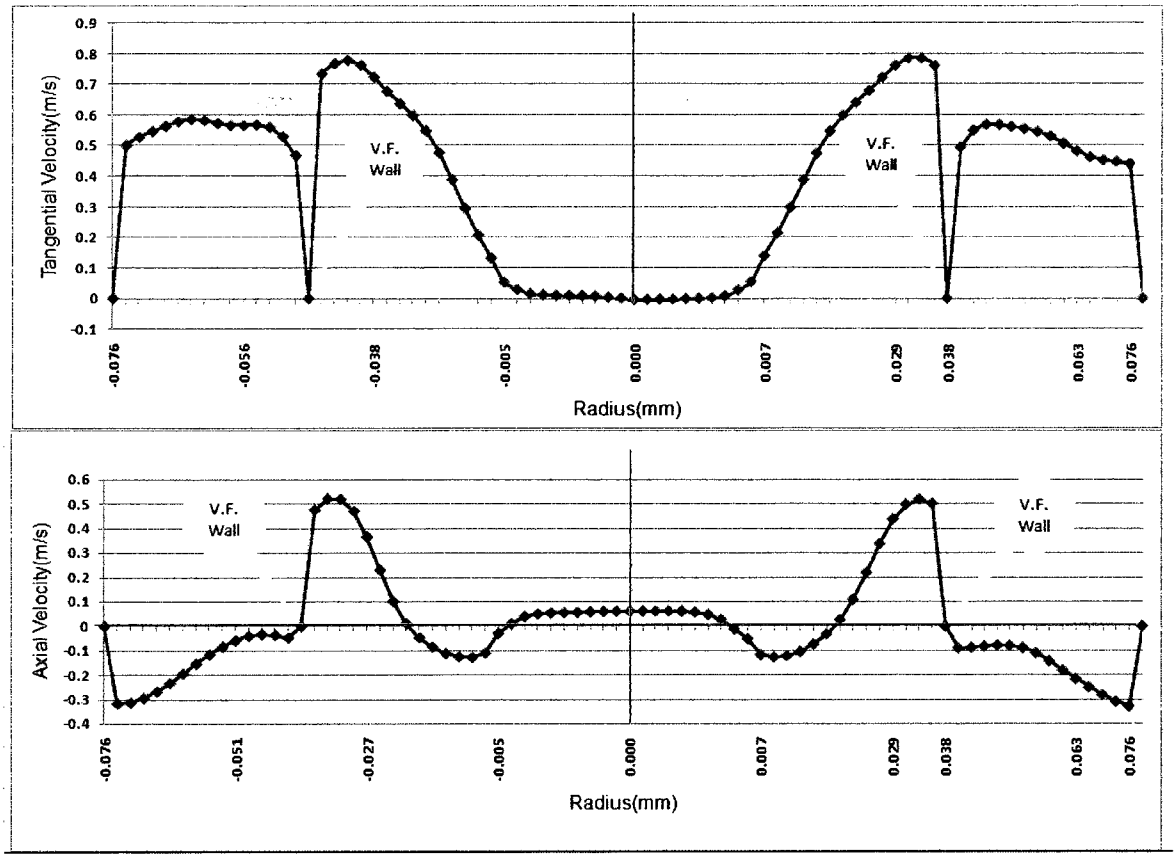

Figure 6.26 Tangential and Axial Velocities at Axial Plane Z=187 mm

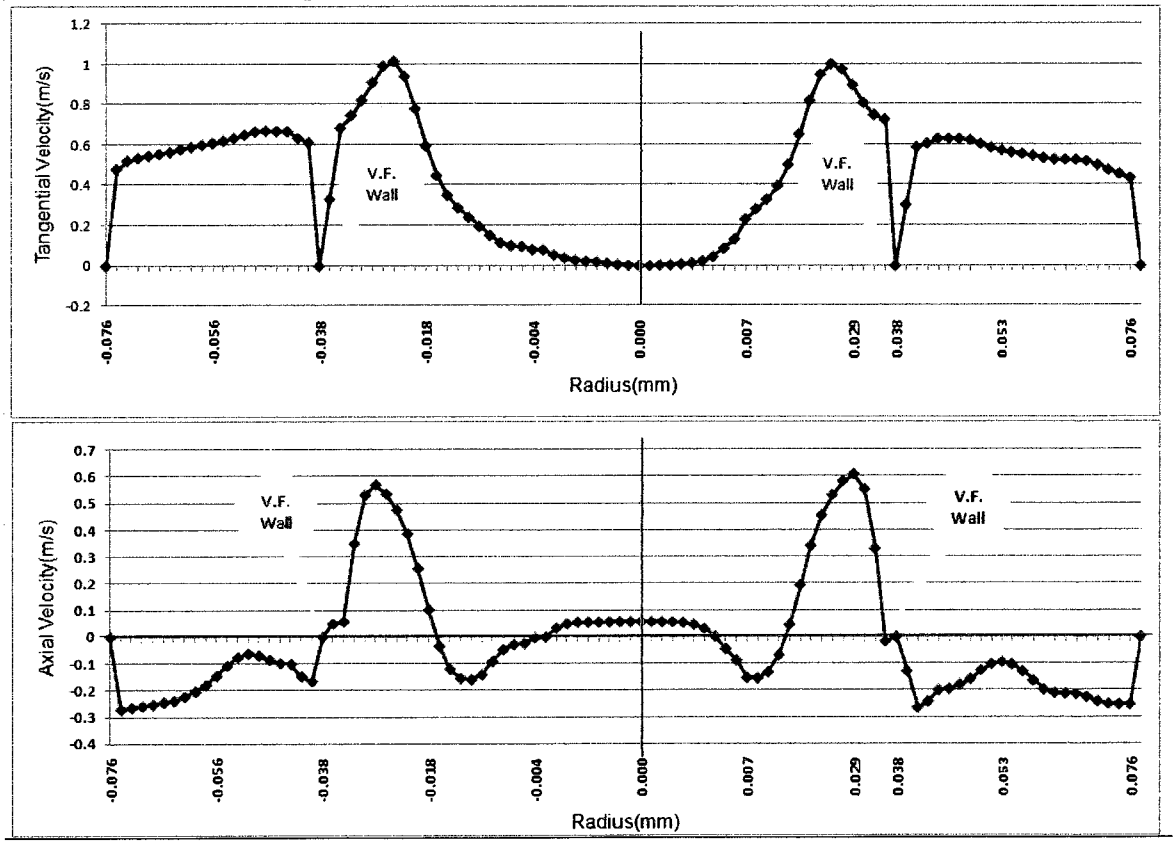

Figure 6.27 Tangential and Axial Velocities at Axial Plane Z=200 mm

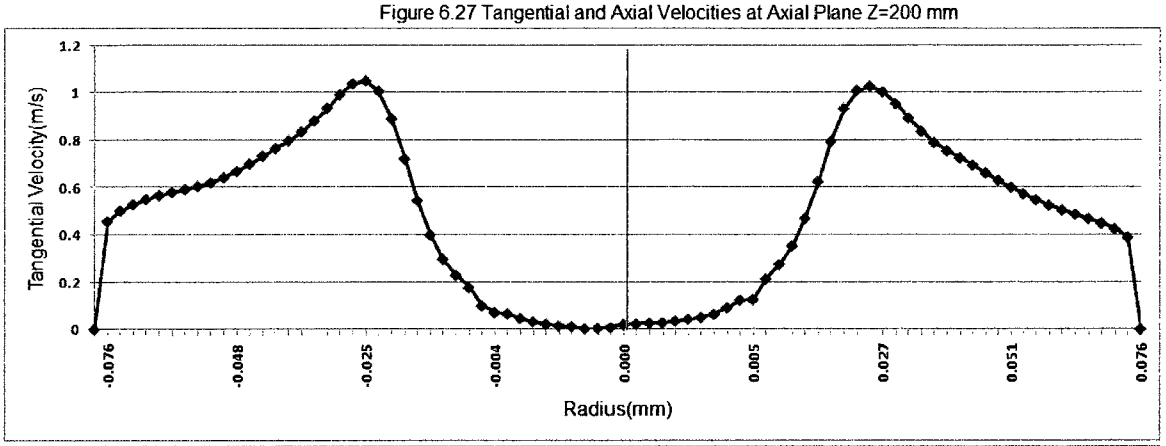

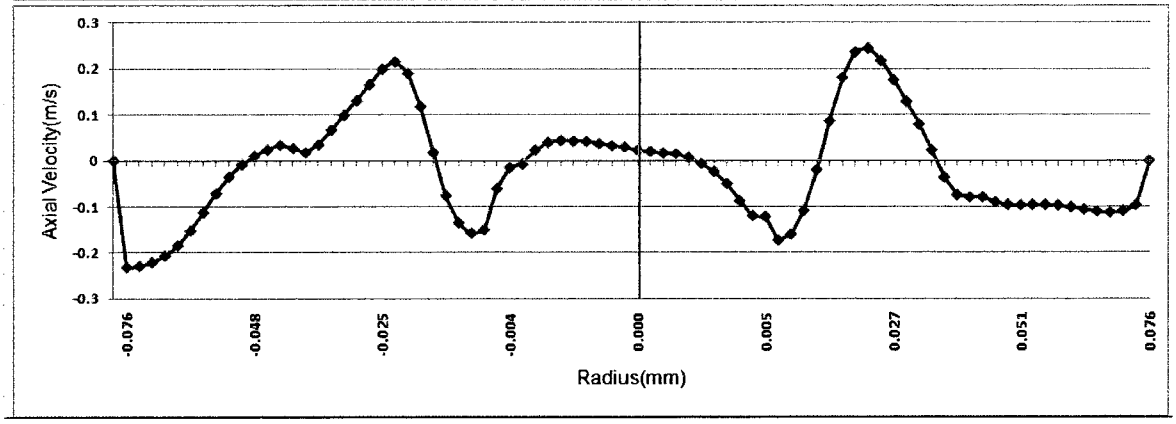

Figure 6.28 Tangential and Axial Velocities at Axial Plane Z=220 mm

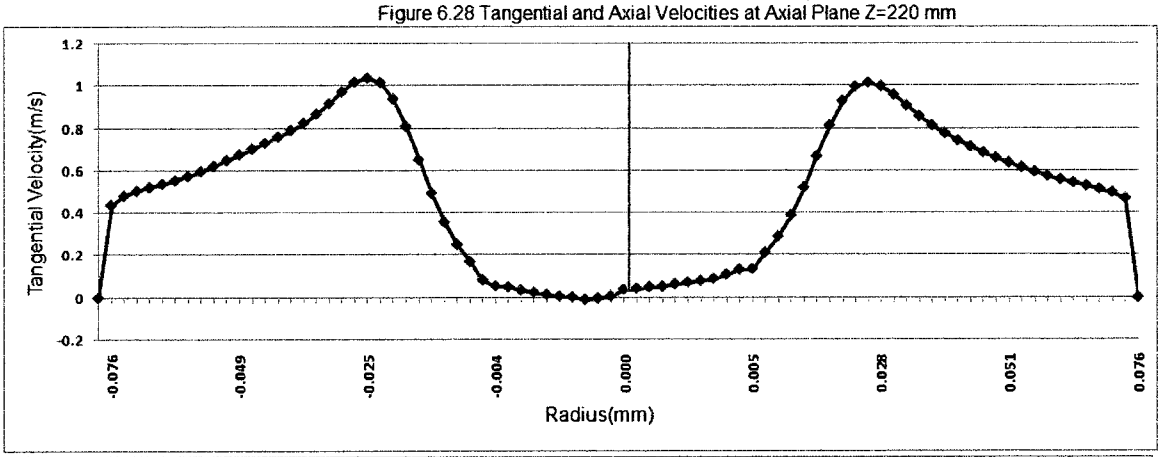

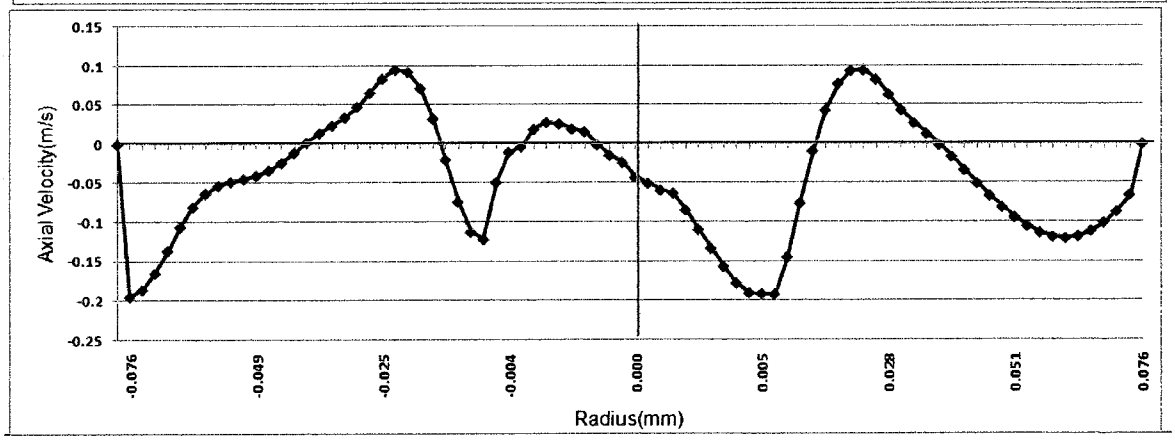

Figure 6.30 Tangential and Axial Velocities at Axial Plane Z=260 mm

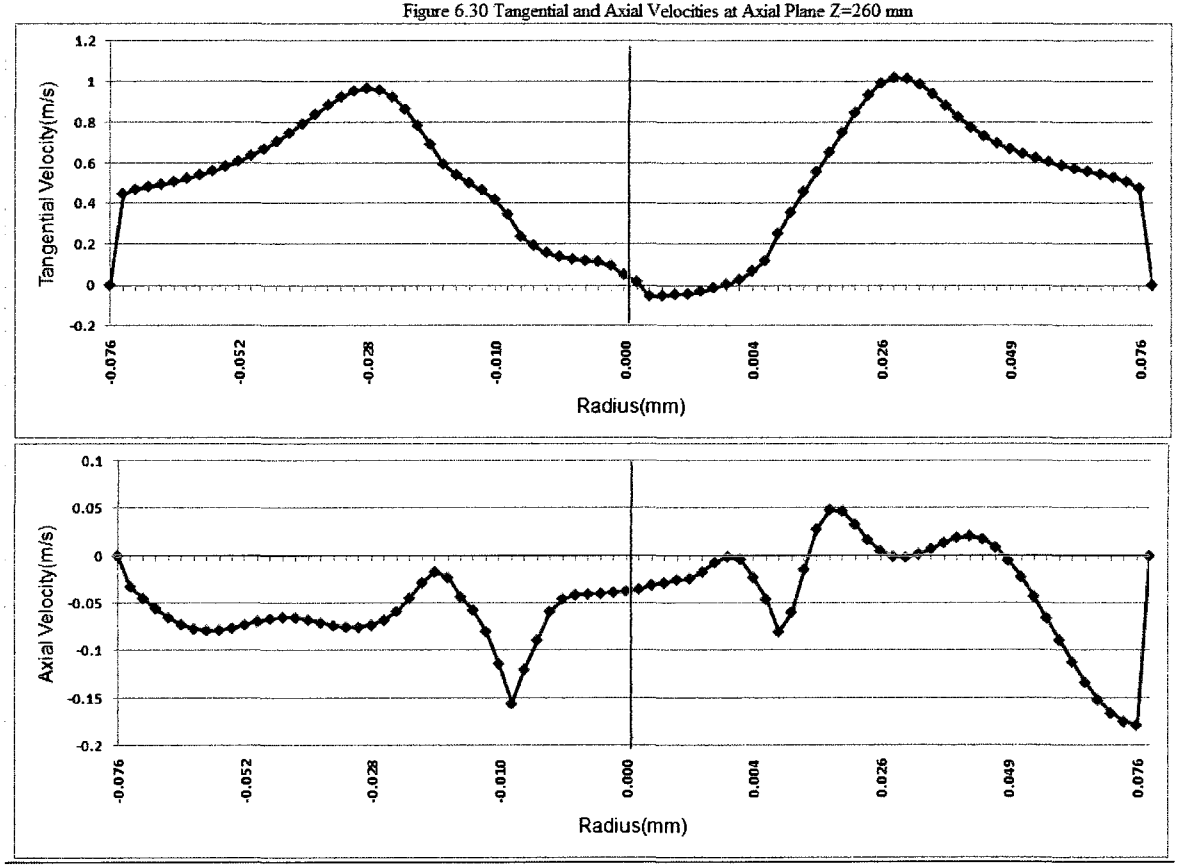

Figure 6.29 Tangential and Axial Velocities at Axial Plane Z=240 mm

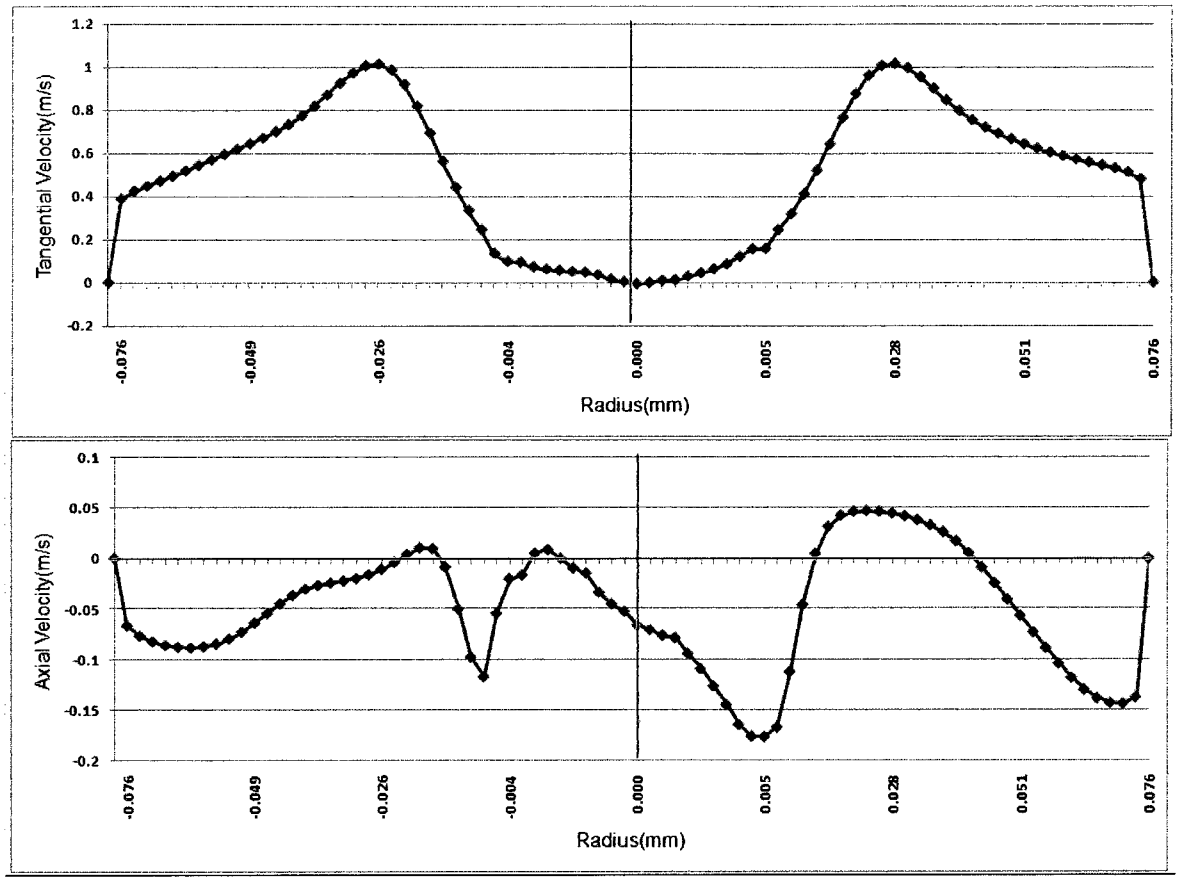

Figure 6.31 Tangential and Axial Velocities at Axial Plane Z=280 mm

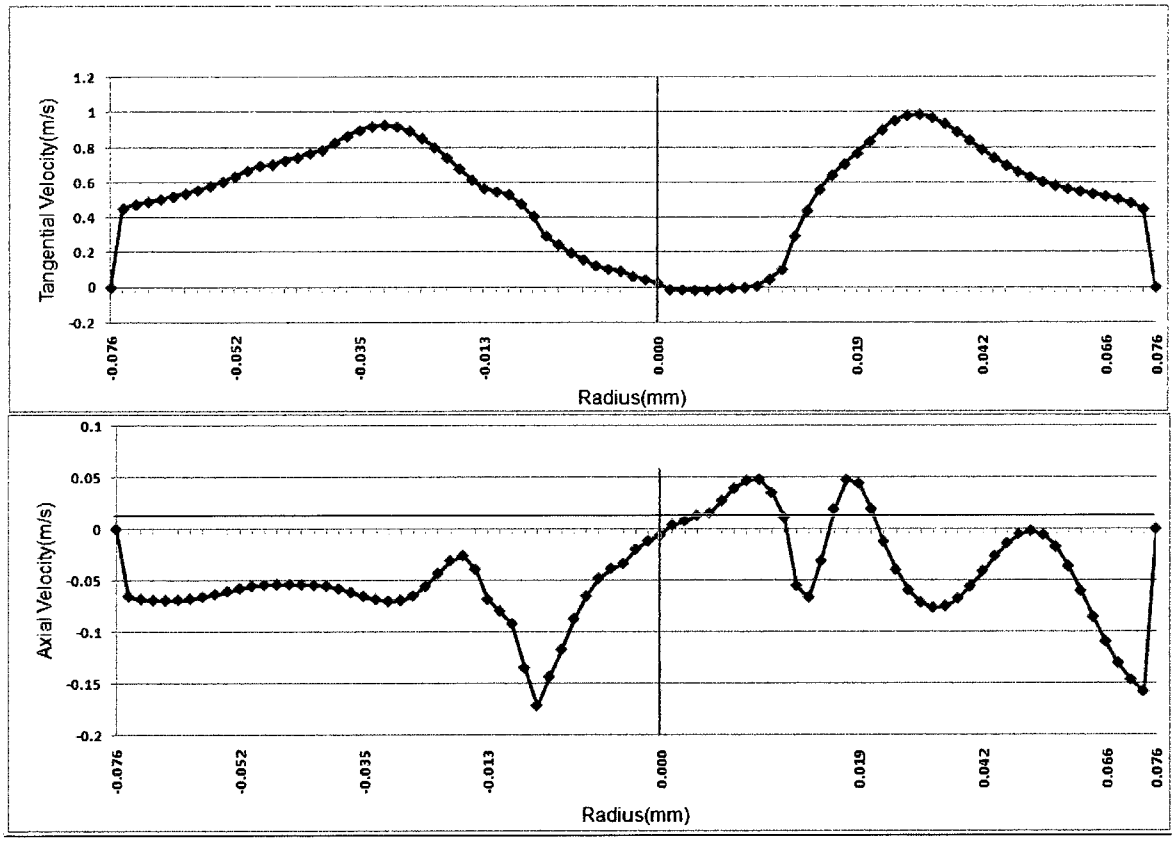

Figure 6.32 Tangential and Axial Velocities at Axial Plane Z=294 mm

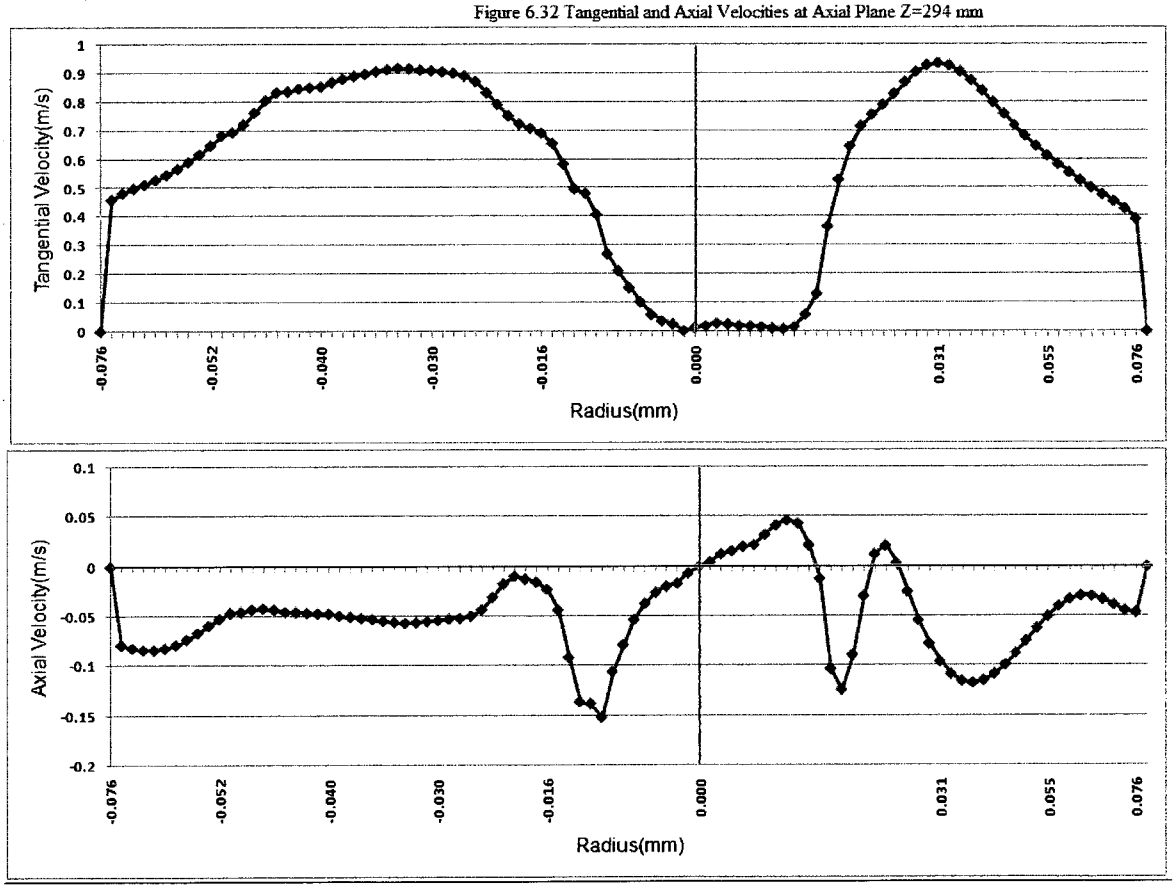

Figure 6.33 Tangential and Axial Velocities at Axial Plane Z=345 mm

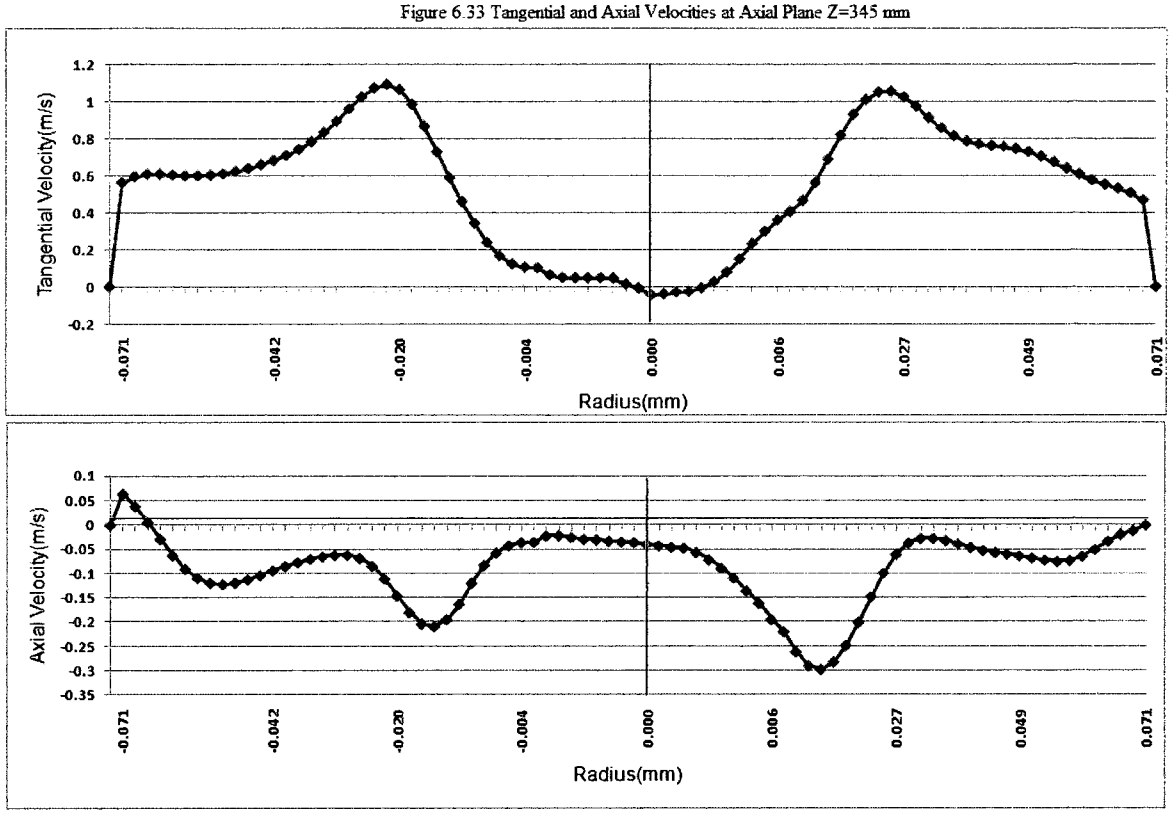

Figure 6.34 Tangential and Axial Velocities at Axial Plane Z=365 mm

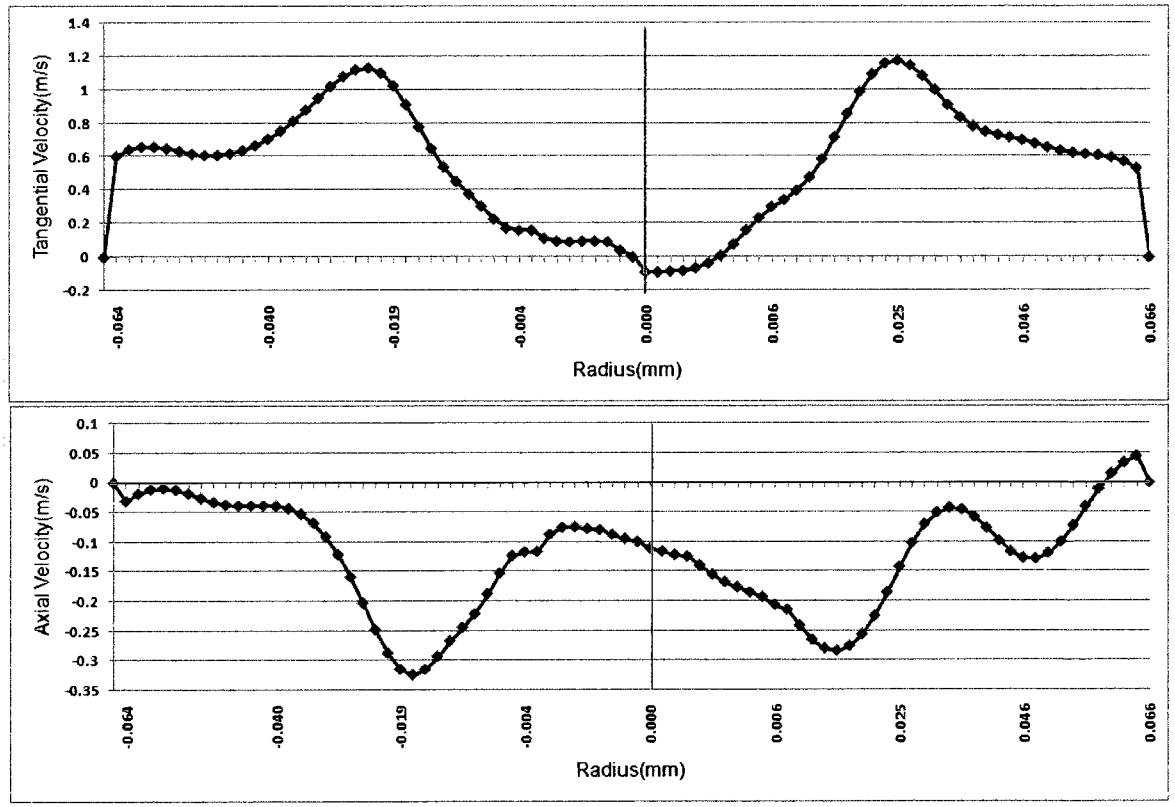

Figure 6.35 Tangential and Axial Velocities at Axial Plane Z=385 mm

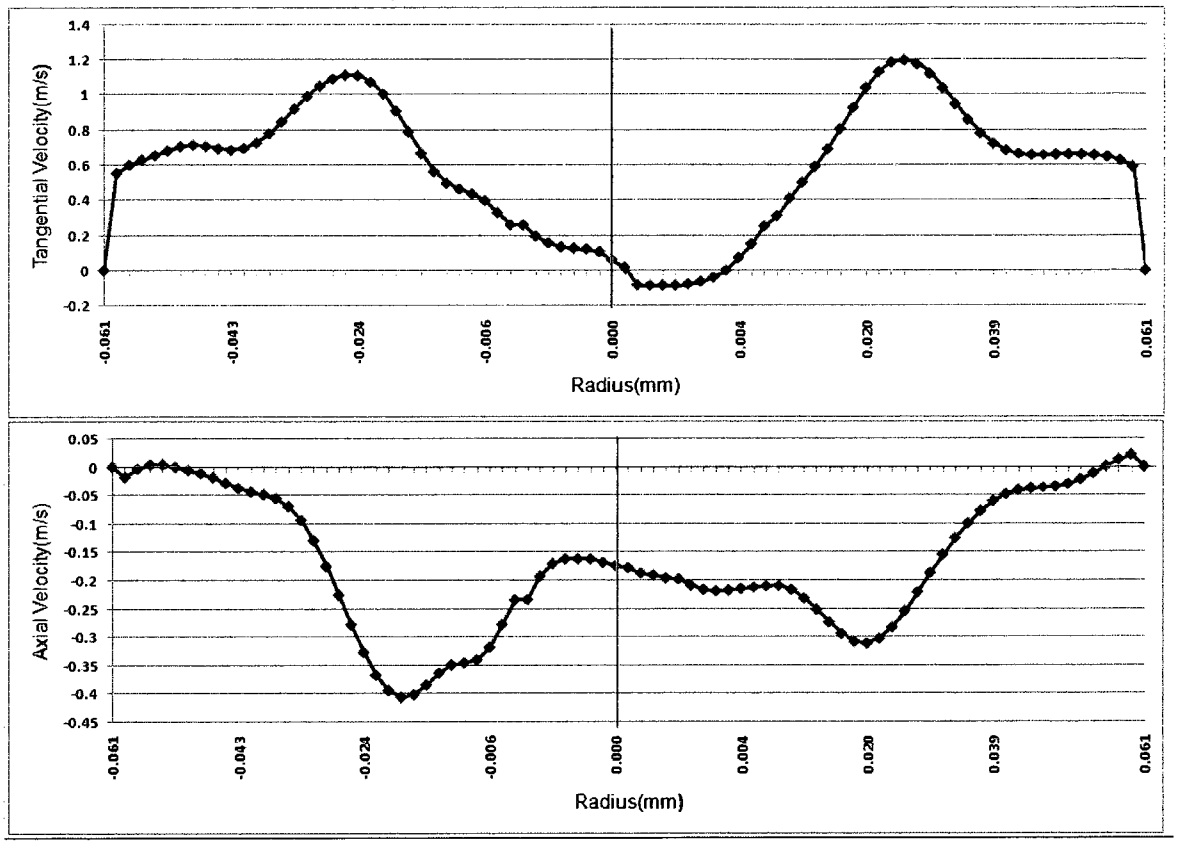

Figure 6.36 Tangential and Axial Velocities at Axial Plane Z=405 mm

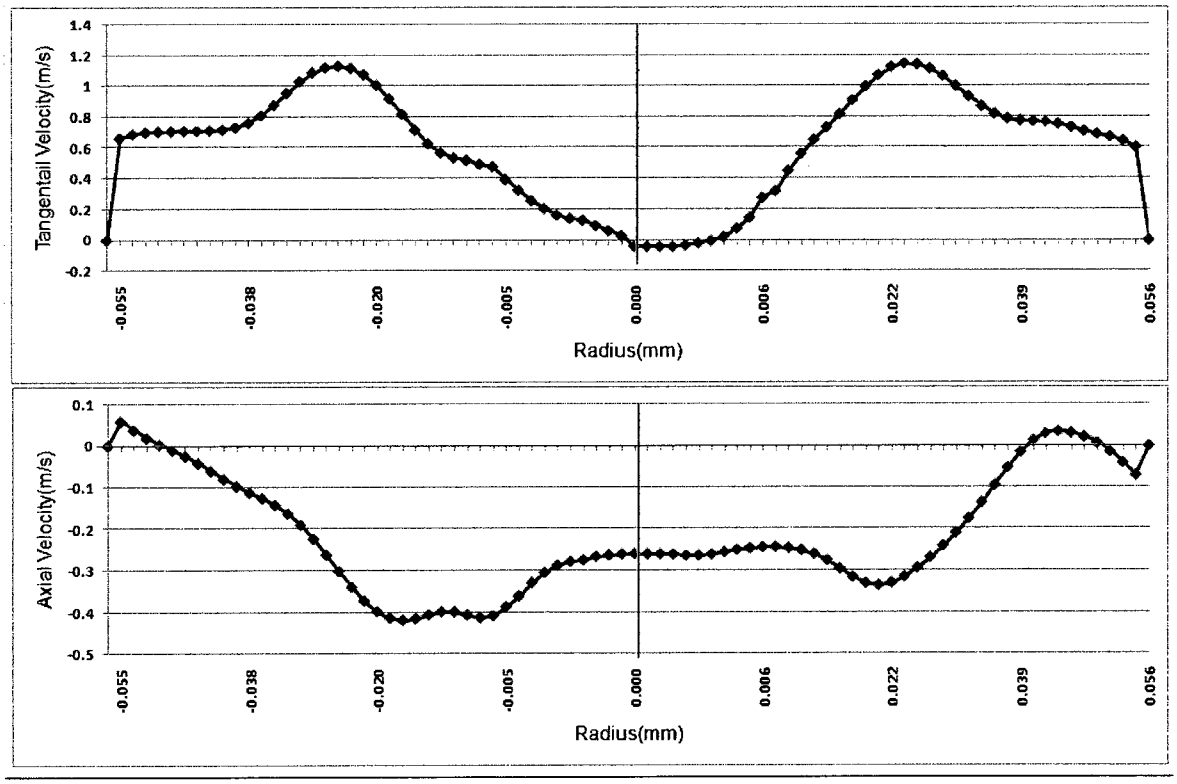

Figure 6.38 Tangential and Axial Velocities at Axial Plane Z=445 mm

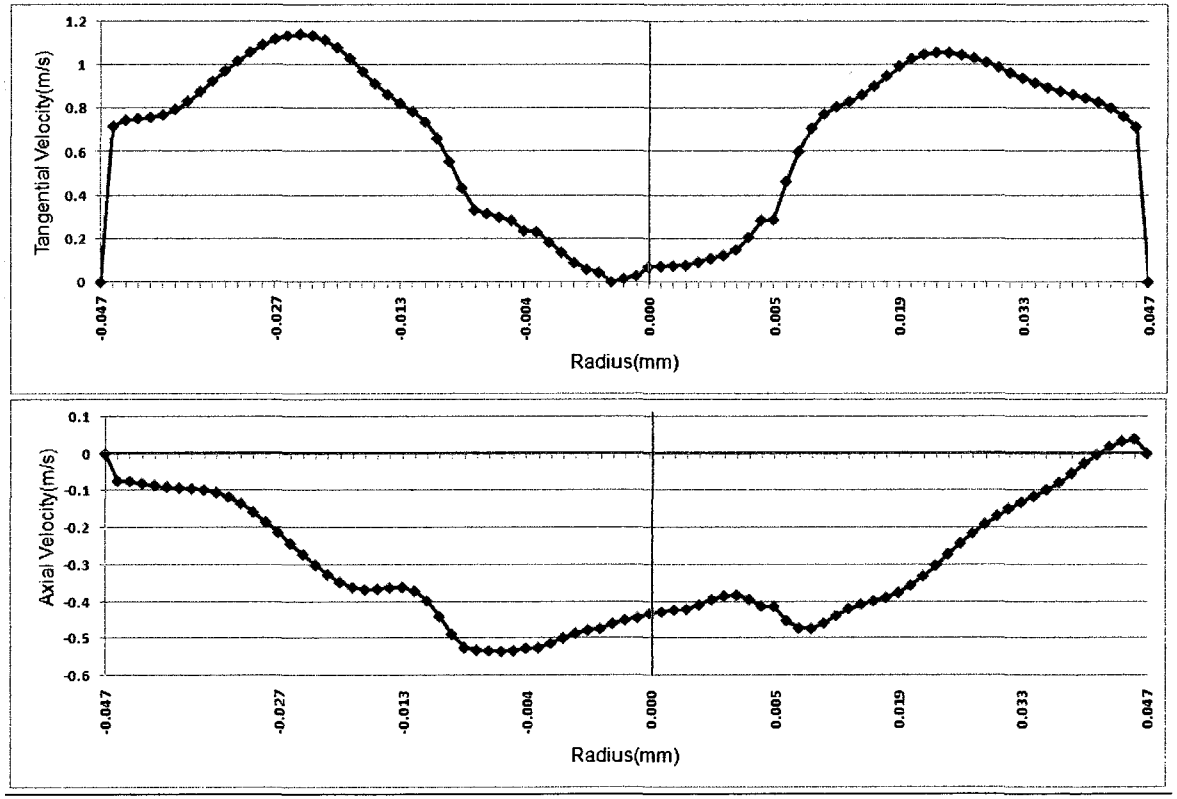

Figure 6.37 Tangential and Axial Velocities at Axial Plane Z=425 mm

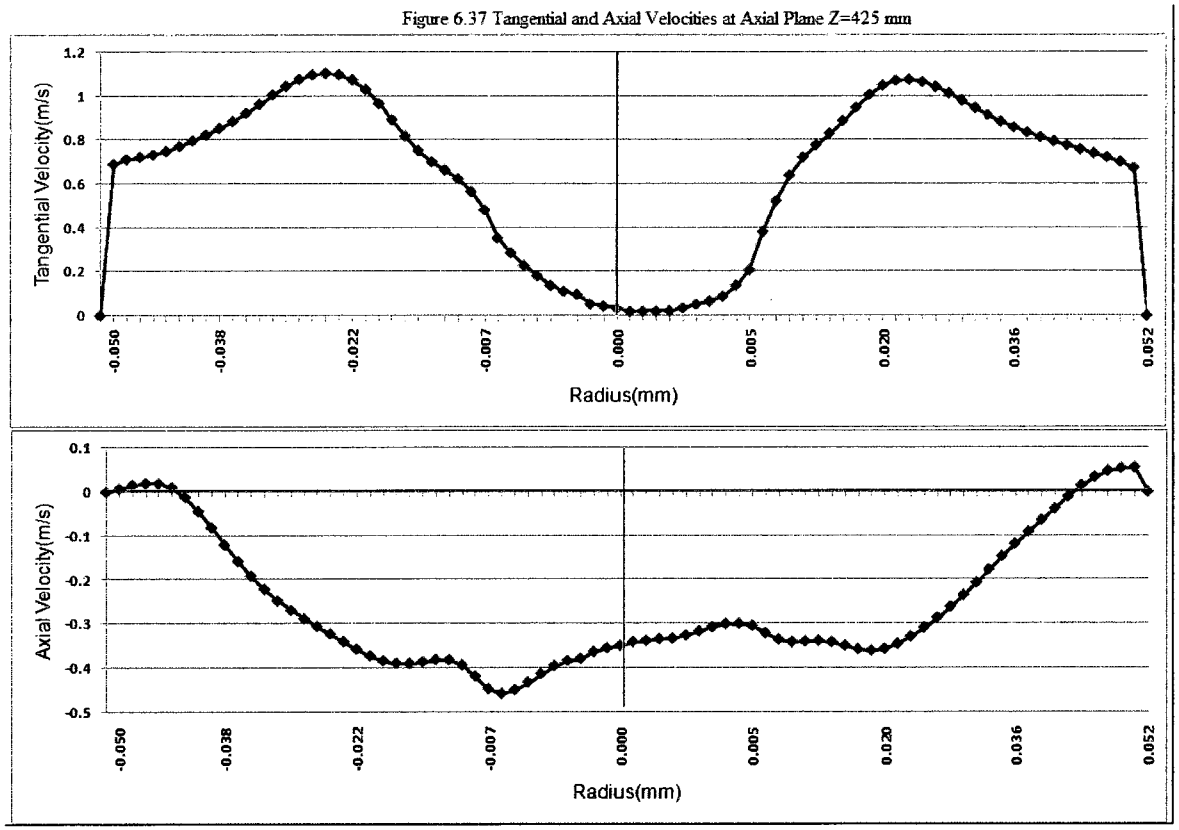

Figure 6.39 Tangential and Axial Velocities at Axial Plane Z=465 mm

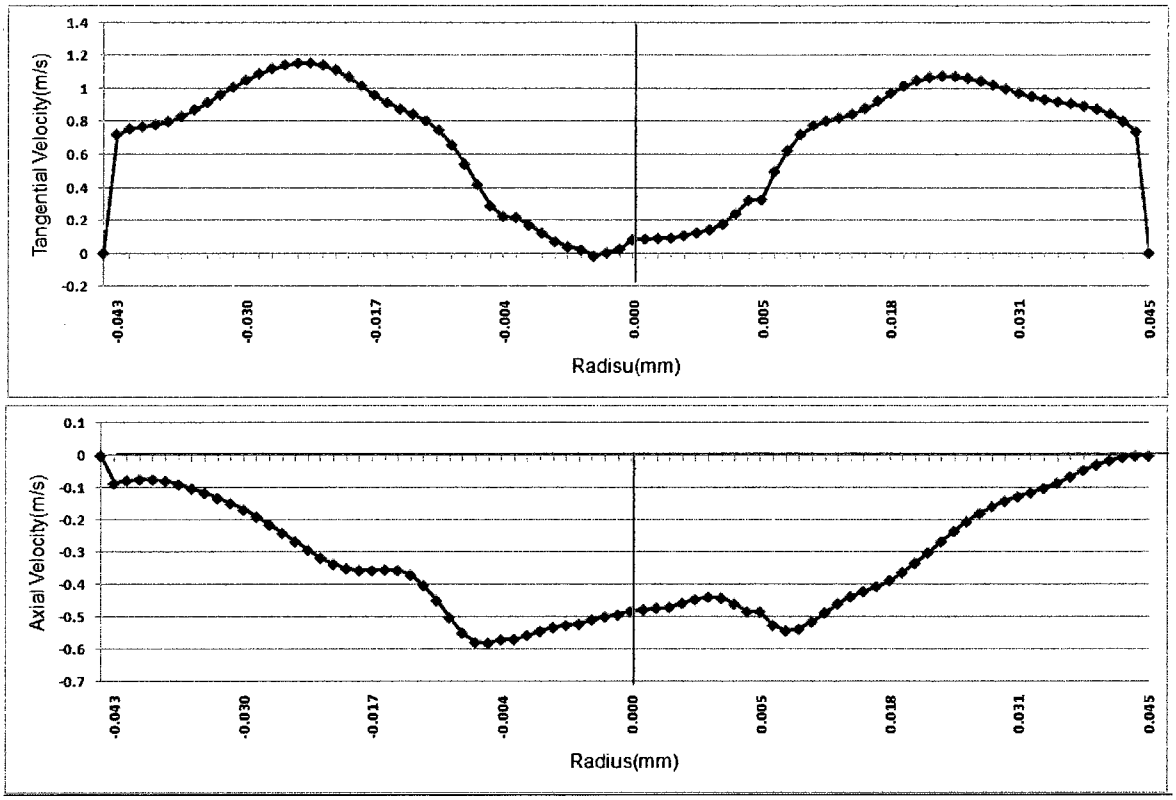

Figure 6.40 Tangential and Axial Velocities at Axial Plane Z=485 mm

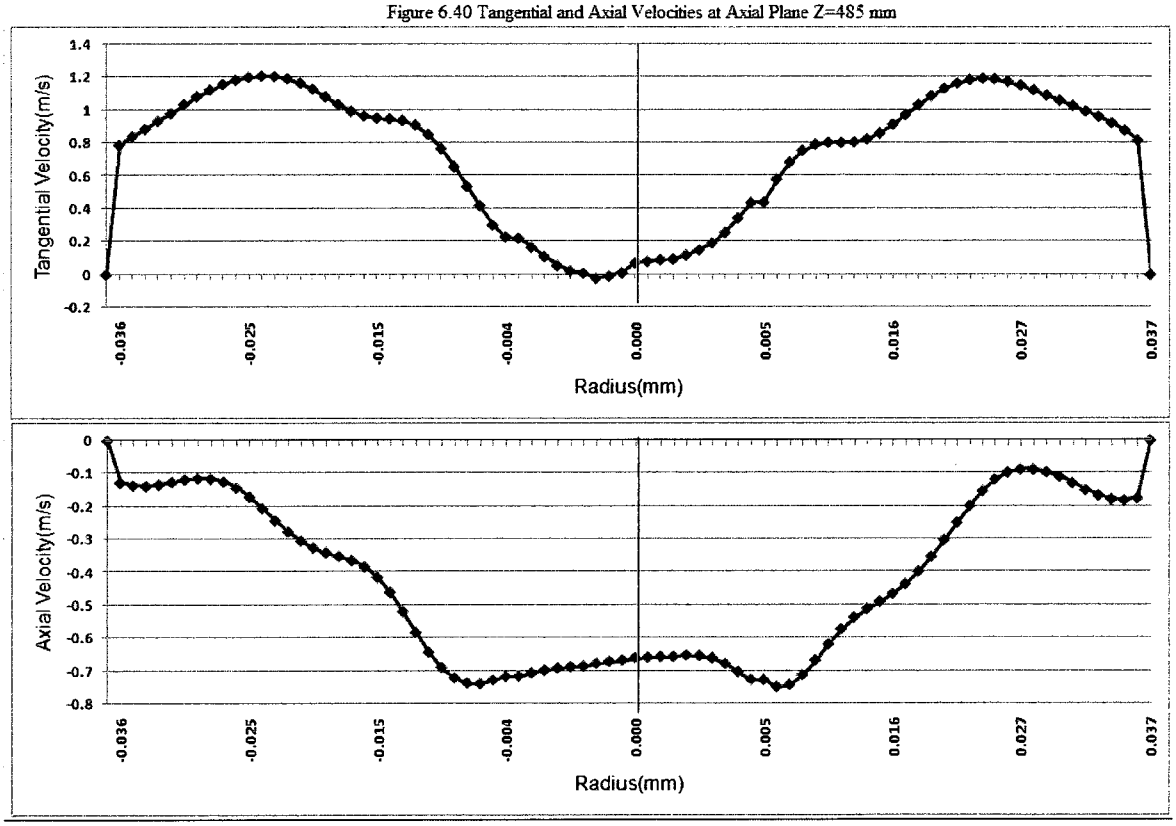

Figure 6.41 Tangential and Axial Velocities at Axial Plane Z=505 mm

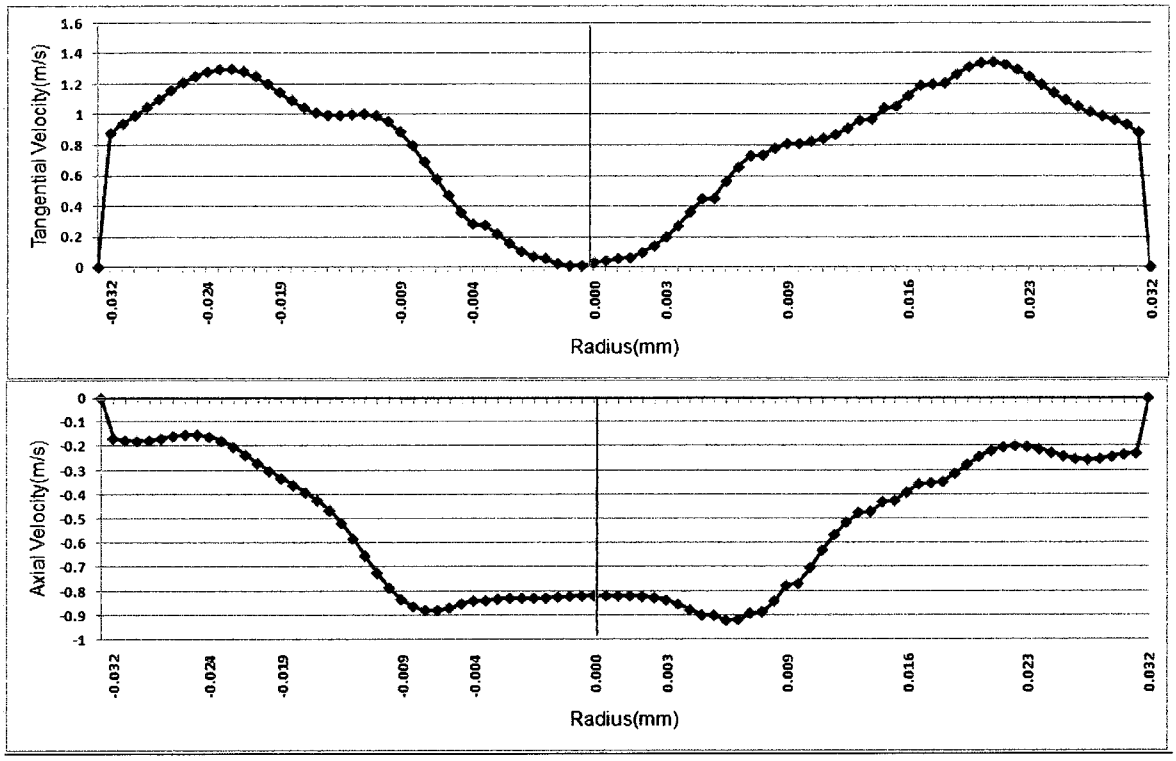

Figure 6.42 Tangential and Axial Velocities at Axial Plane Z=525 mm

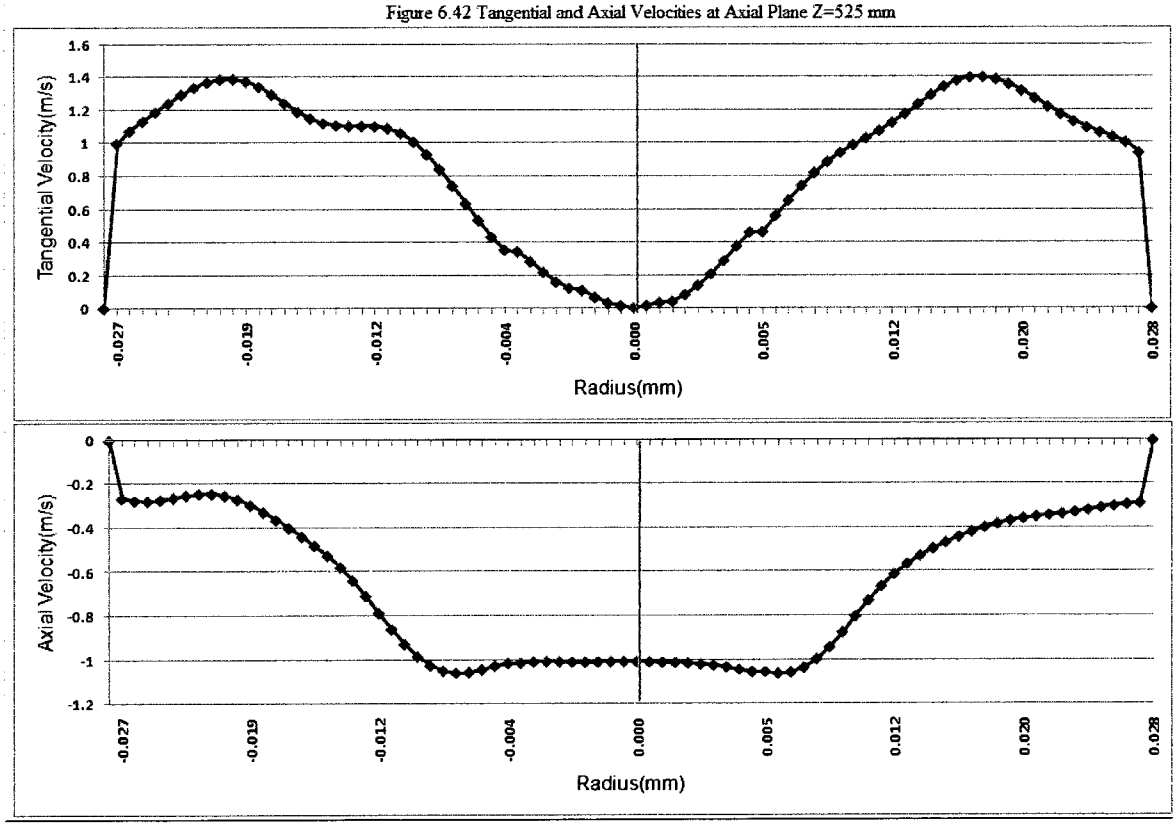

Figure 6.44 Tangential and Axial Velocities at Axial Plane Z=565 mm

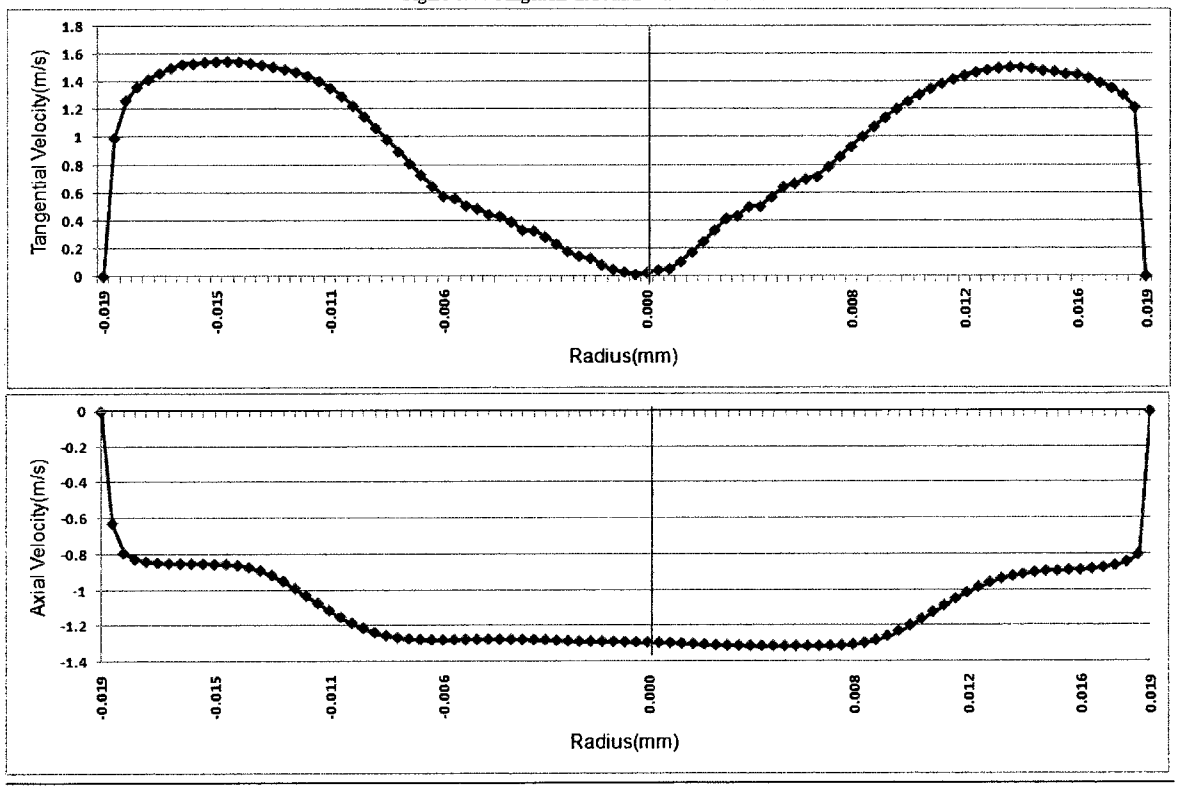

Figure 6.43 Tangential and Axial Velocities at Axial Plane Z=545 mm

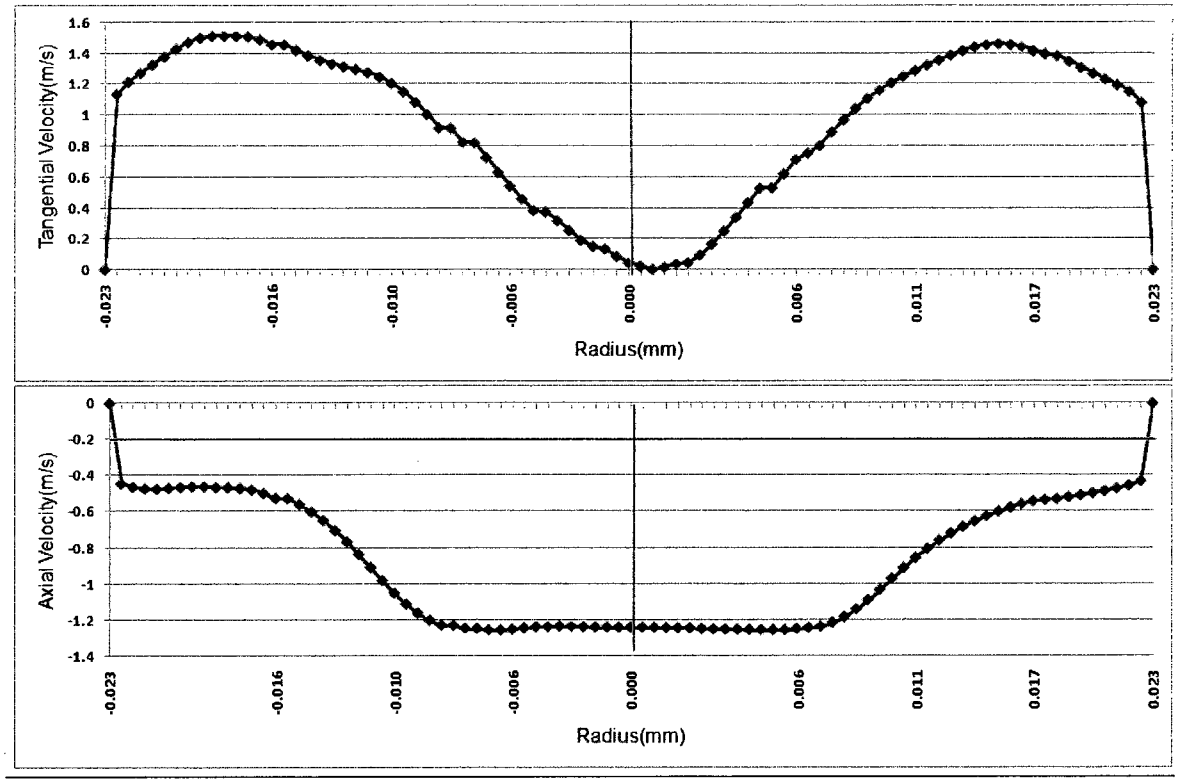

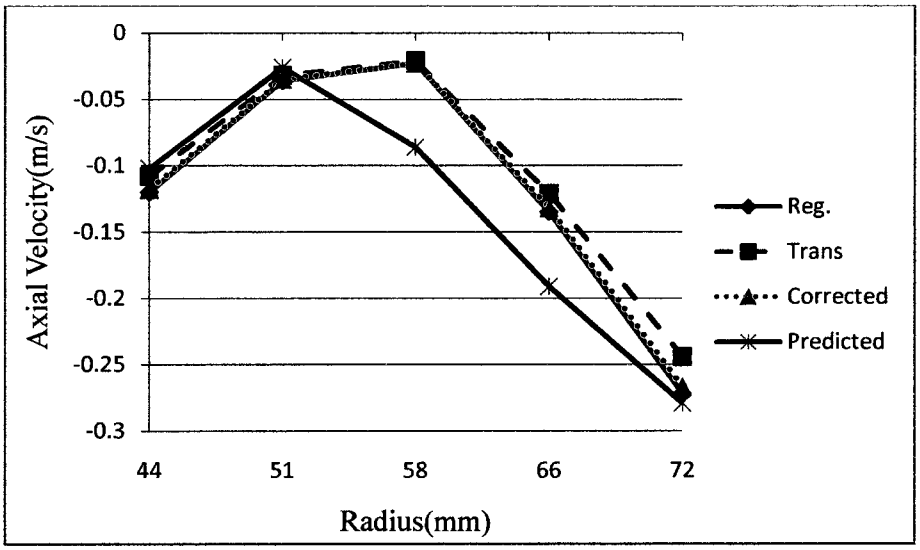

Figure 6.45 Comparison of the axial velocities at axial plane Z=140mm

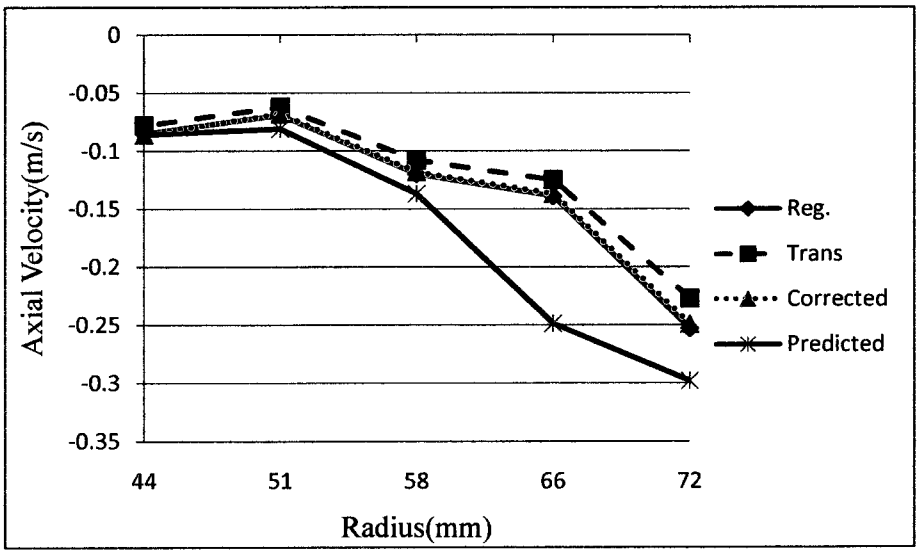

Figure 6.46 Comparison of the axial velocities at axial plane Z=160mm

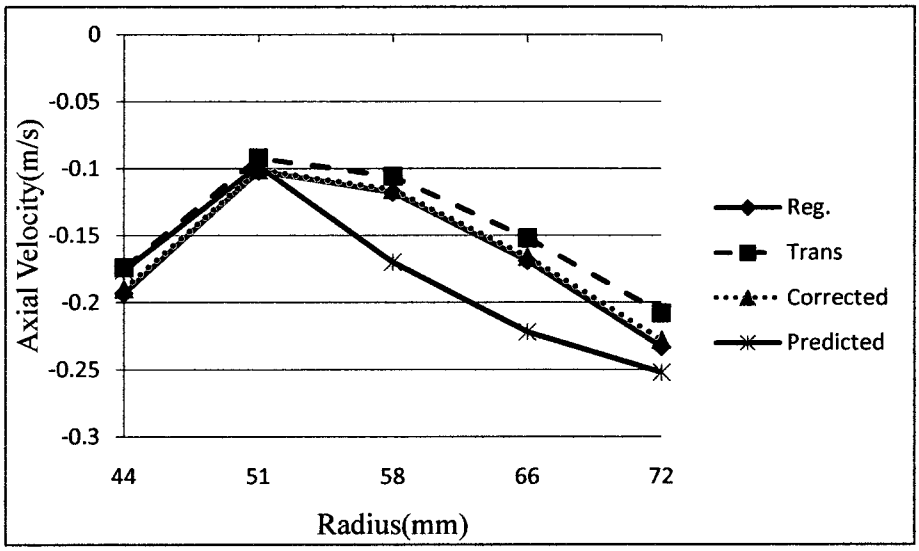

Figure 6.47 Comparison of the axial velocities at axial plane Z=187mm

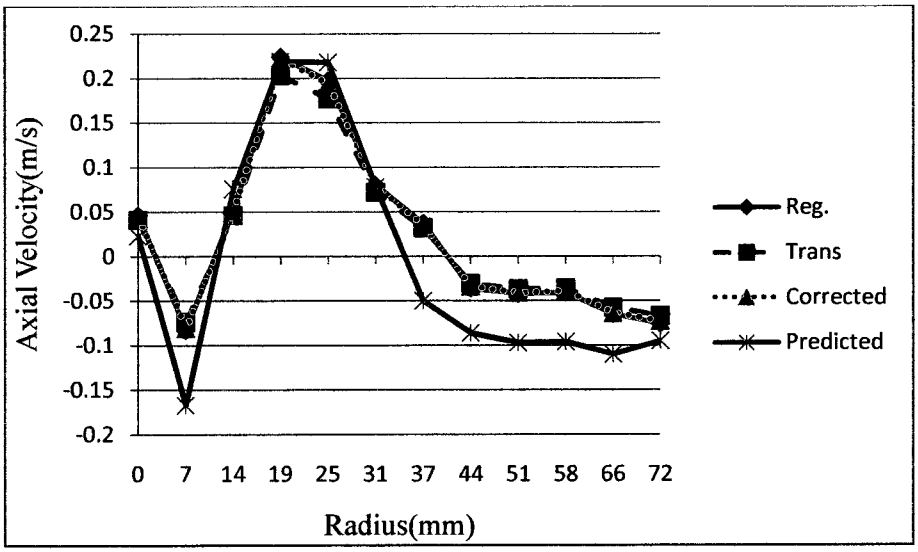

Figure 6.48 Comparison of the axial velocities at axial plane Z=200mm

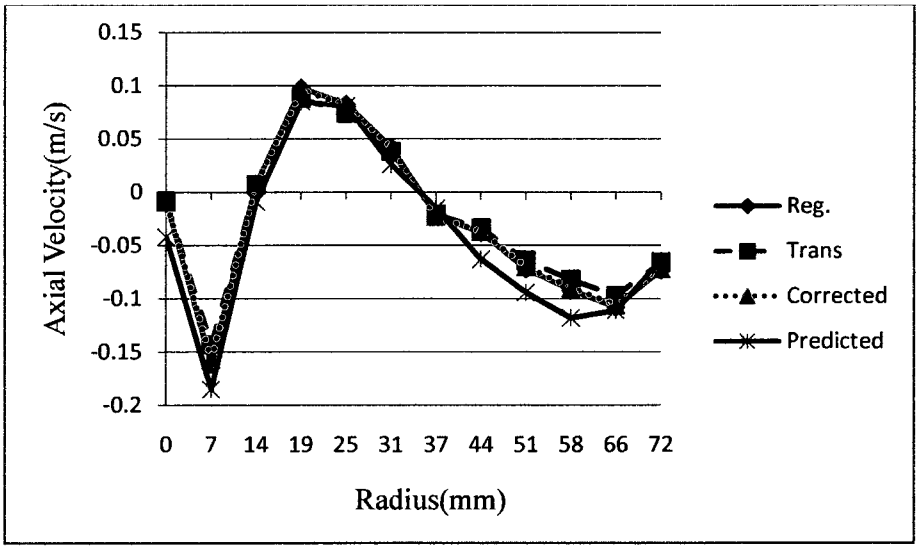

Figure 6.49 Comparison of the axial velocities at axial plane Z=220mm

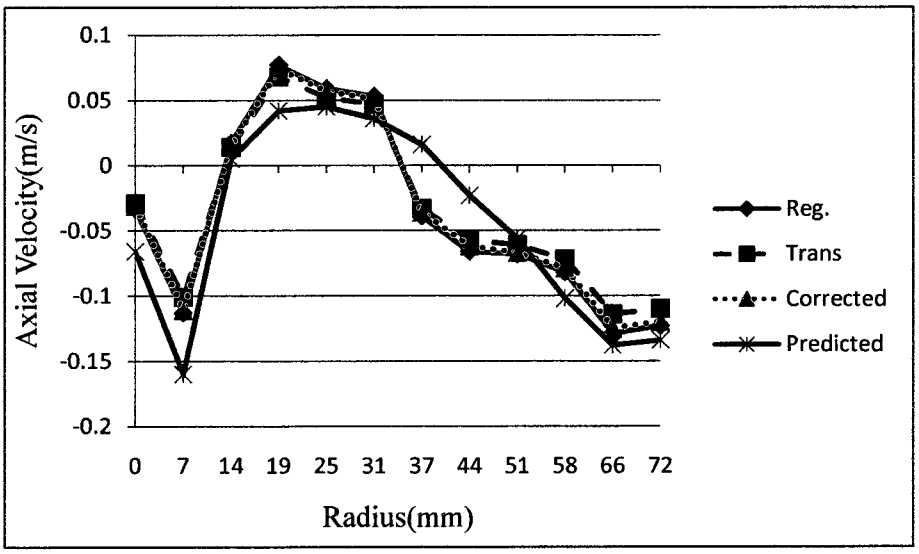

Figure 6.50 Comparison of the axial velocities at axial plane Z=240mm

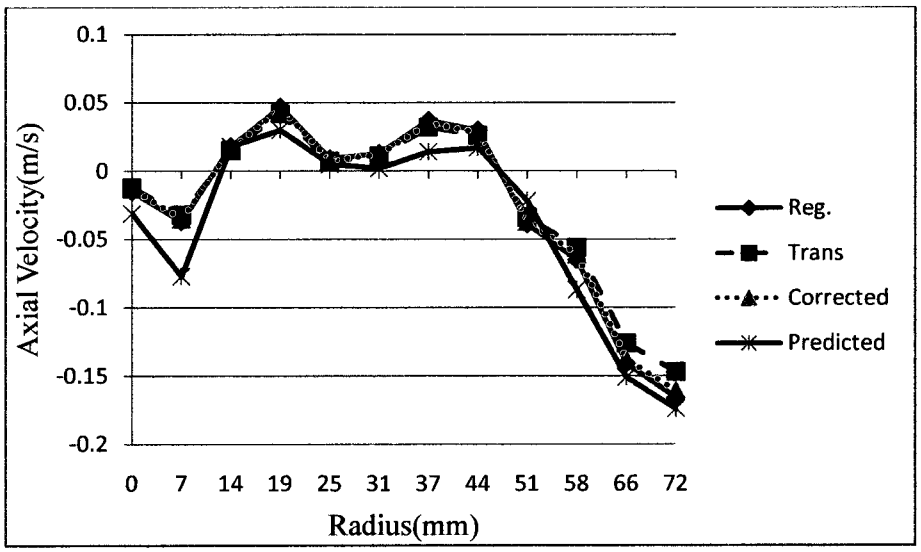

Figure 6.51 Comparison of the axial velocities at axial plane Z=260mm

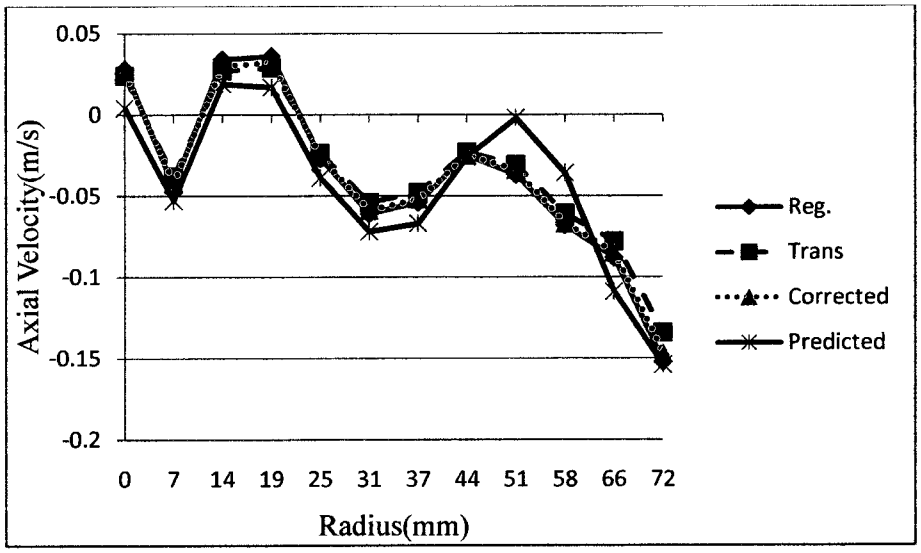

Figure 6.52 Comparison of the axial velocities at axial plane Z=280mm

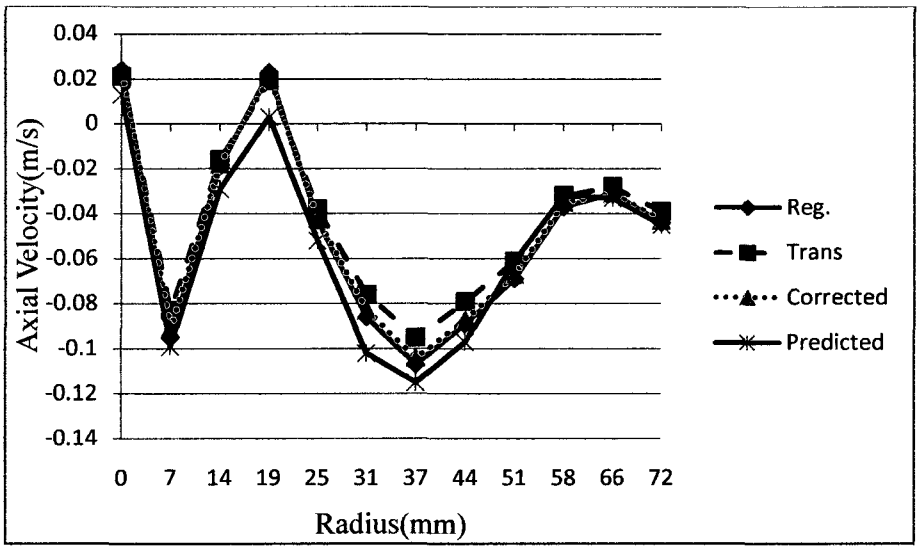

Figure 6.53 Comparison of the axial velocities at axial plane Z=294mm

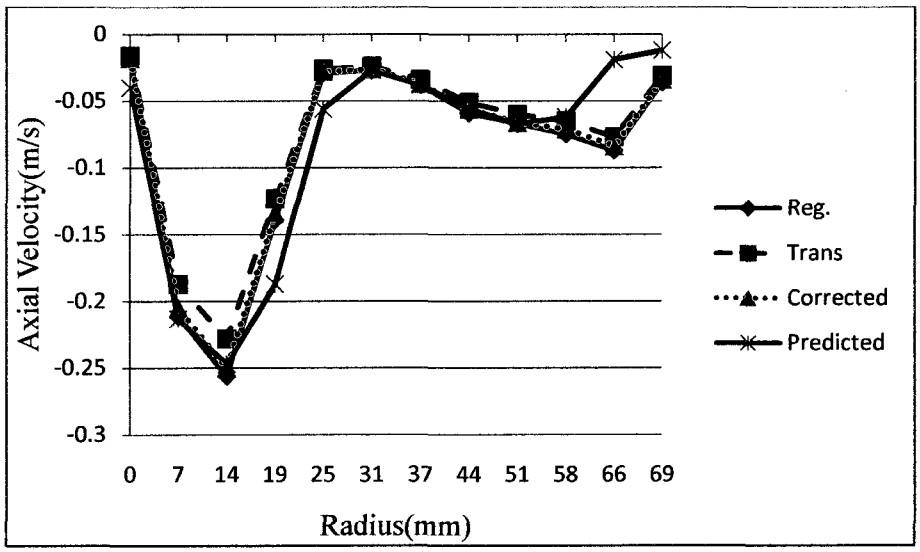

Figure 6.54 Comparison of the axial velocities at axial plane Z=345mm

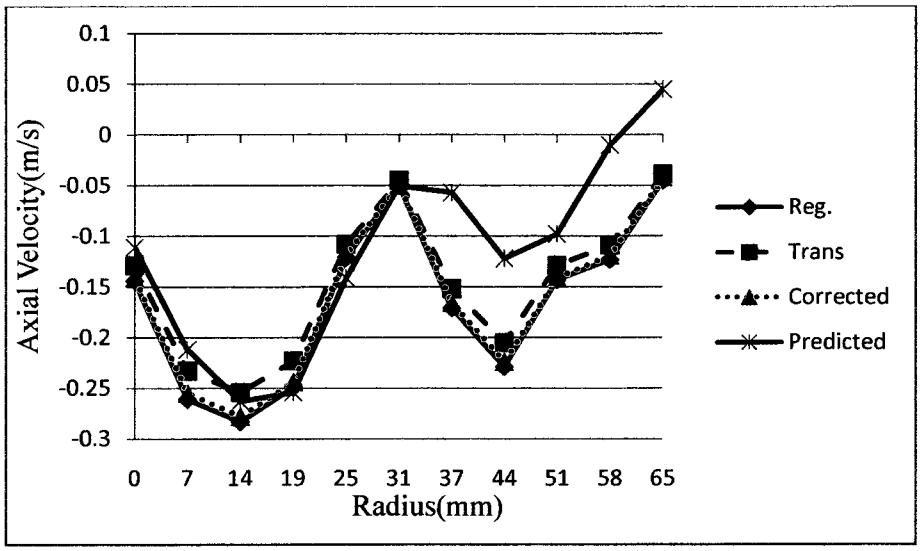

Figure 6.55 Comparison of the axial velocities at axial plane Z=365mm

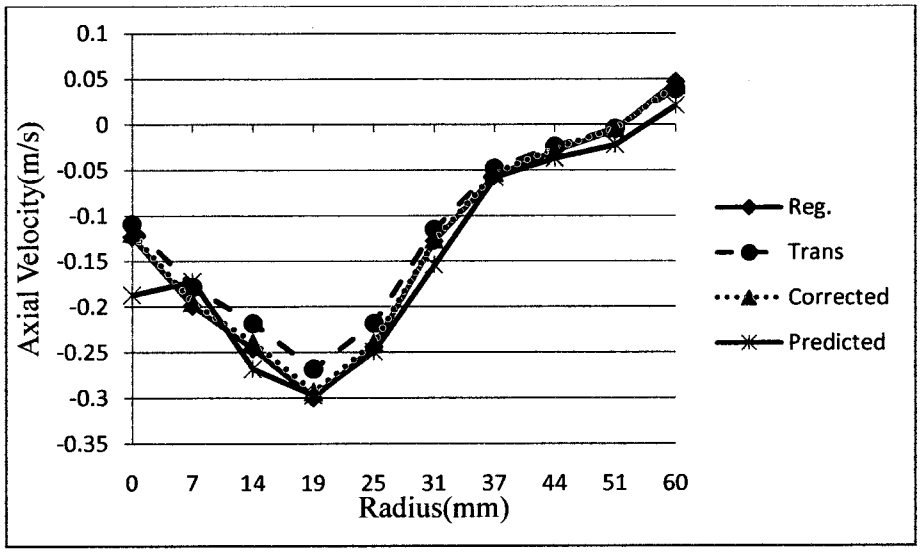

Figure 6.56 Comparison of the axial velocities at axial plane Z=385mm

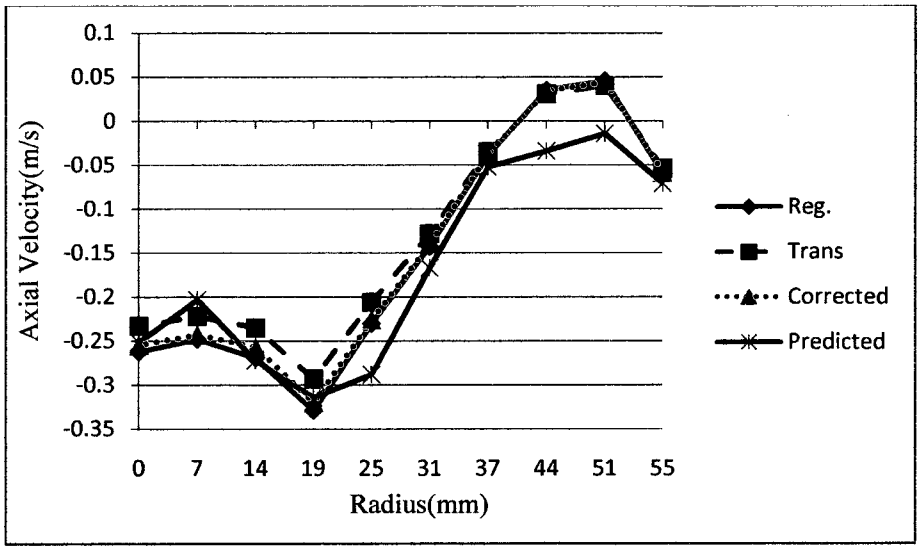

Figure 6.57 Comparison of the axial velocities at axial plane Z=405mm

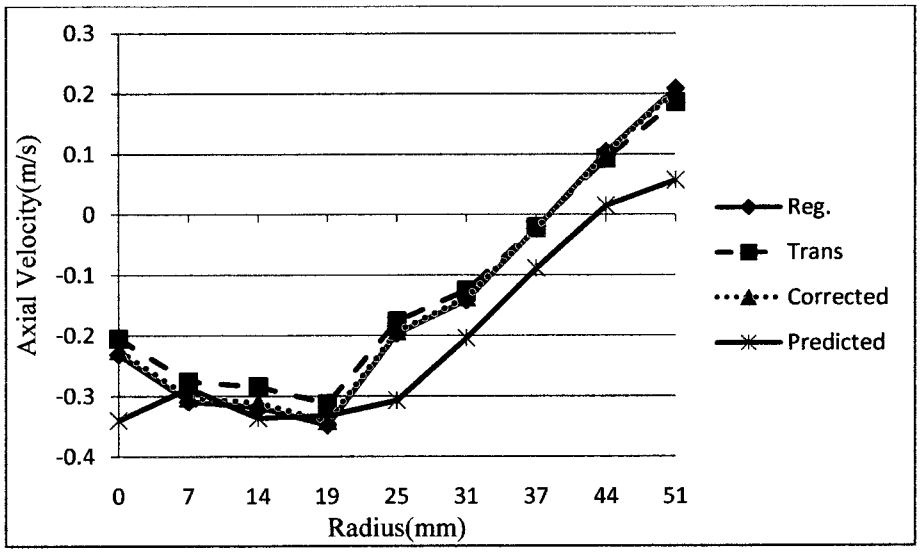

Figure 6.58 Comparison of the axial velocities at axial plane Z=425mm

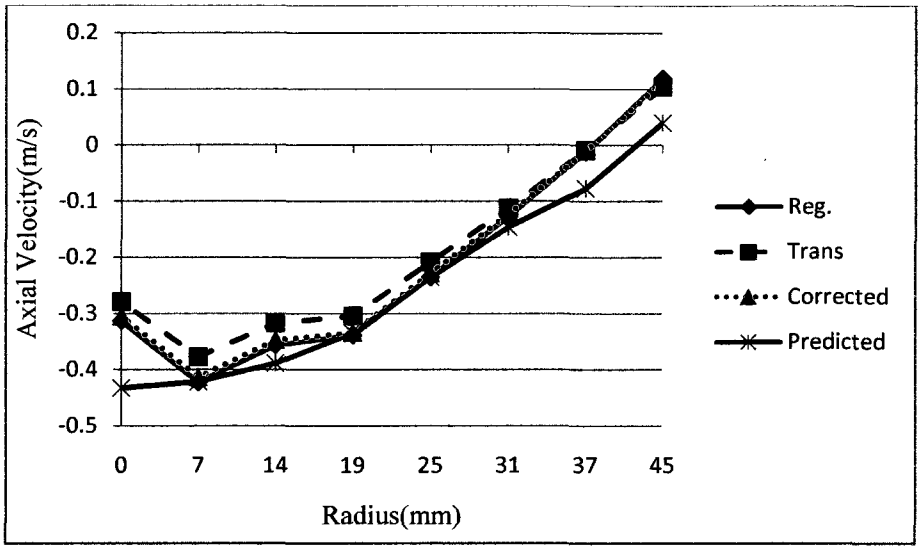

Figure 6.59 Comparison of the axial velocities at axial plane Z=445mm

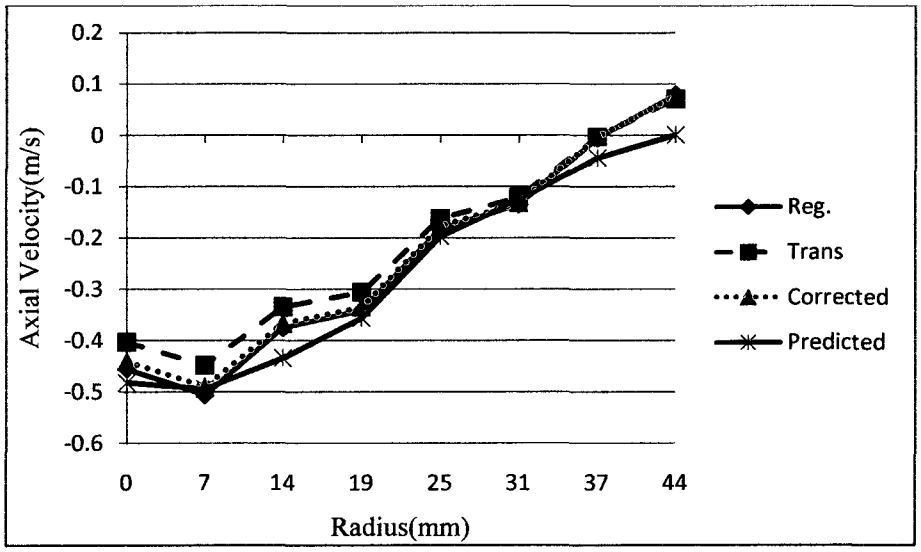

Figure 6.60 Comparison of the axial velocities at axial plane Z=465mm

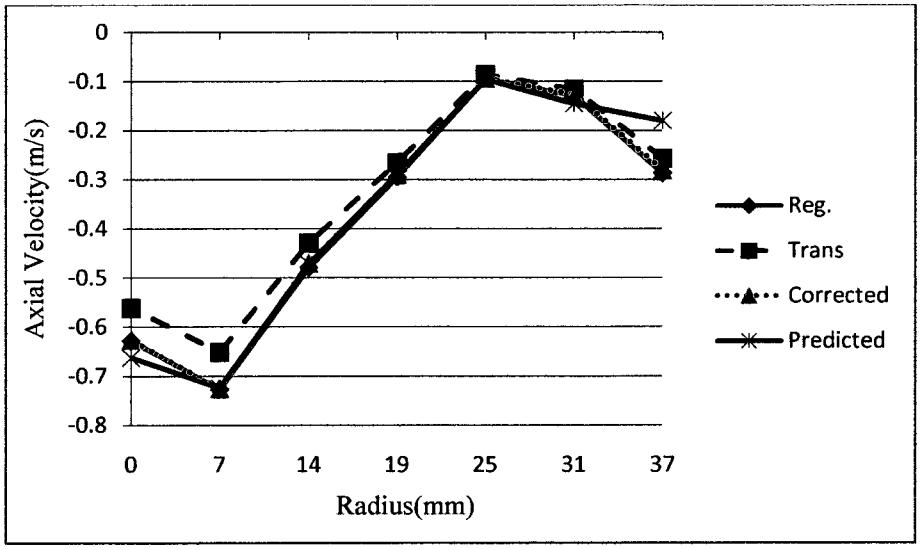

Figure 6.61Comparison of the axial velocities at axial plane Z=485mm

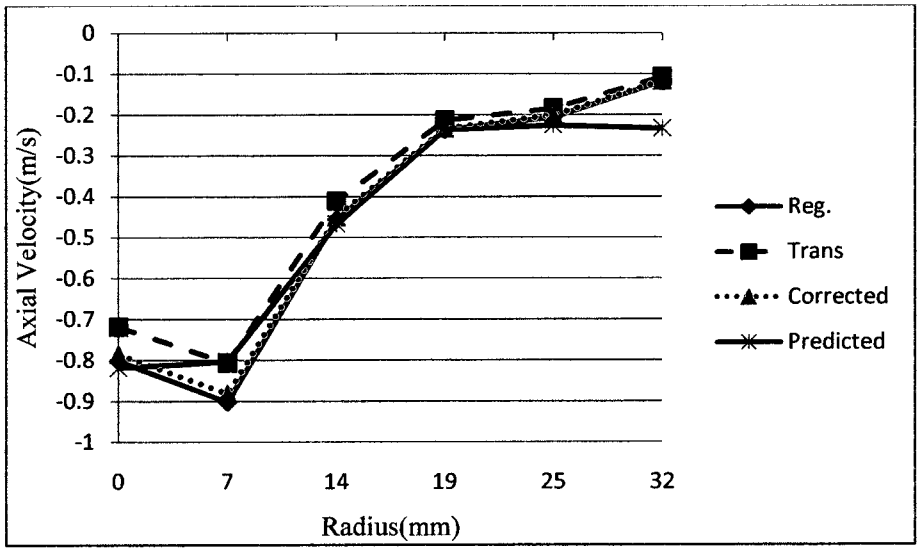

Figure 6.62 Comparison of the axial velocities at axial plane Z=505mm

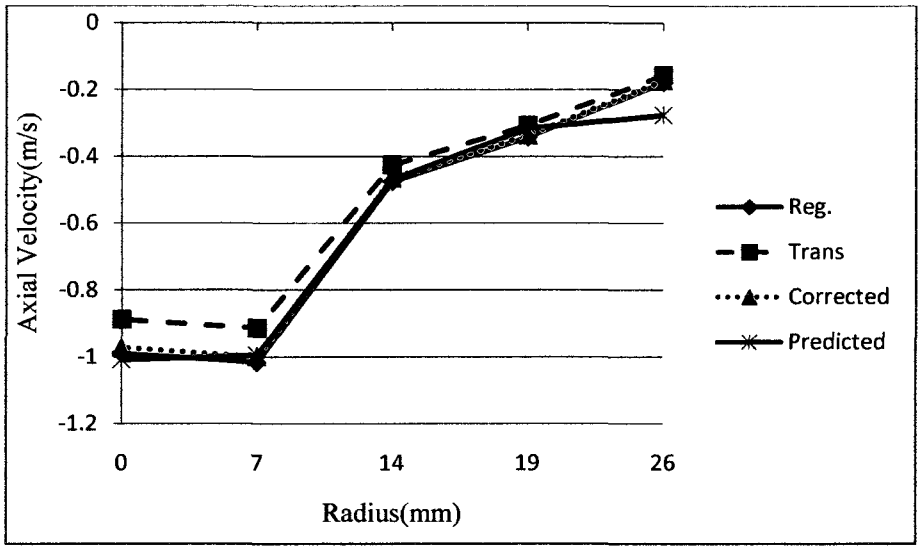

Figure 6.63 Comparison of the axial velocities at axial plane Z=525mm

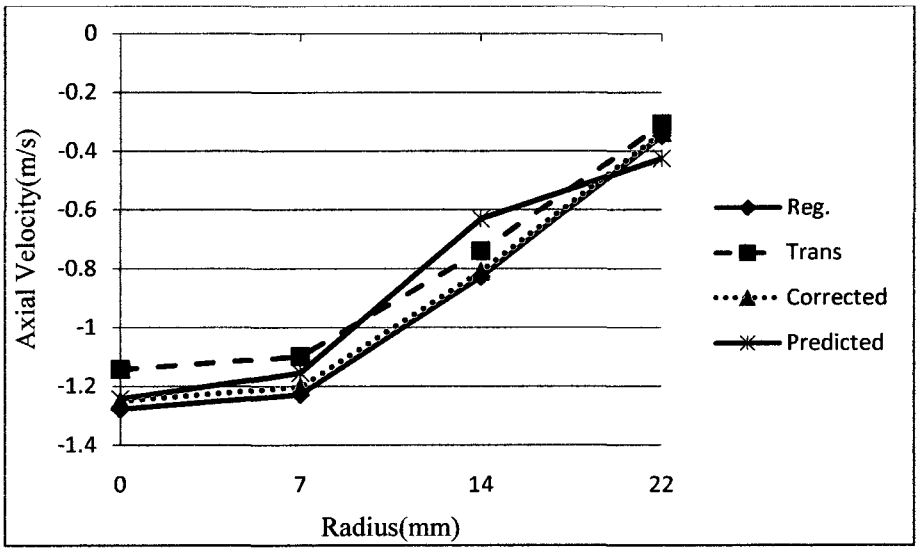

Figure 6.64 Comparison of the axial velocities at axial plane Z=545mm

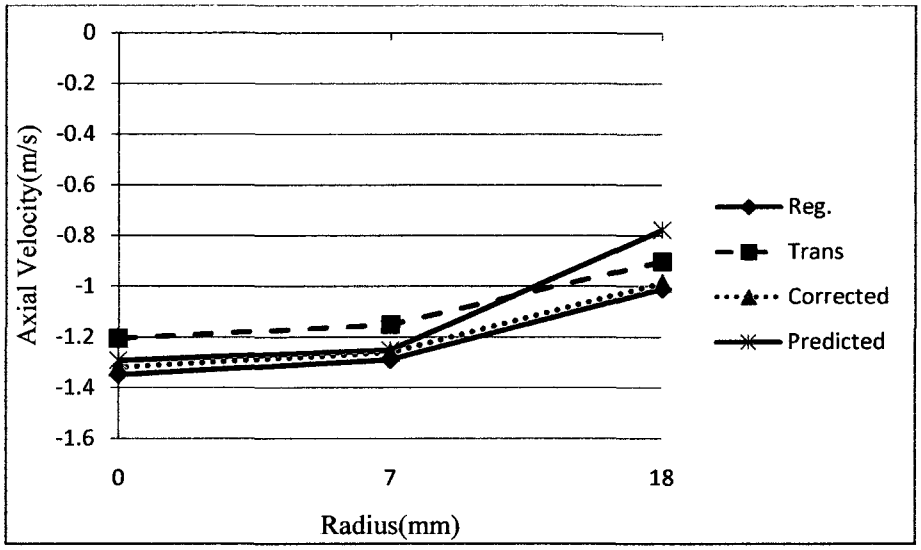

Figure 6.65 Comparison of the axial velocities at axial plane Z=565mm

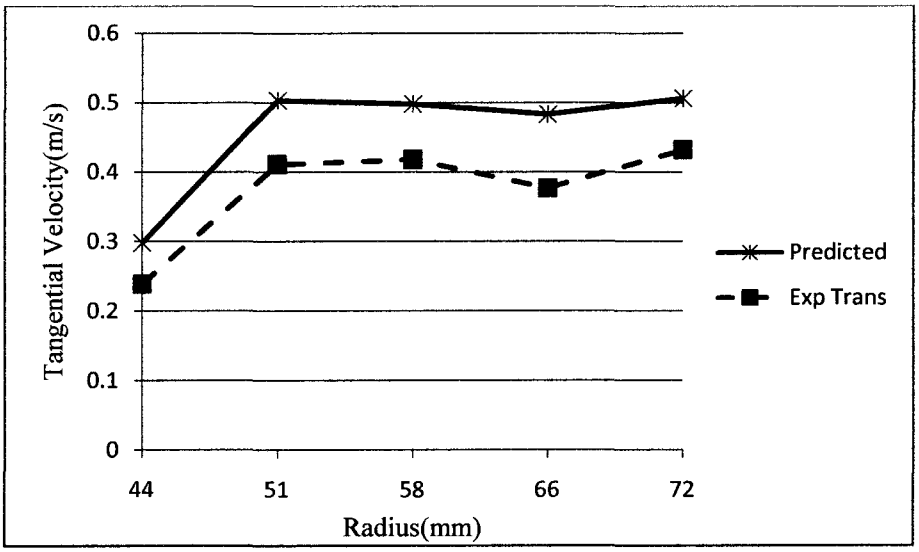

Figure 6.66 Comparison of the tangential velocities at axial plane Z=140mm

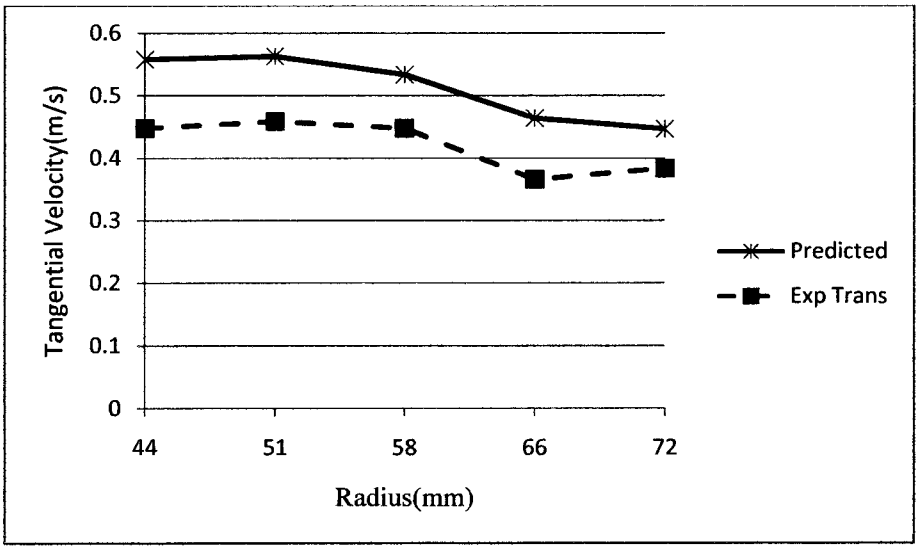

Figure 6.67 Comparison of the tangential velocities at axial plane Z=160mm

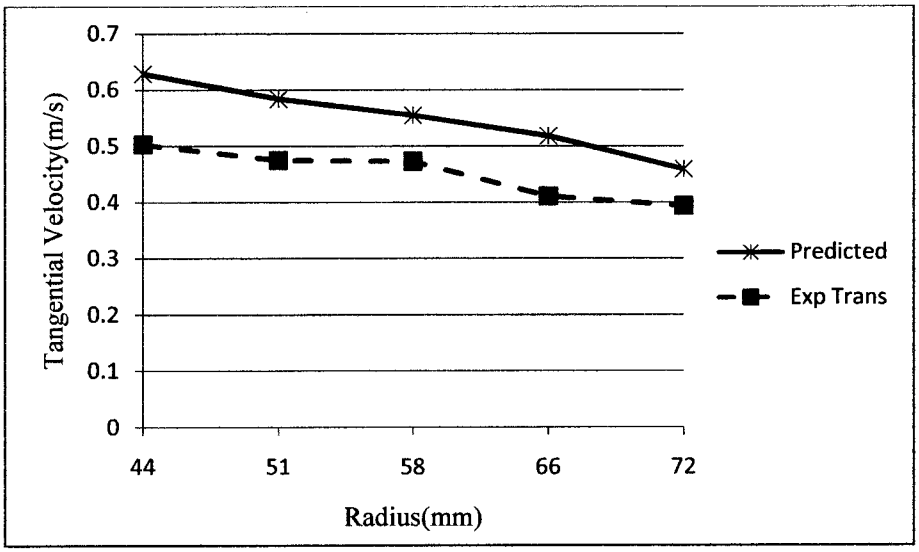

Figure 6.68 Comparison of the tangential velocities at axial plane Z=187mm

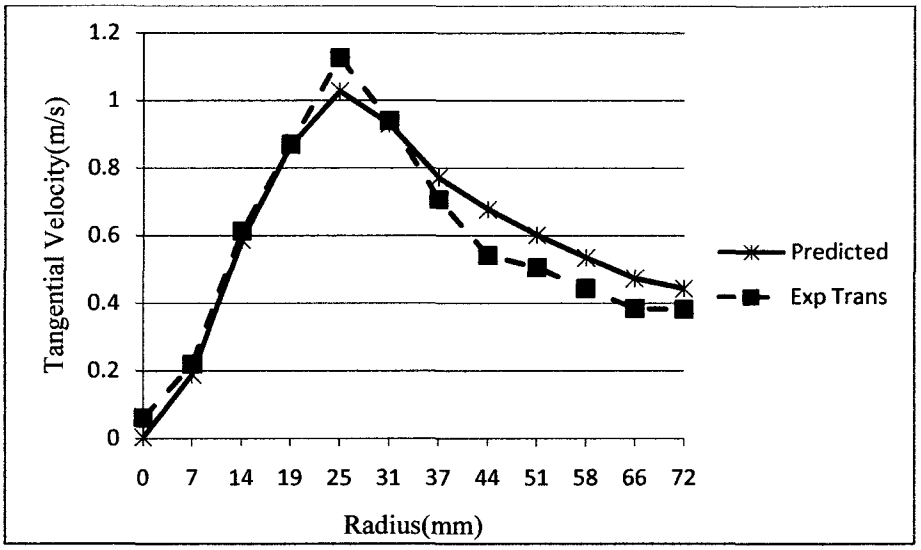

Figure 6.69 Comparison of the tangential velocities at axial plane Z=200mm

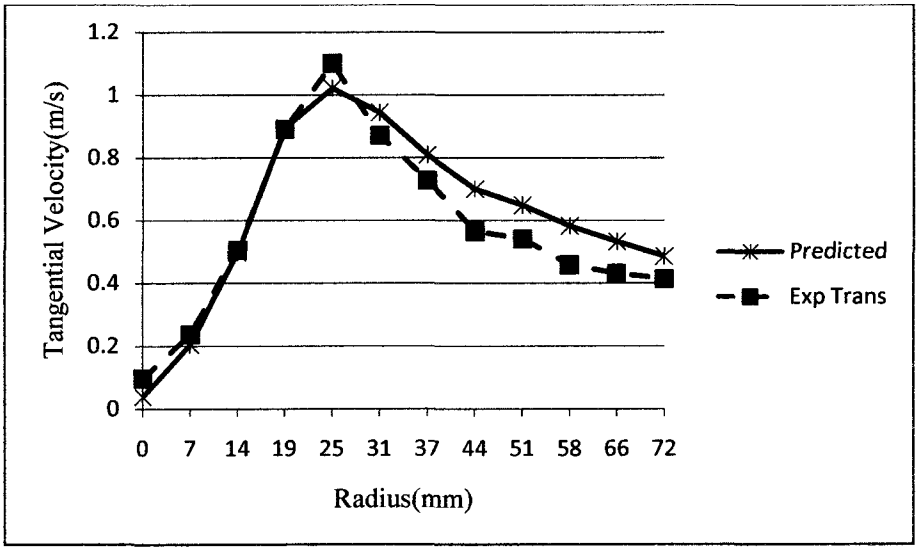

Figure 6.70 Comparison of the tangential velocities at axial plane Z=220mm

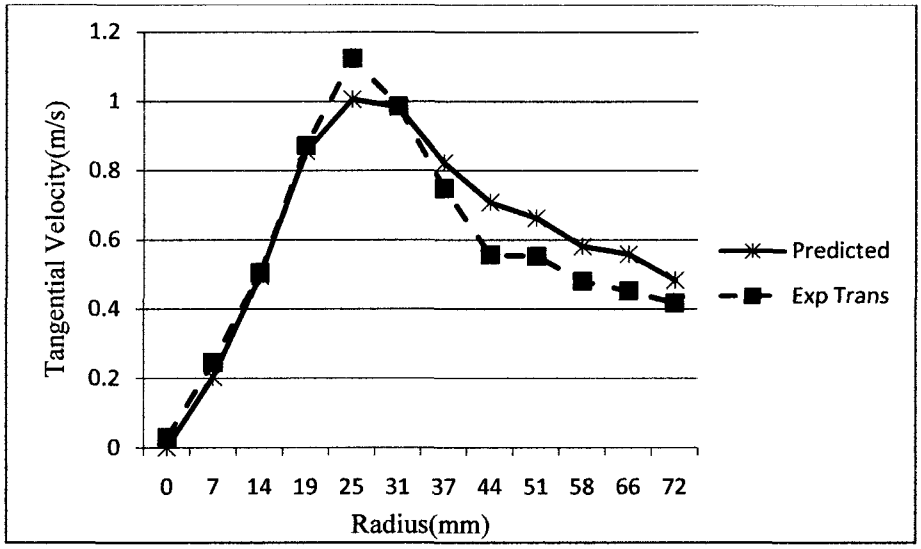

Figure 6.71 Comparison of the tangential velocities at axial plane Z=240mm

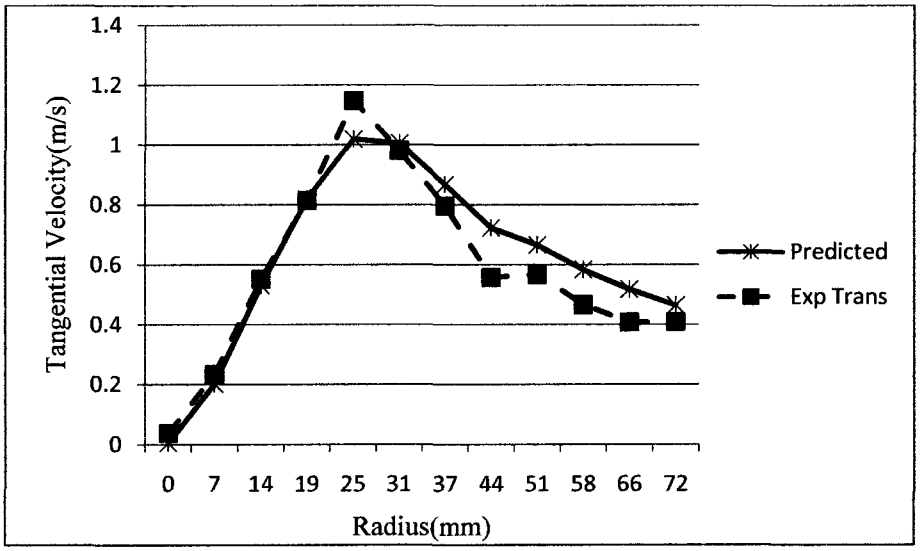

Figure 6.72 Comparison of the tangential velocities at axial plane Z=260mm

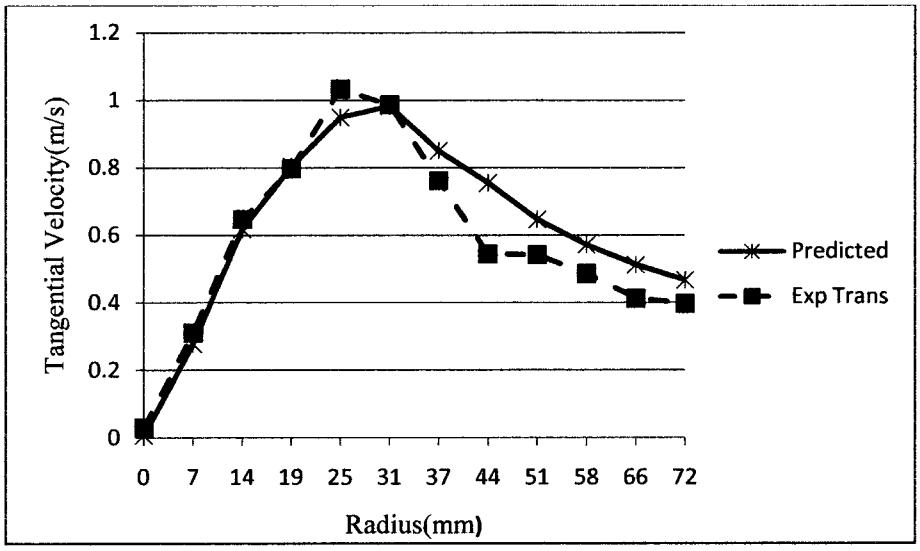

Figure 6.73 Comparison of the tangential velocities at axial plane Z=280mm

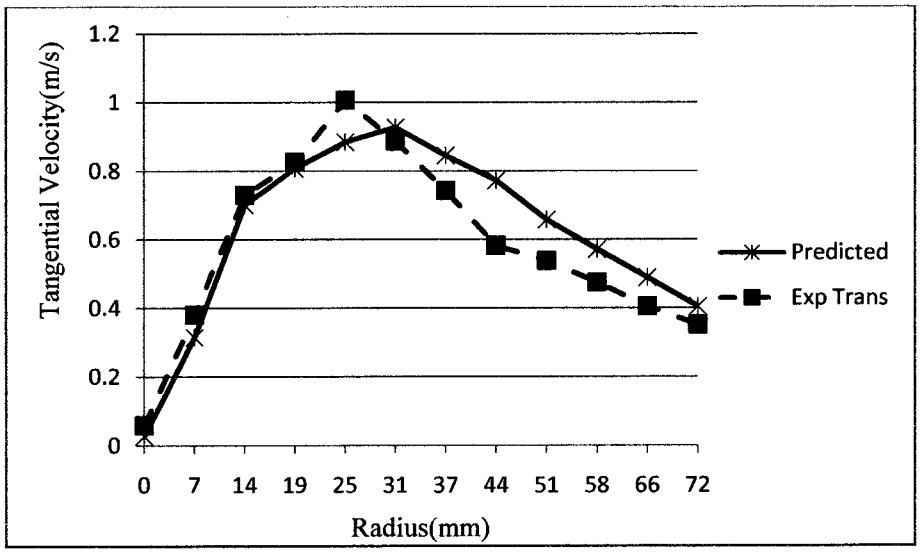

Figure 6.74 Comparison of the tangential velocities at axial plane Z=294mm

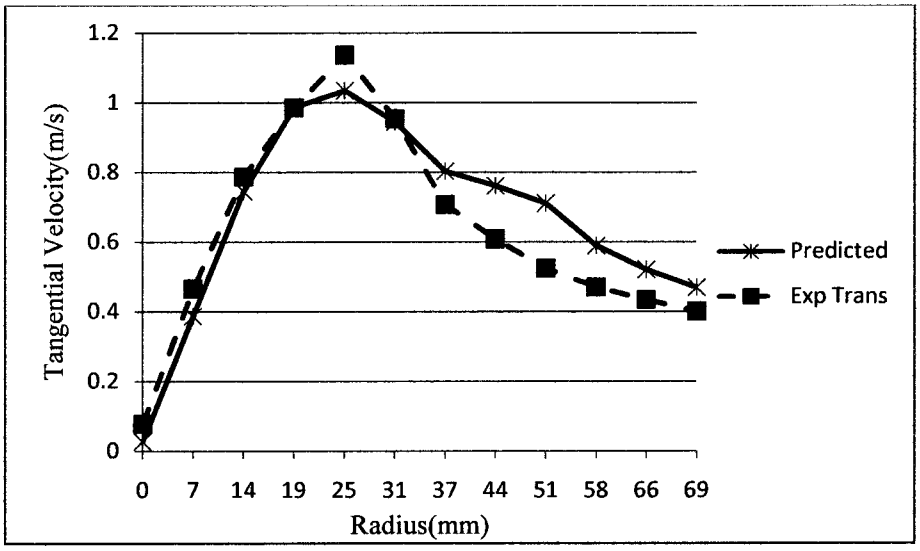

Figure 6.75 Comparison of the tangential velocities at axial plane Z=345mm

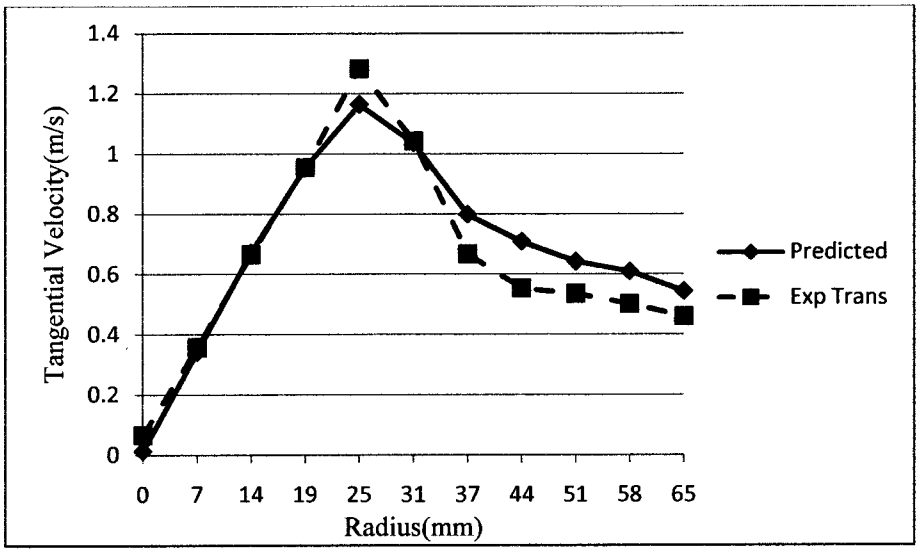

Figure 6.76 Comparison of the tangential velocities at axial plane Z=365mm

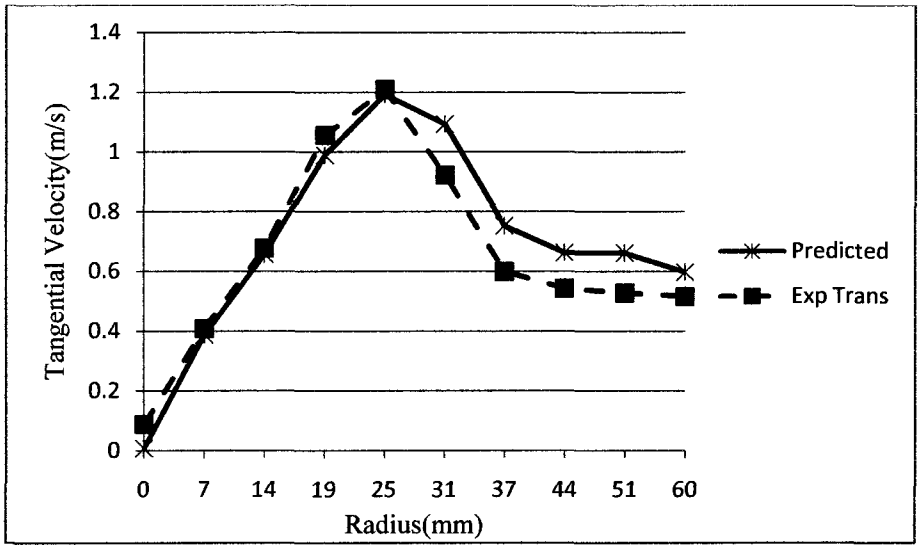

Figure 6.77 Comparison of the tangential velocities at axial plane Z=385mm

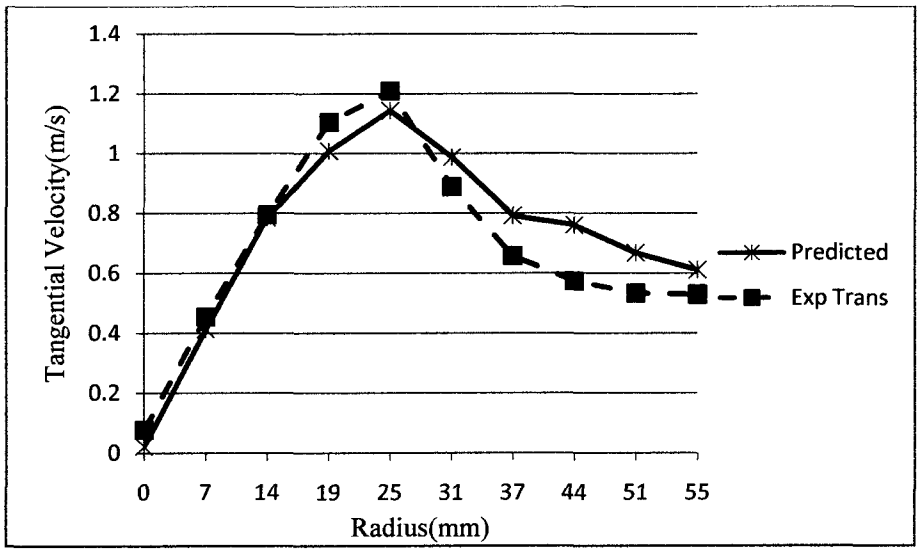

Figure 6.78 Comparison of the tangential velocities at axial plane Z=405mm

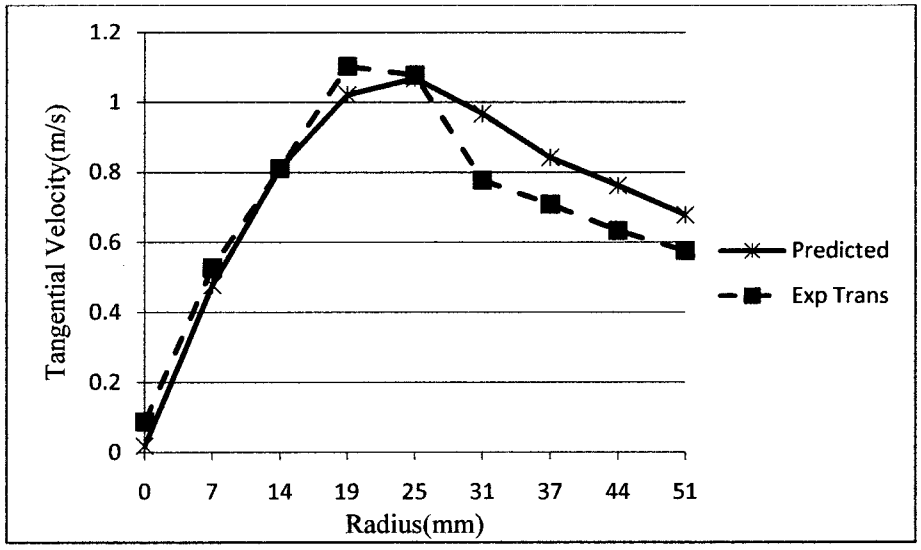

Figure 6.79 Comparison of the tangential velocities at axial plane Z=425mm

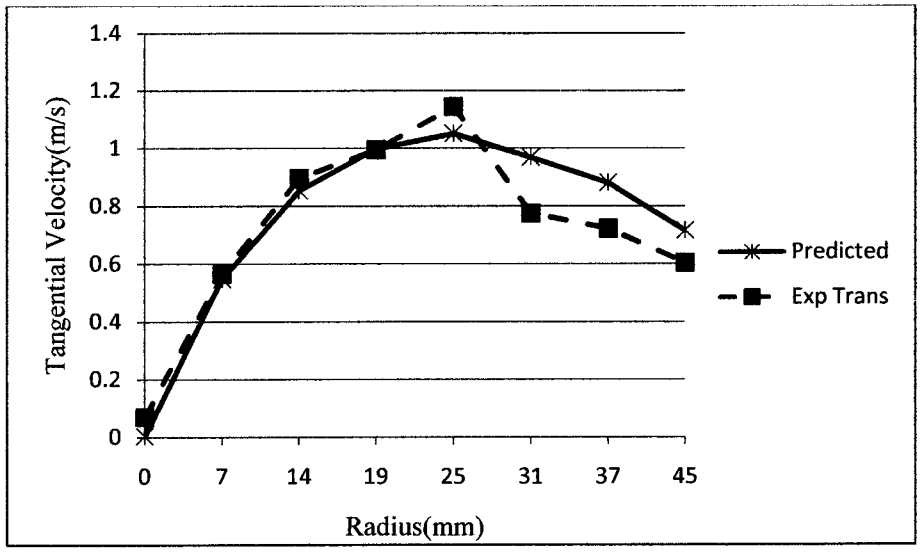

Figure 6.80 Comparison of the tangential velocities at axial plane Z=445mm

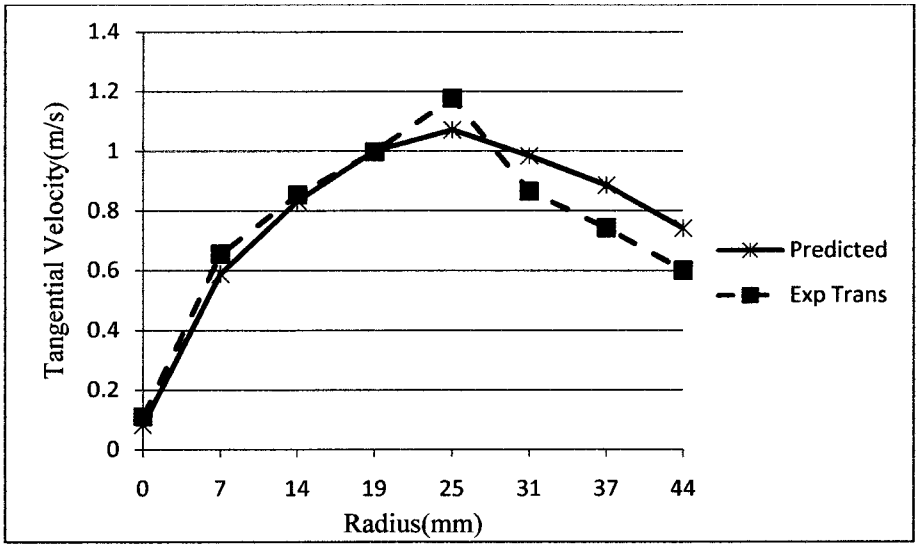

Figure 6.81 Comparison of the tangential velocities at axial plane Z=465mm

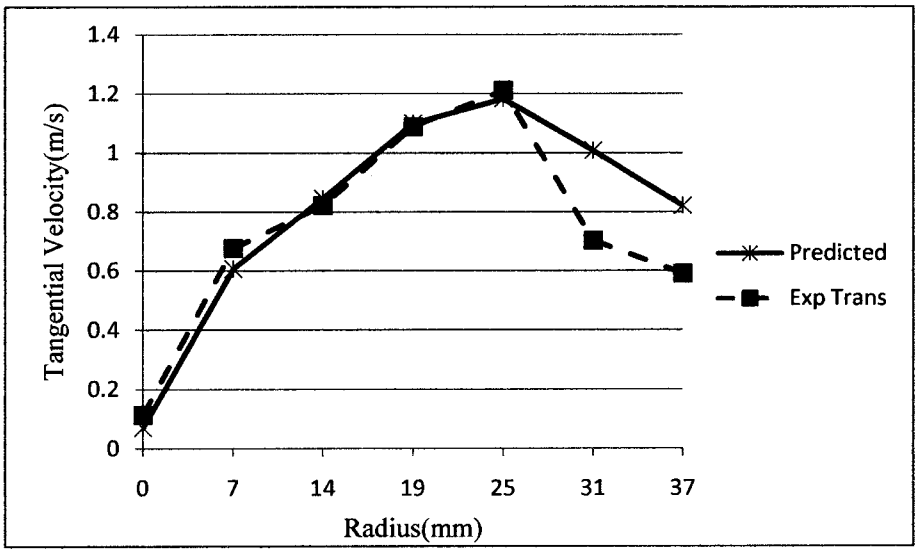

Figure 6.82 Comparison of the tangential velocities at axial plane Z=485mm

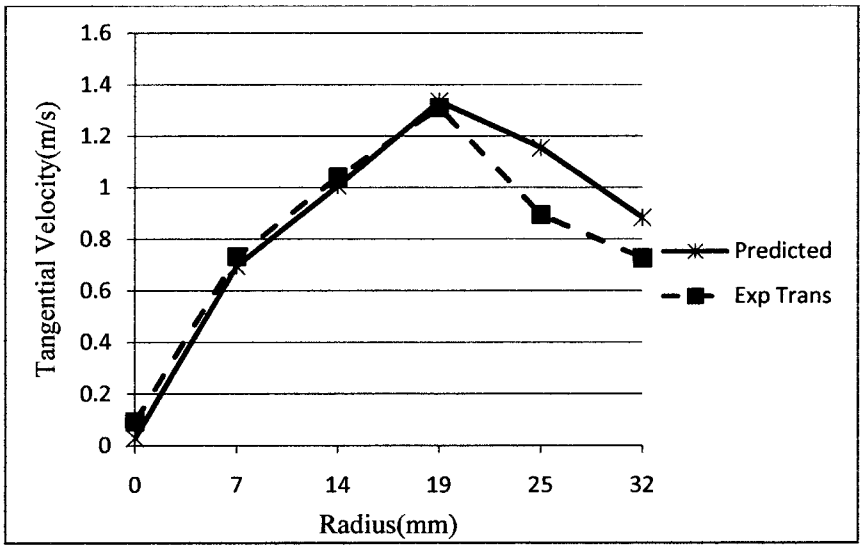

Figure 6.83 Comparison of the tangential velocities at axial plane Z=505mm

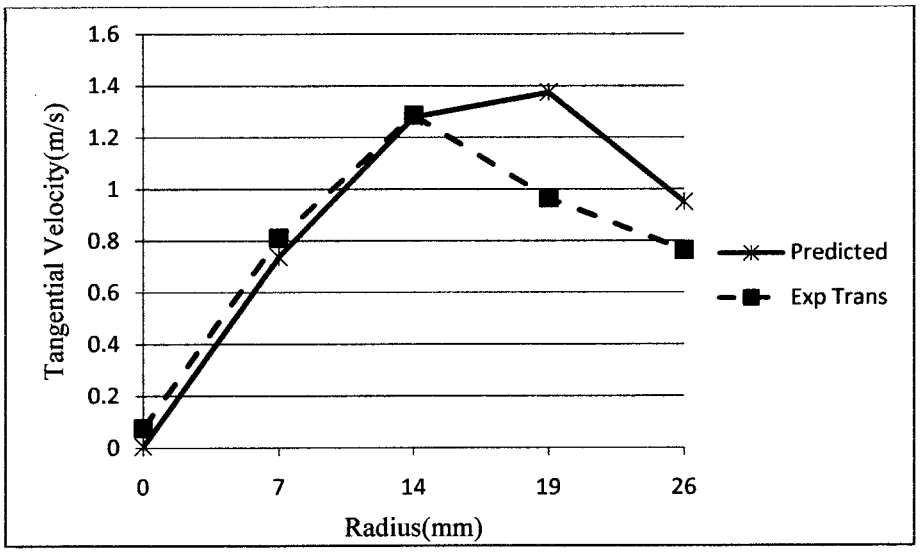

Figure 6.84 Comparison of the tangential velocities at axial plane Z=525mm

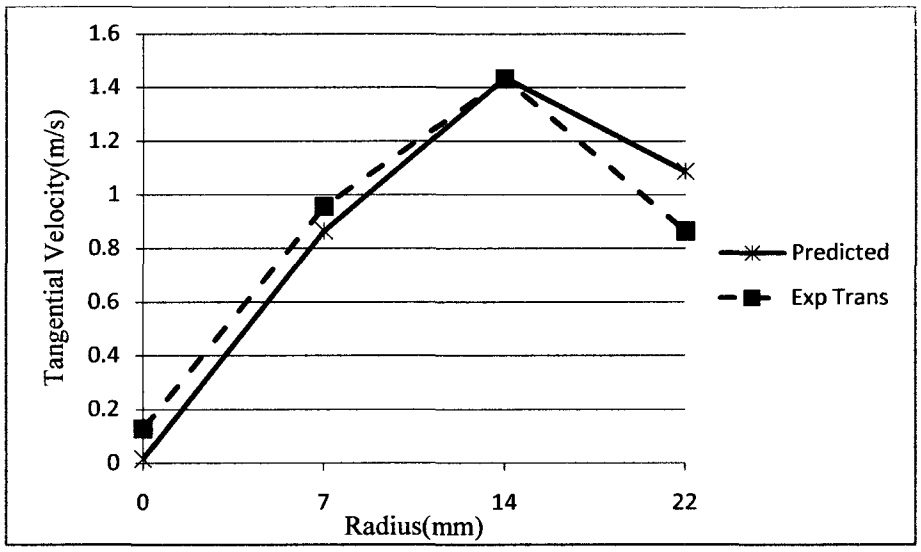

Figure 6.85 Comparison of the tangential velocities at axial plane Z=545mm

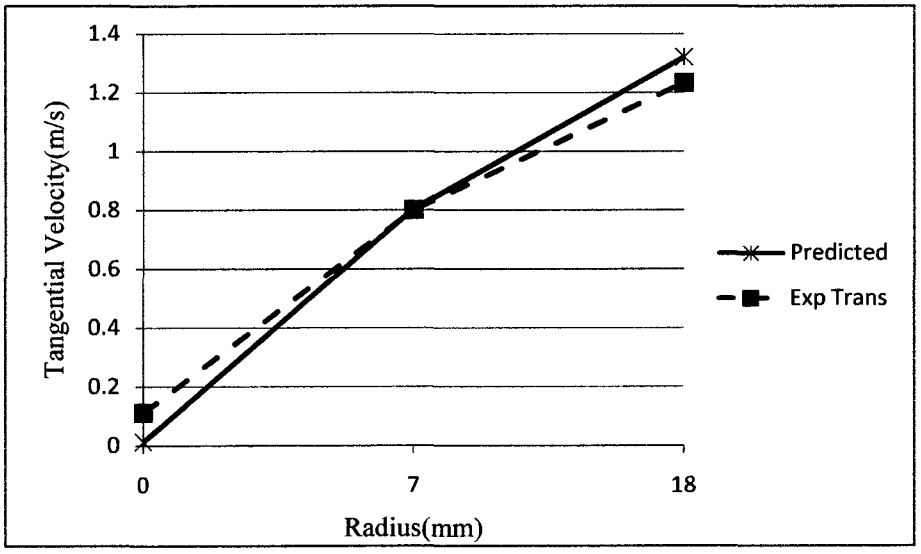

Figure 6.86 Comparison of the tangential velocities at axial plane Z=565mm

Chapter 7

Summary, Conclusions and Recommendation for Further Research

7.1 Summary

In the present study, the characteristics of the flow field inside a 6″ hydrocyclone were investigated. Towards this goal, four major tasks were completed during the course of this study.

To begin with, a test facility to study a 6″ hydrocyclone was designed, drawn and fabricated. Next, the Laser Doppler Anemometry (LDA) was deployed to measure the mean velocity components within the hydrocyclone. As a result of directly operating the LDA, without inclosing rectangular boxes around the walls of the hydrocyclone to reduce the effects of the refraction of the laser beams, two positions for the optical probe were chosen. The first position was the traditional one (called the regular position) in which the two laser beams (green) perpendicularly oriented to each other penetrate the solid wall of the hydrocyclone with one pair of beams set parallel to the hydrocyclone axis. The other horizontal blue laser beam pair penetrates the hydrocyclone from the sides. Therefore, the green and blue beams do not intersect in one crossing point along the LDA axis. This forces one to measure only one component at the same point.

In the second position (called the transform position), the four laser beams (two blue and two green) penetrate the hydrocyclone from the sides of the curved wall.

This was achieved by rotating the optical probe 45° angle, which forced the four beams to intersect at a single point. This new method permitted the measurement of tangential and axial velocity components at a single point. The viability of this procedure was verified using test data.

In the second experimental series, a flow visualization test was conducted by using droplet dye injection technique to qualitatively investigate the flow field patterns of the 6″ hydrocyclone. By tracing the trajectories of droplet dye within hydrocyclone, five different kinds of flow field patterns were observed and recorded on video frames for analysis and comparison with the experimental LDA data.

The short study to predict the flow field characteristics inside the hydrocyclone was attempted using the Computational fluid dynamics (CFD) software. The turbulent model used for this purpose was the Reynolds Stress Model (RSM) as the flow field was highly curved.

7.2 Conclusions

Experiments revealed that the LDA system is able to directly yield velocity component data at a single point, although the hydrocyclone has curved solid walls. To this end one has to orient the LDA optical probe in the transform position, which is suggested in this study, so as to obtain two components of the mean velocities at the same point. The axial velocity profiles obtained in the transform position were corrected for index of refraction effects and the result was very close to the axial velocity profiles obtained in the traditional position of the optical probe. Using the transform position for the probe one can obtain the mean

velocity components in the hydrocyclone flow field. The new suggested method also permits the determination of one of the turbulent intensity in the flow field.

The qualitative results of flow visualization experiments by dye techniques indirectly validated the quantitative measurements of the mean velocities obtained using LDA and gave a good description of the flow characteristics within the 6″ hydrocyclone.

The predicted velocities of CFD agree well with the experimental results of LDA and flow visualization study. RSM provides an accurate prediction for complex flow as in hydrocyclones. A good CFD model permits one to determine the flow characteristics of hydrocyclones for various conditions encountered in the field without recourse to costly test procedures.

7.3 Recommendation for Further Research

The following studies are recommended as a follow-up to this research:

1. Further studies can be made by using the LDA directly in other curved solid wall situations such as circular pipes, by using the new technique presented in this study.
2. It is desirable to insure that the basic results obtained in this research are also applicable at other operating conditions. The effect of particles loading, the effect of different split ratio, the effect of operating with an air core and with higher inlet flow rates. Furthermore, some variations in the hydrocyclone geometry, all of aforementioned should provide valuable information which could provide additional fundamental understanding of using LDA directly in the hydrocyclones.

3. The experiments results provide enough databases to measure the turbulence quantity to get complete analysis through CDF modeling. Theoretical modeling of the flow field within the hydrocyclone may be undertaken to verify the results obtained here.
4. The present flow visualization studies using droplet dye injection enables one to trace the dye path precisely. Using a high speed camera it may be possible to record the stream of a dye in future studies for further analysis.

Appendix 1: References

1- Azbel, D.S. and Cheremisinoff, N.P. (1983) "Fluid Mechanics and Unit Operations" Ann Arbor Science Publishers, the Butterworth Group, Michigan.

2- Bergström, Jonas and Vomhoff, Hannes (2007) "Experimental hydrocyclone flow field studies", Separation and Purification Technology, vol. 53, Issue 1, pp. 8-20.

3- Bhattacharyya, P. (1984) "The flow field inside a conventional hydrocyclone" 2nd International Conference in Hydrocyclones, Bath, England.

4- Boadway, J.D. (1984) "A hydrocyclone with recovery of velocity energy", 2nd International Conference on Hydrocyclones, Bath, England.

5- Bradley D. (1965) "The Hydrocyclone" Pergamum Press.

6- Bradley D. and Pulling D.J. (1959) "Flow patterns in the hydraulic cyclone and their interpretation in terms of performance" Trans Instn. Chem. Engr., vol.37 pp. 34-45.

7- Chine', B. and Concha, F. (2000) "Flow patterns in conical and cylindrical hydrocyclones", Chem. Eng. Journal, vol.80, Issues 1-3, pp. 267-273.

8- Chu, Liang-Yin, Chen, Wen-Mei and Lee, Xiao-Zhong (2002) "Effects of geometric and operating parameters and feed characters on the motion of solid particles in hydrocyclones" Separation and Purification Technology, volume 26, Issues 2-3, pp. 237-246.

9- Chu, L.Y., Chen, W.M., Lee, X.Z. (2002), "Enhancement of hydrocyclone performance by controlling the inside turbulence structure" Chemical Engineering Science, vol.57, pp 207-212.

10- Chu, L.Y. and Chen, W.M. (1993) "Research on the motion of solid particles in a hydrocyclone", sep. Sce. Technol., vol.28, Issue 10, pp.1875-1886

11- Chu, L.Y., Wang, G.J., Yu, W., Zhou, X.T., Chen, W.M and Dai, G.Q. (2004) "Enhancement of hydrocyclone separatism performance by eliminating the air core", Chemical Engineering and Processing vol.43, Issue 12, pp.1441-1448.

12- Coghe, A. and Solero, G. (2002) "Experimental fluid dynamic characterization of a cyclone chamber", Experimental Thermal and Fluid Science, vol. 27, Issue 1, pp. 87-96.

13- Cullivan, J.C, Williams, R.A., Dyakowski, T., and Cross, C.R. (2004) "New understanding of a hydrocyclone flow field and separation mechanism from Computational Fluid Dynamics", Minerals Engineering, vol.17, Issue 5, pp.651-660.

14- Dabir, B. (1983) "Mean velocity measurements in a 3" Hydrocyclone using Laser Doppler Anemometry" Ph .D. Dissertation, Michigan State University.

15- Dabir, B, and Petty, C .A. (1986) "Measurements of mean velocity profiles in a hydrocyclone using Laser Doppler Anemometry", Chem.Eng.Commun.vol.48, pp.377-388.

16- Dabir, B. and Petty, C.A. (1984) "Laser Doppler Anemometry measurements of tangential and axial velocities in a hydrocyclone

operating without an air core" 2nd International Conference on Hydrocyclones, Bath, England.

17- Dai, G.Q., Li, J.M. and Chen, W.M. (1999) "Numerical prediction of the liquid flow within a hydrocyclone", Chemical Engineering Journal, vol.74, Issue 3, pp.217-223.

18- Delgadillo, J.A.G. and Rajamani, R. K. (2005) "A comparative study of three turbulence-closure models for the hydrocyclone problem" International Journal of Mineral Processing vol.77, pp217-230.

19- Drain, L.E. (1980) "The Laser Doppler Technique" A Wiley Interscience Publication, John Wiley & sons.

20- Durrani, T.S., Greated, C.A. (1977) "Laser systems in flow measurement", Plenum Press, New York.

21- Durst, F., Melling, A. And Whitelaw, J.H. (1981) "Principles and practice of Laser-Doppler Anemometry, Academic Press, London.

22- Fanglu, GU and Wenzhen, Li "Measurement and study of velocity field in various cyclones by use of Laser Doppler Anemometry", 3rd International Conference on Hydrocyclones, Oxford, 1987.

23- Fisher, M.J. and Flack, R.D. (2002) "Velocity distribution in a hydrocyclone separator", Exp. Fluids, vol. 32, pp. 302-312.

24- Flagan, Richard C., AND Seinfeld, John H. (1988) "Fundamentals of air pollution engineering", Prentice Hall.

25- Hecht, E. and Zajac, A. (1974) "Optics", Addison-Wesley Publishing Company.

26- Hsieh, K.T. And Rajamani, R.K. (1988) "Phenomenological Model of the Hydrocyclone: Model Development and Verification for Single- Phase Flow" International Journal of Mineral Processing, vol.22, pp223-237.

27- Hsieh, K. T. And Rajamani, R. K. (1991) "Mathematical Model of the Hydrocyclone based on Physics of Fluid Flow" AIChE Journal, vol.37 No.5, pp 735-746.

28- Hsu, C.Y. and Wu, R.M. (2008) "Hot zone in a Hydrocyclone for Particles Escape from Overflow" Drying Technology, vol. 26, pp 1011-1017.

29- Hwang, C.C., Shen, H.Q., Zhu, G. And Khonsari, M.M. (1993) "On the main flow pattern in hydrocyclones", J. Fluids Eng., vol.115, Issue 1, pp. 21-25.

30- Hwang, K.J., Hsueh, W.S. and Nagase, Y. "Mechanism of particle separation in small hydrocyclone" Drying Technology, vol.26, pp 1002-1010.

31- Kelsall D.F. (1952) "A study of the motion of solid particles in a hydraulic cyclone". Trans. Instn. Chem. Engr., vol. 30 pp. 87-108.

32- Kim, E., Chang, G., and Yoon, J.I. (2004) "Numerical analysis of a hydrocyclone in a recirculating aquaculture system", 15th Australasian Fluid Mechanics Conference, The University of Sydney, Australia, 13-17 Dec.

33- Knowles, S.R, Woods, D.R., and Feuerstein, I.A. (1973) "The velocity distribution within a hydrocyclone operating without air-core" Canadian Journal Chemical Engineering, vol. 51, pp.263-271.

34- Lapple C.E. (1951) "Processes use many collector types", Chemical Engineer, vol. 58, PP.144-151.

35- Laser Doppler Anemometry (LDA) by Dantec, www.dantecmt.com, web site.

36- Lilge, E.O. (1962) "Hydrocyclone fundamentals", Transactions of the Institution Min. Metal, vol. 71, pp. 285-337.

37- Luo, Q., Deng, C., Xu, J., and Xiong, G. (1989) "Comparison of the performance of water-sealed and commercial hydrocyclones", Int. J. Miner. Process, vol.25, pp.297.310.

38- Mackenzie, David Leo (1941) and Cornwell, David A. (2008) "Introduction to environment engineering"4th edition, Publisher Dubuque, IA, McGraw-Hill companies.

39- Martinez, L.F., Lavin, A.G., Mahamud, M.M. and Bueno, J.L. (2007) "Improvements in hydrocyclone design flow lines stabilization" Powder Technology, vol.176, issue 1, pp.1-8.

40- Martinez, L.F, Lavin, A.G., Mahamud, M.M. and Bueno, J.L. (2008) "Vortex finder optimum length in hydrocyclone separation", Chemical Engineering and Processing: Process Intensification, vol.47, Issue 2, pp. 192-199.

41- Matvienko, O.V. (2004) "Analysis of turbulence models and investigation of the structure of the flow in a hydrocyclone", Journal of Engineering Physics and Thermophysics, vol.77, no. 2.

42- Monredon, T.C., Hsieh, K.T. and Rajamani, R.K. (1992) "Fluid flow of the hydrocyclone, an investigation of device dimensions, Int. J. Miner Process., vol.35, pp.68-83.

43- Murphy, S., Deflos, R., Pourquie, M. J .B.M. Olujic, Z., Jansens, P.J., and Nieuwstadt, F.T.M. (2007) "Prediction of strongly swirling flow within an

axial hydrocyclone using two commercial CFD codes", Chemical Engineering Science, vol. 62, Issue 6, pp. 1619-1635.

44- Narasimha, M., Sripriya, R. and Banerjee, P.K. (2005) "CFD modelling of hydrocyclone-prediction of cut size" International Journal of Mineral Processing, vol.75, pp53-68.

45- Nowakowski, A.F., Cullivan, J.C., Williams, R. A., and Dyakowski, T. (2004) Application of CFD to modelling of the flow in hydrocyclones. Is this a realizable option or still a research challenge? Minerals Engineering, Vol.17, issue 5, pp 661-669.

46- Peavy, H.S., Tehobanoglons, G. and Rowe, D.R. (1985) "Environmental Engineering", Publisher McGraw-Hill, New York.

47- Peng, W., Boot, P.J.A.J, Hoffmann, A.C., Dries, H. W.A., Kater, J. And Ekker, A. (2001) "Flow in the inlet region in tangential inlet cyclones." Ind. Eng. Chem. Res, vol.40, pp.5649-5655.

48- Qian, Luo and Ji Run, Xu (1992) "The effect of the air core on the flow field within hydrocyclones", 4th International Conference on Hydrocyclones, Southampton.

49- Rajamani, R.K. and Milin, L. (1992) "Fluid-Flow model of the hydrocyclone for concentrated slurry classification", 4th International Conference on Hydrocyclones, Southampton.

50- Rietema K. (1961) "Performance and design of hydrocyclones I, II, III, IV" Chemical Engineering Science, vol. 15, pp. 298 - 325.

51- Rietema, K. and Van Duijn, G. (1983) "Performance of a large–cone-angle hydrocyclone- I, Hydrodynamics" Chemical Engineering Science vol.38, No.10. pp. 1651-1661.

52- Schuetz, S., Mayer, G., Bierdel, M. And Piesche, M. (2004) "Investigations on the flow and separation behaviour of hydrocyclones using computational fluid dynamics" International Journal of Mineral Processing, vol.73, pp 229-237.

53- Sevilla, E.M. and Branion, R.M. R. (1997) "The Fluid dynamics of Hydrocyclones" Journal of Pulp and Paper Science, Vol. 23(2), pp 185-193.

54- Slack, M. D., Del Porte, S. and Engelman, M. S. (2004) "Designing automated computational fluid dynamics modeling tools for hydrocyclone system design" Mineral Engineering, vol.17, pp 705-711.

55- Smyth, I.C., Thew, M.T, and Colman, D.A. (1984) "The effect of split ratio on heavy dispersion liquid-liquid separation in hydrocyclones", 2nd International Conference on Hydrocyclones, Bath, England.

56- Solero, G. And Coghe, A. (2002) "Experimental fluid dynamic characterization of a cyclone chamber" Experimental Thermal and Fluid Science, Vol. 27, pp 78-6.

57- Spellman, F.R., and Whiting, N.E. (2005) "Environmental Engineer's Mathematics Handbook", Boca Raton, Fla. CRC Press.

58- Sripriya, R., Kaulaskar, M.D., Chakraborty, S. And Meikap, B.C. (2007) "Studies on the performance of a hydrocyclone and modeling for flow characterization in presence and absence of air core" Chemical Engineering Science, vol.62, and pp 6391-6402.

59- Svarovsky L. (1977 and 2000) "solid – liquid separation", Chapter 6, 1st edition and 4th edition respectively.

60- Theodore, Louis and Buonicore, Anthony, J. (1988) "Air pollution control equipment" volume I, Particulates, CRC Press.

61- Trawinski, H.F. (1984) "About the practice of Hydrocyclone operation" 2nd International conference on Hydrocyclones, Bath, England paper k2, pp 393-412.

62- Wang, B., Chu, K.W. and Yu, A.B. (2007) "Numerical study of Particle-Fluid Flow in a Hydrocyclone" Int. Eng. Chem. Res. vol. 46, pp 4695-4705.

63- Wang, B. and Yu, A.B. (2006) "Numerical study of particle-fluid flow in hydrocyclones with different body dimensions" Minerals Engineering, vol.19, pp 1022-1033.

64- Wang, B. and Yu, A.B. (2008) "Numerical study of the gas-liquid-solid flow in hydrocyclones with different configuration of vortex finder" Chemical Engineering Journal, vol.135, pp 33-42.

65- Wong, W.O., Wang, X.W. and Zhou, Y. (2007) "Turbulent flow structure in a cylinder-on–cone cyclone" Journal of Fluids Engineering, vol.129, pp. 1179-1185.

66- Zhang, Yuanhui (2005) "Indoor air quality engineering", CRC Press.

Appendix 2

Number of turns made by a fluid particle in a hydrocyclone

The parameter N_t denoting the number of turns in the hydrocyclone as mentioned in chapter 5 is briefly discuss in this appendix. Comparisons between the observed N_t and some approximate mathematical computations were presented as follows.

1- Using Eq. 2.4 where N_t the effective turns of fluid :

$$N_t = \frac{1}{76.2mm}(323.85+\frac{238.25}{2}) = 5.81 \text{ turn} \qquad \text{(A 2.1)}$$

2- Using Theodore et al. (1988) Eq. 2.6

$$N_t = \frac{t_r v_i}{\pi D_c}$$

Here t_r = Residence Time of the fluid stream $= \frac{V}{Q_i}$, and

$$v_i = \text{Inlet Velocity} = \frac{Q_i}{A_i} = \frac{2.32\times10^{-3}m3ls}{0.0762\times0.0635} = 0.480 \text{ m/sec}$$

V is the Volume of hydrocyclone (Fig. 3.9) which measured as below

$$V = \frac{\pi}{4}\{(\frac{H_1}{D_c - D_u})(\frac{D_c^3 - D_u^3}{3}) + D_c^2 H_2 - D_o^2(D_i + Z)\}$$

Hence,

$$V=\frac{\pi}{4}\{(\frac{0.238}{0.1524-0.0381})(\frac{0.1524^3-0.0381^3}{3})+0.1524^2\times0.324-0.0762^2(0.0762+0.113)\}=5.072\times10^{-3}m^3$$

Thus, $t_r = \frac{5.072x10^{-3}}{2.32x10^{-3}} = 2.19$ sec

Therefore, $N_t = \frac{2.19 \, x \, 0.480}{\pi \, x \, 0.1542} = 2.17$ turn (A 2.2)

3) Another approach to compute the number of turns by using the measured mean velocities by LDA:

Because the magnitude of fluid velocity at top of hydrocyclone, near the inlet, is not available due to the shape of inlet assembly that was not suitable for LDA to function properly, refer to the experiment set up in Chapter 3(section3.2), the first available reading was at axial plane140mm below the roof of hydrocyclone which will be used here. The data from the transform case (where the probe tilted 45°), which gives both tangential and axial velocities, are used to approximately compute the number of turns, as follows:

At axial level Z=140 mm and near wall at r = 72 mm:

$V_\theta = 0.432$ m/s

$V_a = -0.244$ m/s

The dye moves downward 100 mm to axial level (Z = 240 mm) in time t_1

$$t_1 = \frac{Z}{V_a} = \frac{0.100}{0.244} = 0.410 \text{ sec}$$

For this time the number of turns is:

$$N_{t_1} = \frac{0.432 \times 0.410}{\pi \times 0.1524} = 0.370 \text{ turn}$$

For the entire cylindrical part, H2 = 324 mm, Fig. 3.9, the number of turns made by fluid is:

$$N_{t_{cy}} = \frac{0.324 \times 0.370}{0.10} = 1.20 \text{ turn}$$

For conical part, at axial level Z=345mm and near the wall (r = 69mm):

$V_\theta = 0.401 m/s$ $V_a = -0.031 m/s$

To reach the apex, the dye in the conical part moves 220mm downward to Z= 565mm

$$t_{conical} + \frac{Z}{V_a} = \frac{0.220}{0.031} = 7.10 \text{ sec}$$

$$N_{t_{conical}} = \frac{V_{\theta t_{conical}}}{\pi D_c} = \frac{0.401 \times 7.10}{\pi \times 0.1524} = 5.875 \text{ turn}$$

It is assumed that the dye moves one full revolution in the cylindrical part and half a revolution in the conical part, therefore, the total number of turns made be fluid for the entire hydrocyclone is:

$$N_t = N_{t_{cy}} + N_{t_{conical}} / 2 = 1.18 + 5.875/2 = 4.12 \text{ turn} \quad \text{(A 2.3)}$$

4) The visual observation for number of turns in the cylindrical and conical parts revealed that the dye moves 3 turns in the cylindrical part (one turn to be added to cover the upper region of hydrocyclone between the dye injection point (at 125mm) and the roof of hydrocyclone, which makes the number of turns in the cylindrical part 4 turns) and another 3 turns in the conical part, which gives 5.5 turn according to the above assumption (3). Therefore, the visual observation gives 5.50 turn (A 2.4)

5) To summarize the result of these approximate computations:

- Eq. 2.4 (A 2.1) gives $N_t = 5.81$ turn
- Eq. 2.6 (A 2.2) gives $N_t = 2.17$ turn
- LDA data for mean velocities(A 2.3) gives $N_t = 4.12$ turn
- The visual observation(A 2.4) gives $N_t = 5.50$ turn

As a conclusion for the total number of turns made by fluid within hydrocyclone, according to Theodore et al. (1988) the value of N_t typically ranges from 3 to 10, therefore, all of the above results are acceptable, however, depending on the feed flow rate, N_t value in hydrocyclone range between 4.0 – 6.0 turn as determined above, therefore, the assumption of 5 turns that proposed by may authors, for a gas cyclone, is justified for a hydrocyclone according to the operating flow conditions presented in this experiment, which enable to use Eq. 2.3 to compute the separation efficiency in hydrocyclone.

A2.1 Conclusions

The aim of this test was to observe the movement of fluid from the dye injection point towards the apex region and to determine the number of turns. In addition, other three different approaches were presented to approximately compute the number of turns made by fluid inside hydrocyclone and compared with that observed with the dye movement.

The result of this test shows that the number of turns are between 4 - 6 is reasonable for the operating flow conditions presented here and it might be used to compute the separation efficiency as given in Eq. 2.3 by Lapple (1951). This attempt provides an experimental data which might be useful to other researchers who look to develop Eq. 2.3 for the hydrocyclone separation efficiency.

Appendix 3: Tables

Table 3.1 Comparisions between Rietema (1961) & Bradley (1965) Hydrocyclones, Lapple's Cyclone (1951) and the used Hydrocyclone

Hydrocyclones Comparision

H.Cyclone Type	Parameters						
	Di/Dc	Do/Dc	ℓ/Dc	H2/Dc	L/Dc	Du/Dc	Cone Angle (θ)
Rietema (1961)	0.28	0.34	0.4	—	5	0.2	10°—20°
Bradley (1965)	0.133 (1/7.5)	0.2 (1/5)	0.33 (1/3)	0.5 (1/2)	6.85	0.07	9°
Hydrocyclone in study	0.5 (1/2)	0.5 (1/2)	1.24	2.125	3.71	0.25 (1/4)	27°

Hydrocyclone/Cyclone Comparision

Hydrocyclone & Cyclone Type	Parameters						
	Di/Dc	Do/Dc	Z1/Dc	H2/Dc	h/Dc	Du/Dc	H1/Dc
Lapple's Cyclone 1951	0.5 (1/2)	0.5 (1/2)	0.125 (1/8)	2	0.25 (1/4)	0.25 (1/4)	2
Hydrocyclone in study	0.5 (1/2)	0.5 (1/2)	0.74 (1/1.35)	2.125	0.417 (1/2.4)	0.25 (1/4)	1.563

Refer to Figure 3.7 for Hydrocyclone Dimensions

Table 3.2 Movement of laser beams inside the hydrocyclone

Movement of Optical Probe (mm) in air	Movement of Laser Beams inside water(Hydrocyclone) (mm)
0	0
5	7
10	14
15	19
20	25
25	31
30	37
35	44
40	51
45	58
50	66
55	72

Table 4.1 Axial Velocity at regular optical probe position, Case "A"
(Fig. 4.1 to Fig. 4.11)

Axial Level (mm)	Radius (mm)	Axial Velocity (m/s)	Axial Level (mm)	Radius (mm)	Axial Velocity (m/s)	Axial Level (mm)	Radius (mm)	Axial Velocity (m/s)
140	44	-0.12	220	72	0.343	294	7	-0.095
	51	-0.036	240	0	-0.033		14	-0.019
	58	-0.023		7	-0.113		19	0.023
	66	-0.135		14	0.017		25	-0.043
	72	-0.272		19	0.077		31	-0.086
160	44	-0.085		25	0.059		37	-0.107
	51	-0.069		31	0.053		44	-0.089
	58	-0.12		37	-0.039		51	-0.069
	66	-0.139		44	-0.066		58	-0.037
	72	-0.253		51	-0.068		66	-0.031
187	44	-0.193		58	-0.082		72	-0.044
	51	-0.102		66	-0.129	345	0	-0.019
	58	-0.118		72	-0.123		7	-0.211
	66	-0.169	260	0	-0.015		14	-0.256
	72	-0.233		7	-0.037		19	-0.139
200	0	0.046		14	0.018		25	-0.029
	7	-0.083		19	0.047		31	-0.027
	14	0.052		25	0.009		37	-0.038
	19	0.224		31	0.013		44	-0.059
	25	0.197		37	0.037		51	-0.067
	31	0.08		44	0.03		58	-0.075
	37	0.037		51	-0.039		66	-0.087
	44	-0.036		58	-0.065		69	-0.036
	51	-0.042		66	-0.141	365	0	-0.144
	58	-0.041		72	-0.166		7	-0.261
	66	-0.065	280	0	0.028		14	-0.283
	72	-0.076		7	-0.044		19	-0.249
220	0	0.109		14	0.034		25	-0.121
	7	0.076		19	0.036		31	-0.05
	14	0.065		25	-0.027		37	-0.171
	19	0.077		31	-0.061		44	-0.229
	25	0.095		37	-0.054		51	-0.143
	31	0.112		44	-0.025		58	-0.123
	37	0.184		51	-0.037		65	-0.045
	44	0.193		58	-0.068			
	51	0.209		66	-0.088			
	58	0.243		72	-0.152			
	66	0.267	294	0	0.024			

Table 4.2 Axial Velocity at regular optical probe position, Case "A" (Fig. 4.12 to Fig. 4.21)

Axial Level (mm)	Radius (mm)	Axial Velocity (m/s)	Axial Level (mm)	Radius (mm)	Axial Velocity (m/s)
385	0	-0.123	465	0	-0.455
	7	-0.199		7	-0.506
	14	-0.246		14	-0.375
	19	-0.3		19	-0.341
	25	-0.244		25	-0.183
	31	-0.128		31	-0.135
	37	-0.056		37	-0.005
	44	-0.029		44	0.079
	51	-0.006	485	0	-0.628
	60	0.047		7	-0.727
405	0	-0.262		14	-0.479
	7	-0.248		19	-0.295
	14	-0.269		25	-0.095
	19	-0.329		31	-0.129
	25	-0.23		37	-0.287
	31	-0.143	505	0	-0.801
	37	-0.039		7	-0.902
	44	0.035		14	-0.456
	51	0.046		19	-0.237
	55	-0.06		25	-0.206
425	0	-0.231		32	-0.118
	7	-0.309	525	0	-0.989
	14	-0.318		7	-1.016
	19	-0.348		14	-0.475
	25	-0.197		19	-0.342
	31	-0.142		26	-0.177
	37	-0.023	545	0	-1.277
	44	0.104		7	-1.228
	51	0.209		14	-0.828
445	0	-0.313		22	-0.347
	7	-0.422	565	0	-1.348
	14	-0.356		7	-1.289
	19	-0.338		18	-1.009
	25	-0.235			
	31	-0.127			
	37	-0.012			
	45	0.119			

Table 4.3 Tangential Velocity (Transform) and Axial Velocity (Transform and Corrected) at 45° optical probe position, Case "B"

Axial Level (mm)	Radius (mm)	Tangential Velocity (m/s)	Axial Velocity (m/s)		Axial Level (mm)	Radius (mm)	Tangential Velocity (m/s)	Axial Velocity (m/s)	
			Transform	Corrected				Transform	Corrected
140	44	0.239	-0.108	-0.119	220	72	0.414	-0.066	-0.072
	51	0.411	-0.032	-0.035	240	0	0.03	-0.029	-0.032
	58	0.418	-0.021	-0.023		7	0.247	-0.101	-0.111
	66	0.377	-0.121	-0.134		14	0.505	0.014	0.016
	72	0.432	-0.244	-0.269		19	0.872	0.068	0.075
160	44	0.448	-0.078	-0.086		25	1.124	0.052	0.057
	51	0.459	-0.062	-0.068		31	0.986	0.047	0.052
	58	0.448	-0.108	-0.119		37	0.749	-0.033	-0.036
	66	0.366	-0.125	-0.138		44	0.557	-0.057	-0.062
	72	0.384	-0.227	-0.25		51	0.553	-0.061	-0.067
187	44	0.503	-0.174	-0.192		58	0.481	-0.072	-0.079
	51	0.475	-0.092	-0.102		66	0.453	-0.114	-0.125
	58	0.473	-0.106	-0.117		72	0.418	-0.11	-0.121
	66	0.411	-0.152	-0.167	260	0	0.038	-0.012	-0.013
	72	0.394	-0.208	-0.23		7	0.234	-0.032	-0.035
200	0	0.061	0.041	0.045		14	0.552	0.015	0.017
	7	0.22	-0.074	-0.081		19	0.814	0.042	0.046
	14	0.614	0.046	0.051		25	1.147	0.007	0.008
	19	0.871	0.203	0.224		31	0.981	0.011	0.012
	25	1.127	0.177	0.194		37	0.796	0.032	0.035
	31	0.94	0.072	0.079		44	0.557	0.026	0.028
	37	0.707	0.032	0.035		51	0.567	-0.034	-0.037
	44	0.542	-0.031	-0.034		58	0.466	-0.056	-0.061
	51	0.506	-0.037	-0.041		66	0.407	-0.126	-0.139
	58	0.444	-0.036	-0.039		72	0.408	-0.147	-0.162
	66	0.385	-0.058	-0.064	280	0	0.031	0.024	0.026
	72	0.382	-0.067	-0.073		7	0.312	-0.038	-0.042
220	0	0.097	-0.008	-0.009		14	0.647	0.027	0.03
	7	0.238	-0.143	-0.157		19	0.798	0.029	0.032
	14	0.506	0.007	0.008		25	1.033	-0.024	-0.026
	19	0.891	0.088	0.097		31	0.987	-0.054	-0.059
	25	1.101	0.074	0.082		37	0.762	-0.048	-0.053
	31	0.871	0.038	0.042		44	0.545	-0.023	-0.025
	37	0.728	-0.021	-0.023		51	0.542	-0.031	-0.034
	44	0.566	-0.034	-0.037		58	0.486	-0.061	-0.067
	51	0.542	-0.064	-0.07		66	0.413	-0.078	-0.086
	58	0.459	-0.082	-0.09		72	0.398	-0.134	-0.148
	66	0.432	-0.097	-0.107					

Table 4.4 Tangential Velocity (Transform) and Axial Velocity (Transform and Corrected) at 45° optical probe position, Case "B"

Axial Level (mm)	Radius (mm)	Tangential Velocity (m/s)	Axial Velocity (m/s)		Axial Level (mm)	Radius (mm)	Tangential Velocity (m/s)	Axial Velocity (m/s)	
			Transform	Corrected				Transform	Corrected
294	0	0.059	0.021	0.023	385	0	0.088	-0.109	-0.12
	7	0.381	-0.083	-0.091		7	0.408	-0.178	-0.197
	14	0.73	-0.016	-0.018		14	0.677	-0.218	-0.241
	19	0.826	0.019	0.021		19	1.055	-0.268	-0.296
	25	1.006	-0.038	-0.042		25	1.209	-0.218	-0.241
	31	0.887	-0.076	-0.083		31	0.922	-0.115	-0.127
	37	0.742	-0.095	-0.105		37	0.599	-0.048	-0.053
	44	0.582	-0.079	-0.087		44	0.543	-0.024	-0.027
	51	0.538	-0.061	-0.067		51	0.528	-0.004	-0.004
	58	0.475	-0.032	-0.035		60	0.516	0.039	0.043
	66	0.405	-0.028	-0.031	405	0	0.077	-0.233	-0.257
	72	0.352	-0.039	-0.043		7	0.454	-0.222	-0.245
345	0	0.078	-0.016	-0.018		14	0.795	-0.235	-0.259
	7	0.466	-0.187	-0.207		19	1.104	-0.293	-0.32
	14	0.787	-0.228	-0.252		25	1.208	-0.206	-0.227
	19	0.986	-0.123	-0.135		31	0.888	-0.128	-0.141
	25	1.136	-0.026	-0.028		37	0.657	-0.035	-0.039
	31	0.954	-0.024	-0.026		44	0.573	0.031	0.034
	37	0.707	-0.034	-0.037		51	0.533	0.04	0.044
	44	0.608	-0.051	-0.056		55	0.529	-0.054	-0.059
	51	0.524	-0.06	-0.066	425	0	0.088	-0.205	-0.226
	58	0.47	-0.065	-0.071		7	0.528	-0.276	-0.304
	66	0.434	-0.077	-0.085		14	0.811	-0.284	-0.311
	69	0.401	-0.031	-0.034		19	1.102	-0.312	-0.344
365	0	0.067	-0.129	-0.142		25	1.077	-0.176	-0.194
	7	0.358	-0.233	-0.257		31	0.777	-0.125	-0.138
	14	0.666	-0.254	-0.281		37	0.708	-0.021	-0.023
	19	0.955	-0.223	-0.246		44	0.633	0.093	0.103
	25	1.283	-0.108	-0.119		51	0.576	0.186	0.205
	31	1.042	-0.045	-0.05	445	0	0.07	-0.279	-0.308
	37	0.667	-0.152	-0.168		7	0.566	-0.377	-0.416
	44	0.554	-0.205	-0.226		14	0.896	-0.317	-0.35
	51	0.536	-0.129	-0.142		19	0.994	-0.304	-0.336
	58	0.502	-0.109	-0.12		25	1.144	-0.208	-0.23
	65	0.46	-0.039	-0.043		31	0.775	-0.112	-0.124
						37	0.722	-0.009	-0.01
						45	0.604	0.104	0.115

Table 4.5 Tangential Velocity (Transform) and Axial Velocity (Transform and Corrected) at 45° optical probe position, Case "B"

Axial Level (mm)	Radius (mm)	Tangential Velocity (m/s)	Axial Velocity (m/s)	
			Transform	Corrected
465	0	0.111	-0.403	-0.442
	7	0.655	-0.448	-0.495
	14	0.854	-0.334	-0.368
	19	0.998	-0.306	-0.337
	25	1.177	-0.162	-0.179
	31	0.865	-0.121	-0.134
	37	0.743	-0.003	-0.003
	44	0.601	0.071	0.078
485	0	0.114	-0.561	-0.62
	7	0.676	-0.651	-0.719
	14	0.822	-0.429	-0.474
	19	1.088	-0.265	-0.292
	25	1.211	-0.086	-0.094
	31	0.702	-0.116	-0.128
	37	0.591	-0.257	-0.284
505	0	0.094	-0.718	-0.793
	7	0.733	-0.806	-0.889
	14	1.042	-0.411	-0.453
	19	1.311	-0.213	-0.235
	25	0.894	-0.184	-0.203
	32	0.727	-0.107	-0.118
525	0	0.076	-0.888	-0.98
	7	0.812	-0.914	-1.009
	14	1.287	-0.425	-0.469
	19	0.965	-0.307	-0.339
	26	0.765	-0.157	-0.173
545	0	0.129	-1.142	-1.26
	7	0.956	-1.098	-1.212
	14	1.432	-0.74	-0.817
	22	0.864	-0.308	-0.34
565	0	0.112	-1.205	-1.33
	7	0.801	-1.151	-1.27
	18	1.234	-0.902	-0.996

Table 4.6 LDA data in regular probe position (Case A)

R [mm]	Z [mm]	Axial Velocity (m/s)	Axial Vel.-RMS (m/s)
44	140	-0.12	0.059
51	140	-0.036	0.047
58	140	-0.023	0.058
66	140	-0.135	0.109
72	140	-0.272	0.164
72	160	-0.253	0.062
66	160	-0.139	0.055
58	160	-0.12	0.072
51	160	-0.069	0.117
44	160	-0.085	0.206
44	187	-0.193	0.071
51	187	-0.102	0.066
58	187	-0.118	0.094
66	187	-0.169	0.122
72	187	-0.233	0.262
0	200	0.046	0.092
7	200	-0.083	0.067
14	200	0.052	0.058
19	200	0.224	0.062
25	200	0.197	0.077
31	200	0.08	0.108
37	200	0.037	0.176
44	200	-0.036	0.197
51	200	-0.042	0.207
58	200	-0.041	0.212
66	200	-0.065	0.252
72	200	-0.076	0.303
72	220	-0.073	0.343
66	220	-0.108	0.267
58	220	-0.092	0.243
51	220	-0.072	0.209
44	220	-0.038	0.193
37	220	-0.022	0.184
31	220	0.0424	0.112
25	220	0.083	0.095
19	220	0.098	0.077
14	220	0.008	0.065
7	220	-0.161	0.076
0	220	-0.009	0.109

Table 4.7 LDA data in regular probe position (Case A)

R [mm]	Z [mm]	Axial Velocity (m/s)	Axial Vel.-RMS (m/s)
0	240	-0.033	0.114
7	240	-0.113	0.085
14	240	0.017	0.087
19	240	0.077	0.092
25	240	0.059	0.084
31	240	0.053	0.076
37	240	-0.039	0.108
44	240	-0.066	0.177
51	240	-0.068	0.205
58	240	-0.082	0.274
66	240	-0.129	0.306
72	240	-0.123	0.376
72	260	-0.166	0.389
66	260	-0.141	0.318
58	260	-0.065	0.258
51	260	-0.039	0.214
44	260	0.03	0.185
37	260	0.037	0.156
31	260	0.013	0.174
25	260	0.009	0.183
19	260	0.047	0.162
14	260	0.018	0.115
7	260	-0.037	0.086
0	260	-0.015	0.115
0	280	0.028	0.121
7	280	-0.044	0.094
14	280	0.034	0.116
19	280	0.036	0.128
25	280	-0.027	0.133
31	280	-0.061	0.155
37	280	-0.054	0.148
44	280	-0.025	0.162
51	280	-0.037	0.201
58	280	-0.068	0.268
66	280	-0.088	0.297
72	280	-0.152	0.394

Table 4.8 LDA data in regular probe position (Case A)

R [mm]	Z [mm]	Axial Velocity (m/s)	Axial Vel.-RMS (m/s)
72	294	-0.044	0.376
66	294	-0.031	0.367
58	294	-0.037	0.349
51	294	-0.069	0.278
44	294	-0.089	0.259
37	294	-0.107	0.232
31	294	-0.086	0.226
25	294	-0.043	0.178
19	294	0.023	0.173
14	294	-0.019	0.098
7	294	-0.095	0.077
0	294	0.024	0.085
0	345	-0.019	0.107
7	345	-0.211	0.083
14	345	-0.256	0.094
19	345	-0.139	0.111
25	345	-0.029	0.151
31	345	-0.027	0.182
37	345	-0.038	0.192
44	345	-0.059	0.248
51	345	-0.067	0.281
58	345	-0.075	0.296
66	345	-0.087	0.305
69	345	-0.036	0.406
65	365	-0.045	0.423
58	365	-0.123	0.413
51	365	-0.143	0.383
44	365	-0.229	0.365
37	365	-0.171	0.291
31	365	-0.05	0.273
25	365	-0.121	0.245
19	365	-0.249	0.205
14	365	-0.283	0.175
7	365	-0.261	0.119
0	365	-0.144	0.163

Table 4.9 LDA data in regular probe position (Case A)

R [mm]	Z [mm]	Axial Velocity (m/s)	Axial Vel.-RMS (m/s)
0	385	-0.123	0.176
7	385	-0.199	0.145
14	385	-0.246	0.202
19	385	-0.3	0.231
25	385	-0.244	0.262
31	385	-0.128	0.247
37	385	-0.056	0.273
44	385	-0.029	0.325
51	385	-0.006	0.358
60	385	0.047	0.446
55	405	-0.06	0.442
51	405	0.046	0.414
44	405	0.035	0.409
37	405	-0.039	0.379
31	405	-0.143	0.347
25	405	-0.23	0.264
19	405	-0.329	0.245
14	405	-0.269	0.201
7	405	-0.248	0.151
0	405	-0.262	0.196
0	425	-0.231	0.211
7	425	-0.309	0.27
14	425	-0.318	0.276
19	425	-0.348	0.257
25	425	-0.197	0.281
31	425	-0.142	0.347
37	425	-0.023	0.356
44	425	0.104	0.449
51	425	0.209	0.578
45	445	0.119	0.689
37	445	-0.012	0.447
31	445	-0.127	0.36
25	445	-0.235	0.308
19	445	-0.338	0.253
14	445	-0.356	0.186
7	445	-0.422	0.154
0	445	-0.313	0.225

Table 4.10 LDA data in regular probe position (Case A)

R [mm]	Z [mm]	Axial Velocity (m/s)	Axial Vel.-RMS (m/s)
0	465	-0.455	0.252
7	465	-0.506	0.255
14	465	-0.375	0.187
19	465	-0.341	0.276
25	465	-0.183	0.346
31	465	-0.135	0.423
37	465	-0.005	0.525
44	465	0.079	0.562
37	485	-0.287	0.644
31	485	-0.129	0.543
25	485	-0.095	0.451
19	485	-0.295	0.369
14	485	-0.479	0.281
7	485	-0.727	0.245
0	485	-0.628	0.283
0	505	-0.801	0.474
7	505	-0.902	0.334
14	505	-0.456	0.47
19	505	-0.237	0.666
25	505	-0.206	0.778
32	505	-0.118	0.872
26	525	-0.177	0.832
19	525	-0.342	0.698
14	525	-0.475	0.476
7	525	-1.016	0.405
0	525	-0.989	0.479
0	545	-1.277	0.467
7	545	-1.228	0.428
14	545	-0.828	0.653
22	545	-0.347	0.734
18	565	-1.009	0.984
7	565	-1.289	0.565
0	565	-1.348	0.646

Table 4.11 LDA data where the optical probe tilted 45°(Case "B")

R [mm]	Z [mm]	Tangential Vel (m/s)	Axial Velocity (m/s)	Tang. Vel.-RMS (m/s)	Axial Vel.-RMS (m/s)
44	140	0.239	-0.108	0.152	0.107
51	140	0.411	-0.032	0.041	0.067
58	140	0.418	-0.021	0.022	0.061
66	140	0.377	-0.121	0.091	0.103
72	140	0.432	-0.244	0.108	0.154
72	160	0.384	-0.227	0.085	0.199
66	160	0.366	-0.125	0.05	0.069
58	160	0.448	-0.108	0.065	0.089
51	160	0.459	-0.062	0.105	0.114
44	160	0.448	-0.078	0.186	0.194
44	187	0.503	-0.174	0.075	0.095
51	187	0.475	-0.092	0.06	0.072
58	187	0.473	-0.106	0.083	0.098
66	187	0.411	-0.152	0.111	0.123
72	187	0.394	-0.208	0.135	0.153
0	200	0.061	0.041	0.083	0.097
7	200	0.22	-0.074	0.063	0.079
14	200	0.614	0.046	0.053	0.136
19	200	0.871	0.203	0.056	0.076
25	200	1.127	0.177	0.072	0.087
31	200	0.94	0.072	0.099	0.114
37	200	0.707	0.032	0.102	0.176
44	200	0.542	-0.031	0.128	0.103
51	200	0.506	-0.037	0.149	0.089
58	200	0.444	-0.036	0.164	0.059
66	200	0.385	-0.058	0.192	0.107
72	200	0.382	-0.067	0.202	0.192
72	220	0.414	-0.066	0.168	0.183
66	220	0.432	-0.097	0.141	0.176
58	220	0.459	-0.082	0.132	0.141
51	220	0.542	-0.064	0.118	0.111
44	220	0.566	-0.034	0.104	0.126
37	220	0.728	-0.021	0.097	0.153
31	220	0.871	0.038	0.079	0.216
25	220	1.101	0.074	0.068	0.164
19	220	0.891	0.088	0.092	0.087
14	220	0.506	0.007	0.116	0.206
7	220	0.238	-0.143	0.129	0.171
0	220	0.097	-0.008	0.188	0.206

Table 4.12 LDA data where the optical probe tilted 45°(Case "B")

R [mm]	Z [mm]	Tangential Vel (m/s)	Axial Velocity (m/s)	Tang. Vel.-RMS (m/s)	Axial Vel.-RMS (m/s)
0	240	0.03	-0.029	0.108	0.111
7	240	0.247	-0.101	0.077	0.089
14	240	0.505	0.014	0.078	0.193
19	240	0.872	0.068	0.087	0.156
25	240	1.124	0.052	0.067	0.191
31	240	0.986	0.047	0.065	0.215
37	240	0.749	-0.033	0.098	0.132
44	240	0.557	-0.057	0.115	0.097
51	240	0.553	-0.061	0.138	0.115
58	240	0.481	-0.072	0.183	0.206
66	240	0.453	-0.114	0.216	0.229
72	240	0.418	-0.11	0.242	0.292
72	260	0.408	-0.147	0.156	0.206
66	260	0.407	-0.126	0.117	0.192
58	260	0.466	-0.056	0.074	0.144
51	260	0.567	-0.034	0.097	0.107
44	260	0.557	0.026	0.167	0.181
37	260	0.796	0.032	0.143	0.157
31	260	0.981	0.011	0.104	0.164
25	260	1.147	0.007	0.127	0.139
19	260	0.814	0.042	0.148	0.121
14	260	0.552	0.015	0.185	0.105
7	260	0.234	-0.032	0.077	0.084
0	260	0.038	-0.012	0.115	0.102
0	280	0.031	0.024	0.111	0.143
7	280	0.312	-0.038	0.087	0.096
14	280	0.647	0.027	0.147	0.179
19	280	0.798	0.029	0.114	0.226
25	280	1.033	-0.024	0.091	0.095
31	280	0.987	-0.054	0.073	0.104
37	280	0.762	-0.048	0.102	0.117
44	280	0.545	-0.023	0.126	0.139
51	280	0.542	-0.031	0.167	0.174
58	280	0.486	-0.061	0.191	0.207
66	280	0.413	-0.078	0.212	0.227
72	280	0.398	-0.134	0.246	0.271

Table 4.13 LDA data where the optical probe tilted 45°(Case "B")

X [mm]	Y [mm]	Tangential Vel (m/s)	Axial Velocity (m/s)	Tang. Vel.-RMS (m/s)	Axial Vel.-RMS (m/s)
72	294	0.352	-0.039	0.242	0.357
66	294	0.405	-0.028	0.233	0.341
58	294	0.475	-0.032	0.216	0.325
51	294	0.538	-0.061	0.202	0.266
44	294	0.582	-0.079	0.174	0.248
37	294	0.742	-0.095	0.111	0.225
31	294	0.887	-0.076	0.078	0.217
25	294	1.006	-0.038	0.063	0.172
19	294	0.826	0.019	0.104	0.205
14	294	0.73	-0.016	0.088	0.097
7	294	0.381	-0.083	0.071	0.089
0	294	0.059	0.021	0.177	0.187
0	345	0.078	-0.016	0.198	0.106
7	345	0.466	-0.187	0.077	0.081
14	345	0.787	-0.228	0.087	0.097
19	345	0.986	-0.123	0.101	0.126
25	345	1.136	-0.026	0.134	0.141
31	345	0.954	-0.024	0.165	0.152
37	345	0.707	-0.034	0.175	0.183
44	345	0.608	-0.051	0.186	0.207
51	345	0.524	-0.06	0.206	0.215
58	345	0.47	-0.065	0.217	0.229
66	345	0.434	-0.077	0.237	0.244
69	345	0.401	-0.031	0.271	0.289
65	365	0.46	-0.039	0.287	0.313
58	365	0.502	-0.109	0.276	0.288
51	365	0.536	-0.129	0.243	0.267
44	365	0.554	-0.205	0.233	0.251
37	365	0.667	-0.152	0.164	0.209
31	365	1.042	-0.045	0.17	0.196
25	365	1.283	-0.108	0.122	0.165
19	365	0.955	-0.223	0.087	0.101
14	365	0.666	-0.254	0.104	0.126
7	365	0.358	-0.233	0.129	0.147
0	365	0.067	-0.129	0.148	0.183

Table 4.14 LDA data where the optical probe tilted 45°(Case "B")

X [mm]	Y [mm]	Tangential Vel (m/s)	Axial Velocity (m/s)	Tang. Vel.-RMS (m/s)	Axial Vel.-RMS (m/s)
0	385	0.088	-0.109	0.161	0.193
7	385	0.408	-0.178	0.132	0.144
14	385	0.677	-0.218	0.108	0.135
19	385	1.055	-0.268	0.083	0.099
25	385	1.209	-0.218	0.058	0.109
31	385	0.922	-0.115	0.083	0.135
37	385	0.599	-0.048	0.025	0.159
44	385	0.543	-0.024	0.147	0.201
51	385	0.528	-0.004	0.193	0.232
60	385	0.516	0.039	0.205	0.258
55	405	0.529	-0.054	0.203	0.257
51	405	0.533	0.04	0.178	0.187
44	405	0.573	0.031	0.233	0.295
37	405	0.657	-0.035	0.144	0.151
31	405	0.888	-0.128	0.114	0.125
25	405	1.208	-0.206	0.084	0.091
19	405	1.104	-0.293	0.122	0.113
14	405	0.795	-0.235	0.182	0.135
7	405	0.454	-0.222	0.137	0.173
0	405	0.077	-0.233	0.187	0.212
0	425	0.088	-0.205	0.273	0.296
7	425	0.528	-0.276	0.243	0.229
14	425	0.811	-0.284	0.101	0.162
19	425	1.102	-0.312	0.023	0.104
25	425	1.077	-0.176	0.055	0.078
31	425	0.777	-0.125	0.076	0.127
37	425	0.708	-0.021	0.122	0.142
44	425	0.633	0.093	0.252	0.282
51	425	0.576	0.186	0.305	0.318
45	445	0.604	0.104	0.223	0.241
37	445	0.722	-0.009	0.155	0.179
31	445	0.775	-0.112	0.083	0.098
25	445	1.144	-0.208	0.061	0.09
19	445	0.994	-0.304	0.123	0.143
14	445	0.896	-0.317	0.167	0.183
7	445	0.566	-0.377	0.181	0.197
0	445	0.07	-0.279	0.204	0.236

Table 4.15 LDA data where the optical probe tilted 45°(Case "B")

X [mm]	Y [mm]	Tangential Vel (m/s)	Axial Velocity (m/s)	Tang. Vel.-RMS (m/s)	Axial Vel.-RMS (m/s)
0	465	0.111	-0.403	0.247	0.246
7	465	0.655	-0.448	0.232	0.241
14	465	0.854	-0.334	0.171	0.185
19	465	0.998	-0.306	0.254	0.265
25	465	1.177	-0.162	0.314	0.323
31	465	0.865	-0.121	0.383	0.395
37	465	0.743	-0.003	0.477	0.488
44	465	0.601	0.071	0.511	0.536
37	485	0.591	-0.257	0.584	0.596
31	485	0.702	-0.116	0.493	0.504
25	485	1.211	-0.086	0.411	0.426
19	485	1.088	-0.265	0.333	0.342
14	485	0.822	-0.429	0.255	0.262
7	485	0.676	-0.651	0.222	0.234
0	485	0.114	-0.561	0.255	0.257
0	505	0.094	-0.718	0.431	0.436
7	505	0.733	-0.806	0.303	0.312
14	505	1.042	-0.411	0.423	0.433
19	505	1.311	-0.213	0.606	0.613
25	505	0.894	-0.184	0.709	0.723
32	505	0.727	-0.107	0.791	0.804
26	525	0.765	-0.157	0.753	0.777
19	525	0.965	-0.307	0.63	0.656
14	525	1.287	-0.425	0.433	0.444
7	525	0.812	-0.914	0.366	0.399
0	525	0.076	-0.888	0.434	0.439
0	545	0.129	-1.142	0.421	0.426
7	545	0.956	-1.098	0.389	0.403
14	545	1.432	-0.74	0.593	0.614
22	545	0.864	-0.308	0.654	0.679
18	565	1.234	-0.902	0.895	0.921
7	565	0.801	-1.151	0.512	0.525
0	565	0.112	-1.205	0.581	0.583

Table 4.16 Turbulent Intensity

R [mm]	Z [mm]	Tangential Vel. U (m/s)	Axial Velocity V (m/s)	Tang. Vel.-RMS $\overline{V\theta'}$ (m/s)	Axial Vel.-RMS $\overline{Va'}$ (m/s)	k (m^2/s^2)	u'	I %
0	280	0.031	0.024	0.111	0.143	1.639E-02	1.045E-01	8.230E-01
7	280	0.312	-0.038	0.087	0.096	8.393E-03	7.480E-02	5.890E-01
14	280	0.647	0.027	0.147	0.179	2.683E-02	1.337E-01	1.053
19	280	0.798	0.029	0.114	0.226	3.204E-02	1.461E-01	1.151
25	280	1.033	-0.024	0.091	0.095	8.653E-03	7.595E-02	5.980E-01
31	280	0.987	-0.054	0.073	0.104	8.073E-03	7.336E-02	5.776E-01
37	280	0.762	-0.048	0.102	0.117	1.205E-02	8.962E-02	7.056E-01
44	280	0.545	-0.023	0.126	0.139	1.760E-02	1.083E-01	8.529E-01
51	280	0.542	-0.031	0.167	0.174	2.908E-02	1.392E-01	1.096
58	280	0.486	-0.061	0.191	0.207	3.967E-02	1.626E-01	1.280
66	280	0.413	-0.078	0.212	0.227	4.824E-02	1.793E-01	1.412
72	280	0.398	-0.134	0.246	0.271	6.698E-02	2.113E-01	1.664

Table 6.1 Velocity Data at axial plane Z=140mm

Radius (mm)	Tangential Velocity (m/s)	Axial Velocity (m/s)	Radius (mm)	Tangential Velocity (m/s)	Axial Velocity (m/s)
-7.609E-02	0.000	0.000	3.920E-04	1.741E-03	4.284E-02
-7.356E-02	4.899E-01	-3.146E-01	6.102E-04	2.342E-03	4.271E-02
-7.104E-02	4.990E-01	-3.288E-01	8.945E-04	3.159E-03	4.256E-02
-6.851E-02	5.035E-01	-3.214E-01	9.923E-04	3.481E-03	4.241E-02
-6.599E-02	5.037E-01	-2.899E-01	1.530E-03	5.369E-03	4.178E-02
-6.346E-02	5.058E-01	-2.299E-01	2.202E-03	7.325E-03	3.972E-02
-6.094E-02	5.167E-01	-1.576E-01	2.891E-03	9.775E-03	3.474E-02
-5.842E-02	5.345E-01	-9.588E-02	3.589E-03	1.581E-02	2.279E-02
-5.590E-02	5.479E-01	-5.201E-02	4.290E-03	3.291E-02	-3.884E-03
-5.336E-02	5.501E-01	-2.274E-02	4.999E-03	5.767E-02	-3.479E-02
-5.082E-02	5.447E-01	-5.334E-03	7.207E-03	1.379E-01	-9.916E-02
-4.828E-02	5.340E-01	2.251E-03	9.414E-03	2.156E-01	-1.184E-01
-4.574E-02	5.119E-01	6.066E-04	1.162E-02	3.058E-01	-1.188E-01
-4.319E-02	4.664E-01	-1.031E-02	1.383E-02	4.045E-01	-9.896E-02
-4.064E-02	3.946E-01	-2.621E-02	1.604E-02	5.045E-01	-5.022E-02
-3.809E-02	0.000	0.000	1.826E-02	5.969E-01	2.340E-02
-3.588E-02	7.115E-01	5.130E-01	2.046E-02	6.720E-01	1.055E-01
-3.367E-02	7.336E-01	4.951E-01	2.267E-02	7.236E-01	1.838E-01
-3.148E-02	7.459E-01	4.533E-01	2.487E-02	7.518E-01	2.554E-01
-2.928E-02	7.523E-01	3.968E-01	2.707E-02	7.626E-01	3.220E-01
-2.708E-02	7.532E-01	3.319E-01	2.926E-02	7.630E-01	3.853E-01
-2.488E-02	7.457E-01	2.641E-01	3.147E-02	7.560E-01	4.435E-01
-2.268E-02	7.222E-01	1.938E-01	3.367E-02	7.413E-01	4.918E-01
-2.047E-02	6.755E-01	1.179E-01	3.588E-02	7.149E-01	5.222E-01
-1.827E-02	6.047E-01	3.670E-02	3.809E-02	0.000	0.000
-1.606E-02	5.163E-01	-3.958E-02	4.063E-02	1.964E-01	-1.743E-01
-1.385E-02	4.194E-01	-9.420E-02	4.316E-02	2.705E-01	-1.199E-01
-1.163E-02	3.219E-01	-1.195E-01	4.569E-02	3.547E-01	-6.441E-02
-9.423E-03	2.294E-01	-1.213E-01	4.822E-02	4.310E-01	-3.208E-02
-7.211E-03	1.456E-01	-1.015E-01	5.077E-02	4.820E-01	-2.482E-02
-4.999E-03	5.778E-02	-2.911E-02	5.331E-02	5.041E-01	-3.660E-02
-4.352E-03	3.197E-02	3.546E-03	5.586E-02	5.056E-01	-6.070E-02
-3.718E-03	1.561E-02	2.824E-02	5.839E-02	4.965E-01	-9.036E-02
-3.058E-03	1.002E-02	3.755E-02	6.092E-02	4.844E-01	-1.211E-01
-2.361E-03	7.592E-03	4.052E-02	6.345E-02	4.774E-01	-1.529E-01
-1.871E-03	6.408E-03	4.103E-02	6.598E-02	4.825E-01	-1.903E-01
-1.641E-03	5.778E-03	4.141E-02	6.851E-02	4.985E-01	-2.337E-01
-9.033E-04	3.478E-03	4.216E-02	7.104E-02	5.110E-01	-2.710E-01
-4.583E-04	2.250E-03	4.251E-02	7.357E-02	4.991E-01	-2.916E-01
-1.612E-04	1.674E-03	4.283E-02	7.610E-02	0.000	0.000

Table 6.2 Velocity Data at axial plane Z=160mm

Radius (mm)	Tangential Velocity (m/s)	Axial Velocity (m/s)	Radius (mm)	Tangential Velocity (m/s)	Axial Velocity (m/s)
-7.614E-02	0.000	0.000	3.921E-04	-3.677E-03	6.202E-02
-7.362E-02	5.022E-01	-3.164E-01	6.025E-04	-3.221E-03	6.200E-02
-7.109E-02	5.290E-01	-3.128E-01	8.939E-04	-2.359E-03	6.198E-02
-6.856E-02	5.479E-01	-2.940E-01	9.952E-04	-2.172E-03	6.179E-02
-6.603E-02	5.650E-01	-2.663E-01	1.529E-03	-9.446E-04	6.098E-02
-6.350E-02	5.801E-01	-2.322E-01	2.200E-03	2.931E-04	5.728E-02
-6.097E-02	5.876E-01	-1.935E-01	2.889E-03	2.377E-03	4.797E-02
-5.844E-02	5.841E-01	-1.530E-01	3.588E-03	8.786E-03	2.757E-02
-5.591E-02	5.742E-01	-1.155E-01	4.288E-03	2.804E-02	-1.116E-02
-5.337E-02	5.674E-01	-8.415E-02	4.999E-03	5.562E-02	-5.056E-02
-5.083E-02	5.677E-01	-5.865E-02	7.207E-03	1.400E-01	-1.172E-01
-4.828E-02	5.694E-01	-4.036E-02	9.414E-03	2.146E-01	-1.261E-01
-4.574E-02	5.616E-01	-3.259E-02	1.162E-02	2.989E-01	-1.213E-01
-4.319E-02	5.311E-01	-3.576E-02	1.383E-02	3.894E-01	-1.045E-01
-4.064E-02	4.695E-01	-4.660E-02	1.604E-02	4.765E-01	-7.413E-02
-3.809E-02	0.000	0.000	1.825E-02	5.490E-01	-3.176E-02
-3.589E-02	7.369E-01	4.761E-01	2.046E-02	6.024E-01	2.634E-02
-3.369E-02	7.699E-01	5.209E-01	2.267E-02	6.430E-01	1.090E-01
-3.149E-02	7.806E-01	5.188E-01	2.487E-02	6.822E-01	2.183E-01
-2.930E-02	7.649E-01	4.708E-01	2.707E-02	7.253E-01	3.376E-01
-2.709E-02	7.258E-01	3.659E-01	2.927E-02	7.647E-01	4.377E-01
-2.489E-02	6.792E-01	2.284E-01	3.147E-02	7.876E-01	4.976E-01
-2.268E-02	6.386E-01	1.014E-01	3.367E-02	7.875E-01	5.194E-01
-2.048E-02	6.002E-01	1.088E-02	3.588E-02	7.643E-01	5.022E-01
-1.827E-02	5.498E-01	-4.643E-02	3.809E-02	0.000	0.000
-1.606E-02	4.781E-01	-8.511E-02	4.063E-02	4.970E-01	-8.985E-02
-1.385E-02	3.893E-01	-1.117E-01	4.317E-02	5.522E-01	-8.762E-02
-1.164E-02	2.954E-01	-1.253E-01	4.570E-02	5.701E-01	-8.261E-02
-9.423E-03	2.079E-01	-1.270E-01	4.823E-02	5.696E-01	-7.905E-02
-7.211E-03	1.323E-01	-1.107E-01	5.079E-02	5.635E-01	-8.008E-02
-4.999E-03	5.284E-02	-2.869E-02	5.334E-02	5.566E-01	-8.927E-02
-4.351E-03	2.961E-02	1.024E-02	5.589E-02	5.473E-01	-1.103E-01
-3.716E-03	1.555E-02	3.948E-02	5.843E-02	5.317E-01	-1.422E-01
-3.056E-03	1.149E-02	5.028E-02	6.097E-02	5.086E-01	-1.790E-01
-2.359E-03	1.011E-02	5.402E-02	6.350E-02	4.831E-01	-2.152E-01
-1.871E-03	9.391E-03	5.527E-02	6.604E-02	4.635E-01	-2.492E-01
-1.640E-03	9.065E-03	5.606E-02	6.857E-02	4.533E-01	-2.811E-01
-9.024E-04	7.521E-03	5.859E-02	7.110E-02	4.490E-01	-3.079E-01
-4.579E-04	3.850E-03	6.004E-02	7.363E-02	4.420E-01	-3.276E-01
-1.610E-04	1.137E-03	6.101E-02	7.616E-02	0.000	0.000

Table 6.3 Velocity Data at axial plane Z=187mm

Radius (mm)	Tangential Velocity (m/s)	Axial Velocity (m/s)	Radius (mm)	Tangential Velocity (m/s)	Axial Velocity (m/s)
-7.620E-02	0.000	0.000	-1.608E-04	3.355E-03	5.721E-02
-7.366E-02	4.787E-01	-2.702E-01	3.917E-04	-6.544E-04	5.751E-02
-7.112E-02	5.203E-01	-2.636E-01	6.106E-04	1.069E-03	5.710E-02
-6.982E-02	5.326E-01	-2.574E-01	8.936E-04	3.633E-03	5.653E-02
-6.858E-02	5.444E-01	-2.517E-01	9.904E-04	4.351E-03	5.619E-02
-6.724E-02	5.537E-01	-2.436E-01	1.529E-03	8.915E-03	5.447E-02
-6.604E-02	5.625E-01	-2.375E-01	2.199E-03	1.438E-02	4.680E-02
-6.350E-02	5.767E-01	-2.219E-01	2.888E-03	2.459E-02	3.114E-02
-6.096E-02	5.880E-01	-2.032E-01	3.587E-03	4.551E-02	2.168E-03
-5.842E-02	5.979E-01	-1.780E-01	4.288E-03	8.662E-02	-4.457E-02
-5.588E-02	6.079E-01	-1.446E-01	5.000E-03	1.318E-01	-8.757E-02
-5.334E-02	6.189E-01	-1.071E-01	7.206E-03	2.311E-01	-1.524E-01
-5.080E-02	6.320E-01	-7.584E-02	9.413E-03	2.814E-01	-1.542E-01
-4.826E-02	6.479E-01	-6.157E-02	1.162E-02	3.291E-01	-1.313E-01
-4.572E-02	6.641E-01	-6.916E-02	1.383E-02	3.952E-01	-6.825E-02
-4.452E-02	6.685E-01	-8.521E-02	1.603E-02	5.004E-01	4.555E-02
-4.340E-02	6.661E-01	-9.764E-02	1.824E-02	6.506E-01	1.946E-01
-4.318E-02	6.656E-01	-1.001E-01	2.045E-02	8.172E-01	3.414E-01
-4.149E-02	6.323E-01	-1.468E-01	2.265E-02	9.462E-01	4.546E-01
-4.064E-02	6.114E-01	-1.653E-01	2.486E-02	9.987E-01	5.311E-01
-3.810E-02	0.000	0.000	2.706E-02	9.729E-01	5.836E-01
-3.708E-02	3.303E-01	5.028E-02	2.927E-02	8.945E-01	6.084E-01
-3.592E-02	6.817E-01	5.807E-02	3.147E-02	8.059E-01	5.516E-01
-3.375E-02	7.445E-01	3.494E-01	3.368E-02	7.465E-01	3.302E-01
-3.158E-02	8.195E-01	5.309E-01	3.589E-02	7.240E-01	-1.738E-02
-2.940E-02	9.075E-01	5.688E-01	3.810E-02	0.000	0.000
-2.719E-02	9.883E-01	5.346E-01	3.943E-02	3.019E-01	-1.281E-01
-2.498E-02	1.012E+00	4.753E-01	4.063E-02	5.869E-01	-2.645E-01
-2.276E-02	9.374E-01	3.867E-01	4.166E-02	6.064E-01	-2.415E-01
-2.055E-02	7.773E-01	2.569E-01	4.315E-02	6.295E-01	-1.992E-01
-1.834E-02	5.943E-01	1.025E-01	4.348E-02	6.292E-01	-1.941E-01
-1.611E-02	4.466E-01	-3.460E-02	4.449E-02	6.284E-01	-1.783E-01
-1.388E-02	3.500E-01	-1.202E-01	4.568E-02	6.224E-01	-1.572E-01
-1.164E-02	2.878E-01	-1.547E-01	4.821E-02	6.031E-01	-1.247E-01
-9.410E-03	2.406E-01	-1.590E-01	5.076E-02	5.849E-01	-1.024E-01
-7.205E-03	1.952E-01	-1.405E-01	5.331E-02	5.709E-01	-9.424E-02
-6.036E-03	1.517E-01	-9.173E-02	5.586E-02	5.610E-01	-1.039E-01
-5.000E-03	1.136E-01	-4.763E-02	5.840E-02	5.532E-01	-1.297E-01
-4.719E-03	9.926E-02	-2.826E-02	6.094E-02	5.446E-01	-1.640E-01
-4.657E-03	9.610E-02	-2.400E-02	6.349E-02	5.331E-01	-1.974E-01
-4.351E-03	8.034E-02	-2.181E-03	6.468E-02	5.266E-01	-2.098E-01
-4.315E-03	7.882E-02	-1.333E-04	6.493E-02	5.250E-01	-2.123E-01
-3.715E-03	5.344E-02	3.382E-02	6.501E-02	5.244E-01	-2.132E-01
-3.055E-03	3.844E-02	4.948E-02	6.603E-02	5.177E-01	-2.238E-01
-2.358E-03	2.822E-02	5.509E-02	6.857E-02	4.983E-01	-2.415E-01
-1.867E-03	2.261E-02	5.573E-02	7.111E-02	4.732E-01	-2.512E-01
-1.639E-03	2.033E-02	5.617E-02	7.231E-02	4.544E-01	-2.525E-01
-9.020E-04	1.341E-02	5.667E-02	7.366E-02	4.339E-01	-2.526E-01
-4.572E-04	6.669E-03	5.706E-02	7.620E-02	0.000	0.000

Table 6.4 Velocity Data at axial plane Z=200mm

Radius (mm)	Tangential Velocity (m/s)	Axial Velocity (m/s)	Radius (mm)	Tangential Velocity (m/s)	Axial Velocity (m/s)
7.619E-02	0.000	0.000	-1.612E-04	7.875E-03	2.996E-02
7.367E-02	3.899E-01	-9.696E-02	-4.572E-04	4.229E-03	3.301E-02
7.115E-02	4.264E-01	-1.089E-01	-9.028E-04	2.248E-03	3.737E-02
6.863E-02	4.501E-01	-1.123E-01	-1.641E-03	1.163E-02	4.253E-02
6.611E-02	4.693E-01	-1.103E-01	-1.864E-03	1.456E-02	4.318E-02
6.359E-02	4.873E-01	-1.056E-01	-2.360E-03	2.147E-02	4.467E-02
6.108E-02	5.059E-01	-1.007E-01	-3.057E-03	3.232E-02	4.031E-02
5.857E-02	5.262E-01	-9.703E-02	-3.717E-03	4.614E-02	2.382E-02
5.606E-02	5.489E-01	-9.556E-02	-4.230E-03	6.543E-02	-7.070E-03
5.353E-02	5.741E-01	-9.599E-02	-4.352E-03	7.000E-02	-1.445E-02
5.101E-02	6.015E-01	-9.668E-02	-4.999E-03	9.940E-02	-6.093E-02
4.848E-02	6.308E-01	-9.548E-02	-7.275E-03	1.759E-01	-1.505E-01
4.596E-02	6.622E-01	-8.967E-02	-9.536E-03	2.282E-01	-1.578E-01
4.344E-02	6.958E-01	-7.865E-02	-1.178E-02	2.971E-01	-1.353E-01
4.093E-02	7.259E-01	-7.922E-02	-1.402E-02	4.003E-01	-7.574E-02
3.841E-02	7.555E-01	-7.429E-02	-1.625E-02	5.459E-01	1.806E-02
3.618E-02	7.906E-01	-3.593E-02	-1.848E-02	7.218E-01	1.187E-01
3.395E-02	8.376E-01	2.324E-02	-2.070E-02	8.914E-01	1.909E-01
3.174E-02	8.944E-01	8.017E-02	-2.293E-02	1.009E+00	2.159E-01
2.953E-02	9.549E-01	1.300E-01	-2.515E-02	1.052E+00	2.001E-01
2.731E-02	1.005	1.766E-01	-2.738E-02	1.040E+00	1.660E-01
2.509E-02	1.029	2.187E-01	-2.961E-02	9.940E-01	1.312E-01
2.287E-02	1.013	2.456E-01	-3.180E-02	9.372E-01	9.965E-02
2.065E-02	9.356E-01	2.377E-01	-3.401E-02	8.832E-01	6.788E-02
1.843E-02	7.955E-01	1.821E-01	-3.621E-02	8.370E-01	3.534E-02
1.621E-02	6.260E-01	8.747E-02	-3.841E-02	7.995E-01	1.802E-02
1.399E-02	4.705E-01	-1.941E-02	-4.092E-02	7.662E-01	2.739E-02
1.176E-02	3.540E-01	-1.083E-01	-4.344E-02	7.344E-01	3.448E-02
9.525E-03	2.745E-01	-1.600E-01	-4.595E-02	7.003E-01	2.406E-02
7.270E-03	2.128E-01	-1.729E-01	-4.846E-02	6.695E-01	1.028E-02
4.999E-03	1.255E-01	-1.215E-01	-5.098E-02	6.432E-01	-8.034E-03
4.957E-03	1.235E-01	-1.194E-01	-5.350E-02	6.221E-01	-3.488E-02
4.289E-03	9.176E-02	-8.739E-02	-5.602E-02	6.059E-01	-7.107E-02
3.588E-03	6.358E-02	-4.971E-02	-5.853E-02	5.932E-01	-1.126E-01
2.889E-03	5.001E-02	-2.361E-02	-6.105E-02	5.814E-01	-1.525E-01
2.200E-03	4.230E-02	-5.956E-03	-6.357E-02	5.678E-01	-1.845E-01
1.529E-03	3.545E-02	7.321E-03	-6.610E-02	5.510E-01	-2.068E-01
9.871E-04	2.774E-02	1.541E-02	-6.862E-02	5.302E-01	-2.208E-01
8.937E-04	2.653E-02	1.684E-02	-7.114E-02	5.034E-01	-2.292E-01
6.168E-04	2.330E-02	2.053E-02	-7.367E-02	4.582E-01	-2.316E-01
3.914E-04	2.054E-02	2.349E-02	-7.619E-02	0.000	0.000

Table 6.5 Velocity Data at axial plane Z=220mm

Radius (mm)	Tangential Velocity (m/s)	Axial Velocity (m/s)	Radius (mm)	Tangential Velocity (m/s)	Axial Velocity (m/s)
7.619E-02	0.000	0.000	-1.612E-04	7.097E-03	-2.334E-02
7.368E-02	4.676E-01	-6.553E-02	-4.575E-04	-2.753E-03	-1.433E-02
7.118E-02	4.965E-01	-8.677E-02	-9.034E-04	-8.776E-03	-9.785E-04
6.868E-02	5.129E-01	-1.009E-01	-1.642E-03	3.158E-03	1.585E-02
6.617E-02	5.274E-01	-1.116E-01	-1.864E-03	6.430E-03	1.923E-02
6.368E-02	5.423E-01	-1.183E-01	-2.362E-03	1.490E-02	2.587E-02
6.118E-02	5.581E-01	-1.207E-01	-3.059E-03	2.474E-02	2.787E-02
5.869E-02	5.751E-01	-1.190E-01	-3.719E-03	3.536E-02	1.900E-02
5.620E-02	5.935E-01	-1.137E-01	-4.195E-03	5.058E-02	-2.990E-03
5.370E-02	6.136E-01	-1.052E-01	-4.352E-03	5.567E-02	-1.031E-02
5.120E-02	6.355E-01	-9.396E-02	-4.999E-03	8.324E-02	-4.903E-02
4.870E-02	6.593E-01	-8.072E-02	-7.299E-03	1.702E-01	-1.221E-01
4.621E-02	6.848E-01	-6.597E-02	-9.593E-03	2.505E-01	-1.126E-01
4.371E-02	7.123E-01	-4.996E-02	-1.189E-02	3.567E-01	-7.385E-02
4.122E-02	7.420E-01	-3.302E-02	-1.416E-02	4.929E-01	-2.000E-02
3.873E-02	7.758E-01	-1.593E-02	-1.643E-02	6.504E-01	3.238E-02
3.649E-02	8.125E-01	-8.959E-04	-1.869E-02	8.085E-01	7.150E-02
3.425E-02	8.561E-01	1.302E-02	-2.093E-02	9.378E-01	9.231E-02
3.203E-02	9.056E-01	2.678E-02	-2.316E-02	1.015E+00	9.491E-02
2.981E-02	9.568E-01	4.345E-02	-2.537E-02	1.037E+00	8.355E-02
2.757E-02	9.978E-01	6.335E-02	-2.761E-02	1.017E+00	6.551E-02
2.534E-02	1.015	8.244E-02	-2.985E-02	9.716E-01	4.776E-02
2.313E-02	9.956E-01	9.461E-02	-3.207E-02	9.173E-01	3.421E-02
2.090E-02	9.282E-01	9.398E-02	-3.428E-02	8.668E-01	2.406E-02
1.866E-02	8.125E-01	7.714E-02	-3.651E-02	8.243E-01	1.405E-02
1.640E-02	6.671E-01	4.296E-02	-3.874E-02	7.900E-01	2.577E-03
1.414E-02	5.189E-01	-8.829E-03	-4.123E-02	7.584E-01	-1.095E-02
1.186E-02	3.893E-01	-7.561E-02	-4.372E-02	7.300E-01	-2.355E-02
9.579E-03	2.881E-01	-1.448E-01	-4.622E-02	7.023E-01	-3.342E-02
7.292E-03	2.134E-01	-1.925E-01	-4.870E-02	6.749E-01	-4.014E-02
4.999E-03	1.359E-01	-1.916E-01	-5.119E-02	6.481E-01	-4.450E-02
4.935E-03	1.335E-01	-1.904E-01	-5.368E-02	6.220E-01	-4.798E-02
4.290E-03	1.101E-01	-1.780E-01	-5.618E-02	5.971E-01	-5.301E-02
3.590E-03	8.972E-02	-1.567E-01	-5.867E-02	5.739E-01	-6.284E-02
2.890E-03	7.976E-02	-1.336E-01	-6.117E-02	5.534E-01	-8.037E-02
2.201E-03	7.229E-02	-1.094E-01	-6.367E-02	5.362E-01	-1.061E-01
1.530E-03	6.375E-02	-8.464E-02	-6.617E-02	5.208E-01	-1.365E-01
9.859E-04	5.221E-02	-6.259E-02	-6.867E-02	5.040E-01	-1.652E-01
8.944E-04	5.022E-02	-5.891E-02	-7.118E-02	4.806E-01	-1.861E-01
6.216E-04	4.413E-02	-4.997E-02	-7.368E-02	4.372E-01	-1.952E-01
3.916E-04	3.866E-02	-4.242E-02	-7.619E-02	0.000	0.000

Table 6.6 Velocity Data at axial plane Z=240mm

Radius (mm)	Tangential Velocity (m/s)	Axial Velocity (m/s)	Radius (mm)	Tangential Velocity (m/s)	Axial Velocity (m/s)
7.619E-02	0.000	0.000	-1.609E-04	5.335E-03	-5.230E-02
7.372E-02	4.811E-01	-1.371E-01	-4.575E-04	1.577E-02	-4.519E-02
7.124E-02	5.130E-01	-1.434E-01	-9.029E-04	3.655E-02	-3.349E-02
6.876E-02	5.311E-01	-1.429E-01	-1.641E-03	4.842E-02	-1.476E-02
6.628E-02	5.460E-01	-1.382E-01	-1.867E-03	5.065E-02	-9.734E-03
6.381E-02	5.598E-01	-1.297E-01	-2.361E-03	5.657E-02	2.725E-05
6.133E-02	5.738E-01	-1.179E-01	-3.058E-03	6.235E-02	8.507E-03
5.886E-02	5.887E-01	-1.038E-01	-3.718E-03	7.254E-02	5.021E-03
5.638E-02	6.052E-01	-8.843E-02	-4.259E-03	9.521E-02	-1.653E-02
5.389E-02	6.237E-01	-7.259E-02	-4.352E-03	9.908E-02	-2.025E-02
5.141E-02	6.443E-01	-5.659E-02	-5.000E-03	1.354E-01	-5.431E-02
4.893E-02	6.669E-01	-4.050E-02	-7.303E-03	2.451E-01	-1.168E-01
4.646E-02	6.919E-01	-2.446E-02	-9.605E-03	3.357E-01	-9.729E-02
4.397E-02	7.207E-01	-8.907E-03	-1.191E-02	4.413E-01	-4.987E-02
4.148E-02	7.551E-01	5.189E-03	-1.420E-02	5.630E-01	-8.717E-03
3.898E-02	7.983E-01	1.714E-02	-1.648E-02	6.938E-01	9.589E-03
3.670E-02	8.473E-01	2.591E-02	-1.875E-02	8.194E-01	1.036E-02
3.445E-02	9.023E-01	3.265E-02	-2.102E-02	9.220E-01	3.990E-03
3.221E-02	9.560E-01	3.774E-02	-2.330E-02	9.886E-01	-3.731E-03
2.997E-02	9.974E-01	4.162E-02	-2.551E-02	1.015E+00	-1.064E-02
2.773E-02	1.017	4.442E-02	-2.776E-02	1.008E+00	-1.614E-02
2.549E-02	1.008	4.618E-02	-3.000E-02	9.746E-01	-1.994E-02
2.327E-02	9.631E-01	4.689E-02	-3.224E-02	9.259E-01	-2.234E-02
2.100E-02	8.789E-01	4.623E-02	-3.448E-02	8.718E-01	-2.414E-02
1.872E-02	7.674E-01	4.249E-02	-3.672E-02	8.200E-01	-2.642E-02
1.645E-02	6.437E-01	3.142E-02	-3.900E-02	7.748E-01	-3.013E-02
1.417E-02	5.217E-01	4.582E-03	-4.150E-02	7.343E-01	-3.640E-02
1.188E-02	4.112E-01	-4.568E-02	-4.400E-02	7.010E-01	-4.476E-02
9.587E-03	3.189E-01	-1.120E-01	-4.649E-02	6.719E-01	-5.433E-02
7.294E-03	2.458E-01	-1.666E-01	-4.895E-02	6.456E-01	-6.388E-02
5.000E-03	1.575E-01	-1.760E-01	-5.142E-02	6.205E-01	-7.248E-02
4.968E-03	1.560E-01	-1.755E-01	-5.390E-02	5.957E-01	-7.940E-02
4.290E-03	1.213E-01	-1.640E-01	-5.638E-02	5.705E-01	-8.423E-02
3.589E-03	8.615E-02	-1.443E-01	-5.886E-02	5.450E-01	-8.698E-02
2.890E-03	6.382E-02	-1.260E-01	-6.133E-02	5.195E-01	-8.798E-02
2.201E-03	4.583E-02	-1.090E-01	-6.380E-02	4.946E-01	-8.751E-02
1.530E-03	3.019E-02	-9.396E-02	-6.628E-02	4.712E-01	-8.557E-02
9.907E-04	1.352E-02	-7.858E-02	-6.876E-02	4.489E-01	-8.208E-02
8.945E-04	1.071E-02	-7.597E-02	-7.123E-02	4.246E-01	-7.635E-02
6.123E-04	1.084E-03	-7.047E-02	-7.371E-02	3.891E-01	-6.633E-02
3.921E-04	-5.593E-03	-6.605E-02	-7.619E-02	0.000	0.000

Table 6.7 Velocity Data at axial plane Z=260mm

Radius (mm)	Tangential Velocity (m/s)	Axial Velocity (m/s)	Radius (mm)	Tangential Velocity (m/s)	Axial Velocity (m/s)
-7.619E-02	0.000	0.000	-1.609E-04	1.666E-02	-3.505E-02
-7.374E-02	4.497E-01	-3.245E-02	3.921E-04	-5.389E-02	-3.086E-02
-7.128E-02	4.706E-01	-4.487E-02	6.036E-04	-5.111E-02	-2.850E-02
-6.883E-02	4.844E-01	-5.543E-02	8.940E-04	-4.485E-02	-2.514E-02
-6.638E-02	4.968E-01	-6.496E-02	9.949E-04	-4.288E-02	-2.382E-02
-6.393E-02	5.102E-01	-7.235E-02	1.530E-03	-2.799E-02	-1.681E-02
-6.149E-02	5.255E-01	-7.692E-02	2.200E-03	-1.200E-02	-6.812E-03
-5.905E-02	5.430E-01	-7.871E-02	2.889E-03	4.908E-03	-8.404E-04
-5.660E-02	5.627E-01	-7.822E-02	3.588E-03	2.792E-02	-3.538E-03
-5.417E-02	5.849E-01	-7.598E-02	4.289E-03	7.093E-02	-2.239E-02
-5.173E-02	6.097E-01	-7.264E-02	4.999E-03	1.207E-01	-4.559E-02
-4.929E-02	6.379E-01	-6.904E-02	7.294E-03	2.542E-01	-8.000E-02
-4.685E-02	6.699E-01	-6.609E-02	9.590E-03	3.583E-01	-5.953E-02
-4.439E-02	7.067E-01	-6.458E-02	1.189E-02	4.604E-01	-1.442E-02
-4.193E-02	7.481E-01	-6.501E-02	1.419E-02	5.585E-01	2.809E-02
-3.947E-02	7.941E-01	-6.730E-02	1.648E-02	6.545E-01	4.865E-02
-3.717E-02	8.405E-01	-7.041E-02	1.878E-02	7.524E-01	4.707E-02
-3.488E-02	8.864E-01	-7.332E-02	2.110E-02	8.498E-01	3.305E-02
-3.261E-02	9.268E-01	-7.510E-02	2.342E-02	9.357E-01	1.686E-02
-3.032E-02	9.561E-01	-7.515E-02	2.569E-02	9.951E-01	5.162E-03
-2.802E-02	9.688E-01	-7.294E-02	2.798E-02	1.021E+00	-6.613E-04
-2.573E-02	9.595E-01	-6.767E-02	3.028E-02	1.017E+00	-1.396E-03
-2.345E-02	9.254E-01	-5.836E-02	3.257E-02	9.887E-01	1.773E-03
-2.113E-02	8.659E-01	-4.462E-02	3.485E-02	9.412E-01	7.480E-03
-1.882E-02	7.855E-01	-2.843E-02	3.714E-02	8.841E-01	1.405E-02
-1.652E-02	6.922E-01	-1.695E-02	3.945E-02	8.281E-01	1.930E-02
-1.422E-02	5.953E-01	-2.278E-02	4.189E-02	7.763E-01	2.105E-02
-1.285E-02	5.427E-01	-4.308E-02	4.435E-02	7.336E-01	1.763E-02
-1.193E-02	5.033E-01	-5.719E-02	4.681E-02	6.989E-01	8.923E-03
-1.100E-02	4.686E-01	-7.960E-02	4.925E-02	6.707E-01	-4.586E-03
-9.614E-03	4.215E-01	-1.136E-01	5.170E-02	6.469E-01	-2.221E-02
-7.307E-03	3.489E-01	-1.559E-01	5.414E-02	6.260E-01	-4.290E-02
-4.999E-03	2.392E-01	-1.199E-01	5.659E-02	6.073E-01	-6.549E-02
-4.351E-03	1.961E-01	-8.893E-02	5.903E-02	5.904E-01	-8.885E-02
-3.716E-03	1.601E-01	-5.856E-02	6.148E-02	5.751E-01	-1.119E-01
-3.056E-03	1.412E-01	-4.538E-02	6.393E-02	5.608E-01	-1.334E-01
-2.359E-03	1.285E-01	-4.122E-02	6.638E-02	5.464E-01	-1.517E-01
-1.871E-03	1.207E-01	-4.049E-02	6.883E-02	5.307E-01	-1.658E-01
-1.640E-03	1.161E-01	-3.979E-02	7.128E-02	5.113E-01	-1.746E-01
-9.024E-04	9.650E-02	-3.860E-02	7.374E-02	4.770E-01	-1.783E-01
-4.579E-04	5.252E-02	-3.719E-02	7.619E-02	0.000	0.000

Table 6.8 Velocity Data at axial plane Z=280mm

Radius (mm)	Tangential Velocity (m/s)	Axial Velocity (m/s)	Radius (mm)	Tangential Velocity (m/s)	Axial Velocity (m/s)
-7.619E-02	0.000	0.000	-4.579E-04	4.378E-02	-1.172E-02
-7.376E-02	4.541E-01	-6.542E-02	-1.609E-04	2.518E-02	-5.994E-03
-7.134E-02	4.758E-01	-6.816E-02	3.920E-04	-1.302E-02	3.907E-03
-6.892E-02	4.912E-01	-6.926E-02	6.046E-04	-1.485E-02	7.721E-03
-6.649E-02	5.055E-01	-6.941E-02	8.939E-04	-1.688E-02	1.300E-02
-6.408E-02	5.208E-01	-6.892E-02	9.942E-04	-1.659E-02	1.511E-02
-6.167E-02	5.381E-01	-6.780E-02	1.529E-03	-1.081E-02	2.729E-02
-5.925E-02	5.578E-01	-6.599E-02	2.200E-03	-4.919E-03	3.924E-02
-5.684E-02	5.803E-01	-6.353E-02	2.889E-03	-1.652E-03	4.679E-02
-5.445E-02	6.059E-01	-6.068E-02	3.588E-03	8.201E-03	4.781E-02
-5.204E-02	6.349E-01	-5.783E-02	4.288E-03	4.387E-02	3.472E-02
-4.964E-02	6.677E-01	-5.547E-02	4.999E-03	1.010E-01	1.096E-02
-4.769E-02	6.969E-01	-5.443E-02	7.295E-03	2.926E-01	-5.521E-02
-4.723E-02	7.039E-01	-5.407E-02	9.593E-03	4.400E-01	-6.656E-02
-4.580E-02	7.272E-01	-5.378E-02	1.190E-02	5.588E-01	-3.137E-02
-4.478E-02	7.436E-01	-5.398E-02	1.420E-02	6.434E-01	1.882E-02
-4.336E-02	7.680E-01	-5.463E-02	1.651E-02	7.074E-01	4.754E-02
-4.233E-02	7.855E-01	-5.539E-02	1.881E-02	7.694E-01	4.417E-02
-3.988E-02	8.278E-01	-5.818E-02	2.112E-02	8.364E-01	1.916E-02
-3.754E-02	8.663E-01	-6.170E-02	2.344E-02	9.020E-01	-1.235E-02
-3.521E-02	8.988E-01	-6.540E-02	2.581E-02	9.548E-01	-3.999E-02
-3.289E-02	9.208E-01	-6.853E-02	2.817E-02	9.846E-01	-5.961E-02
-3.056E-02	9.291E-01	-7.022E-02	3.052E-02	9.896E-01	-7.163E-02
-2.821E-02	9.217E-01	-6.940E-02	3.285E-02	9.725E-01	-7.658E-02
-2.584E-02	8.968E-01	-6.490E-02	3.518E-02	9.382E-01	-7.504E-02
-2.348E-02	8.550E-01	-5.590E-02	3.751E-02	8.925E-01	-6.771E-02
-2.116E-02	8.017E-01	-4.337E-02	3.985E-02	8.419E-01	-5.596E-02
-1.885E-02	7.424E-01	-3.112E-02	4.229E-02	7.899E-01	-4.128E-02
-1.655E-02	6.809E-01	-2.619E-02	4.473E-02	7.417E-01	-2.649E-02
-1.425E-02	6.171E-01	-3.942E-02	4.716E-02	6.988E-01	-1.380E-02
-1.256E-02	5.667E-01	-6.849E-02	4.958E-02	6.622E-01	-5.221E-03
-1.194E-02	5.488E-01	-7.982E-02	5.200E-02	6.312E-01	-2.064E-03
-1.142E-02	5.326E-01	-9.211E-02	5.441E-02	6.055E-01	-5.801E-03
-9.622E-03	4.780E-01	-1.349E-01	5.681E-02	5.841E-01	-1.747E-02
-7.309E-03	4.091E-01	-1.714E-01	5.923E-02	5.661E-01	-3.646E-02
-4.999E-03	2.944E-01	-1.436E-01	6.165E-02	5.507E-01	-6.038E-02
-4.351E-03	2.444E-01	-1.171E-01	6.407E-02	5.367E-01	-8.580E-02
-3.716E-03	1.962E-01	-8.754E-02	6.649E-02	5.226E-01	-1.098E-01
-3.056E-03	1.582E-01	-6.546E-02	6.891E-02	5.066E-01	-1.303E-01
-2.359E-03	1.229E-01	-4.807E-02	7.134E-02	4.860E-01	-1.466E-01
-1.870E-03	1.040E-01	-3.863E-02	7.376E-02	4.490E-01	-1.580E-01
-1.640E-03	9.321E-02	-3.377E-02	7.619E-02	0.000	0.000
-9.023E-04	6.188E-02	-1.967E-02			

Table 6.9 Velocity Data at axial plane Z=294mm

Radius (mm)	Tangential Velocity (m/s)	Axial Velocity (m/s)	Radius (mm)	Tangential Velocity (m/s)	Axial Velocity (m/s)
-7.619E-02	0.000	0.000	-3.716E-03	1.519E-01	-5.317E-02
-7.378E-02	4.587E-01	-7.892E-02	-3.056E-03	1.023E-01	-3.695E-02
-7.137E-02	4.813E-01	-8.191E-02	-2.359E-03	5.794E-02	-2.586E-02
-6.896E-02	4.968E-01	-8.362E-02	-1.870E-03	3.632E-02	-1.975E-02
-6.655E-02	5.114E-01	-8.369E-02	-1.640E-03	2.565E-02	-1.685E-02
-6.415E-02	5.273E-01	-8.200E-02	-9.022E-04	1.926E-03	-6.537E-03
-6.175E-02	5.454E-01	-7.844E-02	-4.577E-04	1.258E-02	1.752E-04
-5.935E-02	5.661E-01	-7.310E-02	-1.609E-04	1.886E-02	4.561E-03
-5.695E-02	5.899E-01	-6.642E-02	3.920E-04	2.810E-02	1.278E-02
-5.456E-02	6.171E-01	-5.914E-02	6.058E-04	2.479E-02	1.593E-02
-5.217E-02	6.480E-01	-5.220E-02	8.939E-04	1.935E-02	2.028E-02
-4.978E-02	6.828E-01	-4.657E-02	9.935E-04	1.835E-02	2.201E-02
-4.914E-02	6.930E-01	-4.561E-02	1.529E-03	1.524E-02	3.215E-02
-4.738E-02	7.210E-01	-4.298E-02	2.200E-03	1.143E-02	4.164E-02
-4.494E-02	7.625E-01	-4.181E-02	2.889E-03	7.963E-03	4.668E-02
-4.250E-02	8.048E-01	-4.310E-02	3.588E-03	1.604E-02	4.354E-02
-4.086E-02	8.319E-01	-4.546E-02	4.289E-03	5.904E-02	2.164E-02
-4.066E-02	8.355E-01	-4.569E-02	4.999E-03	1.305E-01	-1.212E-02
-4.006E-02	8.454E-01	-4.635E-02	7.297E-03	3.658E-01	-1.032E-01
-3.975E-02	8.498E-01	-4.690E-02	9.600E-03	5.286E-01	-1.242E-01
-3.957E-02	8.525E-01	-4.724E-02	1.191E-02	6.452E-01	-8.881E-02
-3.848E-02	8.681E-01	-4.922E-02	1.423E-02	7.146E-01	-2.975E-02
-3.770E-02	8.797E-01	-5.046E-02	1.655E-02	7.551E-01	1.253E-02
-3.694E-02	8.886E-01	-5.176E-02	1.887E-02	7.891E-01	2.105E-02
-3.620E-02	8.960E-01	-5.294E-02	2.122E-02	8.274E-01	3.457E-03
-3.537E-02	9.045E-01	-5.428E-02	2.358E-02	8.683E-01	-2.524E-02
-3.399E-02	9.119E-01	-5.568E-02	2.594E-02	9.040E-01	-5.389E-02
-3.303E-02	9.168E-01	-5.658E-02	2.830E-02	9.272E-01	-7.765E-02
-3.070E-02	9.153E-01	-5.612E-02	3.065E-02	9.344E-01	-9.573E-02
-3.009E-02	9.110E-01	-5.475E-02	3.299E-02	9.260E-01	-1.083E-01
-2.970E-02	9.083E-01	-5.387E-02	3.533E-02	9.050E-01	-1.154E-01
-2.912E-02	9.041E-01	-5.255E-02	3.767E-02	8.746E-01	-1.174E-01
-2.834E-02	8.994E-01	-5.183E-02	4.002E-02	8.382E-01	-1.147E-01
-2.757E-02	8.897E-01	-4.972E-02	4.245E-02	7.978E-01	-1.082E-01
-2.598E-02	8.700E-01	-4.308E-02	4.487E-02	7.570E-01	-9.884E-02
-2.362E-02	8.315E-01	-3.051E-02	4.730E-02	7.172E-01	-8.737E-02
-2.125E-02	7.905E-01	-1.721E-02	4.970E-02	6.798E-01	-7.480E-02
-1.891E-02	7.504E-01	-9.361E-03	5.211E-02	6.447E-01	-6.198E-02
-1.743E-02	7.224E-01	-1.248E-02	5.451E-02	6.121E-01	-4.999E-02
-1.659E-02	7.081E-01	-1.533E-02	5.691E-02	5.814E-01	-3.976E-02
-1.583E-02	6.904E-01	-2.281E-02	5.932E-02	5.526E-01	-3.252E-02
-1.428E-02	6.547E-01	-4.358E-02	6.173E-02	5.255E-01	-2.927E-02
-1.196E-02	5.827E-01	-9.143E-02	6.414E-02	5.001E-01	-2.963E-02
-9.633E-03	4.961E-01	-1.363E-01	6.655E-02	4.761E-01	-3.305E-02
-9.241E-03	4.804E-01	-1.382E-01	6.896E-02	4.525E-01	-3.870E-02
-7.313E-03	4.076E-01	-1.519E-01	7.137E-02	4.265E-01	-4.444E-02
-4.999E-03	2.703E-01	-1.059E-01	7.378E-02	3.901E-01	-4.645E-02
-4.351E-03	2.109E-01	-7.854E-02	7.619E-02	0.000	0.000

Table 6.10 Velocity Data at axial plane Z=345mm

Radius (mm)	Tangential Velocity (m/s)	Axial Velocity (m/s)	Radius (mm)	Tangential Velocity (m/s)	Axial Velocity (m/s)
7.091E-02	0.000	0.000	-4.574E-04	1.456E-02	-3.466E-02
6.873E-02	4.676E-01	-1.157E-02	-9.022E-04	4.704E-02	-3.310E-02
6.655E-02	5.081E-01	-1.914E-02	-1.640E-03	4.887E-02	-3.041E-02
6.438E-02	5.320E-01	-3.343E-02	-1.867E-03	4.810E-02	-2.927E-02
6.220E-02	5.535E-01	-5.005E-02	-2.359E-03	4.801E-02	-2.590E-02
6.002E-02	5.782E-01	-6.417E-02	-3.056E-03	5.013E-02	-2.167E-02
5.776E-02	6.084E-01	-7.277E-02	-3.716E-03	6.401E-02	-2.279E-02
5.553E-02	6.417E-01	-7.472E-02	-4.326E-03	1.036E-01	-3.545E-02
5.335E-02	6.746E-01	-7.208E-02	-4.351E-03	1.053E-01	-3.596E-02
5.114E-02	7.045E-01	-6.760E-02	-4.539E-03	1.232E-01	-4.205E-02
4.895E-02	7.287E-01	-6.333E-02	-5.000E-03	1.669E-01	-5.709E-02
4.674E-02	7.459E-01	-5.985E-02	-5.908E-03	2.387E-01	-8.279E-02
4.451E-02	7.565E-01	-5.650E-02	-7.229E-03	3.432E-01	-1.201E-01
4.230E-02	7.632E-01	-5.206E-02	-9.434E-03	4.607E-01	-1.636E-01
4.010E-02	7.712E-01	-4.589E-02	-1.164E-02	5.886E-01	-1.947E-01
3.791E-02	7.864E-01	-3.856E-02	-1.382E-02	7.273E-01	-2.090E-01
3.571E-02	8.144E-01	-3.170E-02	-1.598E-02	8.656E-01	-2.037E-01
3.352E-02	8.575E-01	-2.728E-02	-1.817E-02	9.848E-01	-1.803E-01
3.132E-02	9.130E-01	-2.767E-02	-2.036E-02	1.063E+00	-1.462E-01
2.912E-02	9.726E-01	-3.709E-02	-2.254E-02	1.091E+00	-1.115E-01
2.692E-02	1.023	-6.036E-02	-2.473E-02	1.072E+00	-8.445E-02
2.472E-02	1.053	-9.871E-02	-2.694E-02	1.023E+00	-6.832E-02
2.252E-02	1.050	-1.478E-01	-2.914E-02	9.591E-01	-6.196E-02
2.033E-02	1.010	-2.001E-01	-3.133E-02	8.929E-01	-6.178E-02
1.814E-02	9.299E-01	-2.475E-01	-3.352E-02	8.330E-01	-6.486E-02
1.595E-02	8.179E-01	-2.819E-01	-3.571E-02	7.828E-01	-6.985E-02
1.378E-02	6.890E-01	-2.971E-01	-3.796E-02	7.419E-01	-7.652E-02
1.160E-02	5.632E-01	-2.898E-01	-4.021E-02	7.090E-01	-8.469E-02
9.410E-03	4.664E-01	-2.613E-01	-4.246E-02	6.818E-01	-9.399E-02
7.217E-03	4.070E-01	-2.197E-01	-4.473E-02	6.587E-01	-1.037E-01
6.290E-03	3.622E-01	-1.951E-01	-4.690E-02	6.395E-01	-1.124E-01
5.000E-03	3.002E-01	-1.609E-01	-4.906E-02	6.236E-01	-1.191E-01
4.289E-03	2.340E-01	-1.357E-01	-5.119E-02	6.113E-01	-1.220E-01
3.587E-03	1.494E-01	-1.093E-01	-5.335E-02	6.030E-01	-1.193E-01
2.888E-03	7.988E-02	-8.879E-02	-5.553E-02	5.991E-01	-1.092E-01
2.200E-03	2.751E-02	-7.133E-02	-5.776E-02	5.997E-01	-9.009E-02
1.529E-03	-5.778E-03	-5.657E-02	-6.002E-02	6.037E-01	-6.209E-02
9.917E-04	-2.455E-02	-4.733E-02	-6.220E-02	6.083E-01	-2.892E-02
8.938E-04	-2.794E-02	-4.567E-02	-6.438E-02	6.080E-01	6.103E-03
6.086E-04	-3.725E-02	-4.239E-02	-6.655E-02	5.948E-01	3.805E-02
3.919E-04	-4.293E-02	-3.995E-02	-6.873E-02	5.622E-01	6.410E-02
-1.608E-04	-6.474E-03	-3.612E-02	-7.091E-02	0.000	0.000

Table 6.11 Velocity Data at axial plane Z=365mm

Radius (mm)	Tangential Velocity (m/s)	Axial Velocity (m/s)	Radius (mm)	Tangential Velocity (m/s)	Axial Velocity (m/s)
6.611E-02	0.000	0.000	-4.580E-04	4.288E-02	-9.452E-02
6.410E-02	5.326E-01	4.459E-02	-9.023E-04	9.415E-02	-8.771E-02
6.209E-02	5.732E-01	3.356E-02	-1.640E-03	9.570E-02	-7.953E-02
6.009E-02	5.971E-01	1.496E-02	-1.869E-03	9.492E-02	-7.804E-02
5.808E-02	6.095E-01	-1.025E-02	-2.359E-03	9.206E-02	-7.454E-02
5.608E-02	6.165E-01	-3.993E-02	-3.056E-03	9.545E-02	-7.569E-02
5.393E-02	6.245E-01	-7.215E-02	-3.716E-03	1.139E-01	-8.760E-02
5.183E-02	6.378E-01	-9.978E-02	-4.336E-03	1.611E-01	-1.163E-01
4.982E-02	6.570E-01	-1.189E-01	-4.351E-03	1.622E-01	-1.170E-01
4.777E-02	6.796E-01	-1.284E-01	-4.465E-03	1.737E-01	-1.233E-01
4.574E-02	7.005E-01	-1.273E-01	-5.000E-03	2.277E-01	-1.527E-01
4.368E-02	7.175E-01	-1.165E-01	-6.067E-03	3.041E-01	-1.879E-01
4.160E-02	7.323E-01	-9.804E-02	-7.080E-03	3.767E-01	-2.214E-01
3.953E-02	7.513E-01	-7.675E-02	-9.118E-03	4.532E-01	-2.447E-01
3.749E-02	7.836E-01	-5.778E-02	-1.116E-02	5.393E-01	-2.672E-01
3.546E-02	8.364E-01	-4.542E-02	-1.316E-02	6.498E-01	-2.934E-01
3.343E-02	9.108E-01	-4.233E-02	-1.514E-02	7.794E-01	-3.154E-01
3.139E-02	9.992E-01	-5.031E-02	-1.716E-02	9.127E-01	-3.244E-01
2.936E-02	1.084	-7.026E-02	-1.919E-02	1.025E+00	-3.148E-01
2.732E-02	1.148	-1.019E-01	-2.121E-02	1.101E+00	-2.877E-01
2.528E-02	1.176	-1.420E-01	-2.324E-02	1.131E+00	-2.482E-01
2.323E-02	1.160	-1.854E-01	-2.529E-02	1.120E+00	-2.029E-01
2.120E-02	1.095	-2.250E-01	-2.733E-02	1.081E+00	-1.593E-01
1.918E-02	9.898E-01	-2.558E-01	-2.937E-02	1.022E+00	-1.214E-01
1.714E-02	8.584E-01	-2.755E-01	-3.140E-02	9.527E-01	-9.096E-02
1.512E-02	7.178E-01	-2.834E-01	-3.343E-02	8.812E-01	-6.817E-02
1.313E-02	5.872E-01	-2.799E-01	-3.551E-02	8.138E-01	-5.262E-02
1.113E-02	4.788E-01	-2.651E-01	-3.759E-02	7.549E-01	-4.353E-02
9.099E-03	4.011E-01	-2.410E-01	-3.967E-02	7.060E-01	-3.944E-02
7.070E-03	3.445E-01	-2.143E-01	-4.179E-02	6.671E-01	-3.854E-02
6.269E-03	3.024E-01	-2.060E-01	-4.382E-02	6.387E-01	-3.891E-02
5.000E-03	2.359E-01	-1.927E-01	-4.583E-02	6.195E-01	-3.891E-02
4.289E-03	1.654E-01	-1.848E-01	-4.782E-02	6.099E-01	-3.730E-02
3.588E-03	7.916E-02	-1.764E-01	-4.982E-02	6.098E-01	-3.314E-02
2.888E-03	1.332E-02	-1.673E-01	-5.183E-02	6.187E-01	-2.654E-02
2.200E-03	-3.457E-02	-1.548E-01	-5.393E-02	6.338E-01	-1.868E-02
1.529E-03	-6.395E-02	-1.396E-01	-5.608E-02	6.492E-01	-1.205E-02
9.907E-04	-7.999E-02	-1.246E-01	-5.808E-02	6.591E-01	-9.248E-03
8.937E-04	-8.208E-02	-1.221E-01	-6.009E-02	6.592E-01	-1.154E-02
6.112E-04	-8.710E-02	-1.159E-01	-6.209E-02	6.428E-01	-1.902E-02
3.916E-04	-8.881E-02	-1.110E-01	-6.410E-02	6.040E-01	-3.094E-02
-1.609E-04	1.848E-03	-9.970E-02	-6.611E-02	0.000	0.000

Table 6.12 Velocity Data at axial plane Z=385mm

Radius (mm)	Tangential Velocity (m/s)	Axial Velocity (m/s)	Radius (mm)	Tangential Velocity (m/s)	Axial Velocity (m/s)
-6.130E-02	0.000	0.000	3.913E-04	-8.200E-02	-1.869E-01
-5.946E-02	5.559E-01	-1.804E-02	6.124E-04	-8.448E-02	-1.907E-01
-5.763E-02	6.018E-01	-3.572E-03	8.935E-04	-8.510E-02	-1.954E-01
-5.579E-02	6.319E-01	3.831E-03	9.902E-04	-8.491E-02	-1.973E-01
-5.395E-02	6.573E-01	3.780E-03	1.529E-03	-7.729E-02	-2.085E-01
-5.212E-02	6.829E-01	-4.848E-04	2.200E-03	-6.286E-02	-2.159E-01
-5.010E-02	7.074E-01	-5.832E-03	2.888E-03	-3.950E-02	-2.187E-01
-4.814E-02	7.168E-01	-1.139E-02	3.587E-03	8.233E-04	-2.173E-01
-4.630E-02	7.096E-01	-1.898E-02	4.289E-03	7.280E-02	-2.141E-01
-4.444E-02	6.950E-01	-2.876E-02	5.000E-03	1.510E-01	-2.118E-01
-4.261E-02	6.873E-01	-3.756E-02	6.216E-03	2.528E-01	-2.100E-01
-4.074E-02	6.970E-01	-4.379E-02	6.920E-03	3.117E-01	-2.090E-01
-3.885E-02	7.286E-01	-4.854E-02	8.785E-03	4.136E-01	-2.164E-01
-3.689E-02	7.819E-01	-5.567E-02	1.065E-02	5.026E-01	-2.314E-01
-3.498E-02	8.496E-01	-6.952E-02	1.249E-02	5.931E-01	-2.513E-01
-3.307E-02	9.233E-01	-9.371E-02	1.429E-02	6.938E-01	-2.731E-01
-3.116E-02	9.937E-01	-1.295E-01	1.615E-02	8.099E-01	-2.937E-01
-2.928E-02	1.053	-1.748E-01	1.802E-02	9.311E-01	-3.074E-01
-2.742E-02	1.094	-2.254E-01	1.988E-02	1.044E+00	-3.107E-01
-2.554E-02	1.115	-2.775E-01	2.175E-02	1.135E+00	-3.022E-01
-2.365E-02	1.111	-3.261E-01	2.365E-02	1.189E+00	-2.823E-01
-2.175E-02	1.076	-3.665E-01	2.553E-02	1.201E+00	-2.540E-01
-1.989E-02	1.008	-3.934E-01	2.741E-02	1.177E+00	-2.208E-01
-1.804E-02	9.103E-01	-4.051E-01	2.927E-02	1.123E+00	-1.868E-01
-1.617E-02	7.913E-01	-4.007E-01	3.115E-02	1.042E+00	-1.543E-01
-1.431E-02	6.674E-01	-3.834E-01	3.302E-02	9.505E-01	-1.251E-01
-1.251E-02	5.648E-01	-3.627E-01	3.489E-02	8.604E-01	-9.943E-02
-1.067E-02	4.974E-01	-3.484E-01	3.678E-02	7.827E-01	-7.764E-02
-8.800E-03	4.635E-01	-3.448E-01	3.868E-02	7.238E-01	-6.036E-02
-6.928E-03	4.359E-01	-3.398E-01	4.063E-02	6.856E-01	-4.815E-02
-6.249E-03	3.982E-01	-3.177E-01	4.254E-02	6.660E-01	-4.104E-02
-5.000E-03	3.291E-01	-2.772E-01	4.441E-02	6.589E-01	-3.779E-02
-4.351E-03	2.606E-01	-2.339E-01	4.630E-02	6.591E-01	-3.638E-02
-4.348E-03	2.602E-01	-2.336E-01	4.814E-02	6.618E-01	-3.457E-02
-3.716E-03	1.953E-01	-1.921E-01	5.010E-02	6.636E-01	-3.022E-02
-3.056E-03	1.567E-01	-1.705E-01	5.212E-02	6.623E-01	-2.207E-02
-2.359E-03	1.342E-01	-1.621E-01	5.395E-02	6.580E-01	-1.152E-02
-1.870E-03	1.273E-01	-1.620E-01	5.579E-02	6.490E-01	6.758E-04
-1.640E-03	1.224E-01	-1.622E-01	5.763E-02	6.300E-01	1.236E-02
-9.024E-04	1.072E-01	-1.681E-01	5.946E-02	5.931E-01	2.067E-02
-4.585E-04	6.011E-02	-1.739E-01	6.130E-02	0.000	0.000
-1.610E-04	1.664E-02	-1.776E-01			

Table 6.13 Velocity Data at axial plane Z=405mm

Radius (mm)	Tangential Velocity (m/s)	Axial Velocity (m/s)	Radius (mm)	Tangential Velocity (m/s)	Axial Velocity (m/s)
5.650E-02	0.000	0.000	-1.609E-04	2.823E-02	-2.608E-01
5.483E-02	6.030E-01	-7.124E-02	-4.587E-04	6.141E-02	-2.632E-01
5.316E-02	6.449E-01	-4.097E-02	-9.023E-04	9.449E-02	-2.661E-01
5.149E-02	6.694E-01	-1.427E-02	-1.640E-03	1.287E-01	-2.746E-01
4.982E-02	6.879E-01	6.722E-03	-1.870E-03	1.406E-01	-2.787E-01
4.817E-02	7.081E-01	2.155E-02	-2.359E-03	1.621E-01	-2.874E-01
4.627E-02	7.337E-01	3.148E-02	-3.056E-03	2.048E-01	-3.051E-01
4.446E-02	7.550E-01	3.453E-02	-3.716E-03	2.561E-01	-3.294E-01
4.279E-02	7.664E-01	2.970E-02	-4.351E-03	3.242E-01	-3.615E-01
4.105E-02	7.704E-01	1.322E-02	-5.000E-03	3.920E-01	-3.875E-01
3.934E-02	7.745E-01	-1.524E-02	-6.499E-03	4.765E-01	-4.090E-01
3.759E-02	7.886E-01	-5.260E-02	-6.773E-03	4.919E-01	-4.130E-01
3.579E-02	8.204E-01	-9.460E-02	-8.482E-03	5.180E-01	-4.071E-01
3.404E-02	8.703E-01	-1.360E-01	-1.019E-02	5.338E-01	-3.993E-01
3.232E-02	9.334E-01	-1.745E-01	-1.186E-02	5.661E-01	-3.992E-01
3.061E-02	1.001	-2.091E-01	-1.349E-02	6.259E-01	-4.064E-01
2.890E-02	1.064	-2.402E-01	-1.518E-02	7.145E-01	-4.155E-01
2.718E-02	1.113	-2.685E-01	-1.689E-02	8.173E-01	-4.194E-01
2.547E-02	1.142	-2.937E-01	-1.858E-02	9.183E-01	-4.141E-01
2.375E-02	1.147	-3.151E-01	-2.028E-02	1.007E+00	-3.986E-01
2.203E-02	1.124	-3.300E-01	-2.203E-02	1.075E+00	-3.728E-01
2.029E-02	1.072	-3.357E-01	-2.376E-02	1.116E+00	-3.397E-01
1.858E-02	9.967E-01	-3.305E-01	-2.548E-02	1.130E+00	-3.016E-01
1.689E-02	9.082E-01	-3.157E-01	-2.719E-02	1.120E+00	-2.621E-01
1.517E-02	8.174E-01	-2.952E-01	-2.891E-02	1.087E+00	-2.237E-01
1.348E-02	7.320E-01	-2.748E-01	-3.065E-02	1.029E+00	-1.899E-01
1.185E-02	6.518E-01	-2.601E-01	-3.239E-02	9.549E-01	-1.627E-01
1.017E-02	5.617E-01	-2.511E-01	-3.414E-02	8.772E-01	-1.422E-01
8.471E-03	4.508E-01	-2.458E-01	-3.594E-02	8.090E-01	-1.264E-01
6.768E-03	3.188E-01	-2.428E-01	-3.768E-02	7.603E-01	-1.125E-01
6.321E-03	2.754E-01	-2.437E-01	-3.940E-02	7.312E-01	-9.751E-02
5.000E-03	1.469E-01	-2.462E-01	-4.108E-02	7.171E-01	-8.017E-02
4.288E-03	7.586E-02	-2.500E-01	-4.279E-02	7.116E-01	-6.048E-02
3.587E-03	2.225E-02	-2.556E-01	-4.446E-02	7.099E-01	-4.171E-02
2.888E-03	-3.466E-03	-2.610E-01	-4.627E-02	7.085E-01	-2.477E-02
2.200E-03	-1.789E-02	-2.637E-01	-4.816E-02	7.058E-01	-1.023E-02
1.529E-03	-3.175E-02	-2.638E-01	-4.982E-02	7.028E-01	2.999E-03
9.902E-04	-4.148E-02	-2.611E-01	-5.149E-02	6.984E-01	1.894E-02
8.936E-04	-4.219E-02	-2.606E-01	-5.316E-02	6.876E-01	3.774E-02
6.135E-04	-4.156E-02	-2.602E-01	-5.483E-02	6.617E-01	5.892E-02
3.913E-04	-3.985E-02	-2.600E-01	-5.650E-02	0.000	0.000

Table 6.14 Velocity Data at axial plane Z=425mm

Radius (mm)	Tangential Velocity (m/s)	Axial Velocity (m/s)	Radius (mm)	Tangential Velocity (m/s)	Axial Velocity (m/s)
5.170E-02	0.000	0.000	-1.609E-04	3.312E-02	-3.487E-01
5.019E-02	6.738E-01	5.571E-02	-4.590E-04	4.357E-02	-3.543E-01
4.869E-02	7.023E-01	5.424E-02	-9.024E-04	5.263E-02	-3.628E-01
4.718E-02	7.222E-01	4.781E-02	-1.640E-03	9.560E-02	-3.781E-01
4.567E-02	7.405E-01	3.406E-02	-1.871E-03	1.099E-01	-3.833E-01
4.418E-02	7.582E-01	1.486E-02	-2.359E-03	1.367E-01	-3.945E-01
4.244E-02	7.775E-01	-1.069E-02	-3.056E-03	1.813E-01	-4.127E-01
4.078E-02	7.958E-01	-3.755E-02	-3.716E-03	2.276E-01	-4.319E-01
3.926E-02	8.140E-01	-6.349E-02	-4.351E-03	2.860E-01	-4.491E-01
3.769E-02	8.351E-01	-9.058E-02	-5.000E-03	3.525E-01	-4.575E-01
3.614E-02	8.585E-01	-1.178E-01	-6.615E-03	4.816E-01	-4.469E-01
3.455E-02	8.849E-01	-1.464E-01	-8.161E-03	5.658E-01	-4.181E-01
3.290E-02	9.149E-01	-1.766E-01	-9.707E-03	6.240E-01	-3.927E-01
3.130E-02	9.473E-01	-2.062E-01	-1.121E-02	6.638E-01	-3.812E-01
2.974E-02	9.811E-01	-2.344E-01	-1.267E-02	7.014E-01	-3.809E-01
2.819E-02	1.014	-2.609E-01	-1.421E-02	7.520E-01	-3.856E-01
2.664E-02	1.043	-2.853E-01	-1.576E-02	8.181E-01	-3.894E-01
2.508E-02	1.065	-3.079E-01	-1.728E-02	8.931E-01	-3.890E-01
2.354E-02	1.075	-3.279E-01	-1.882E-02	9.668E-01	-3.834E-01
2.198E-02	1.071	-3.448E-01	-2.042E-02	1.030E+00	-3.722E-01
2.042E-02	1.049	-3.562E-01	-2.198E-02	1.074E+00	-3.571E-01
1.884E-02	1.006	-3.603E-01	-2.355E-02	1.098E+00	-3.400E-01
1.729E-02	9.496E-01	-3.568E-01	-2.510E-02	1.105E+00	-3.226E-01
1.575E-02	8.885E-01	-3.486E-01	-2.666E-02	1.097E+00	-3.053E-01
1.420E-02	8.315E-01	-3.406E-01	-2.823E-02	1.077E+00	-2.877E-01
1.266E-02	7.795E-01	-3.374E-01	-2.980E-02	1.046E+00	-2.687E-01
1.120E-02	7.229E-01	-3.392E-01	-3.139E-02	1.007E+00	-2.470E-01
9.694E-03	6.407E-01	-3.406E-01	-3.302E-02	9.640E-01	-2.212E-01
8.154E-03	5.234E-01	-3.347E-01	-3.462E-02	9.229E-01	-1.911E-01
6.612E-03	3.816E-01	-3.206E-01	-3.619E-02	8.861E-01	-1.572E-01
5.000E-03	2.082E-01	-3.038E-01	-3.771E-02	8.541E-01	-1.205E-01
4.289E-03	1.376E-01	-2.991E-01	-3.926E-02	8.246E-01	-8.089E-02
3.588E-03	8.832E-02	-2.996E-01	-4.078E-02	7.983E-01	-4.409E-02
2.888E-03	6.539E-02	-3.068E-01	-4.244E-02	7.726E-01	-1.130E-02
2.200E-03	5.188E-02	-3.160E-01	-4.418E-02	7.497E-01	1.062E-02
1.529E-03	3.550E-02	-3.256E-01	-4.567E-02	7.342E-01	1.914E-02
9.897E-04	2.156E-02	-3.326E-01	-4.718E-02	7.231E-01	1.979E-02
8.935E-04	1.981E-02	-3.339E-01	-4.869E-02	7.129E-01	1.551E-02
6.150E-04	1.944E-02	-3.374E-01	-5.019E-02	6.906E-01	7.497E-03
3.912E-04	1.905E-02	-3.403E-01	-5.170E-02	0.000	0.000

Table 6.15 Velocity Data at axial plane Z=445mm

Radius (mm)	Tangential Velocity (m/s)	Axial Velocity (m/s)	Radius (mm)	Tangential Velocity (m/s)	Axial Velocity (m/s)
4.690E-02	0.000	0.000	-9.025E-04	6.933E-04	-4.591E-01
4.555E-02	7.133E-01	4.007E-02	-1.640E-03	4.386E-02	-4.733E-01
4.421E-02	7.632E-01	3.373E-02	-1.867E-03	5.875E-02	-4.773E-01
4.286E-02	8.007E-01	1.898E-02	-2.360E-03	8.964E-02	-4.856E-01
4.152E-02	8.280E-01	-2.326E-03	-3.057E-03	1.378E-01	-4.986E-01
4.019E-02	8.472E-01	-2.579E-02	-3.716E-03	1.836E-01	-5.125E-01
3.860E-02	8.637E-01	-5.290E-02	-4.290E-03	2.313E-01	-5.248E-01
3.710E-02	8.787E-01	-7.732E-02	-4.351E-03	2.364E-01	-5.261E-01
3.575E-02	8.951E-01	-9.708E-02	-4.842E-03	2.836E-01	-5.323E-01
3.433E-02	9.159E-01	-1.149E-01	-5.000E-03	2.990E-01	-5.341E-01
3.294E-02	9.390E-01	-1.311E-01	-5.180E-03	3.154E-01	-5.327E-01
3.151E-02	9.636E-01	-1.482E-01	-5.361E-03	3.319E-01	-5.313E-01
3.004E-02	9.882E-01	-1.675E-01	-6.456E-03	4.330E-01	-5.243E-01
2.858E-02	1.011	-1.896E-01	-7.840E-03	5.542E-01	-4.880E-01
2.718E-02	1.031	-2.143E-01	-9.224E-03	6.608E-01	-4.400E-01
2.579E-02	1.046	-2.419E-01	-1.057E-02	7.364E-01	-3.972E-01
2.440E-02	1.055	-2.715E-01	-1.187E-02	7.840E-01	-3.709E-01
2.300E-02	1.056	-3.017E-01	-1.324E-02	8.214E-01	-3.608E-01
2.162E-02	1.048	-3.302E-01	-1.463E-02	8.619E-01	-3.618E-01
2.022E-02	1.028	-3.554E-01	-1.600E-02	9.120E-01	-3.658E-01
1.882E-02	9.932E-01	-3.750E-01	-1.738E-02	9.694E-01	-3.669E-01
1.740E-02	9.482E-01	-3.885E-01	-1.881E-02	1.028E+00	-3.608E-01
1.601E-02	9.015E-01	-3.973E-01	-2.022E-02	1.078E+00	-3.467E-01
1.463E-02	8.612E-01	-4.057E-01	-2.163E-02	1.114E+00	-3.258E-01
1.324E-02	8.312E-01	-4.184E-01	-2.302E-02	1.134E+00	-3.005E-01
1.186E-02	8.068E-01	-4.374E-01	-2.442E-02	1.140E+00	-2.720E-01
1.056E-02	7.728E-01	-4.580E-01	-2.583E-02	1.134E+00	-2.422E-01
9.215E-03	7.076E-01	-4.728E-01	-2.723E-02	1.118E+00	-2.125E-01
7.835E-03	6.008E-01	-4.716E-01	-2.865E-02	1.092E+00	-1.839E-01
6.453E-03	4.626E-01	-4.514E-01	-3.012E-02	1.058E+00	-1.573E-01
5.000E-03	2.869E-01	-4.124E-01	-3.157E-02	1.017E+00	-1.345E-01
4.981E-03	2.847E-01	-4.118E-01	-3.298E-02	9.723E-01	-1.169E-01
4.289E-03	2.071E-01	-3.932E-01	-3.435E-02	9.252E-01	-1.050E-01
3.588E-03	1.502E-01	-3.817E-01	-3.575E-02	8.759E-01	-9.784E-02
2.889E-03	1.232E-01	-3.838E-01	-3.710E-02	8.320E-01	-9.450E-02
2.200E-03	1.084E-01	-3.941E-01	-3.860E-02	7.940E-01	-9.239E-02
1.529E-03	9.218E-02	-4.080E-01	-4.019E-02	7.688E-01	-8.972E-02
9.853E-04	7.696E-02	-4.205E-01	-4.152E-02	7.578E-01	-8.587E-02
8.938E-04	7.474E-02	-4.225E-01	-4.286E-02	7.527E-01	-8.012E-02
6.239E-04	7.307E-02	-4.277E-01	-4.421E-02	7.450E-01	-7.436E-02
3.911E-04	7.037E-02	-4.321E-01	-4.555E-02	7.175E-01	-7.361E-02
-1.608E-04	2.980E-02	-4.435E-01	-4.690E-02	0.000	0.000
-4.582E-04	1.560E-02	-4.496E-01			

Table 6.16 Velocity Data at axial plane Z=465mm

Radius (mm)	Tangential Velocity (m/s)	Axial Velocity (m/s)	Radius (mm)	Tangential Velocity (m/s)	Axial Velocity (m/s)
4.460E-02	0.000	0.000	-1.608E-04	2.559E-02	-4.932E-01
4.333E-02	7.396E-01	1.966E-04	-4.580E-04	3.637E-03	-4.993E-01
4.206E-02	8.030E-01	-4.926E-03	-9.025E-04	-1.765E-02	-5.087E-01
4.079E-02	8.474E-01	-1.488E-02	-1.640E-03	2.335E-02	-5.218E-01
3.952E-02	8.771E-01	-2.892E-02	-1.866E-03	3.824E-02	-5.253E-01
3.826E-02	8.958E-01	-4.502E-02	-2.360E-03	7.093E-02	-5.325E-01
3.675E-02	9.101E-01	-6.518E-02	-3.057E-03	1.222E-01	-5.437E-01
3.532E-02	9.219E-01	-8.455E-02	-3.717E-03	1.712E-01	-5.565E-01
3.405E-02	9.354E-01	-1.004E-01	-4.281E-03	2.193E-01	-5.686E-01
3.270E-02	9.540E-01	-1.144E-01	-4.351E-03	2.253E-01	-5.702E-01
3.139E-02	9.759E-01	-1.271E-01	-5.000E-03	2.881E-01	-5.804E-01
3.004E-02	1.000	-1.409E-01	-6.374E-03	4.176E-01	-5.783E-01
2.864E-02	1.025	-1.579E-01	-7.677E-03	5.414E-01	-5.494E-01
2.726E-02	1.047	-1.789E-01	-8.981E-03	6.590E-01	-5.023E-01
2.594E-02	1.064	-2.042E-01	-1.025E-02	7.493E-01	-4.486E-01
2.462E-02	1.075	-2.338E-01	-1.146E-02	8.070E-01	-4.023E-01
2.331E-02	1.077	-2.664E-01	-1.276E-02	8.451E-01	-3.700E-01
2.199E-02	1.070	-3.005E-01	-1.406E-02	8.769E-01	-3.558E-01
2.068E-02	1.051	-3.330E-01	-1.535E-02	9.146E-01	-3.538E-01
1.936E-02	1.018	-3.624E-01	-1.665E-02	9.619E-01	-3.563E-01
1.803E-02	9.754E-01	-3.863E-01	-1.800E-02	1.017E+00	-3.564E-01
1.669E-02	9.266E-01	-4.050E-01	-1.933E-02	1.071E+00	-3.500E-01
1.538E-02	8.816E-01	-4.203E-01	-2.065E-02	1.115E+00	-3.364E-01
1.408E-02	8.469E-01	-4.369E-01	-2.196E-02	1.143E+00	-3.169E-01
1.277E-02	8.241E-01	-4.588E-01	-2.328E-02	1.156E+00	-2.928E-01
1.147E-02	8.067E-01	-4.868E-01	-2.460E-02	1.156E+00	-2.666E-01
1.025E-02	7.796E-01	-5.151E-01	-2.592E-02	1.145E+00	-2.399E-01
8.977E-03	7.229E-01	-5.370E-01	-2.725E-02	1.123E+00	-2.140E-01
7.676E-03	6.262E-01	-5.420E-01	-2.863E-02	1.091E+00	-1.895E-01
6.373E-03	4.969E-01	-5.253E-01	-3.000E-02	1.053E+00	-1.675E-01
5.000E-03	3.267E-01	-4.839E-01	-3.133E-02	1.010E+00	-1.483E-01
4.979E-03	3.243E-01	-4.832E-01	-3.261E-02	9.645E-01	-1.317E-01
4.289E-03	2.419E-01	-4.595E-01	-3.393E-02	9.171E-01	-1.161E-01
3.588E-03	1.775E-01	-4.416E-01	-3.519E-02	8.736E-01	-1.021E-01
2.889E-03	1.441E-01	-4.382E-01	-3.661E-02	8.329E-01	-8.885E-02
2.200E-03	1.256E-01	-4.451E-01	-3.811E-02	8.013E-01	-7.871E-02
1.529E-03	1.085E-01	-4.574E-01	-3.935E-02	7.830E-01	-7.407E-02
9.854E-04	9.278E-02	-4.699E-01	-4.061E-02	7.703E-01	-7.356E-02
8.938E-04	9.031E-02	-4.720E-01	-4.187E-02	7.567E-01	-7.697E-02
6.231E-04	8.738E-02	-4.771E-01	-4.313E-02	7.218E-01	-8.647E-02
3.911E-04	8.340E-02	-4.815E-01	-4.439E-02	0.000	0.000

Table 6.17 Velocity Data at axial plane Z=485mm

Radius (mm)	Tangential Velocity (m/s)	Axial Velocity (m/s)	Radius (mm)	Tangential Velocity (m/s)	Axial Velocity (m/s)
3.729E-02	0.000	0.000	-1.609E-04	1.188E-02	-6.685E-01
3.626E-02	8.159E-01	-1.762E-01	-4.577E-04	-8.185E-03	-6.723E-01
3.523E-02	8.763E-01	-1.823E-01	-9.025E-04	-2.111E-02	-6.783E-01
3.420E-02	9.221E-01	-1.794E-01	-1.640E-03	1.023E-02	-6.866E-01
3.317E-02	9.600E-01	-1.672E-01	-1.866E-03	2.294E-02	-6.886E-01
3.215E-02	9.919E-01	-1.508E-01	-2.360E-03	5.596E-02	-6.925E-01
3.091E-02	1.026	-1.299E-01	-3.057E-03	1.102E-01	-6.991E-01
2.974E-02	1.058	-1.107E-01	-3.716E-03	1.669E-01	-7.079E-01
2.870E-02	1.089	-9.680E-02	-4.276E-03	2.227E-01	-7.171E-01
2.761E-02	1.121	-8.857E-02	-4.351E-03	2.303E-01	-7.183E-01
2.654E-02	1.150	-8.810E-02	-5.000E-03	3.012E-01	-7.294E-01
2.543E-02	1.174	-9.699E-02	-6.127E-03	4.206E-01	-7.406E-01
2.429E-02	1.188	-1.187E-01	-7.191E-03	5.353E-01	-7.385E-01
2.317E-02	1.191	-1.538E-01	-8.256E-03	6.551E-01	-7.224E-01
2.208E-02	1.183	-1.987E-01	-9.289E-03	7.653E-01	-6.905E-01
2.101E-02	1.163	-2.496E-01	-1.028E-02	8.511E-01	-6.447E-01
1.994E-02	1.131	-3.023E-01	-1.134E-02	9.095E-01	-5.845E-01
1.886E-02	1.087	-3.532E-01	-1.241E-02	9.374E-01	-5.200E-01
1.780E-02	1.033	-3.983E-01	-1.346E-02	9.467E-01	-4.615E-01
1.672E-02	9.725E-01	-4.365E-01	-1.452E-02	9.518E-01	-4.156E-01
1.564E-02	9.120E-01	-4.664E-01	-1.563E-02	9.653E-01	-3.838E-01
1.454E-02	8.595E-01	-4.904E-01	-1.672E-02	9.928E-01	-3.648E-01
1.347E-02	8.237E-01	-5.123E-01	-1.781E-02	1.034E+00	-3.524E-01
1.241E-02	8.058E-01	-5.384E-01	-1.888E-02	1.080E+00	-3.411E-01
1.134E-02	8.023E-01	-5.740E-01	-1.996E-02	1.127E+00	-3.261E-01
1.028E-02	8.029E-01	-6.199E-01	-2.104E-02	1.165E+00	-3.047E-01
9.287E-03	7.924E-01	-6.687E-01	-2.212E-02	1.191E+00	-2.767E-01
8.252E-03	7.553E-01	-7.142E-01	-2.321E-02	1.204E+00	-2.432E-01
7.190E-03	6.831E-01	-7.440E-01	-2.434E-02	1.207E+00	-2.065E-01
6.126E-03	5.800E-01	-7.503E-01	-2.547E-02	1.198E+00	-1.716E-01
5.000E-03	4.392E-01	-7.284E-01	-2.656E-02	1.181E+00	-1.435E-01
4.980E-03	4.366E-01	-7.277E-01	-2.762E-02	1.156E+00	-1.252E-01
4.289E-03	3.445E-01	-7.042E-01	-2.870E-02	1.122E+00	-1.163E-01
3.588E-03	2.566E-01	-6.788E-01	-2.974E-02	1.082E+00	-1.150E-01
2.889E-03	1.942E-01	-6.618E-01	-3.091E-02	1.034E+00	-1.185E-01
2.200E-03	1.508E-01	-6.542E-01	-3.215E-02	9.807E-01	-1.264E-01
1.529E-03	1.190E-01	-6.535E-01	-3.317E-02	9.333E-01	-1.340E-01
9.863E-04	9.474E-02	-6.573E-01	-3.420E-02	8.846E-01	-1.388E-01
8.938E-04	9.053E-02	-6.579E-01	-3.523E-02	8.381E-01	-1.366E-01
6.205E-04	8.045E-02	-6.600E-01	-3.626E-02	7.876E-01	-1.286E-01
3.913E-04	7.135E-02	-6.618E-01	-3.729E-02	0.000	0.000

Table 6.18 Velocity Data at axial plane Z=505mm

Radius (mm)	Tangential Velocity (m/s)	Axial Velocity (m/s)	Radius (mm)	Tangential Velocity (m/s)	Axial Velocity (m/s)
3.249E-02	0.000	0.000	8.935E-04	5.690E-02	-8.186E-01
3.161E-02	8.819E-01	-2.298E-01	6.168E-04	4.171E-02	-8.182E-01
3.073E-02	9.347E-01	-2.340E-01	3.912E-04	2.992E-02	-8.179E-01
2.985E-02	9.635E-01	-2.436E-01	-1.612E-04	8.993E-03	-8.197E-01
2.897E-02	9.884E-01	-2.517E-01	-4.576E-04	9.646E-03	-8.213E-01
2.810E-02	1.015	-2.553E-01	-9.028E-04	2.395E-02	-8.241E-01
2.705E-02	1.051	-2.519E-01	-1.641E-03	5.755E-02	-8.276E-01
2.605E-02	1.095	-2.409E-01	-1.865E-03	7.011E-02	-8.281E-01
2.517E-02	1.142	-2.268E-01	-2.360E-03	1.036E-01	-8.284E-01
2.424E-02	1.194	-2.125E-01	-3.057E-03	1.585E-01	-8.289E-01
2.333E-02	1.246	-2.021E-01	-3.717E-03	2.176E-01	-8.322E-01
2.239E-02	1.292	-1.982E-01	-4.273E-03	2.762E-01	-8.388E-01
2.142E-02	1.327	-2.031E-01	-4.351E-03	2.845E-01	-8.397E-01
2.046E-02	1.343	-2.181E-01	-5.000E-03	3.600E-01	-8.515E-01
1.954E-02	1.338	-2.424E-01	-5.957E-03	4.711E-01	-8.684E-01
1.863E-02	1.311	-2.746E-01	-6.862E-03	5.789E-01	-8.782E-01
1.772E-02	1.263	-3.118E-01	-7.767E-03	6.914E-01	-8.779E-01
1.690E-02	1.205	-3.465E-01	-8.647E-03	7.981E-01	-8.633E-01
1.680E-02	1.197	-3.513E-01	-9.491E-03	8.872E-01	-8.335E-01
1.669E-02	1.189	-3.560E-01	-1.039E-02	9.550E-01	-7.855E-01
1.589E-02	1.121	-3.902E-01	-1.130E-02	9.923E-01	-7.229E-01
1.508E-02	1.051	-4.244E-01	-1.220E-02	1.004E+00	-6.525E-01
1.497E-02	1.042	-4.289E-01	-1.310E-02	1.000E+00	-5.820E-01
1.405E-02	9.694E-01	-4.684E-01	-1.405E-02	9.939E-01	-5.170E-01
1.394E-02	9.627E-01	-4.731E-01	-1.497E-02	9.963E-01	-4.647E-01
1.312E-02	9.100E-01	-5.129E-01	-1.590E-02	1.013E+00	-4.233E-01
1.221E-02	8.690E-01	-5.653E-01	-1.681E-02	1.046E+00	-3.904E-01
1.131E-02	8.434E-01	-6.284E-01	-1.774E-02	1.092E+00	-3.612E-01
1.040E-02	8.268E-01	-7.012E-01	-1.865E-02	1.146E+00	-3.327E-01
9.602E-03	8.105E-01	-7.679E-01	-1.957E-02	1.201E+00	-3.024E-01
9.494E-03	8.093E-01	-7.762E-01	-2.049E-02	1.249E+00	-2.698E-01
8.646E-03	7.805E-01	-8.407E-01	-2.145E-02	1.282E+00	-2.357E-01
7.871E-03	7.354E-01	-8.846E-01	-2.241E-02	1.297E+00	-2.035E-01
7.766E-03	7.302E-01	-8.904E-01	-2.334E-02	1.295E+00	-1.777E-01
6.862E-03	6.562E-01	-9.172E-01	-2.424E-02	1.278E+00	-1.606E-01
5.957E-03	5.642E-01	-9.195E-01	-2.517E-02	1.248E+00	-1.523E-01
5.000E-03	4.512E-01	-8.995E-01	-2.605E-02	1.209E+00	-1.524E-01
4.981E-03	4.488E-01	-8.989E-01	-2.705E-02	1.158E+00	-1.586E-01
4.289E-03	3.622E-01	-8.768E-01	-2.810E-02	1.099E+00	-1.682E-01
3.588E-03	2.727E-01	-8.535E-01	-2.897E-02	1.047E+00	-1.756E-01
2.888E-03	1.991E-01	-8.368E-01	-2.985E-02	9.926E-01	-1.791E-01
2.200E-03	1.405E-01	-8.267E-01	-3.073E-02	9.393E-01	-1.756E-01
1.529E-03	9.579E-02	-8.211E-01	-3.161E-02	8.780E-01	-1.670E-01
9.872E-04	6.256E-02	-8.190E-01	-3.249E-02	0.000	0.000

Table 6.19 Velocity Data at axial plane Z=525mm

Radius (mm)	Tangential Velocity (m/s)	Axial Velocity (m/s)	Radius (mm)	Tangential Velocity (m/s)	Axial Velocity (m/s)
2.769E-02	0.000	0.000	-1.609E-04	1.413E-02	-1.007
2.696E-02	9.416E-01	-2.866E-01	-4.571E-04	3.082E-02	-1.007
2.622E-02	1.006	-2.902E-01	-9.025E-04	6.512E-02	-1.008
2.549E-02	1.039	-2.980E-01	-1.640E-03	1.072E-01	-1.009
2.476E-02	1.067	-3.067E-01	-1.865E-03	1.218E-01	-1.009
2.403E-02	1.095	-3.158E-01	-2.360E-03	1.586E-01	-1.008
2.318E-02	1.133	-3.255E-01	-3.057E-03	2.187E-01	-1.007
2.237E-02	1.177	-3.337E-01	-3.717E-03	2.826E-01	-1.008
2.163E-02	1.223	-3.404E-01	-4.262E-03	3.426E-01	-1.014
2.086E-02	1.273	-3.473E-01	-4.351E-03	3.524E-01	-1.015
2.011E-02	1.320	-3.552E-01	-5.000E-03	4.318E-01	-1.027
1.934E-02	1.360	-3.653E-01	-5.783E-03	5.330E-01	-1.044
1.853E-02	1.389	-3.789E-01	-6.529E-03	6.350E-01	-1.056
1.776E-02	1.403	-3.955E-01	-7.275E-03	7.411E-01	-1.059
1.700E-02	1.401	-4.153E-01	-8.003E-03	8.431E-01	-1.049
1.624E-02	1.383	-4.383E-01	-8.707E-03	9.326E-01	-1.025
1.549E-02	1.346	-4.640E-01	-9.450E-03	1.008	-9.843E-01
1.474E-02	1.295	-4.926E-01	-1.020E-02	1.061	-9.278E-01
1.399E-02	1.238	-5.246E-01	-1.094E-02	1.091	-8.596E-01
1.323E-02	1.180	-5.624E-01	-1.169E-02	1.103	-7.850E-01
1.247E-02	1.126	-6.078E-01	-1.246E-02	1.105	-7.083E-01
1.170E-02	1.077	-6.637E-01	-1.323E-02	1.104	-6.386E-01
1.095E-02	1.033	-7.286E-01	-1.399E-02	1.109	-5.770E-01
1.021E-02	9.901E-01	-8.003E-01	-1.475E-02	1.123	-5.247E-01
9.456E-03	9.431E-01	-8.740E-01	-1.551E-02	1.151	-4.788E-01
8.711E-03	8.871E-01	-9.417E-01	-1.627E-02	1.192	-4.381E-01
8.005E-03	8.217E-01	-9.954E-01	-1.702E-02	1.243	-3.997E-01
7.276E-03	7.430E-01	-1.035	-1.778E-02	1.297	-3.627E-01
6.529E-03	6.547E-01	-1.056	-1.856E-02	1.344	-3.270E-01
5.783E-03	5.621E-01	-1.061	-1.935E-02	1.377	-2.948E-01
5.000E-03	4.638E-01	-1.053	-2.012E-02	1.392	-2.691E-01
4.976E-03	4.609E-01	-1.053	-2.087E-02	1.390	-2.517E-01
4.289E-03	3.767E-01	-1.042	-2.163E-02	1.371	-2.431E-01
3.588E-03	2.877E-01	-1.031	-2.237E-02	1.340	-2.433E-01
2.889E-03	2.076E-01	-1.023	-2.318E-02	1.296	-2.503E-01
2.200E-03	1.384E-01	-1.018	-2.404E-02	1.242	-2.614E-01
1.529E-03	8.258E-02	-1.014	-2.476E-02	1.190	-2.711E-01
9.874E-04	4.102E-02	-1.011	-2.549E-02	1.134	-2.769E-01
8.939E-04	3.422E-02	-1.010	-2.623E-02	1.074	-2.745E-01
6.175E-04	1.655E-02	-1.009	-2.696E-02	9.993E-01	-2.640E-01
3.916E-04	3.466E-03	-1.007	-2.769E-02	0.000	0.000

Table 6.20 Velocity Data at axial plane Z=545mm

Radius (mm)	Tangential Velocity (m/s)	Axial Velocity (m/s)	Radius (mm)	Tangential Velocity (m/s)	Axial Velocity (m/s)
2.289E-02	0.000	0.000	-9.023E-04	8.520E-02	-1.240
2.230E-02	1.082	-4.308E-01	-1.640E-03	1.345E-01	-1.240
2.171E-02	1.154	-4.549E-01	-1.865E-03	1.508E-01	-1.240
2.113E-02	1.197	-4.718E-01	-2.359E-03	1.900E-01	-1.238
2.054E-02	1.234	-4.851E-01	-3.056E-03	2.529E-01	-1.236
1.995E-02	1.271	-4.966E-01	-3.716E-03	3.168E-01	-1.235
1.931E-02	1.311	-5.080E-01	-4.272E-03	3.743E-01	-1.237
1.868E-02	1.350	-5.187E-01	-4.351E-03	3.825E-01	-1.238
1.809E-02	1.386	-5.296E-01	-5.000E-03	4.590E-01	-1.244
1.785E-02	1.399	-5.348E-01	-5.606E-03	5.413E-01	-1.251
1.749E-02	1.418	-5.425E-01	-6.194E-03	6.303E-01	-1.256
1.689E-02	1.444	-5.578E-01	-6.782E-03	7.254E-01	-1.255
1.629E-02	1.460	-5.764E-01	-7.362E-03	8.223E-01	-1.247
1.567E-02	1.464	-5.985E-01	-7.382E-03	8.254E-01	-1.246
1.506E-02	1.458	-6.236E-01	-7.930E-03	9.161E-01	-1.230
1.447E-02	1.443	-6.519E-01	-7.951E-03	9.190E-01	-1.229
1.387E-02	1.419	-6.835E-01	-8.518E-03	1.006	-1.202
1.328E-02	1.391	-7.191E-01	-9.109E-03	1.086	-1.162
1.268E-02	1.358	-7.594E-01	-9.695E-03	1.154	-1.112
1.209E-02	1.325	-8.045E-01	-1.028E-02	1.207	-1.051
1.149E-02	1.290	-8.555E-01	-1.089E-02	1.248	-9.819E-01
1.090E-02	1.253	-9.112E-01	-1.149E-02	1.277	-9.094E-01
1.030E-02	1.212	-9.709E-01	-1.210E-02	1.299	-8.366E-01
9.706E-03	1.165	-1.031	-1.270E-02	1.316	-7.678E-01
9.117E-03	1.111	-1.088	-1.330E-02	1.335	-7.044E-01
8.524E-03	1.047	-1.140	-1.389E-02	1.358	-6.490E-01
7.935E-03	9.725E-01	-1.182	-1.448E-02	1.388	-6.009E-01
7.364E-03	8.919E-01	-1.214	-1.508E-02	1.423	-5.600E-01
6.784E-03	8.045E-01	-1.236	-1.567E-02	1.459	-5.269E-01
6.462E-03	7.546E-01	-1.243	-1.569E-02	1.460	-5.258E-01
6.196E-03	7.135E-01	-1.249	-1.630E-02	1.491	-4.985E-01
5.607E-03	6.215E-01	-1.254	-1.690E-02	1.511	-4.784E-01
5.000E-03	5.307E-01	-1.255	-1.727E-02	1.513	-4.705E-01
4.982E-03	5.283E-01	-1.255	-1.748E-02	1.515	-4.660E-01
4.289E-03	4.357E-01	-1.254	-1.749E-02	1.515	-4.656E-01
3.588E-03	3.406E-01	-1.252	-1.810E-02	1.502	-4.598E-01
2.888E-03	2.497E-01	-1.251	-1.868E-02	1.473	-4.601E-01
2.200E-03	1.668E-01	-1.250	-1.931E-02	1.431	-4.646E-01
1.529E-03	9.668E-02	-1.248	-1.995E-02	1.380	-4.701E-01
9.883E-04	4.457E-02	-1.245	-2.054E-02	1.328	-4.736E-01
8.938E-04	3.615E-02	-1.245	-2.113E-02	1.275	-4.727E-01
6.151E-04	1.649E-02	-1.243	-2.171E-02	1.219	-4.636E-01
3.917E-04	2.221E-03	-1.242	-2.230E-02	1.138	-4.453E-01
-1.608E-04	2.341E-02	-1.240	-2.289E-02	0.000	0.000
-4.571E-04	4.521E-02	-1.240			

Table 6.21 Velocity Data at axial plane Z=565mm

Radius (mm)	Tangential Velocity (m/s)	Axial Velocity (m/s)	Radius (mm)	Tangential Velocity (m/s)	Axial Velocity (m/s)
-1.905E-02	0.000	0.000	3.917E-04	1.253E-02	-1.291
-1.868E-02	9.946E-01	-6.247E-01	6.133E-04	2.522E-02	-1.292
-1.858E-02	1.267	-7.923E-01	8.937E-04	4.269E-02	-1.294
-1.810E-02	1.363	-8.265E-01	9.890E-04	5.093E-02	-1.294
-1.763E-02	1.418	-8.409E-01	1.529E-03	1.025E-01	-1.298
-1.716E-02	1.462	-8.466E-01	2.199E-03	1.710E-01	-1.302
-1.668E-02	1.500	-8.492E-01	2.888E-03	2.491E-01	-1.305
-1.621E-02	1.527	-8.505E-01	3.587E-03	3.316E-01	-1.308
-1.609E-02	1.532	-8.510E-01	4.289E-03	4.149E-01	-1.310
-1.574E-02	1.543	-8.518E-01	4.440E-03	4.343E-01	-1.310
-1.537E-02	1.548	-8.543E-01	4.985E-03	4.995E-01	-1.312
-1.527E-02	1.548	-8.547E-01	5.000E-03	5.013E-01	-1.312
-1.480E-02	1.545	-8.608E-01	5.465E-03	5.698E-01	-1.313
-1.433E-02	1.535	-8.719E-01	5.931E-03	6.428E-01	-1.313
-1.386E-02	1.522	-8.899E-01	6.081E-03	6.655E-01	-1.314
-1.340E-02	1.507	-9.161E-01	6.297E-03	6.984E-01	-1.314
-1.293E-02	1.491	-9.499E-01	6.396E-03	7.146E-01	-1.313
-1.246E-02	1.470	-9.890E-01	6.861E-03	7.866E-01	-1.312
-1.200E-02	1.442	-1.031	7.328E-03	8.596E-01	-1.310
-1.153E-02	1.404	-1.073	7.794E-03	9.331E-01	-1.305
-1.106E-02	1.356	-1.113	8.261E-03	1.006	-1.296
-1.059E-02	1.296	-1.150	8.728E-03	1.076	-1.280
-1.012E-02	1.227	-1.184	9.194E-03	1.143	-1.258
-9.649E-03	1.150	-1.213	9.660E-03	1.204	-1.230
-9.179E-03	1.067	-1.237	1.013E-02	1.259	-1.198
-8.714E-03	9.821E-01	-1.254	1.059E-02	1.308	-1.162
-8.249E-03	8.957E-01	-1.265	1.106E-02	1.350	-1.124
-7.784E-03	8.102E-01	-1.272	1.152E-02	1.387	-1.085
-7.319E-03	7.272E-01	-1.276	1.199E-02	1.419	-1.048
-6.854E-03	6.480E-01	-1.278	1.246E-02	1.446	-1.013
-6.391E-03	5.741E-01	-1.278	1.293E-02	1.469	-9.827E-01
-6.293E-03	5.586E-01	-1.278	1.340E-02	1.486	-9.570E-01
-5.928E-03	5.061E-01	-1.277	1.387E-02	1.499	-9.367E-01
-5.767E-03	4.835E-01	-1.277	1.434E-02	1.504	-9.216E-01
-5.464E-03	4.438E-01	-1.276	1.481E-02	1.504	-9.104E-01
-5.365E-03	4.313E-01	-1.276	1.528E-02	1.495	-9.018E-01
-5.000E-03	3.899E-01	-1.276	1.575E-02	1.480	-8.947E-01
-4.351E-03	3.306E-01	-1.277	1.585E-02	1.475	-8.936E-01
-4.277E-03	3.249E-01	-1.277	1.622E-02	1.456	-8.881E-01
-3.716E-03	2.816E-01	-1.279	1.627E-02	1.454	-8.875E-01
-3.056E-03	2.309E-01	-1.282	1.669E-02	1.427	-8.812E-01
-2.359E-03	1.773E-01	-1.285	1.716E-02	1.393	-8.734E-01
-1.865E-03	1.426E-01	-1.287	1.763E-02	1.355	-8.626E-01
-1.640E-03	1.273E-01	-1.287	1.811E-02	1.307	-8.427E-01
-9.021E-04	7.934E-02	-1.288	1.858E-02	1.215	-8.015E-01
-4.570E-04	4.717E-02	-1.289	1.905E-02	0.000	0.000
-1.608E-04	2.923E-02	-1.289			